ROBUST AIRCRAFT SUBSYSTEM CONCEPTUAL ARCHITECTING

A Dissertation
Presented to
The Academic Faculty

by

David W. Jackson

In Partial Fulfillment
of the Requirements for the Degree
Doctor of Philosophy in the
School of Aerospace Engineering

Georgia Institute of Technology
December 2013

ROBUST AIRCRAFT SUBSYSTEM CONCEPTUAL ARCHITECTING

Approved by:

Professor Dimitri Mavris, Advisor
School of Aerospace Engineering
Georgia Institute of Technology

Professor Daniel Schrage
School of Aerospace Engineering
Georgia Institute of Technology

Dr. Elena Garcia
School of Aerospace Engineering
Georgia Institute of Technology

Assistant Professor Brian German
School of Aerospace Engineering
Georgia Institute of Technology

Dr. Michael Armstrong
Aerospace Systems Engineering Specialist
Rolls-Royce

Mr. Alexander Schneegans
President
PACE America, Inc.

Date Approved: 15 November 2013

To my parents,

Tom and Hope Jackson

ACKNOWLEDGEMENTS

I want to thank my advisor, Professor Dimitri Mavris who has provided great insight into my work and invaluable support along the way. I would like to express my appreciation for all the great experiences and all that I have learned while being a member of the Aerospace Systems Design Laboratory and for all of Dr. Mavris' time and guidance. I would also like to thank Dr. Elena Garcia who has provided extremely useful input and many hours of very insightful feedback. I would also like to thank Dave Rumney and Caio A. Ferreira from the Parker Hannifin Corporation who provided expert opinion and input with regards to ranges for actuator weights. I would like to thank all of the members of my committee: Dr. Schrage, Dr. German, Dr. Garcia, and Mr. Schneegans. All of whom have taken time from their schedule to provide me with valuable input and assistance. Finally, I would like to thank my family and friends for their support.

TABLE OF CONTENTS

LIST OF TABLES

LIST OF FIGURES

LIST OF SYMBOLS

α	Acceleration, $m/(sec^2)$
ΔPr	Pressure Loss, psi
δ	Deflection Angle, rad
η	Efficiency
μ	Mean
ρ	Density, Kg/m^3
σ	Standard Deviation
A	Area, m^2
b	Span, m
c	Chord, m
C_D	Coefficient of Drag
c_{wsp}	Chord of Wing at Spoiler, m
D	Diameter, in
D_i	Number of Designs in Row i
F	Force, N
f	Friction Factor
G	Gearing Ratio
k	Coefficient

l Length, ft

$LStrue(XY)$ Link Strength Between X and Y

M Hinge Moment, Nm

m Mass, Kg

N Number of Design Alternatives

n Load Factor

P Power, HP

P_{in} Input Power, KW

P_{out} Output Power, KW

P_B Power Extraction from Baseline, HP

P_{EDS} Power Extraction from EDS, HP

P_M Power Extraction from Map, HP

Pr Pressure, Pa

Q Flow Rate, $(m^3)/sec$

Q_{GPM} Flow Rate, GPM

R_i ith Response

S Variance-Covariance Matrix

S_{sp} Spoiler Area, m^2

SG Specific Gravity

SNR Signal to Noise Ratio

T Number of Tests

Ti^2 Hotelling's Tsquared

$TOGW$ Design Takeoff Gross Weight, LB

V Velocity, m/sec

W Weight, LB

W_N Aircraft Weight, N

x_i ith Observation

x_t Target Vector

y_{sp} Spanwise Location of Spoiler, m

SUMMARY

Aircraft subsystems, such as the Environmental Control System, the Flight Control System, and the Anti-Icing System, are key components in modern aircraft, the impact and significance of which have been constantly increasing. Furthermore, the architecture selection of these subsystems has overall system-level effects. Despite the significant effects of architecture selections, existing methods for determining the architecture, especially early in design, are similar to the use of traditional point solutions and do not capture much of the design space. However, energy optimized aircraft and more electric aircraft are two approaches that attempt to improve the platform-level impacts of subsystems by utilizing non-traditional architectures. These initiatives have several expected benefits over the use of the traditional subsystem architecture and are being explored to replace the traditionally powered systems. Therefore, several system-level studies have examined more electric aircraft concepts which, although they have provided useful insight, have left several gaps that require further investigation.

Currently, aircraft subsystems are rarely examined during the conceptual design phase, despite the fact that this phase has a significant influence on aircraft cost and performance. For this reason, there is a critical need to examine subsystem architecture trades and investigate the design space during the conceptual design of an aircraft. Traditionally, after the aircraft conceptual design phase, subsystems are developed in a process that begins with the point selection of the architecture, then continues with its development and analysis, and concludes in the detailed development of the subsystems. The choice of the point design of the architecture to be developed can be made using simplified models to explore the design space. This

method known as conceptual architecting is explored in this dissertation. To this end, the impact and classification of uncertainty on conceptual architecting is determined utilizing Bayesian distributions and a developed modeling and simulation environment. In addition, due to the presence of epistemic uncertainty, a process using uncertainty distributions and Bayesian Networks is developed to determine the effect of this uncertainty on the robustness of the designs.

This dissertation also focuses on bringing actuation subsystem architecture trades into conceptual design because of the significant cost impact of this design phase and the interdependence of vehicle sizing with the subsystems impact on the aircraft. A methodology to examine the design space of aircraft subsystem architectures during the conceptual design of aircraft, while incorporating this coupling, is presented herein and applied specifically to actuation architectures. As part of this methodology, the architectures are compared, utilizing a modeling and simulation environment. Specifically, the proposed methodology uses conceptual physics-based models of the subsystems that were integrated with an aircraft sizing and synthesis algorithm and an engine core sizing algorithm. Using this methodology, uncertainty is captured on the subsystems properties to enable the selection of robust designs.

The application of the proposed methodology is examined using the experiments herein. The interdependence of vehicle sizing with the subsystems impact on the aircraft was studied within the experiments for different passenger classes of aircraft. The extent of these interdependencies is examined experimentally and found to be significant. As a result, this coupling must be captured to enable better informed decision making. In addition, the capturing of uncertainty and robust design selection was demonstrated experimentally for subsystem architectures. The determination of the driving sources of uncertainty was demonstrated utilizing Bayesian Networks. Finally, overall, the proposed methodology was seen to provide additional benefits over the use of a point driven design by capturing the coupling between aircraft sizing

and subsystem architecture platform-level impacts while exploring the architecture design space.

CHAPTER I

MOTIVATION AND PROBLEM DEFINITION

1.1 Introduction

Aircraft internal subsystems play a significant role in today's aircraft. These subsystems enable the aircraft to perform many essential functions including moving the primary flight controls, carrying passengers in comfort, operating the instruments, and communicating. These subsystems over decades of development have evolved into one standard architecture [120], which is currently being challenged by novel concepts such as energy optimized aircraft and the More Electric Aircraft (MEA) [46], [59], [120].

For such novel architectures to be fully considered, their impact on the aircraft design should be closely examined. Specifically, the impact of the subsystem architecture trades on the aircraft sizing should be explored. Such an analysis should allow the quantification of the impact of uncertainty on the robustness of the different designs. The creation of a methodology to enable this analysis leads to the Research Objective of this dissertation.

Research Objective: To create and examine a methodology for capturing subsystem architecture trades and their coupling with aircraft sizing.

The question of how to achieve this objective creates the Motivating Research Question for this work.

Motivating Research Question: How can the objective of creating and examining a methodology for capturing subsystem architecture trades and their coupling with aircraft sizing be achieved?

1.2 Aircraft Subsystems

1.2.1 Role, Definition, and Impact

According to Raymer [115], aircraft subsystems include hydraulic power systems, electrical systems, avionics, and auxiliary power systems. A close equivalent to the term subsystems is Aircraft Equipment Systems (AES). The American Institute of Aeronautics and Astronautics (AIAA) Energy Optimized Aircraft and Equipment Systems (EOASYS) Program Committee [17] defines aircraft subsystems (or AES) as hidden systems of the aircraft that are essential to performance, safety, controllability and comfort. Examples of aircraft subsystems pointed out by the EOASYS Committee are Environmental Control, Thermal Systems, Flight Control, anti-ice systems, Braking, power generation and distribution, and the fuel system [17].

For the purposes of this dissertation, the EOASYS AES definition will be used to define aircraft internal subsystems. As noted in the definition [17], these subsystems are key to the aircraft's functionality. They provide the movement of the flight controls, the fuel, cabin comfort, and even ice protection [17]. Not only do these subsystems provide key functionality, but they also contribute to the aircraft empty weight and impact its size. According to Stinton [127], the combination of the hydraulic, electrical, and pneumatic systems is approximately 6 to 12 percent of the total design gross weight, which impacts the overall aircraft size and performance.

As discussed in the chapter regarding the methodology, this dissertation focuses on the case study of possible significant changes in the actuation systems to capture these trades and demonstrate the methodology and its usefulness. Specifically, trades between the traditional hydraulic actuation, electric actuation, and hybrid systems are performed. The selection of such a case study limits the scope of the required modeling and the size of the examined design space. Also, as discussed later, this case study enables true evaluation of the MEA technology of an Electro-Hydrostatic Actuator(EHA) and the potential replacement of a traditional power system (hydraulics)

with a more electrical concept. The rest of the architecture was held constant as the current traditional architecture to enable comparison of the results with existing aircraft in the examined passenger classes.

1.3 Aircraft Subsystems Architectures

1.3.1 Definition

In order to explore aircraft subsystem architectures, it is first necessary to define what is meant by these architectures. To start, this discussion, briefly reviews of what is meant in the literature by the term architecture. Moir and Seabridge [92] examined and broke down into a structure the systems architectures for military aircraft fulfilling different roles. Dahmann, Fujimoto, and Weatherly [34] when discussing architecture in the context of simulations within the United States Department of Defense (DoD), used the following definition for architecture: "major functional elements, interfaces, and design rules, pertaining as feasible to all simulation applications, and providing a common framework within which specific system architectures can be defined."

For the purposes of this work, an architecture is defined as the components that make up a system, their arrangement, and their interconnections. A system is defined as a set of components and connections that fulfill a given purpose. In this work, an aircraft subsystems architecture is defined by a selection of the distribution network (interconnections between components and how they are routed), the power source for each subsystem component, and the components themselves. The power source for each component includes the type of power used and the location of the source of that power. This selection implies the determination of which technologies may be used for that component. For example, for each component that is electrically driven, this selection would include the specification of the electrical bus (and therefore the generator) powering each component and the distribution network used for routing

the wiring. An example of a subsystem architecture, specifically of the hydraulically driven flight control actuation system of the Airbus A-320 is shown in Figure 1. The actuators are identified by which system (yellow, green, and blue) and therefore which pumps power the actuators. In this example, the pumps primarily derive their power either from shaft power extraction from the engines or from electrical sources. Among other impacts, the type of power selected can indicate the selection of a technology that requires that type of power for a particular component. As a result of this impact, combined with the fact that components are a part of subsystem architectures, the subsystem architecture selection is directly related to the technology selection for the internal subsystem components.

A distribution network is the set of pathways created or used for routing connections between components. These connections can be electrical wires, pneumatic pipes, or hydraulic lines. The selection of the route network is highly constrained by the locations of components, such as the fuel tank and the passenger cabin. An example of a route network can be seen below in Figure 2 where the set of red lines running through the aircraft (in this case, a notional Boeing 737-800 aircraft) is the currently selected route network which runs around such features as a passenger cabin. Connections between components are primarily run through these conduits.

1.3.2 Traditional Subsystem Architectures

Aircraft typically utilize a traditional point-driven design for their subsystem architecture selection [120] and [46]. In this architecture, most of the aircraft power generated by the aircraft engines from burning fuel is used for propulsion with the remainder of the power created by the engines converted to non-propulsive power of different types. Traditionally, this power is converted into four forms of power utilized to drive the various aircraft subsystems. These forms of power include pneumatic, hydraulic, mechanical, and electrical power. Pneumatic power is traditionally used for

the Environmental Control System (ECS) and Wing Anti-Icing (WAI). This form of power is typically extracted from the engines' high pressure compressors in the form of bleed air. Mechanical power is drawn from the engines to provide input power to hydraulic pumps, electrical generators, and other components. Electrical power is used for several systems, including the avionics, galleys, entertainment, and lights [120]. This power distribution configuration represents the traditional subsystems architecture that has evolved to become the current traditional standard architecture for transport aircraft [120] and [46]. The fact that subsystem architectures are typically chosen utilizing a point-design based off of this traditional architecture leads to Observation 1.

Observation 1: Subsystem architectures are typically a traditionally selected point-driven design.

1.3.3 Impact

The impact of subsystem architecture selections can be significant. If the selected architecture is changed, then the weight, energy use, and power flows of the subsystems will change [120], [51], [46], and [27]. The power flows change because either the distribution network itself changes to another configuration or some components draw power from different sources (and possibly different types of power). If this occurs, the connections between the components must be updated accordingly. This change in the links between components and their routing can significantly change the power flow, the line losses, and the weight of the connections. These changes may be extensive and can be complex to evaluate. However, as shown later in this dissertation, these changes can be captured using modeling and simulation. These differences, in addition to the possible changes to the weight and efficiency of the components themselves and to their power sources such as pumps or generators, lead to the differences in weight, power draw and power flows between different subsystem

architectures [120], [51], [27], and [46]. The resulting change in levels of shaft power extraction and bleed air flow drawn from the engines will affect fuel burn and possibly engine core sizing [120], [51], [27], and [46]. The changes in fuel burn and possibly the engine core size along with the different subsystem weight lead to a different aircraft Take Off Gross Weight (TOGW), and therefore a different size aircraft [51] and [27]. Changes in the subsystems architecture leading to a different aircraft sizing lead to Observation 2.

Observation 2: Variations in the subsystems architecture can lead to significant platform-level impacts.

1.4 Energy Optimized Aircraft and More Electric Aircraft

Energy optimized aircraft and more electric aircraft are two types of subsystem architectures under study in the current aerospace industry that challenge the traditional architecture status quo. This section discusses these architectures, why and how they are being examined, and the fact that further analysis is needed.

1.4.1 Energy Optimized Aircraft

The economics of the airline industry are creating a great demand for reducing the cost of operating aircraft [46]. This is partially motivated by a large increase in fuel prices in recent years [65] and [133]. These problems create a demand for fuel-efficient aircraft. An increase in fuel efficiency could reduce the operations cost of the aircraft and the amount of emissions from the aircraft (because less fuel is burned) as well as allow the aircraft to be resized to be smaller or allow an increase in payload (or range).

This desire for fuel efficiency leads to the concept of energy optimized aircraft. There are different ways to achieve such an energy optimized aircraft [46]. These options include optimizing aircraft equipment systems and engines, optimizing the aircraft, and optimizing the solutions to the aircraft required functions [46]. The Power

Optimized Aircraft project focused on the first two of these options and attempted to minimize non-propulsive power usage [46]. However, there are many different groups studying energy optimized aircraft, and each group seems to have a slightly different definition of energy optimized aircraft and goal or focus for their research. For example, the United States Air Force (USAF) created the Integrated Vehicle Energy Technology Demonstration (INVENT) program with goals of increasing aircraft range, endurance, and cooling capacity [14] and [139]. More Electric Aircraft (MEA) is one approach to enable the creation of the highest efficiency within the aircraft level energy balance [59].

1.4.2 More Electric Aircraft

More Electric Aircraft (MEA) or the related All Electric Aircraft (AEA) are aircraft containing more electrical components allowing a reduction or elimination in the use of traditional types of power. This enables the realization of several benefits. One such benefit is a possible reduction in weight of the related systems due to consequences such as the reduction or elimination of heavy hydraulic lines and components. Another potential benefit is a reduction in power demand from these systems. It is currently believed that electrically driven systems have more future efficiency improvement potential than their traditional counterparts. AEA and MEA are not new concepts. In fact, their origins trace back to World War II. However, AEA was unfeasible until recently. The implementation of this concept is now feasible due to the progression of technology in which several discoveries have enabled MEA. [120] MEA and AEA serve as challengers to the current traditional subsystems architecture and have several potential benefits.

1.4.2.1 Expected Benefits

There are several expected benefits of MEA and AEA. One of these is the reduction or elimination of bleed air removed from the compressor of the engine [120]. Another

possible benefit is the removal of centralized hydraulic system components and distribution lines [120]. By reducing the weight of the subsystems, companies can increase the possible payload (or range) of the aircraft, or resize the aircraft, improving its size, cost, and needed amount of fuel.

The needed amount of fuel might also be reduced by a reduction in the energy demand of the internal systems. The Power Optimized Aircraft (POA) project found that electrical components are generally more efficient than their counterparts [46]. This increase in efficiency could result in a lower magnitude of power used by these systems leading to a reduction in the total amount of fuel burned. This reduction in fuel burn has several potential impacts. First, the emissions will be reduced since less fuel would be burned. Second, the cost to the airlines of operating the aircraft will be reduced due to less fuel being used per flight. This is particularly important in the current competitive market. Among other economic developments in recent years, fuel prices have risen significantly, increasing the need for fuel efficiency [65] and [133]. This can be illustrated from Figure 3 which shows the increase in fuel prices.

As a result of their location on the technology S-curve, electrical technologies have more potential room for growth in performance and weight. A technology S-curve has been shown, based off historical studies of technologies to represent a common progression of the application of a given technology if the technology is successful [75]. The S-curve illustrates that, as more and more development and time are invested in a particular technology, eventually the technology becomes more mature and closer to being able to perform at its maximum capacity [75]. When this occurs, more and more development is needed for a given amount of performance gain. Because the traditional architecture of the subsystems for transport aircraft has been developed over decades, traditional technologies likely are higher on the curve and therefore have less room for growth in their performance [120]. Switching to other technologies,

such as the use of electrical components in non-traditional roles, allows the use of a different S-curve, which may have more room for improvement in future development. This growth potential could help with the current challenges of using more electrical technologies on aircraft, such as that the weight of the electrical systems have a tendency to be higher [46] than that of the traditional systems they are replacing. This use of MEA components could actually act to increase the aircraft size or total fuel burn, making MEA potentially not as beneficial as it may seem.

More Electric Aircraft have already started to come into existence. For example, the B-787 has electrical brakes, WAI, ECS, and engine starting systems [46]. Figure 4 shows an increasing trend in the electrical power generation capacity of aircraft. This trend exists but is at least partially due to, the emergence of MEA as additional systems and components have been added to the aircraft over time, including entertainment systems that require electrical power. For example, on the Airbus A-380, powering the In Flight Entertainment (IFE) currently takes 50-60kVA [93]. The additional power that modern systems require increases the importance of making the internal subsystems as efficient as possible.

1.4.2.2 More Electric Aircraft Components

MEA components are electrical components from systems that are traditionally powered by non-electrical sources. In an MEA, these components are being examined to be replaced by electrically powered systems. These systems include traditional pneumatically powered systems such as the WAI, ECS, and the engine starting systems [120], all of which along with electrical brakes are being demonstrated in an electrically powered architecture and can be examined from their implementation on the B-787 [46]. In the B-787 ECS, there are two electrically powered air conditioning packs [93]. The total B-787 ECS pressurization electrical power draw is approximately 500 kVA [93]. On the B-787, the WAI is done by electrically powered heating mats within the

wings, consuming approximately 100kVA [93]. Also being examined in the industry is a more electrical engine, such as the more electric Trent 500 developed for the POA [93]. Another more electrical engine architecture can be seen in the B-787, which has a no engine bleed architecture [102]. The more electrical engine contains electrical fuel and oil pumps, actuators for various purposes, and other electrical components [93].

MEA systems and components also include systems and components that are being examined to replace hydraulically powered systems and components. This includes the use of electrical brakes instead of hydraulic brakes [93]. The B-787 has electrically powered brakes demonstrating this technology and allowing a chance to examine it in operation [93] and [46]. Also, the use of electrically driven pumps to replace some of the engine driven hydraulic pumps is a MEA concept being implemented in the B-787 [93]. Some other MEA/AEA components that are being examined to replace some of the hydraulic powered systems are Electro-Hydrostatic Actuators (EHAs) and Electro-Mechanical Actuators (EMAs) [93]. These actuators will be used to move the control surfaces on the aircraft. The EMA uses an electrical motor to drive a mechanical component such as a ballscrew to move the surface. An EHA has an electrically powered pump that provides pressurized hydraulic fluid that stays within the EHA and pushes on a piston to move a mechanical component that moves the control surface [68]. Examples of an EMA and an EHA are shown in Figure 5. The use of EMAs and EHAs could help reduce or eliminate the need for the central hydraulic systems. EHAs have been used on the Airbus A-380 and the F-35 [93]. Although all of the MEA components and systems have some apparent advantages, a complete platform level examination has to be done to determine if they are better than the traditional architecture and, if so, which mixture of MEA and traditional components and systems is best for a given aircraft design.

1.4.2.3 More Electric Aircraft System Level Studies

Since MEA and AEA were proposed in 1945 [27], there have been several system-level studies to examine these concepts. This section gives an overview of selected studies.

In 1985 the National Aeronautics and Space Administration (NASA) published a study entitled the Integrated Digital/Electric Aircraft (IDEA) Concepts Study [51] and [27]. This study examined a new 250-300 seat transport aircraft envisioned to replace a Lockheed L1011 [27] and [51]. The IDEA systems included the use of EMAs for the flight controls, electrically powered brakes, an electroimpulse WAI, and a self-contained ECS that used ram air and a vapor cycle [51]. The study compared IDEA with a baseline aircraft configuration. These configurations can be seen in Figure 6, which illustrates the size difference between the traditional baseline and the more electrical IDEA. The study found an overall weight savings of 7034 lb through the use of these technologies, removal of the related traditional components, and a reduction in the needed fuel [51]. This impact, combined with the fact that the size of the aircraft determines the required performance from the subsystems, helps lead to Observation 3. For example, the hinge moments which vary with aircraft size, in turn define part of the required performance from the flight control system. Observation 3 is also drawn from these facts: that the weight of different subsystems is historically a function of TOGW, that different power extraction and bleed requirements can impact engine core sizing and therefore aircraft size, and that electrically driven subsystems have different weight and power requirements and therefore affect aircraft sizing [120], [51], [27], [60], [121], and [46].

Observation 3: Subsystem architecture platform-level impacts are coupled with the sizing of the aircraft.

It should be clarified that what is meant by the platform-level impacts in this context is the subsystem weight, power extraction, and amount of bleed air used to power the subsystems. These metrics are used because these parameters impact aircraft and

engine core sizing directly. The subsystem weight impacts the aircraft TOGW [121] (and this is also shown in the experimental results), and the power extraction and bleed may impact fuel burn and engine core sizing. The selection of these metrics for characterizing subsystem impacts is discussed further in the Subsystem Modeling Metrics section later in this dissertation.

The IDEA study contributed several useful analyses examining electrical subsystem architecture impacts but did not consider several important questions such as these: Could a mixture of some of these technologies and a conventional architecture enable even better gains? If so, which mixtures of these technologies have which advantages?

In the 2000's, the European Union (EU) Power Optimized Aircraft (POA) project had the goal of reducing cost by optimizing the aircraft equipment systems (AES) and engines as well as the aircraft as a whole [46]. The project had a goal of reducing fuel burn and non-propulsive power use while increasing reliability [120]. The POA looked at several types of systems with the goal of reducing fuel burn and power use [46]. These systems included engine electrical systems, aircraft electrical systems, actuation systems, and pneumatic systems [46]. The POA study found that the electrical systems used instead of traditional systems have a tendency to be heavier but more efficient [46]. The POA study used a virtual iron bird to model the different aircraft system architectures [25]. Modelica models of the different systems were used together in the virtual iron bird [25]. The virtual iron bird used inverse dynamics for modeling the aircraft systems [25]. The virtual iron bird applied distributions on the current draw of the components and ran a Monte Carlo Simulation (MCS) to account for uncertainty [25]. The fact that these subsystems can be modeled, as demonstrated by programs such as POA [25] and [46], to determine the system-level impact of different architectures leads to Observation 4.

Observation 4: Physics-based modeling and simulation can quantify the system-level impact of different subsystem architectures.

A continuation EU project from the POA is the project More Open Electrical Technologies (MOET) [90], which examines the creation of various MEA electrical technologies and integrates them into aircraft and creates a design environment for power by wire [90]. MOET performs a comparison between baseline aircraft of different sizes and a version of the aircraft with the application of selected MEA technologies [90]. MOET also utilizes Modelica for modeling systems, including a Modelica environment that MOET created for the design of the electrical systems [26].

Observation 5 is derived from the characteristics of the coupling between aircraft sizing and subsystem architecture impacts on the aircraft. Specifically, the historic increase of subsystem weight with TOGW [121] along with the coupling seen in Observation 3 creating an increase in aircraft size when subsystems are heavier and demand more power. This would lead to a higher fuel burn and possibly a larger engine core, along with a possible increase in demands on the subsystems when the aircraft is larger. The positive relationship between aircraft sizing and subsystem architecture impacts leads to Observation 5. An example of the possible increase in demands on the subsystem with an increase in TOGW is larger loads on the flight controls. These loads increase with TOGW as the wing area will increase with TOGW and as the wing area increases, the hinge moment increases, as can be seen utilizing the volume coefficient [115] and [60].

Observation 5: The covariances and correlations between architecture impacts and aircraft size are likely to be positive.

Again, it should be clarified that what is meant by the platform-level impacts in this context is the subsystem weight, power extraction, and amount of bleed air used to power the subsystems. These metrics are utilized because they may impact aircraft and engine core sizing directly. The Subsystem Modeling Metrics section later

in the dissertation further discusses the selection of these metrics for characterizing subsystem impacts.

There are several other MEA programs. These include programs such as Totally Integrated More Electric Systems (TIMES), NASA's Electric Flight Systems Workshop, and a 1988-1989 Cranfield College of Aeronautics study [27] and [120]. Also, the B-787's use of MEA technologies demonstrates that MEA technologies are becoming more and more feasible [93] and [46].

Previous system-level MEA studies primarily considered a static portfolio of technologies compared to selected baseline aircraft. This was similar to using a different point design of the subsystems without exploring different subsystem architectures. For the most part, these studies did not examine the effect of the given technology on multiple aircraft sizes. Energy optimized aircraft are considered the future of civil aviation. To achieve this energy optimization, trades in the subsystem architectures need to be examined earlier in the design process that capture the coupling with aircraft sizing. A methodology for capturing the coupling of subsystem architecture impacts on the aircraft with aircraft sizing is demonstrated later within this dissertation, for actuation architectures.

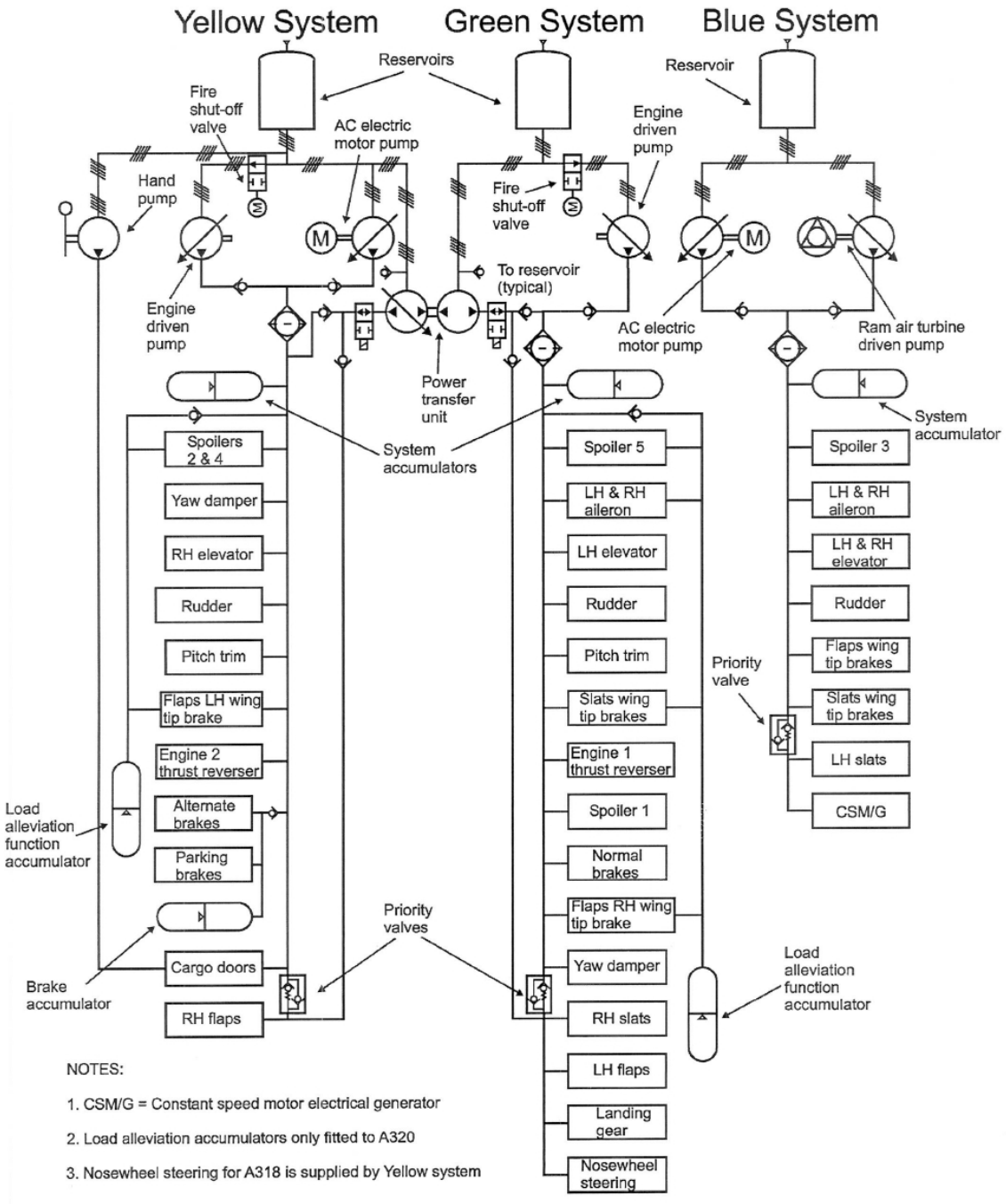

Figure 1: Airbus A-320 Hydraulic System Architecture [4]

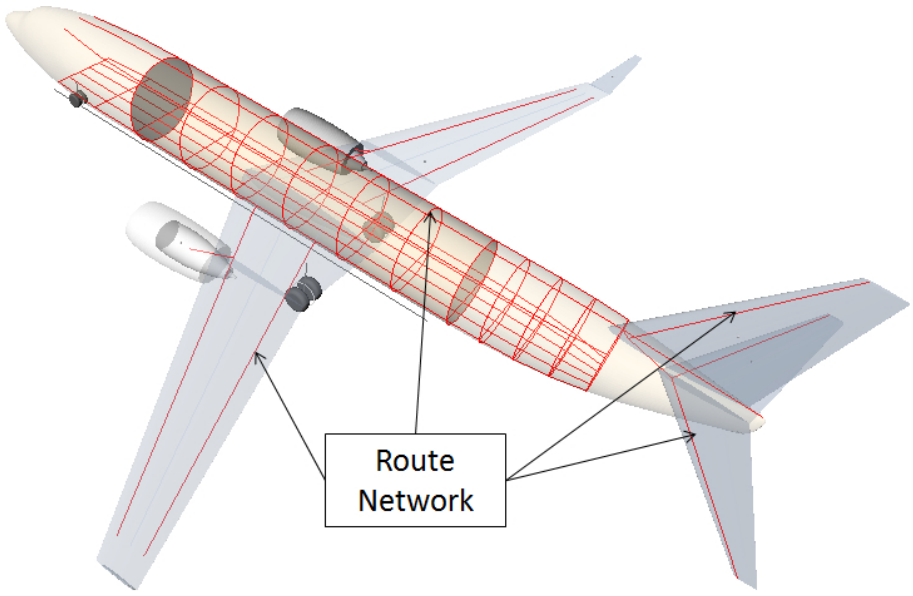

Figure 2: Example Distribution Network

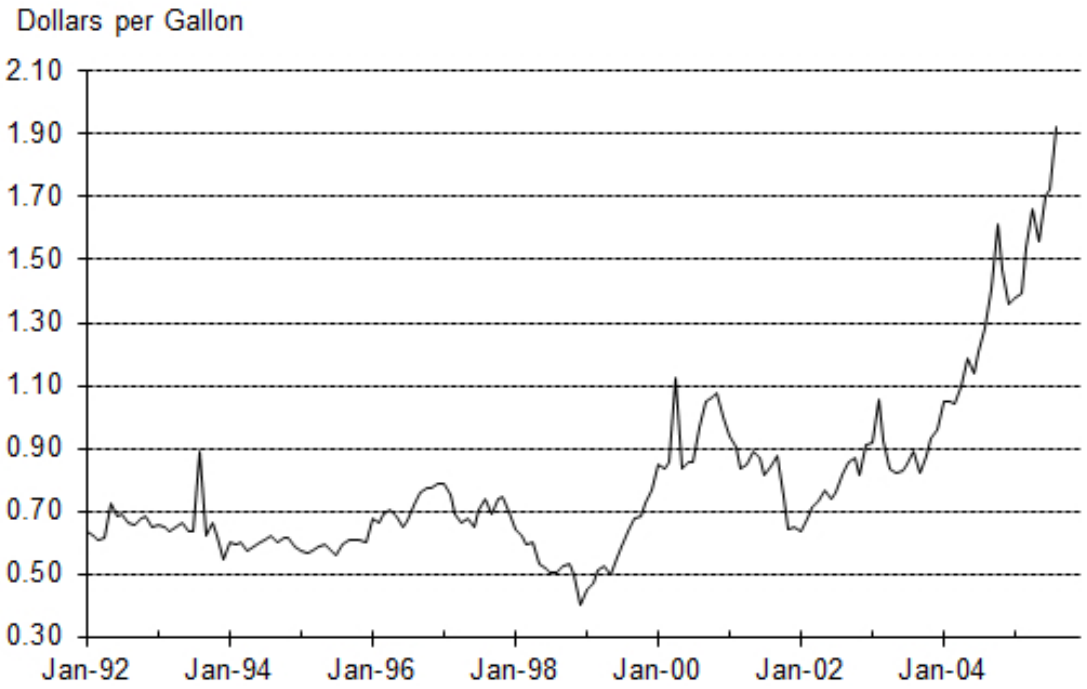

Figure 3: Jet Fuel Prices Adapted from [133]

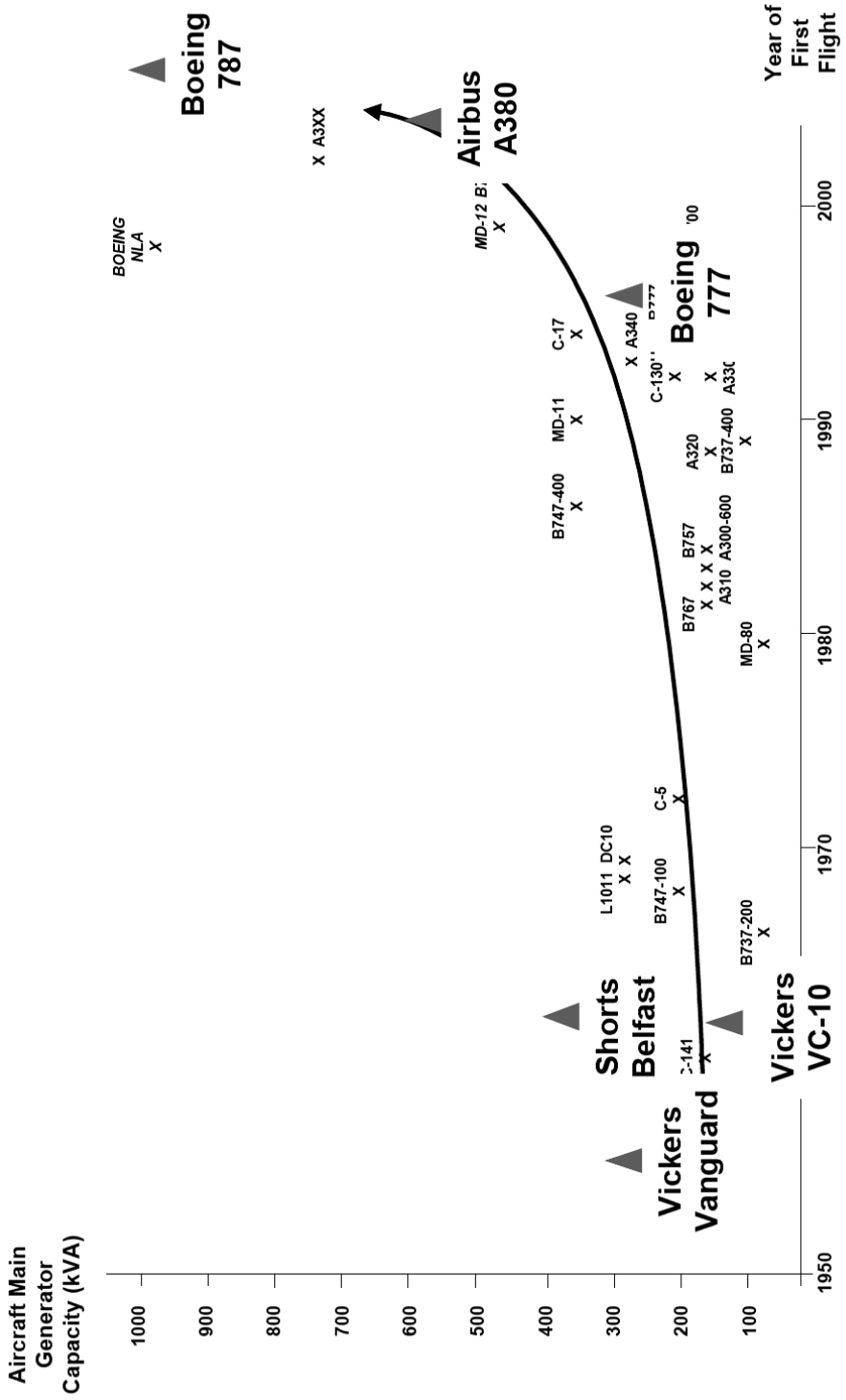

Figure 4: Aircraft Electrical Power Generation [91]

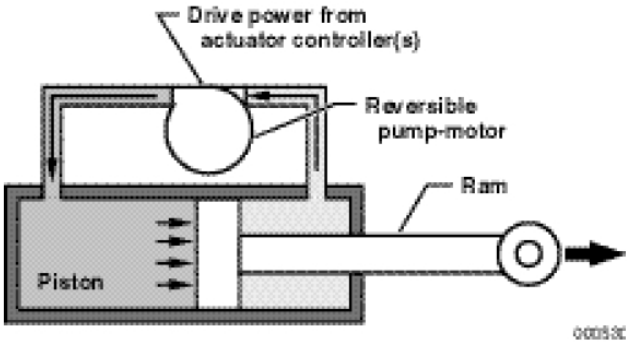

(a) Electrohydrostatic Actuator (EHA).

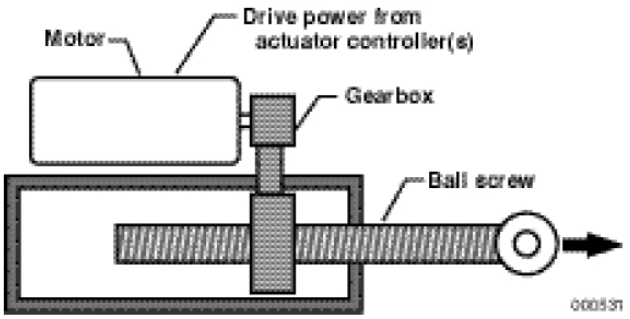

(b) Electromechanical Actuator (EMA).

Figure 5: EMA and EHA [68]

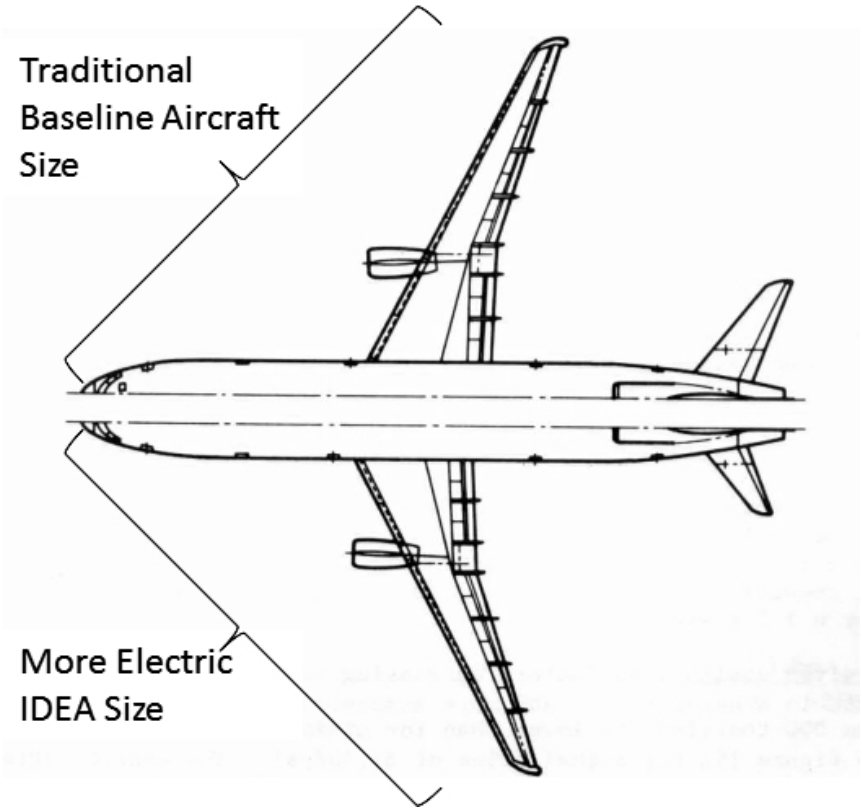

Figure 6: Integrated Digital/Electric Aircraft Comparison to Baseline adapted from [51]

CHAPTER II

SUBSYSTEM DESIGN METHODS AND PROCESSES

2.1 Traditional Consideration of Subsystems within Conceptual Design

Traditionally, subsystem designs are not examined during the conceptual design phase of an aircraft. Therefore, aircraft subsystems do not typically impact the initial design and layout of aircraft directly [115]. It is usually, later in the design cycle that the needs of the subsystems are accounted for by the designer [115]. The subsystems and their hardware vary widely among classes of aircraft making some rules of thumb for including subsystems in conceptual design more difficult to create and implement [115]. While many of the systems' components are small and are not considered during the initial stages of creating layouts of the aircraft, some components are currently considered important when creating the layouts [60]. To illustrate this, Raymer [115] states that the hydraulic system impacts the conceptual design of most aircraft only in the provision of space for the engine driven pumps. Also, the Auxiliary Power Unit's (APU) location must be considered in the design layout of the aircraft. Specifically, the APU is often placed within the tail in transport aircraft [115] and [60]. Additionally, the positions of the avionics bay and antennas are important considerations in the aircraft layout. The avionics bay is often placed in front of or below the cockpit [115] and [60]. The location of the fuel tanks is another internal subsystems-related component that must be considered in a layout [60].

The aircraft subsystems also impact the TOGW weight calculation primarily through a portion of the empty weight. This contribution can be calculated based on historical (or otherwise created) fractions of the weight [60]. For example, Howe

[60] aggregates the weight of the subsystems, landing gear, and equipment into one value that is calculated using a tabulated fraction of the TOGW. Similarly, Jenkinson, Simpkin, and Rhodes [67] give fractions created from historical data for different types of transport aircraft to use for the faction of the mass of the fixed equipment (including subsystems such as the flight control system) to the takeoff mass. Jenkinson, Simpkin, and Rhodes [67] use these fractions because items within the fixed equipment group vary greatly among different aircraft. Stinton [127] gives weight fractions to use for all the subsystems combined (between 0.06 to 0.12) and for some different subsystems by themselves including the electrical systems(0.03), deicing systems (0.006), and the hydraulic and pneumatic systems (0.03). Stinton [127] points out that these ratios vary among aircraft and the numbers mentioned were averages that were suggested by the author to be used to represent the weight fractions. Stinton [127] also contains ratios to use for fuel systems. During conceptual design, as part of the aircraft geometry (and related to the control systems) the size of the control surfaces can also be estimated from empirical data (using volume coefficients) [60] and [115].

As discussed above, the weight of different subsystems is historically a function of TOGW. This variation of the historical weight impact of subsystems with aircraft size (and therefore passenger class) leads to Observation 5. This historical function can be a function of TOGW [121]. As a result, the impacts of the subsystems vary with TOGW. The fact that subsystem weights are historically a function of TOGW as discussed above can also be seen in Roskam [121], and this leads to Observation 7.

Observation 6: The magnitude of the impact of the coupling between the platform-level impacts of the subsystem architecture on the platform and aircraft sizing may vary with aircraft passenger class.

Observation 7: Aircraft subsystem weights are historically a function of the TOGW.

It should be noted that Observation 7 is based on historical trends which are based on previous aircraft which utilized traditional subsystem architectures. The exact trend may not be the same for non-traditional architectures. However, the performance requirements on the subsystems (such as hinge moments) are a function of aircraft size, so Observation 7 is probably still correct for these non-traditional architectures.

2.2 Traditional Development of Subsystems

Development of aircraft subsystems is typically during the later phases of design. This can be see in Moir [93], who discusses the consideration of subsystems within different aircraft design phases. Specifically, Moir [93] separated the aircraft product life cycle into concept, definition, design, build, test, operate, and refurbish or retire phases. In Moir's [93] description of the aircraft design process, subsystems are primarily dealt with in the definition and design phases. In the definition phase, the architectures of the subsystems are determined, the interface documentation and installation characteristics are defined, the system performance is determined and designers use an intermediate level of modeling and experimental models [93]. The architectures of the subsystems are often determined based on the traditional architecture. During the design phase, subsystems are designed in detail and suppliers are selected [93]. This detailed design defines more detailed models of the systems. Moir [93] noted that the iteration between suppliers and aircraft manufactures can extend into later phases of this process. It also should be observed that two levels of models of the subsystems are used depending on the level of development However, conceptual models of different architectures, are not typically used during the design process. Conceptual models can be defined as simplified models treating systems and components with simplified relationships. The use of such models could enable trades between architectures. Conceptual modeling would utilize a simplified representation

of systems using physical relationships and available data to determine the impact of different architectures on the platform. If the needed data to generate the models is not available, then it still is possible to utilize relationships or data from similar aircraft or components, and then update the models when the data becomes available. This proposed simplified modeling enables the study of conceptual architecting as presented in the section on conceptual architecting.

Subsystem architecting can be viewed as a process as well. First, the architecture is determined mostly using block diagrams and interface documentation [93] and [140]. The architecture is typically based off of the traditional subsystem architecture which is illustrated in an SAE document [4] listing details of the hydraulic systems of many commercial aircraft. Then, suppliers are selected and the subsystems are designed in detail [93]. These detail designs deal with details such as the size of the hydraulic lines. When subsystems are designed, there are many regulations and guidelines that must be followed [93]. Moir [93] gives an overview of some of the standards that must be followed during this process. One of the considerations during subsystem design is safety and reliability [93]. Moir [93] also gives an overview of different safety and reliability assessment processes and methods. These include Functional Hazard Analysis, Preliminary System Safety Analysis, System Safety Analysis, Common Cause Analysis, and Fault Tree Analysis [93]. As discussed previously, subsystems include systems such as the environmental control system and the hydraulic system (used for purposes such as flight control). These subsystems would be developed as described above. There are descriptions of these systems, the typical types of components they may contain, and the principles they operate on available in literature, such as Moir [93], Keller [73], Neese [101], and Thompson and Campbell [131]. There are also descriptions available concerning the detailed design of these subsystems such as found in Moir [93], Keller [73], and Thompson and Campbell [131]. This design can include details such as the determination of the size of the lines within the hydraulic system,

the pressure within the lines, the design of the hydraulic components such as actuators and valves, heat loads and dissipation, and many other details of these systems [93], [131], and [73]. This level of detail required for the subsystem design may be part of the reason for the traditional limited consideration of subsystems within conceptual design.

In newer aircraft, suppliers can have much more control of subsystem design but are still given requirements and limitations. This leads to platform integration issues; it is still considered as a point selection of the architecture and is not part of conceptual design [36]. For example, when designing the B-787, Boeing selected some technologies and suppliers before the design of the subsystems [36]. Also, advances in computer modeling allow the use of detailed dynamic modeling with testing data in the place of some of the interface documents [140]. This concept is being examined as part of the INVENT program [140]. However, the selection of the architecture itself is still similar to a point solution often based off of the traditionally used architecture.

2.3 Requirement Analysis for Subsystems

As mentioned above, in the development of subsystems, there are many regulations and guidelines that must be followed [93]. Moir [93] gives an overview of some of the standards that must be followed during this process. The subsystems must be designed to meet the applicable requirements, which may have come from several different stakeholders from different levels as described by the International Council on Systems Engineering (INCOSE) [66] as shown in Figure 7.

It should be noted that not all subsystem requirements are available or determined by the conceptual phase of design. Available requirements will include all aircraft certification regulations such as FAA AC 25.1309-1A [5] and JAA AMJ 25.1309 [2]. The subsystems are also impacted by other regulations and system specific requirements: for example, "the ventilation system must be designed to provide each occupant with

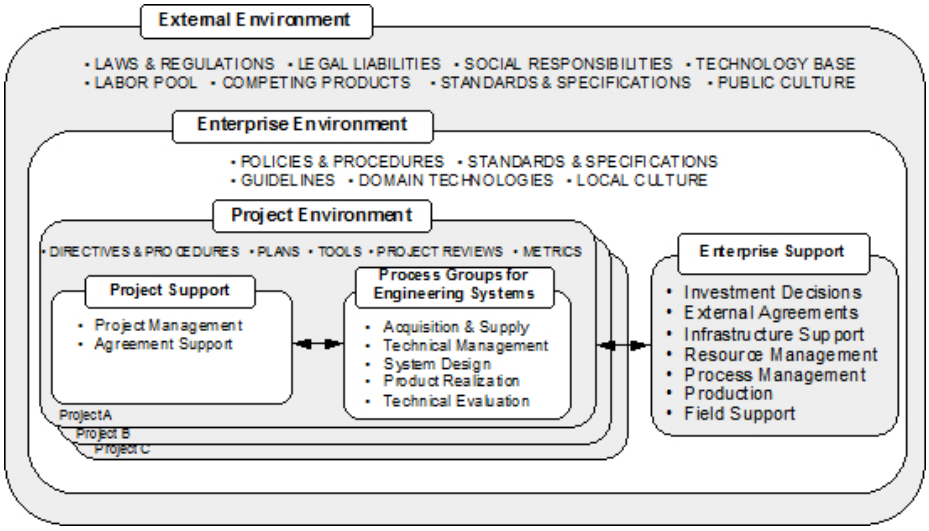

Figure 7: Subsystem Requirement Sources [66]

an airflow containing at least 0.55 pounds of fresh air per minute." -FAR 25.831 [10]. The available requirements impact system sizing and create constraints on the architecture design space. Platform-driven requirements are derived from higher level platform requirements. These are derived from the design mission and required functions using a requirements flow-down after a functional breakdown. Many of these derived subsystem requirements may not yet be determined by conceptual design. These platform-driven requirements may include required functions performed by the systems, selection of the architecture, and needed performance from the subsystems [93]. In order to study subsystem architectures at such an early phase of design, it will be necessary to use the available platform-level requirements and mission to determine the applicable subsystem level requirements.

Current systems engineering processes, such as the one shown in Figure 8 (from DAU [37]) and the NASA systems engineering process described in the NASA Systems Engineering Handbook [97], are utilized to determine the subsystem level requirements from the identified requirements from the stakeholders. These processes determine platform-level requirements from the required mission and other defined requirements and standards. These platform-level requirements are then used in a

functional decomposition and analysis to determine lower level requirements. These lower level requirements could then be used for the subsystem design [37] and [97]. Moir [93] discusses requirements capturing for subsystems design and presents two approaches: top-down and bottom-up.

2.4 Conceptual Architecting of Subsystems

As discussed previously, subsystem architecture selection is not typically considered during conceptual design. Therefore, the impacts of the architecture selection on the TOGW and fuel burn are neglected [115] and [60]. If these impacts are considered earlier it can improve the accuracy of the conceptual design. Part of the reason this dissertation proposes that the architecture trades be determined during conceptual design is that this design phase (and requirement definition) requires fewer funds but determines and commits a large percentage of the final life cycle cost of the aircraft (nearly 70 percent) [105]. The subsystem architecture is often selected as a point design based on the traditional architecture a practice which negates the potential benefits in weight and efficiency from exploring the architecture design space. Currently subsystems' impacts coupling with aircraft sizing is neglected. As a result of these issues, traditional methods of architecture selection cannot adequately capture the impact of subsystem architecture trades.

The current point-driven architecture selection philosophy contains several gaps, one of which is the lack of early study and identification of the architecture by exploration of the architecture design space, examined in this dissertation as conceptual architecting. Conceptual architecting alone is not a new concept. de Tenorio [36] and Armstrong [21] and [20] partially examined this important topic in their dissertations. Conceptual architecting is a similar concept to conceptual aircraft design, which uses simplified trends and analyses to determine the overall characteristics of the aircraft. Conceptual architecting uses models of the different possible subsystems

Figure 8: Defense Systems Engineering Process [37]

to determine the impacts of a given architecture on the platform earlier in the design process [21]. These impacts are then compared and the desired architecture is developed in the later design processes that are currently used. Without such a step, there is not a way to rapidly explore the subsystem architecture design space to identify the desired architecture. Conceptual architecting is not currently being utilized in industry. Richards et. al [119] discuss the need for conceptual architecting within survivability system design for aerospace systems. They point out that trades involving survivability could be performed to improve the overall design instead of treating survivability as only a constraint [119]. Examining trades of conceptual architectures and their impact on aircraft sizing is the primary focus of the later proposed methodology. This concept enables the use of desired architectures including energy optimized in the aircraft design and allows the inclusion of this information earlier in the design process because only simplified models are used, which can be created and utilized even during conceptual design. This approach would represent a significant step forward in the design space exploration of aircraft subsystem architectures.

2.4.1 Challenging Aspects of Architecture Design Space Exploration

The subsystem architecture design space is the set of all possible architecture designs. Exploring this space would make it possible to find the best subsystem architecture for a given problem. This exploration is done in the proposed methodology discussed later in this proposal. There are many aspects of subsystem architecture design space exploration that makes this exploration very difficult. First, this exploration is a combinatorial problem because there is a huge constrained design space of all possible subsystem architectures.

The size of such a design space can expand very quickly. For example, a design space for a new transport aircraft in the 150-passenger class (and selected subsystems) is shown in the screen shot from an Interactive Reconfigurable Matrix of Alternatives

(IRMA) shown in Figure 9. An IRMA uses a Matrix of Alternatives to examine such a design space and calculates the approximate computational time to examine all of the design alternatives. Such computational times become unwieldy for large matrices [43]. In an IRMA, the complex system being examined is decomposed into its important functions and features each placed in a row in the matrix and each alternative solution to that function placed in the columns for the corresponding row. Such a matrix allows a better understanding of the potential solutions to the problem. If the rows are independent, the number of possible designs is the number of entries of each row multiplied together [43] as shown in equation (1). Figure 9 shows an IRMA from a Long Range Strike mission (discussed in [43]) adapted for aircraft subsystems as can be seen in the systems section which is illustrated in Figure 10. This example helps illustrate the combinatorial nature of examining even a portion of the architecture design space.

$$N = \prod D_i \tag{1}$$

Because of the combinatorial nature of this problem, previous methods traditionally examined only a point solution for the architecture. To address this weakness, the proposed methodology herein must appropriately define and examine the architecture design space. Also, subsystems have dynamic impacts on the platform, a condition which violates any static impact assumptions. These dynamic impacts of subsystems include time varying power and heat loads. Another important aspect of this problem is that the impact of the subsystem architecture can be coupled with the sizing of the aircraft. That is, the dynamic impact of architectures can vary as the aircraft size varies. As discussed later in this dissertation, uncertainty is a very challenging aspect of this problem.

Figure 9: Example of IRMA for Aircraft Subsystems adapted from [43]

Systems	ECS Technology
	Fuel Tank Location
	Number of Generators
	Engine Driven Pumps
	AC Motor Pumps
	Flight Control Tech
	Braking Technology
	WAI
	# of Hydraulic Systems

Figure 10: Excerpt of IRMA for Aircraft Systems adapted from [43]

2.4.2 Gaps in Existing Methods for Conceptual Architecting

There are existing methodologies that can assist with Conceptual Architecting. However, there are several gaps in these existing methodologies. This section examines selected particularly relevant existing concepts and their gaps.

2.4.2.1 Numerical Subsystem Optimization

One existing method for assisting with an implementation of Conceptual Architecting is the numerical optimization of subsystems as examined by de Tenorio for his dissertation [36], a concept which provides part of the foundation for this concept of examining different subsystem architectures. This part of de Tenorio's work focuses on optimizing the sizing of aircraft subsystems using models of subsystems with different architectures selected for study [36]. These models were optimized using a multi-level Coordinated Optimization technique [36]. The concept of subsystem sizing in an optimum fashion is a useful contribution. Some additional concepts explored by de Tenorio include the use of SysML modeling of architectures, to examine alternative subsystem architectures discussed in the section on the generation of feasible alternatives [36]. However, there were some limitations in the presented methodology. de Tenorio's work assumed fixed aircraft size and captured the impact of subsystems changing size as a change in the aircraft range [36]. However, this did not fully capture the coupling of subsystem impacts and aircraft sizing. As a result, de Tenorio's [36] work did not fully examine subsystem architecture trades, including

their coupling with aircraft sizing, which is a gap that this dissertation fills. In addition, the models used did not not capture the full dynamics of the impacts of the subsystems [36]. de Tenorio's work had no consideration of uncertainty, neglecting the impact of uncertainty which could change the solutions selected by the designer [36]. Despite these gaps, this work provided a very useful foundation for the work within this dissertation and presented many useful new concepts.

2.4.2.2 Subsystem Reliability and Architecture Generation

Armstrong's dissertation work made several additional useful contributions relating to subsystem sizing requirements, his work examined subsystem reliability and load shedding [21]. Armstrong explored the important subject of reliability with the consideration of a degree of failure for components rather than merely labeling as failed or not failed [21]. Armstrong examined optimal load shedding as well [21], and his work provided important contributions to load shedding, reliability theory, and failure considerations. These concepts could be used in helping to evaluate the reliability impacts of subsystem architectures within extensions of this work. The examined sizing requirements include architecture specific off-nominal sizing requirements [21]. The concept of considering a component as being partially failed and the implications are very important contributions to reliability theory. Finally, Armstrong in his Master's thesis created a method and a tool called ADEN for generating subsystem architectures to examine the use of functional analysis [20]. Such a concept is very useful for the generation of feasible alternatives of subsystem architectures. This concept from Armstrong's work is examined further in the section on generating feasible alternatives of architectures to consider [20]. Although Armstrong's many contributions were useful his research did not examine subsystem architecture trades during aircraft conceptual design while capturing the coupling of these trades with aircraft sizing [20] and [21]. The filling of such a gap is the focus of this dissertation.

2.4.2.3 TIES and TIES based methods

Another methodology that can assist in studying subsystem architectures is the Technology Identification, Evaluation, and Selection (TIES) methodology, which was created for the design of complex systems due a the paradigm shift in design methods and was presented in Kirby's PhD dissertation [75]. This methodology enables the infusion and assessment of technologies within a complex system design [75]. TIES studies technologies (which form part of the subsystem architecture) and in a more general fashion, can be used to examine subsystem architectures. TIES provides several useful concepts for the development of the proposed methodology but does have several gaps which the proposed methodology fills. These gaps are discussed later in this section.

An overview of the steps of TIES can be seen in Figure 11 [75]. The techniques used in TIES are selected for their robustness and generality. Further detail of this process can be found in Kirby's dissertation [75].

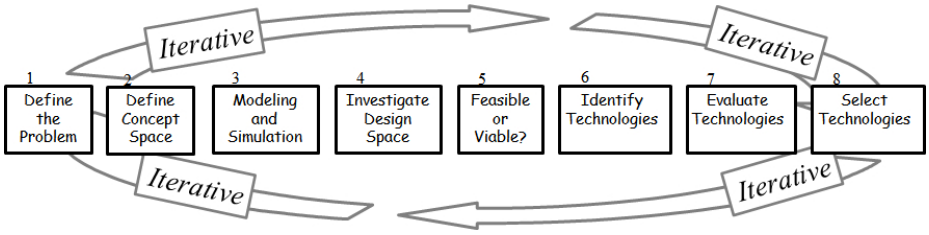

Figure 11: TIES Process Overview Adapted From [75]

Kirby [75] noted that TIES, as presented, assumes that the k-factor (scaling factor) values are independent of the selection of different points in the design space and from one another. As this implies, TIES assumes that the k-factor distributions are independent of the aircraft sizing and from one another. Therefore, TIES does not effectively capture technologies whose effect is changed depending on the results of aircraft sizing and analysis. Subsystem technologies and architectures, such as the use of electrical actuators, have a difference in impact depending on variables such as

the aerodynamic loads and mission profile, which relate to the aircraft sizing.

TIES compares the minimum set of technologies to achieve requirements. However, in the case of subsystem architecture selection, the different potential subsystem technologies may all achieve the stated requirements. TIES captures uncertainties in technology impact through the application of distributions on technology impact factors. The distribution parameters are treated as constants for a given technology, and any dependence on architecture is neglected. TIES does not capture effects of varying subsystem architecture as the k-factor distributions are treated as the same for different architectures containing the same technologies. However, TIES presents several useful concepts exploited in the proposed methodology, such as the use of distributions placed on parameters in the modeling and simulation environment to capture uncertainty.

There are also new methods derived from TIES. One such method is a new approach for technology selection, called the Bi-level method, which enables the designer to gain additional insights and provides additional speed to technology selection [134]. The Bi-level method enables the designer to find moderate and quick design solutions that are helpful when the number of possible technology combinations is very high. This method uses gradient based optimization algorithms partially due to their speed. True to the Bi-level method's name, this method uses a bi-level (two level) optimization process. In the first of these two levels, the vector of technology impact factors (also known as k-factors) is optimized to make the responses as close as possible to the desired values while keeping the design within the constraints. Once this optimum k-factor vector is determined, a second level of optimization is performed to find the combination of technologies that create the k-factor vector closest to the desired k-factor vector [134]. As this and other TIES derived methods have similar assumptions to TIES, they have many of the same limitations as discussed above. These include the inability to capture dependence between the k-factors themselves

and between the k-factors and aircraft sizing. Additionally, TIES derived methods do not capture the impacts of varying the architecture on the k-factor distributions. Finally, these methods try to fulfill the requirements and are not as applicable if all the alternatives meet the given requirements as can happen when comparing aircraft internal subsystem architectures.

CHAPTER III

CAPTURING THE IMPACT OF UNCERTAINTY

3.1 Impact and Classification of Uncertainty

Uncertainty impacts all attempts to examine the natural and physical environment surrounding society [118]. Uncertainty is very important to identify and analyze when examining complex systems [55]. If uncertainty is not properly treated, poor managerial decisions can result [117]. In fact, the consideration of uncertainty can result in different decisions [117]. Uncertainty is important in many different fields including subsystem architecture trades. This is illustrated by the weight gain the Boeing 787 program experienced when integrating a new subsystem architecture [6]. The following quote from the Boeing 787 Chief Engineer (Michael K. Sinnett) describes this phenomenon.

> "When we decided on electric pressurization, it lowered the aircraft weight by 1000-2000 lb [...] but the numbers got muddied as the 787 got integrated. It is hard to say where the weight has gone." [6]

Uncertainty also appears in the use of computer codes (which can be utilized in the analysis of subsystem conceptual architecting) [42]. In fact, Elishakoff, Kulisch, Elishakoff, Di Paola, Chernousko, Bernardini, Baratta, and Zuccaro [42] wrote a book that is specifically about uncertainty analysis for computer codes. Within engineering, there has been a recognition of the fact that uncertainty is important and needs to be considered [42].

As discussed later in this section, uncertainty due to a lack of knowledge exists within conceptual subsystem architecture trades and can have a great impact on the aircraft. Uncertainties, especially uncertainty due to a lack of knowledge, also have

a huge impact on many of the current risk management problems [114]. Furthermore, these uncertainties play an even larger role when there is less knowledge or evidence available [114]. Engineering risk analyses often use probabilistic methods to attempt to capture uncertainties [114]. Risk assessments have shifted from using point estimates to creating distributions to reflect variability and uncertainty [132]. Probabilistic Risk Analysis (PRA) techniques have risen in use to try to account quantitatively for uncertainty in risk assessments [132]. PRAs are being used for analyses involving spacecraft, waste storage, chemical plants, and nuclear power plants [113], and similar methods may be applied to conceptual architecting as discussed later in this dissertation.

It is necessary to identify the classification of the types of uncertainties that exist within conceptual architecting trades in order to determine how they can be examined within the trades. There have been different attempts to create methodologies for classifying uncertainty [118]. Many people have divided uncertainty into categories called epistemic and aleatory uncertainties [114] and [56]. According to Pate-Cornell [114], aleatory uncertainty is randomness in samples, and epistemic uncertainty is uncertainty due to a lack of knowledge concerning fundamental phenomena. Hlavacek, Chleboun, and Babuska [56] cite similar definitions: aleatory as inherent variation in a system, and epistemic as lack of knowledge during the modeling of a system. After pointing out that other frameworks for categorizing uncertainty exist, Parry [113] discusses similar definitions for aleatory and epistemic uncertainties , and states that the distinction between those two types of uncertainty was important. It should be noted that the epistemic uncertainty as discussed in Parry [113] is associated with a model, which seems specific to Probabilistic Risk Analysis (PRA) as discussed in [113]. Helton and Burmaster [55] make similar statements defining aleatory and epistemic uncertainties and stating the importance of such an distinction. One author calls this uncertainty due to a lack of knowledge *uncertainty* while calling variation within

a population *variability* [132]. This is a similar categorization equating epistemic uncertainty with the word *uncertainty* and calling aleatory uncertainty *variability*. Hofer [57] states that all uncertainty is epistemic because if perfect knowledge was obtained, there would be no aleatory uncertainty. In a Statistics book, Navidi [100] referred to uncertainty as the standard deviation of the measuring process of a random variable. This concept is similar to aleatory uncertainty and does not include the uncertainty due to a lack of knowledge.

It should be noted that other frameworks for classifying uncertainty exist but are not as applicable to conceptual architecting. One such framework for classifying uncertainty comes from researchers within the subject area of ecology in which Regan, Colyvan, and Burgman [118] divide uncertainty into two types: epistemic and linguistic uncertainty. In this framework, epistemic uncertainty is uncertainty due to a lack of knowledge about a system's state while linguistic uncertainty is uncertainty due to issues such as ambiguous vocabulary [118]. This framework further divided epistemic uncertainty into six categories: subjective judgment, model uncertainty, natural variation, inherent randomness, systematic error, and measurement error [118]. For the remainder of this paper, the framework of dividing uncertainty into epistemic and aleatory (or leaving them combined as the overall uncertainty) will generally be used as these are the primary types of uncertainty observed within conceptual architecture trades.

Uncertainty in subsystem architecture trades exists on the platform-level impact of the subsystems due to a lack of knowledge (epistemic) and slight random variations between individual aircraft and components (aleatory). This lack of knowledge is due to the fact that the selected technologies and architectures may not have been used on this aircraft (or at all) previously. This is similar to the uncertainty distributions on k-factors due to uncertainty of the application of a new technology in TIES [75]. As a result, the exact weights and efficiencies of the different components and their

distribution systems are not deterministic numbers; rather, they have a distribution that describes the different possible values of these parameters and their probabilities. These distributions are not necessarily known, as it is a lack of knowledge that causes them not to be a set of deterministic values.

There is also uncertainty in the impact on the system performance of integrating the subsystems together, as was demonstrated by the B-787 weight gain during integration [6]. This uncertainty further impacts the exact weight and efficiency and other characteristics of the integrated components. There is also uncertainty in the weight and efficiency due to variations between different manufactured copies of the same components or aircraft. It is important to account for these uncertainties to find a robust design of the aircraft and its subsystems.

Observation 8: Subsystem architecture impacts have epistemic and aleatory uncertainty in various characteristics of the integrated components such as weight and efficiency.

3.2 Quantifying and Accounting for Uncertainty

As discussed in the last subsection, uncertainty plays an important role in many diverse areas of study including conceptual architecture trades. Possibly as a result of its widespread applicability and importance, many different ways of examining uncertainty exist. This section highlights and examines selected methods for quantifying and accounting for uncertainty to determine appropriate methods for use within conceptual architecture trades. The selection of the appropriate method is discussed further in the section discussing the proposed methodology.

Both aleatory and epistemic uncertainties appear in aircraft subsystem architecture trades. The difference between aleatory and epistemic uncertainties is partially based on the definition of probability [114]. The determination of a probability tries to create a quantitative view of the uncertainty associated with a given event [71].

Probability has two significantly different interpretations: the Bayesian and frequentist views of probability [114]. The frequentists define probability as the limiting frequency of independent observations of a phenomenon [114]. The Bayesians view probability as a degree of belief [114]. This degree of belief can be based on expert opinions and supporting data [114]. Although the frequentist probabilities are objectively using sample data, they have limitations in their applicability for capturing uncertainties [114]. Specifically, frequentist probabilities can handle only aleatory uncertainties and only when there are sufficient samples [114]. The variability of distributions of random variables can be captured in the variance and standard deviation of the sample [138]. This variability is also known as the random (aleatory) uncertainty [100].

A statistical treatment of aleatory uncertainty, such as using a sample variance [138], requires repeated measurements [100] which may not always be possible depending on the specific problem being studied (such as in the use or application of subsystem architectures which have never been utilized). However, Bayesian probability and statistics can use all available information to assess probabilities and can handle aleatory and epistemic uncertainties [114]. In Bayesian probability and statistics, these uncertainties can be combined into single probability values or distributions [114]. Despite the fact that categorizing uncertainty can be important, it may not always be best to separate the uncertainty into different categories within an analysis including in the analysis of subsystem architectures [57]. This is at least partially due to the fact that the separation of the uncertainties into different computations is costly [57]. Hofer [57] describes the situations for which he believes it is appropriate and not appropriate to separate the sources of uncertainty. The use of Bayesian distributions combine different forms of uncertainty into one distribution per variable, which captures epistemic and aleatory uncertainty [114]. As there is considerable epistemic uncertainty in subsystem architecture trades due to a lack of knowledge

concerning requirements and the weight and efficiency of the integrated components, Bayesian distributions can be applied on parameters impacted by uncertainty within these trades. This concept leads to Observation 9.

Observation 9: Probability distributions can be created and applied on parameters within the modeling and simulation environment to capture uncertainty in those parameters.

Once the uncertainty is captured by Bayesian (and/or frequentist) probability distributions of random variables, the impact of the uncertainty on the variables must be examined. To determine the impact of the uncertainty on the (potentially higher or system-level) output variables of interest from the analysis, additional analyses must be performed. Sensitivity analysis is one method for examining the impact of uncertainty [132]. Traditionally, sensitivity analysis varies one input to an analysis at a time and examines the change in the outputs as the input variable is run through its entire possible range [132]. Two-way sensitivity analysis is another common way to examine the impact of uncertainty, and is a similar type of analysis [132]. In two-way sensitivity analysis, two different inputs are varied simultaneously and the resulting outputs from the models are plotted [132].

As the number of variables from which to examine the impact of uncertainty increases, the uncertainty impact analysis usually becomes a probabilistic uncertainty analysis, often using Monte Carlo simulations [132]. For example, in PRA the most widely used technique for the propagation of uncertainty is the use of Monte Carlo [113]. The below quote points out in [55] from [98] that the National Research Council [98] views the analysis of uncertainty as an important task that should be done whenever possible. The National Research Council [98] and [55] also pointed out the possible use of sensitivity analysis or Monte Carlo analysis to quantify the uncertainties and also suggested that the risk estimates should be in distributions instead of point estimates.

> "Where possible, sensitivity analysis, Monte Carlo parameter uncertainty analysis, or another approach to quantifying uncertainty should be used. Reducible uncertainties (related to ignorance and sample size) and irreducible (stochastic) uncertainties should be clearly distinguished. Quantitative risk estimates, if presented, should be expressed in terms of distributions rather than as point estimates (especially worst-case scenarios)." [98] and [55]

Monte Carlo simulations provide a means to examine the impact of the distributions of subsystem level uncertainty on the platform level. Monte Carlo methods are numerical methods that use sequences of random numbers to run a simulation [38]. Often in Monte Carlo methods, the physical system under study is modeled and simulated directly [38]. Monte Carlo methods require that the modeled system be described by probability density functions (PDFs), which must be determined before the simulation can proceed [38]. The Monte Carlo simulation randomly samples the PDFs and runs many simulations [38]. The results are then analyzed to determine the mean and variance of the desired results [38]. Monte Carlo algorithms contain most or all of the following components: PDFs, random number generators, sampling rules, scoring, error estimation, variance reduction techniques, and parallelization and vectorization [38]. Several different Monte Carlo methods exist. Some of these methods include importance sampling, rejection sampling, the Metropolis method, and Gibbs sampling [81]. In [81], D.J.C. Mackay gives a good discussion of each of these methods while Hlavacek, Chleboun, and Babuska's [56] book contains among other topics a summary of the application of Monte Carlo simulations.

Monte Carlo methods are also widely and routinely used [38] and [56]. For example, Joy [72] gives an introduction to applying Monte Carlo simulations to studying the interaction of an electron beam with a solid. In fact, Joy [72] concluded that Monte Carlo simulations were well suited, powerful tools for the modern microscopist.

Binder and Heermann [28] discuss the application of Monte Carlo methods to physics and include a chapter that acts as a guide to practical work with Monte Carlo methods and also contains some theoretical foundations of Monte Carlo methods. Monte Carlo simulations have also been used in Civil Engineering for tasks such as estimating the failure probability of a given structure [24]. In such an analysis, the need for possible variance reduction techniques is demonstrated by the fact that the estimated probability of failure approaches the true value as the number of simulation runs approaches infinity, which could become a computational issue [24]. In this example, the variance reduction techniques are used to increase the accuracy while not increasing the required number of runs [24]. Monte Carlo simulations can also be used for Probabilistic Risk Analysis (PRA) [74]. In the case of the pioneering Probabilistic Risk Analysis study, Monte Carlo simulations were used even to determine the overall impact of uncertainty on the estimated risks [74]. This was done by using lognormal distributions for events and probability of failures within the analyses [74].

Monte Carlo simulations are one of the most commonly used methods within design and will likely work well for subsystem conceptual architecting. However, there are several other approaches to characterizing and quantifying uncertainty [129] and [42]. Probabilistic methods are sometimes difficult to apply to engineering [42]. Partially as a result of the fact, other techniques for dealing with uncertainty exist [42]. However, as discussed later in this dissertation, the application of these methods to subsystem architectures has possible disadvantages compared to the use of Monte Carlo simulations. For the reader's reference, some of these other methods include Classical Sets, Fuzzy and Rough Sets, Possibility Theory, Evidence Theory, Interval Probabilities and Analysis, and Info-Gap [129].

The approaches previous subsystem related trade studies used to capture their uncertainty were examined and are described below. This includes the POA program,

which applied distributions on the current (or flow/power) draw of the different components within the VIB modeling environment [25]. The Virtual Iron Bird (VIB) was an integrated modeling environment of aircraft system models used to examine the power demands of systems and their architectures [25]. In the POA program, once the distributions were applied to the component current/power demands, Monte Carlo simulations were run pulling values out of these distributions to capture the uncertainty's impact on the parameters of interest [25]. The Monte Carlo simulations were viewed as an enabler to allow the creation of the distributions on the metrics of interest [25]. Additionally, since the runs of the Monte Carlo simulations were independent of each other, the runs could be run on parallel computing clusters [25].

In the paper by Gurnani and Lewis [50], a process for including uncertainty in a decentralized subsystems design is discussed. In this process, each subsystem is designed in a decentralized environment, and design variable values for the subsystem were passed from one subsystem designer to the next [50]. The authors propose the creation of a set of values for each design variable by pulling values out of distribution placed around the design variable's selected value and passing this set to the next subsystem designer [50]. They further propose using this concept in a second stage where a nonlocal objective function is formed for optimizing the subsystems [50].

In the paper by Du and Chen [40], the authors present a Modified Concurrent Subsystem Method for Uncertainty Analysis (MCSSUA) for use in Multidisciplinary Design Optimization (MDO). MCSSUA is a more efficient and improved variant of the Concurrent Subsystem Uncertainty Analysis method (CSSUA) [40]. Du and Chen [40] discuss both of those methods and a third method called the System Uncertainty Analysis (SUA) method. The SUA method approximates the output variables and their variances by taking Taylor expansions of the output variables and linking variables and then uses a sensitivity analysis (using first order derivatives) [40]. CUSSA assists with the ability to use parallel computations when computing the variance

of outputs of a system [40]. CSSUA uses a system-level optimizer to force the targeted and calculated values of linking variables between subsystems to converge [40]. CUSSA assumes the linking variables are independent of one another and the inputs (a source of inaccuracy of this method) and the method calculates the mean and variance of the output variables by using the information obtained by the optimization [40]. MCSSUA is simply a modified version of CUSSA and has the following primary steps: determine the means of the linking variables, find the system output mean, and estimate the system output variance (using the same concept as SUA to estimate the variance) [40]. Du and Chen [40] note that all three methods are only approximation methods for the uncertainty, the approximations cannot generally capture the output distributions, and they are sometimes susceptible to errors due to approximations such as the use of Taylor expansions.

Since there is a considerable amount of uncertainty in this problem of comparing the impact of various subsystems and their architectures, it is desirable to find an architecture that is robust to the uncertainty. By robust it is meant that its platform-level impacts are not widely distributed due to uncertainty. According to Gurnani and Lewis [50], robust designs are "designs that are insensitive to changes in input parameters and errors in system analyses" [50].

3.3 Robust Design

Once the resulting distributions of the metrics of interest are determined, it is necessary to try to determine which architectures result in designs that are robust to these sources of uncertainty. This raises the topic of robust design. For such a discussion to be complete, it is first necessary to discuss what is meant by robustness. In this work, robust is used to mean that the desired result is insensitive to changes in the noise or uncertainty variables and that the result is consistently close to the desired value [88] and [138]. According to Fowlkes and Creveling [48], "A product or process

is said to be robust when it is insensitive to the effects of sources of variability, even though the sources themselves have not been eliminated." Also, according to Park [111], "Robust design is an engineering methodology for optimizing the product and process conditions which are minimally sensitive to the various causes of variation, and which produce high-quality products with low development and manufacturing costs." The purpose of robust parameter design is the determination of values of the design (control or controllable) variables that create responses that are insensitive to changes in the values of the noise (factors) variables [138] and [88]. Genichi Taguchi is one of the founders of the modern concept of design for robustness [88] and [138]. Taguchi's approach includes the use of orthogonal arrays of experimental designs for the control and noise variables [88]. Taguchi uses Signal to Noise Ratio (SNR) as a metric to summarize the mean and variance of the response. This summary statistic then allowed the designer to compare designs' robustness by this one variable. Taguchi used different mathematical definitions for SNR depending on the goals of the designer [88]. These SNR definitions are listed in equations (2), (3), (4), and (5) below. These can be quantified for parameters such as TOGW for subsystem architecture trades.

When the designer wishes to minimize the response [88], [111], [48], and [138]:

$$SNR = -10log\sum(((R_i)^2)/(T)) \tag{2}$$

When the designer wishes to maximize the response [88], [111], [48], and [138]:

$$SNR = -10log\sum((1/((Ri_i)^2))/(T)) \tag{3}$$

When the designer is trying to meet a target in the response, Taguchi had two definitions of SNR [88], [111], [48], and [138].

When the variance can be changed independently of the mean [88] and [48]:

$$SNR = -10log(\sigma^2) \tag{4}$$

When the variance cannot be changed independently of the mean [88], [111], [48], and [138]:

$$SNR = -10log((\mu^2)/\sigma^2) \tag{5}$$

There are several other approaches to capture the robustness of a design. One such approach to examine robustness of a design is to examine the mean and variance separately instead of combined into SNR [138]. One shortcoming of all of the approaches discussed so far is that they are not as applicable when there is more than one response as there might be when doing comparisons of subsystem architectures. However, there are some approaches for examining multiple responses that could happen in subsystem architecture trades. The driving metric examined in the case study was TOGW, allowing SNR to be sufficient. In Abraham [13], two such approaches are discussed. In the first of these approaches, SNRs are calculated for each response and then combined into a desirability function [13]. The other approach discussed in [13] extended the first approach by adding weights on the desirability of the responses in the desirability function [13]. One disadvantage of the approaches discussed in [13] is the fact that this distills all the comparisons among the designs to one metric whose values would change as these weights are varied. In Hui [63], a generalized multivariate distance from a multivariate target is used to examine robustness. This uses Hotelling's Tsquared shown in equation (6).

As shown in [63]:

$$Ti^2 = (x_i - x_t)(S^{-1})(x_i - x_t) \tag{6}$$

Another applicable robust design method is Robust Design Simulation (RDS) which is discussed in [87] and [85]. RDS applies probabilistics to design and examines the objective as a distribution caused by the effects of distributions on noise or uncertainty variables [87] and [85]. This enables the capturing of the impact of

uncertainty on parameters[87]. RDS examines the identification of a robust design [87] and [85] and is an alternative to Taguchi's approach for examining robustness of subsystem architectures by applying distributions to the noise variables which result in distributions of the design's responses.

3.4 Analysis of the Impact of Uncertainty

As discussed earlier in this chapter, uncertainties on subsystem architecture trades can have significant impacts. This was illustrated by an unexpected subsystem weight gain when integrating the subsystems on the B-787 [6]. The below quote from the Boeing 787 Chief Engineer (Michael K. Sinnett) discusses this phenomenon. (This quote is repeated from an above section to emphasize its significance.)

> "When we decided on electric pressurization, it lowered the aircraft weight by 1000-2000 lb [...] but the numbers got muddied as the 787 got integrated. It is hard to say where the weight has gone." [6]

To minimize such unexpected weight gains, the uncertainty needs to be accounted for and explored. The sources of uncertainty with the highest amount of platform-level impact should be identified for further study to help minimize such occurrences. This concept leads to Observation 10 which is listed below.

Observation 10: Uncertainties on subsystem traits with the highest platform-level impacts should be identified.

There are several different means and metrics that can be examined in determining which sources of uncertainty have the largest impact. Selected methods are examined and discussed below. Correlation values between the variables can be used to examine which of the variables have impacts on the TOGW. There are limitations to this approach as correlations measure how linear the relationship is and not necessarily the strength of this connection [138]. A related parameter, covariance, also examines only if there is a linear relationship [138]. It should be noted that other types of correlation

coefficients exist that could also serve to help in such an analysis, for example the Browing Distance Covariance [128]. These metrics could further assist in such an analysis but cannot be utilized for predictive analysis. Analysis of Variance (ANOVA) also provides an alternative method for identifying which parameters contribute to the variability of the response [88]. ANOVA is a widely utilized statistical concept and is discussed in [88], [100], and [138]. This and the previously discussed methods can be used to help identify which variables may have the largest impact on the response. Depending on the type of metric used, this identification may be imprecise, for example correlations look at how linear the response is, information which will not necessarily be the same as is desired [138]. Several existing tests and methods, including those previously discussed, can help identify which variables may be driving the response. However, the use of Bayesian Networks and strength between the links as discussed below can not only be used to identify this information potentially just as accurately but can also be used for further analysis as desired during the design process as is discussed below. The utilization of the Bayesian Networks for further predictive analysis [52], in addition to identifying which noise variables are driving the response is the reason that this method is selected for further examination.

A Bayesian Network "is a graphical model that efficiently encodes the joint probability distribution (physical or Bayesian) for a large set of variables" [52]. An example of a Bayesian Network (in this case created for detecting credit card fraud) can be seen in Figure 12. There are several important advantages to the use of Bayesian Networks. These include the ability to effectively deal with missing data, study causal relationships, predict future events using the causal relationships, and be an efficient mean for avoiding overfit of data (which is an important advantage as overfitting the data could reduce the accuracy of some of the above described approaches) [52]. The ability of Bayesian Networks to study causal relationships can be very useful to better understand these relationships. Once these relationships are captured using Bayesian

Networks, the network can be used to make predictions. The ability of Bayesian Networks to make such predictions can be used when no experiments are run [52]. If a Bayesian Network of the subsystem design impact could be made, this predictive analysis might be used to further study the impacts of determined values of noise parameters throughout the development of the subsystems, and create a predictive analysis of the impact on the desired response (TOGW). Such an analysis could be useful to the designers and developers of the subsystem to see potential platform-level impacts of different component properties that they are designing. This analysis would be performed during the design of the subsystem components to track and estimate the TOGW impact of the design. Such an analysis could be quite useful, but would be performed by the designers of the subsystems during aircraft development, as a result, the predictive application of a Bayesian Network is not the focus of this work. However, the capabilities of such an analysis are more of an important motivation as to the reason that the creation of such a model could be significantly superior to other forms of statistical analysis for examining which of the noise variables are driving the response because the model enables this predictive analysis.

The use of Bayesian Networks to examine link strength between noise variables and responses could be quite useful as it would enable the above described additional predictive analysis during development of the subsystems. Ebert-Uphoff [41] explores how to measure link strengths within Discrete Bayesian Networks, so in order to use this concept, the subsystem data must be discretized. Ebert-Uphoff [41] defines two measures of link strength, blind average link strength (a local strength based on the child node disregarding the frequency of occurrence for parents) and true average link strength (taking into account the entire network) [41]. For reference, the utilized formula for true link strength is written in equation (7) below [41]. The strength of the links (and how this strength is defined) between variables in discrete Bayesian Networks, representing the variables and their impact as is described in [41], can

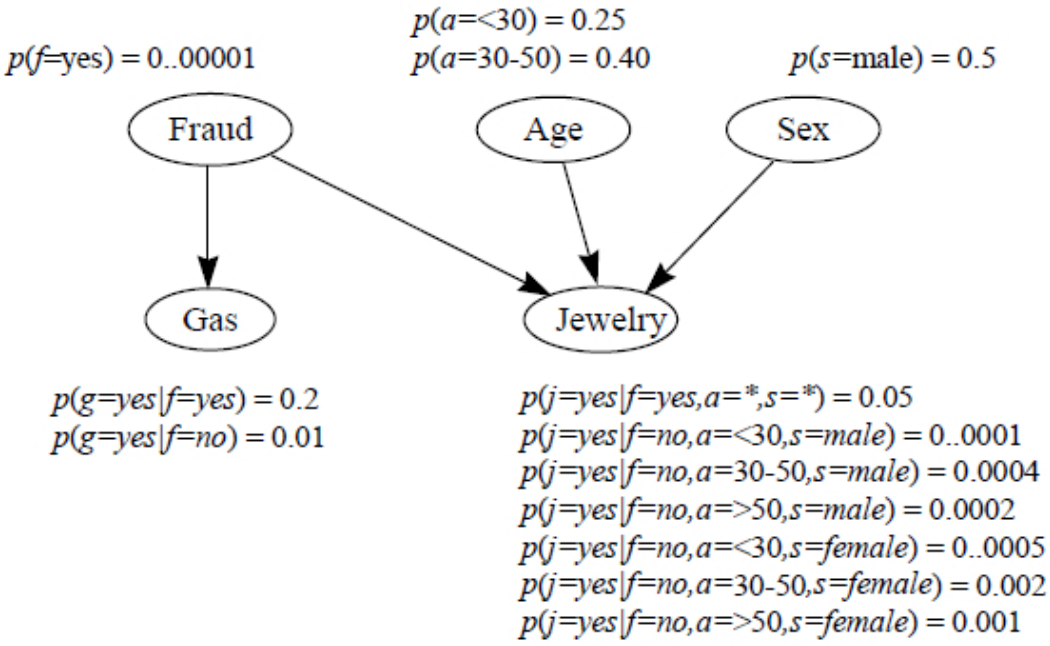

Figure 12: Example Bayesian Network [52]

also potentially capture the impact of different sources of uncertainty. It should be pointed out that such an analysis is not a common use of Bayesian Networks, as it is not utilizing the predictive analysis capabilities of Bayesian Networks. The determination of the impact of the noise variables could be done by calculating the link strengths between nodes in a network such as the one in Figure 13. Such a network could be used for examining the link strengths and potentially for some of the previously discussed predictive analysis. If there is available data and computational resources, the network structure shown in Figure 14 could also be examined, which is another unique advantage over traditional statistical analysis as more insight could be gained on intermediate variables. Due to a possible equivalence in accuracy of using Bayesian Networks for studying the relationship between the noise variables and the response and the additional analysis enabled by Bayesian Networks during the development of subsystems, the use of Bayesian Networks to examine the strength

of the link between noise variables and the response is selected and further explored and utilized in the section on the proposed methodology to examine the subsystem architecture design space. This equivalence is examined in the experiments by cross-referencing the results with an ANOVA analysis and correlation values. In order to examine this design space, it is necessary to determine feasible alternatives within the design space to be examined as discussed in the next chapter.

As discussed in [41]:

$$LStrue(XY) = \sum \mathrm{P(x,z)} \times \sum \mathrm{P(y|x,z)} \times \mathrm{log2(P(y|x,z)/P(y|z))} \tag{7}$$

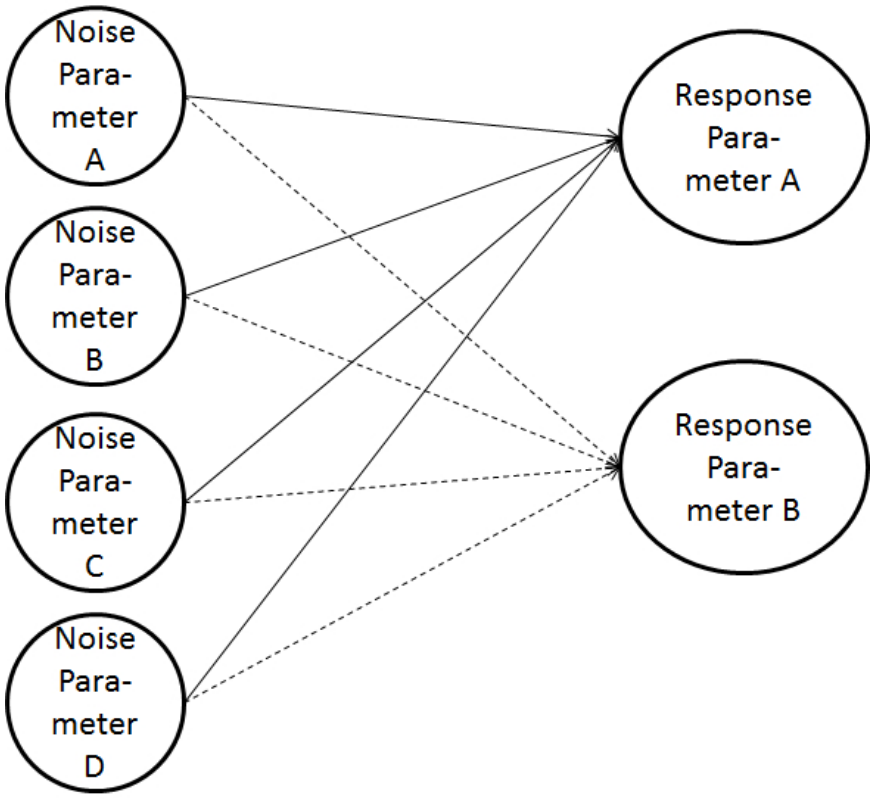

Figure 13: Examined Bayesian Network Structure

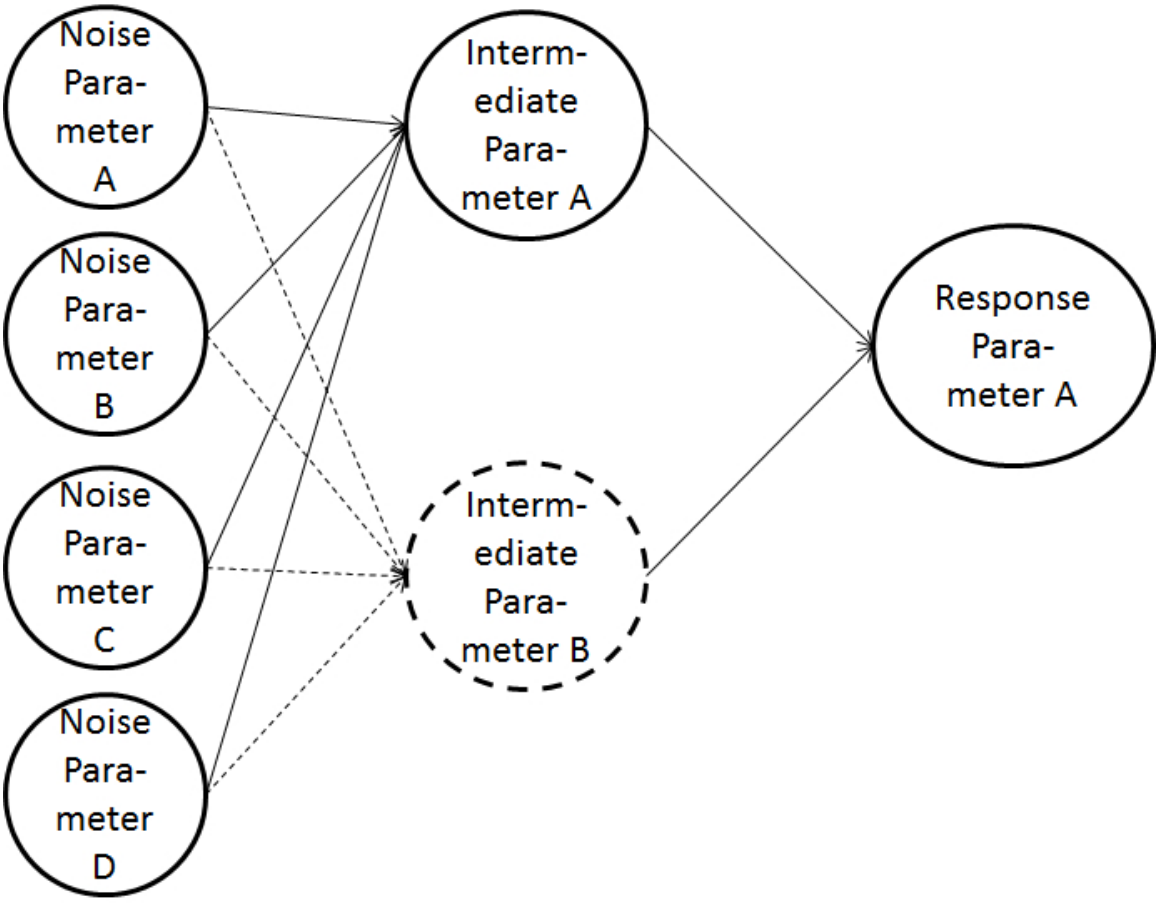

Figure 14: Examined Bayesian Network Structure

CHAPTER IV

METHODOLOGY FOR AIRCRAFT SUBSYSTEM ARCHITECTURE SELECTION

When starting the formulation of the proposed methodology, the generic decision-making process shown in Figure 15 (which was adapted from [125]) was applied to the concept of robust subsystem conceptual architecting. This dissertation applies these steps of a generic decision-making process to the topic of Robust Aircraft Subsystem Conceptual Architecting. The application of the first few steps of this generic process to the problem of aircraft subsystem architecture trades has been addressed in previous studies such as Armstrong's Masters Thesis [20], which addresses among other topics, the generation of alternatives. However, the previous studies did not capture the coupling of these trades with aircraft and engine core sizing. The primary gap in the current state of the art was in the last two steps of this decision making process (evaluating alternatives and making a selection). To address this gap, the proposed methodology was created to address the gap in these two steps and enable robust conceptual subsystem architecting. This methodology is called Methodology for AIrcraft subsystem Architecture selection or MAIA. MAIA enables conceptual architecting of subsystems during aircraft conceptual design, more efficient aircraft, the capturing of platform-level impacts of various subsystem architectures, and capturing the impact of uncertainty. (The methodology is named after Maia, the Greek and Roman goddess [8], [49], and [35].)

The Overarching Research Question comes from the overall desire to create a methodology that improves the current State of the Art (SOA).

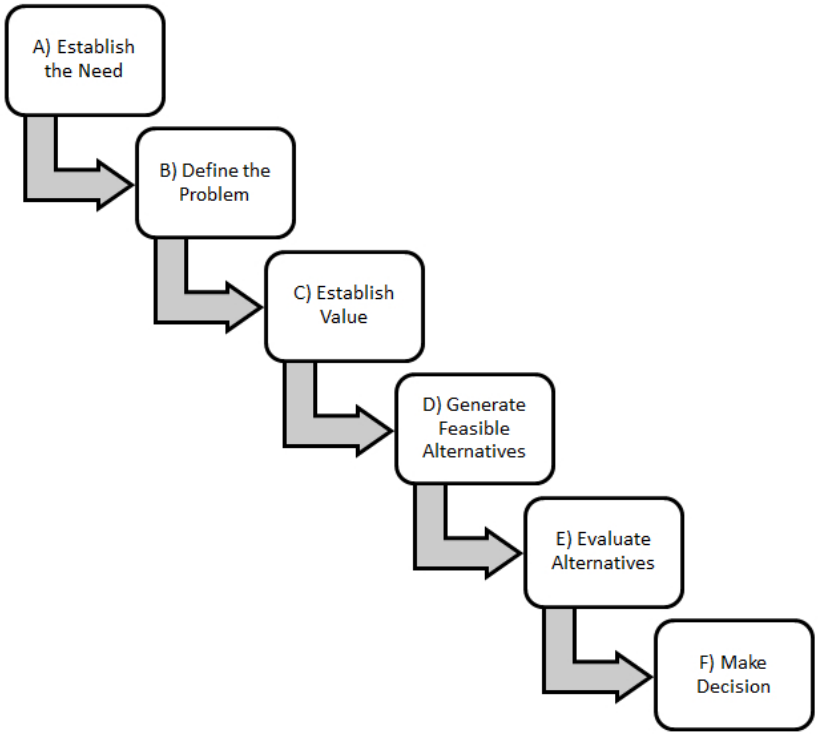

Figure 15: Generic Decision Making Process adapted from [125]

Overarching Research Question: How does the proposed Methodology compare to the current SOA?

In an attempt to answer this question, Observations 1, 2, and 3 (previously stated) are now reviewed.

Observation 1: Subsystem architectures are typically a traditionally selected point-driven design.

This would limit the design space that is examined, potentially neglecting superior designs.

Observation 2: Variations in the subsystems architecture can lead to significant platform-level impacts.

These impacts may be significant and may be improved by exploring the architecture design space.

Observation 3: Subsystem architecture platform-level impacts are coupled with the sizing of the aircraft.

This coupling is not captured in the current SOA. Capturing this may enable truly energy optimized aircraft

These observations lead to the Overarching Hypothesis, which hypothesizes that capturing this coupling and exploring the design space enables a significant improvement in architecture selection.

Overarching Hypothesis: Capturing of the coupling between aircraft sizing and subsystem architecture impacts and exploring the architecture design space enables a significantly better architecture selection than a point-driven design.

An overview of MAIA can be seen in Figure 16. This methodology is derived and discussed in the remainder of this section.

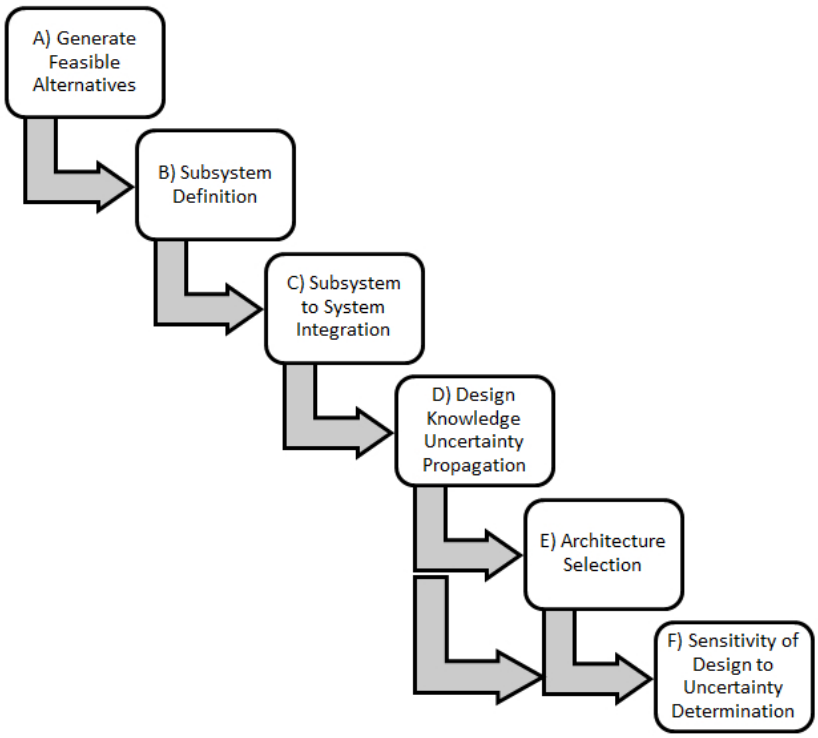

Figure 16: MAIA

MAIA should be implemented during the conceptual design phase of the aircraft. This selection is made is partially because of the large impact of this design phase on aircraft cost and the ease of changing the design during the conceptual design phase as shown in Figure 17 [44]. The use of MAIA enables more accurate aircraft sizing

due to replacement of the historical data used for subsystem weight (as discussed in the chapter on Subsystem Design Methods and Processes) by the use of more accurate data, even capturing the impact of subsystems on aircraft engine core sizing. Specifically, MAIA would be implemented late in the conceptual phase, after the selection of an aircraft configuration, determination of T/W and W/S, and an initial aircraft sizing which assumes the use of the traditional architecture to determine a baseline size. This timing is because the aircraft sizing and modeling within MAIA utilizes this information. The aircraft sizing could be updated and made more accurate with utilizing MAIA. This increase in accuracy is useful due to the ease of changing the design earlier in the design process and the large impact of the early design phases on the total cost as seen in Figure 17 [44]. Such analysis would take additional effort and time earlier in the design process, but as demonstrated in the experiments, the impact of this analysis on the magnitude of TOGW and the robustness of the determined TOGW value to uncertainty is significant. This is done in the conceptual phase partially due to the increased cost of design changes later in the design processes as seen in Figure 18 [107]. The shift of design knowledge (and therefore effort such as MAIA) and freedom earlier in the design process is part of a desired paradigm shift in design discussed in [84]. Such a paradigm shift allows for more design definition and freedom at lower cost commitment within the earlier design phases. MAIA could help enable such a design process.

MAIA also enables selection of the desired architecture that would lead to the smallest and most robust aircraft size. This enables an analytical selection of a subsystem architecture earlier in the design process. Because MAIA captures the impact of architecture trades on aircraft sizing, it enables selection of architectures that minimize aircraft size. As demonstrated in the experiments, MAIA also enables selection of an architecture that allows for a design that is robust to sources of uncertainty, which, as will be discussed later in this dissertation, can help minimize weight growth

during development.

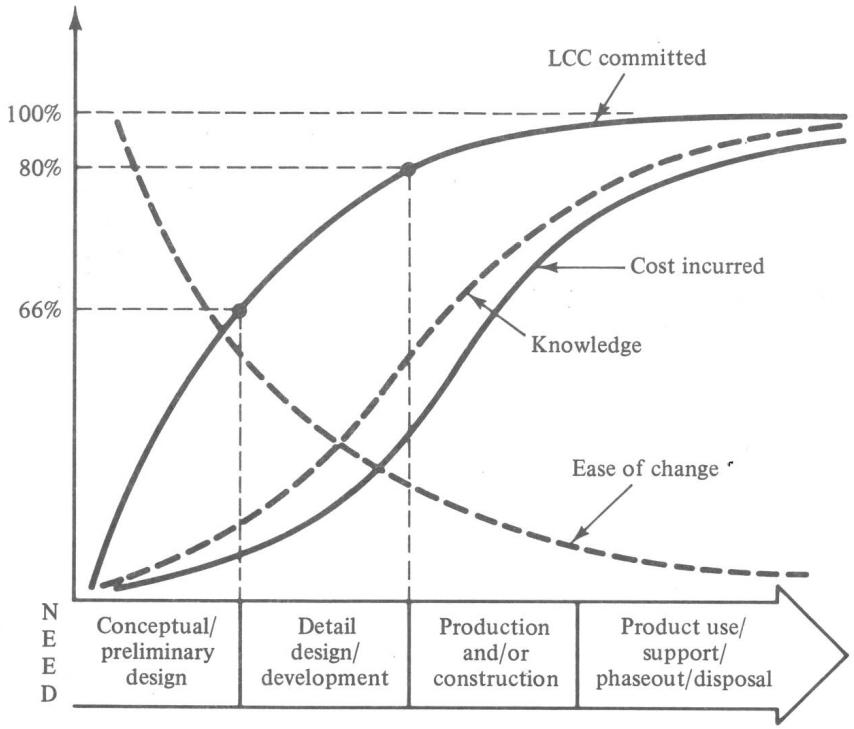

Figure 17: Life Cycle Cost by Design Phase [44]

4.1 Generate Feasible Alternatives

The first step in MAIA is to generate feasible alternatives (Step A). The subsection below examines the current state of the art in different methods that could be utilized for this step for subsystem architecting. Later in this section, a method is selected and applied to MAIA.

4.1.1 Current State Of the Art

There are many existing methods for determining the feasible alternatives. This section examines and discusses some of these methods that are are applicable for subsystem architecting.

The aerospace industry has traditionally treated the selection of subsystem architectures as a traditional point design [120] and [46]. To remind the reader, in this

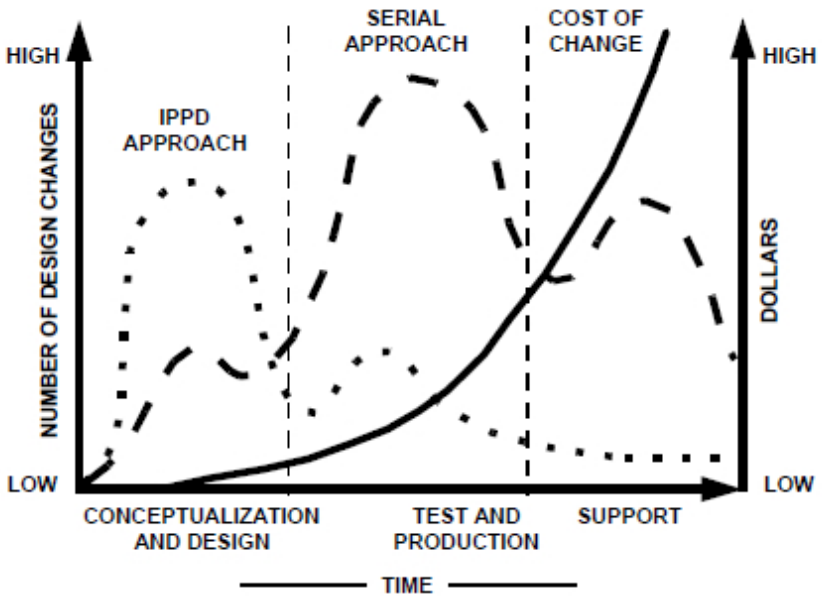

Figure 18: Cost of Design Changes [107]

architecture most of the aircraft power generated by the aircraft engines from burning fuel is used for propulsion, with the remainder of the power created by the engines converted to non-propulsive power of different types. Traditionally, this power is converted into four forms of power (pneumatic, hydraulic, mechanical, and electrical) to then be used by aircraft subsystems [120]. The traditional distribution of the use of these types of power represents the subsystems architecture that has evolved to become the current traditional standard architecture for transport aircraft [120] and [46].

Subsystem architectures are typically chosen utilizing a point design based on this traditional architecture. The selection of such a point design generates one alternative, the traditional architecture. The use of such a traditional architecture is a possible way for generating feasible alternatives to utilize. However, this selection does not explore much of the architecture design space, neglecting possibly superior designs.

The use of an All Electric Aircraft (AEA), as was discussed in Chapter 1, is also the selection of a point design that sets one possible feasible alternative to utilize but also explores little of the architecture design space (if selecting this architecture

without exploring others), again neglecting possibly superior designs.

Conceptual architecting, as discussed in Chapter 2, attempts to examine the architecture designs earlier in the design process. Authors such as de Tenorio [36] and Armstrong [21] and [20] have previously examined this important topic. (Contributions of de Tenorio [36] and Armstrong [21] to architecture generation for conceptual architecting are discussed later in this section.) Conceptual architecting uses models of the different possible subsystems to determine the impacts of a given architecture on the platform earlier in the design process [21]. These impacts are then compared and the desired architecture is used in the later design processes that are currently used. Without such a step, there is not a way to rapidly explore the subsystem architecture design space to identify the desired architecture. Conceptual architecting is not currently being utilized in industry. Examining trades of conceptual architectures and their impact on aircraft sizing is the primary focus of the later proposed methodology. This concept enables the use of desired architectures, such as energy optimized, in the aircraft design and allows the inclusion of this information earlier in the design process. As only simplified models are used, they can be created and utilized even during conceptual design. This would represent a significant step forward in the design space exploration of aircraft subsystem architectures.

There are several possible methods to create the alternatives that are examined in conceptual architecting. One method is the use of an IRMA, which were created to help designers make objective choices to reduce the design space. IRMA is based on the science of morphology. Morphological Analysis was created by F. Zwicky [142] and [43]. IRMAs create a functional to physical system decomposition which results in a Matrix of Alternatives. The complex system is decomposed into its important functions and features. Each of these is placed in a row in the matrix and each alternative solution to that function placed in the columns for the corresponding row. Such a matrix allows a better understanding of the potential solutions to the problem

[43].

Once the functional to physical decomposition is completed (resulting in a Matrix of Alternatives [43]), there are multiple ways to generate alternatives utilizing this design space. One method is to examine every possible architecture. Such a design space can become large very quickly. For example, a design space for a new transport aircraft in the 150-passenger class (and its subsystems) is shown in the screen shot from an IRMA shown in Figure 9. An IRMA uses a Matrix of Alternatives to examine such a design space and approximately calculates the computational time to examine all of the design alternatives. Such computational times become unwieldy for large matrices [43]. Another method is to narrow down the design space utilizing the IRMA by making selections that reduce the number of choices. Such a concept could be implemented by subject matter experts. This reduces the computational time required to examine the remaining architectures but limits the examined architecture design space. The IRMA uses a Multi-Attribute Decision Making (MADM) technique called Technique for Ordered Preference by Similarity to Ideal Solution (TOPSIS) to help narrow down the options [43], which can help reduce the size of the design space. TOPSIS is rooted in the concept that the chosen design should be closest in distance to the positive-ideal solution and furthest from the negative-ideal solution. For reference, the mathematical computations for creating a TOPSIS analysis are discussed in [64]. The selection of a point design from the matrix or alternatives (such as the traditional architecture) is also another way to select a feasible alternative, as was discussed previously in this section.

Finally, once the design space is determined utilizing the IRMA, feasible alternatives must be generated from the remaining design space. One such way to achieve this is the use of a Design of Experiments (DOE). A DOE is a structured way for selecting cases to run for an experiment, and the different types of DOEs are widely utilized, and are discussed in [88], [138] and [100].

Armstrong in his Master's thesis [20] described a method for generating and examining subsystem architectures. Armstrong's work used a functional approach for the definition of architectures [20], examining the functional architecture definition and tools that can be utilized to fully define architectures [20]. This work thoroughly examined the generation of architectures early in the design process [20]. As previously discussed, the examination of architectures earlier in the design process shifts more cost and effort to the early design phases. However, this is done partially due to the previously discussed impact of these phases on cost and the ease of changes earlier in the design process [107], [44], and [84].

The functional definition of architectures methodology discussed in Armstrong's Masters thesis utilized the concept of functional induction [20]. The concept of functional induction [86] assists with a functional decomposition during systems definition and during a functional decomposition of the mission. Functional induction was created for subsystem architecture definition from requirements [86] and could assist in the creation of the IRMA. Functional induction is discussed in [86] but, as shown below in Figure 19, is essentially the determination of required functions that are created (or induced) by the selection of a physical solution for any required function. Armstrong uses functional induction within a chain of functional solutions and a functional to physical mapping [20]. Specifically, Armstrong used functional induction in a new concept similar in purpose and function to a modified IRMA which he calls a Adaptive Reconfigurable Matrix of Alternatives (ARM) [20]. Armstrong created a process and an environment for subsystem architecture definition utilizing this ARM [20]. This environment is called ADEN by Armstrong and is shown in Figure 22 (although his tool focused on steps 3-5 in Figure 20) [20]. The ADEN environment was created by Armstrong to facilitate the process for the function-based architecture definition shown in Figure 20 and is discussed further in his Master's thesis [20]. Tools for these steps of architecture design are listed in Figure 21 and are

discussed in Armstrong's thesis [20]. These tools including Armstrong's tool shown in Figure 22, and the process shown in Figure 20 provides an environment for the selection of subsystem architectures [20]. For further information on these tools, the reader is referred to Armstrong's thesis [20].

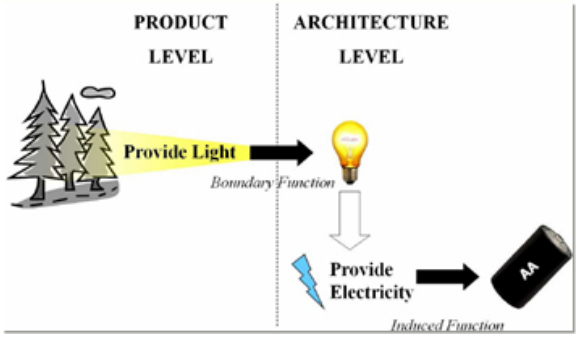

Figure 19: Functional Induction Example [86]

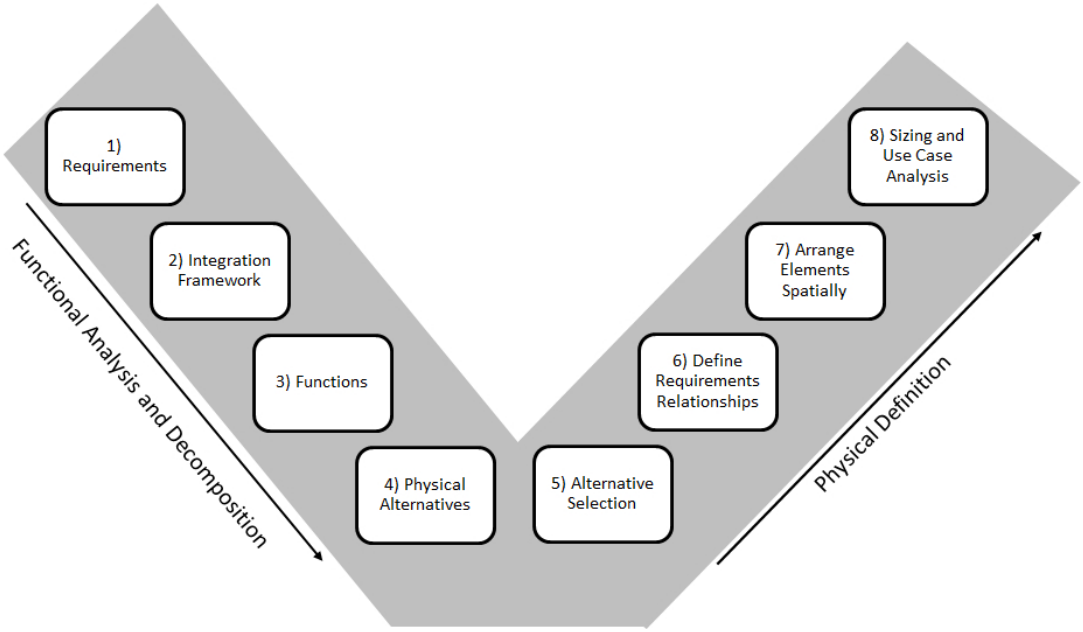

Figure 20: Process for Function based Architecture Definition adapted from [20]

As discussed previously, de Tenorio [36] in his PhD dissertation also examines exploration of architectures during conceptual design. Although de Tenorio [36] does not capture the coupling of these trades with aircraft and engine core sizing (addressed by this dissertation), he provides many important contributions to this topic including

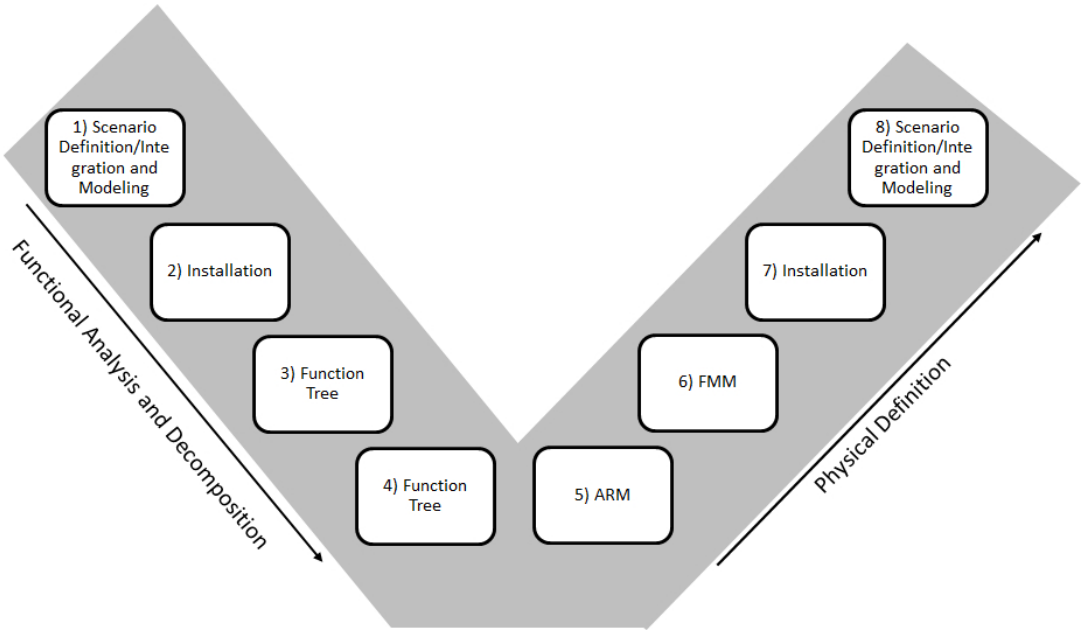

Figure 21: Tools for Function based Architecture Definition adapted from [20]

Figure 22: ADEN Environment [20]

the generation of architectures to study. de Tenorio [36] examines a model-based architecting methodology. de Tenorio [36] utilizes SysML models of architectures that are generated, and then meta models of these SysML models are created. Then, analysis is preformed for a given architecture to size and optimize the subsystems within the architecture. The types of models utilized by de Tenorio [36] enable rapid modeling setup of different architectures that could be utilized for an architecture design space exploration. The architecture design process examined in de Tenorio's work [36] is shown in Figure 23. In de Tenorio's work [36], the generation of the architectures to be studied is performed by an architecture generation team.

As discussed above, there are several existing concepts to assist with generating feasible alternatives within MAIA. These include the work described above from de Tenorio [36] and Armstrong [21] and [20], who explored the generation of these architectures. One such well suited concept specific to generating aircraft subsystem architectures is discussed in Armstrong Master's thesis, in which he describes a method for generating and examining subsystem architectures [20]. For examining a part of the subsystem architecture design space in this work, the selection of test architectures was made as discussed in the section below on the test case selection.

4.1.2 Test Case Selection

4.1.2.1 Selected Test Aircraft Configuration

In the case of civil jet transport aircraft, the layout of the aircraft has primarily been an evolutionary process, starting with the Comet and the Boeing 707 [67]. Modern transport aircraft are little different in configuration from these predecessors but have improvements in areas such as engine efficiencies, range, and passenger capacity [67]. As part of a search for better configurations, designers have examined different unconventional concepts [67]. Although these concepts present possible advantages, the commercial risks in developing these concepts is currently viewed as unacceptable [67]. As a result, the conventional configuration may continue to be used for the

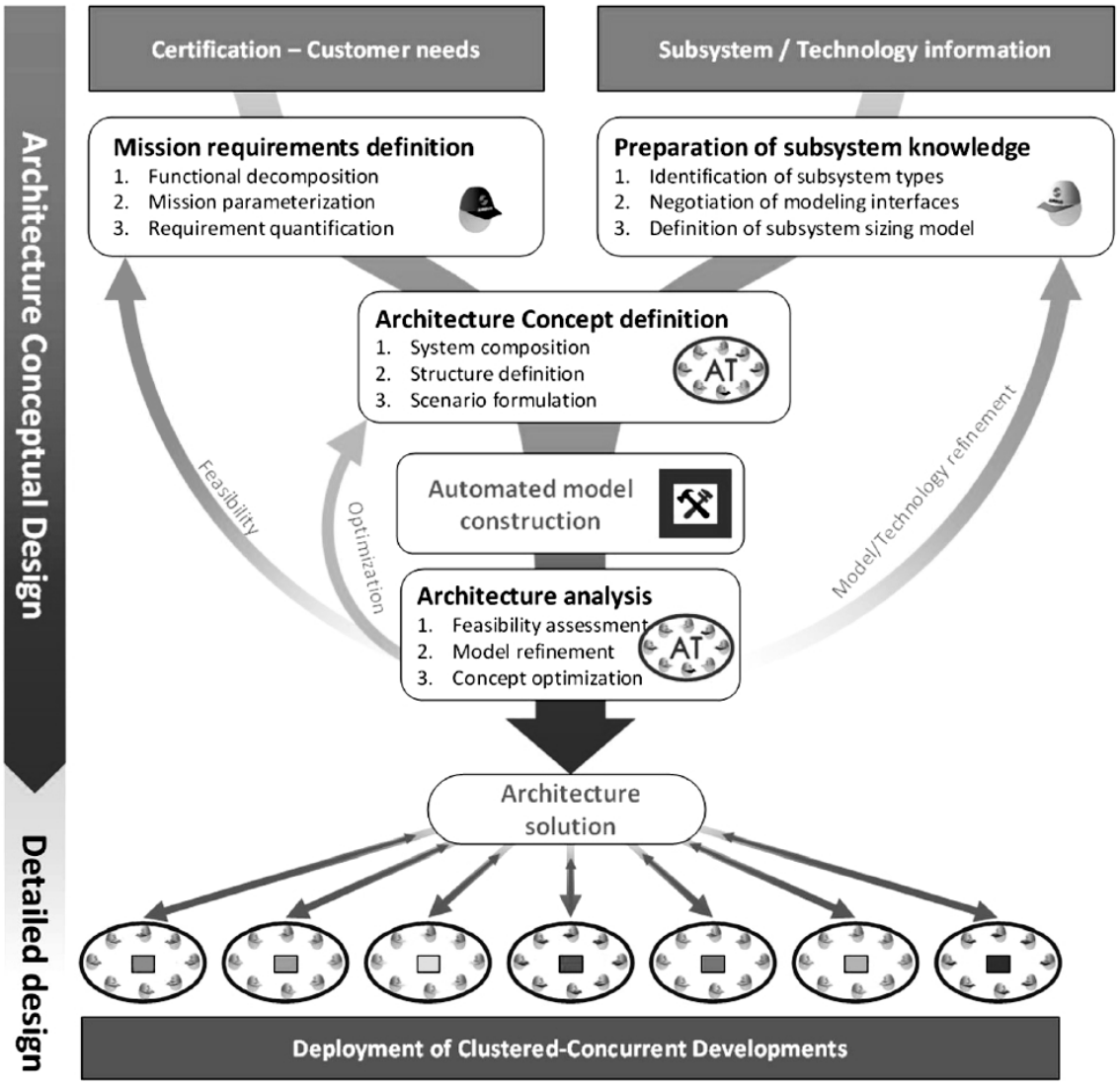

Figure 23: Architecture Design Process [36]

time being [67]. This configuration typically has a centrally positioned cylindrical fuselage, a low trapezoidal moderately swept cantilever monoplane wing, podded engines, retractable tricycle landing gear, and rear mounted separate vertical and horizontal tail/control surfaces [67] and [60]. An example of such a layout is the Boeing 777 [67]. Newberry and Eckels [104] discuss other transport design topics, among which are the selection and design of the interior, which include selecting the layout of the cabin (diameter and seating) along with the number and location of lavatories and galleys [104]. For reference, Anderson [18] discusses the case studies of the Boeing 727 and Boeing 707 design including their layouts.

Alternatives for the determination of the aircraft configuration include the use of a matrix of alternatives, design space exploration/trade studies, engineering judgment, and historically based configuration selection (as the selected test case is a civil transport). For the selection of a test case, the selected method is the use of a matrix of alternatives to determine the possible platform design space and a historical configuration-based selection. This was selected because the selected case study of transport aircraft utilize historically similar configurations and to reduce the scope of required analysis and trades.

The selected aircraft configuration to use as a test case for this dissertation is a potential replacement to the 150 passenger (B-737) class of aircraft. For reference, Table 1 lists some of the basic characteristics of the Boeing 737-800. This aircraft configuration is selected for at least two reasons. First, Boeing and several other aerospace companies are planning to create new aircraft in this area [109] and [108]. Second, the 150-passenger class of aircraft makes up a significant portion of the airline fleet [15]. This is illustrated in Table 2, which shows a breakdown of several aggregated United States passenger and cargo mainline aircraft fleets at the end of 2010 [15]. The fact that several industry entities plan to create new aircraft in this category and the influence of this class of aircraft due to its share of the total fleet size make this class

of aircraft an interesting and appropriate test case.

Table 1: Boeing 737-800 Basic Characteristics [29]

Metric	Performance
Passenger Capacity in 2 Class Configuration	162 Passengers
Passenger Capacity in 1 Class Configuration	189 Passengers
Cargo Space	$1555 ft^3$
Engine Type	CFM56-7
Maximum Thrust	27300 lb
Fuel Capacity	6875 gallons
MTOW	174200 lb
Range	3115 nm
Cruise Speed	0.785 Mach

Table 2: Selected US Cargo and Passenger Airlines Fleet Breakdown as of the End of 2010 [15]

Aircraft	Number
A300	124
A310	56
A318	9
A319	279
A320	382
A321	53
A330	51
B717	101
B727	76
B737	1248
B747	92
B757	611
B767	318
B777	150
Other	705
Total	4255

4.1.2.2 Selected Test Aircraft Subsystem Architectures

The selection of the configuration and its required mission and performance determine the functional part of the functional to physical mapping for the creation of a matrix of alternatives. Possible physical solutions are then filled into this matrix. Such a matrix

is shown in Figure 9. To limit the scope of the required modeling, architecture trades are limited to trades in the flight control actuation systems. This selection was made to limit the scope of the modeling and to capture trades involving a traditional power system (hydraulic) and a MEA concept of electrical actuation. To make the results comparable to the current 150-passenger class of aircraft, the rest of the architecture is fixed as the traditional aircraft architecture. The architecture is fixed to the current traditional architecture with one important exception: the flight control actuation system. Specifically, this exception is varying each individual actuator to be an EHA from a hydraulic actuator and back, and adjusting the wiring and piping (distribution elements) and generator and pump sizing (power sources) to account for this change. This decision is made to enable true evaluation of the MEA technology of an EHA. The design space of all possible combinations of hydraulic and EHA actuators (and their consequences such as changes in the distribution system) are examined. This method of selecting architectures is also utilized in order to limit the scope of the analysis of the demonstration of MAIA. This limitation in scope is performed partially due to the fact that there are several well developed methods for the generation of alternatives. These include the utilized approach, and the work of de Tenorio [36] and Armstrong [21] and [20], and others as previously discussed. An example of an examined architecture can be seen in Figure 24. (The figure was created utilizing the aircraft diagram from [31].) This figure shows the modeled actuation loads and, for a given architecture, whether or not the control surface (or Landing Gear) is powered by EHAs or hydraulic actuators.

4.2 Subsystem Definition

The second step of MAIA (Step B) is to define the subsystems and to determine their system-level impacts. The desire to capture these impacts came from Observation 2.

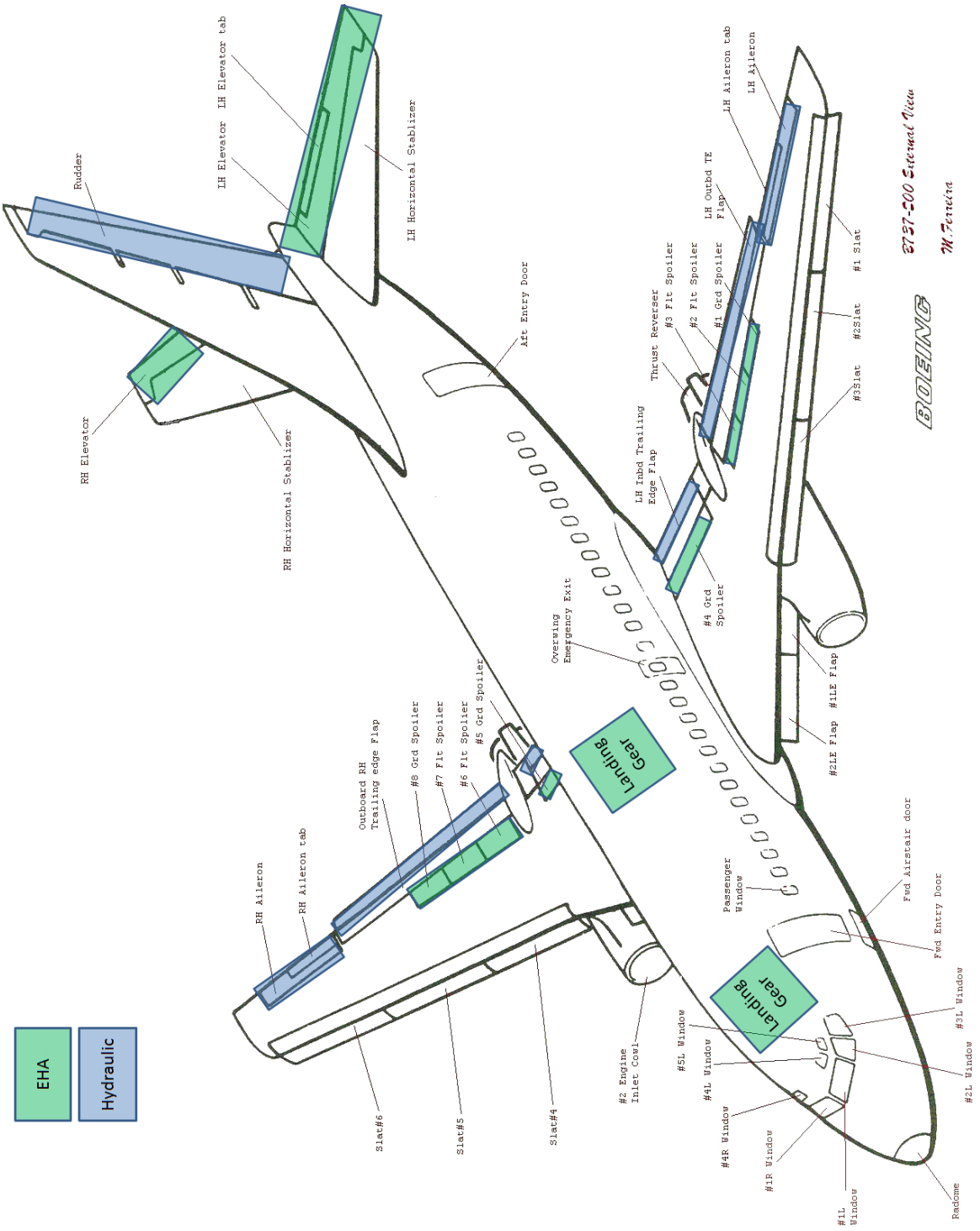

Figure 24: Example Architecture adapted from [31]

Observation 2: Variations in the subsystems architecture can lead to significant platform-level impacts.

The system-level impact can be captured by either physical experiments with the subsystems or models of their impacts. Physical experiments involving their components and their integration and impact on an aircraft were impractical to this effort due to the cost and unavailability of the needed parts and aircraft. The impact can also be determined using computational physics-based modeling of the aircraft subsystems. Such a concept has been implemented previously; for example, the European Union (EU) Power Optimized Aircraft (POA) project utilized modeling of aircraft subsystems to examine their impacts [25].

Physics-based modeling and simulation of the desired aircraft subsystems was performed for this step as described in the section on the modeling environment. This environment enables evaluation of the impact of the different examined subsystem architectures. To review, step B of MAIA is utilizing models of the aircraft subsystems to examine the system-level impact. The ability to perform this analysis was also presented previously in Observation 4.

Observation 4: Physics-based modeling and simulation can quantify the system-level impact of different subsystem architectures.

4.2.1 Subsystem Modeling Metrics

As discussed in the section on energy optimized aircraft, the energy efficiency of the aircraft subsystems can be important to capture, and many possible metrics can be used to examine this energy efficiency. These include, but are not limited to, the following: exergy (available useful work) loss [95], energy usage [95], subsystem weight [95], fuel burn impact [95], and environmental impacts (such as NOx emissions). However, the aircraft subsystems all derive their energy from power drawn

off of the engines in the form of shaft power extraction and bleed air. They are typically architected utilizing this power in a traditional point-based design as previously discussed[120] and [46]. As a result, the impact of changes to a subsystem architecture can be determined by the change in power drawn off of the engines in terms of the shaft power extraction and bleed air. This impact can be considered along with the weight of the subsystems which impact the aircraft sizing through their contributions to the empty weight of the aircraft. These metrics must be determined to enable analysis of the impacts of the subsystems on aircraft sizing. For this study, the metrics of shaft power extraction, bleed air, and subsystem weight were utilized as they contain the primary system-level impacts of subsystem architecture trades.

4.3 Subsystem to System Integration

MAIA step C is to examine the subsystem to system integration. This step is designed to capture the coupling between aircraft sizing and the platform-level impacts of subsystem architectures. The creation of such a step is motivated by Observations 2 and 3. These observations also lead to Research Question 1. This Research Question examines the magnitude of the impact of the coupling of subsystem architectures to platform-level impacts.

Observation 2: Variations in the subsystems architecture can lead to significant platform-level impacts.

Observation 3: Subsystem architecture platform-level impacts are coupled with the sizing of the aircraft.

Research Question 1: What is the magnitude of the coupling between the subsystem architectures platform-level impacts and aircraft size?

To determine this, it is first necessary to capture this coupling utilizing a modeling and simulation environment. This environment can utilize the subsystem models created for step B. The creation of those models was based on Observation 4.

Observation 4: Physics-based modeling and simulation can quantify the system-level impact of different subsystem architectures.

The created modeling environment must be capable of determining the system-level and platform-level impacts of the subsystems. The system-level impacts can be found from physics-based models of subsystems as was discussed in step B.

The subsystem impact can then be utilized to examine the platform-level impact. There are different alternatives for this determination. One alternative is the use of physical experiments which were excluded due to cost. Another is the use of aircraft and engine sizing algorithms. The engine sizing algorithm may be needed due to the impact of the subsystems on power extraction and, therefore, possibly on engine core size, as discussed in the modeling section. A third alternative is the use of simplified sizing relationships. Aircraft sizing refers to the process that calculates the weight of the aircraft that is necessary to carry its required payload through a desired mission profile [115]. The weight is very important as it sizes the entire aircraft [106]. There are different levels of fidelity and complexity in sizing procedures [115]. The simplest calculation uses the weight of similar previously manufactured aircraft [115]. There are also sizing techniques that use various computer codes and/or include results from experiments such as wind tunnel tests [115]. Major airframe companies use detailed sizing computer software which calculates the thrust required and the fuel flow for each of the segments that comprise the design mission profile [115]. The software attempts to meet mission requirements by changing TOGW in an iterative fashion [115]. For example, Huff [61] discusses computerized design synthesis programs including a program owned by Vought called Aircraft Synthesis and Analysis Program (ASAP). ASAP uses statistical data to size the aircraft and uses different modules to further analyze the potential design [61]. Almost all design synthesis codes are comprised of modules from different disciplines [61]. Another example of such a code can be seen in Newberry, and DeFilippo [103] which discusses

the sizing and synthesis code ACSYNT developed by National Aeronautics and Space Administration (NASA) Ames. ACSYNT combines three different types of code: aircraft sizing, aircraft performance, and optimization [103]. This software allows the designer to optimize the size of the designed aircraft for a design mission and performance requirements [103]. Such codes are important in the competitive aircraft market [61] and can capture the sizing impacts of changes in subsystem architectures through the use of architecture impacts, as determined by physics-based modeling and simulation.

As a result of a desire for accuracy, aircraft sizing algorithms are utilized in this work over simplified sizing relationships. The system-level impacts of the subsystems are computed by models made for step B and then passed to aircraft (and engine) sizing algorithms. The subsystem models are integrated with a sizing and synthesis environment to determine the platform-level impacts in a deterministic fashion as discussed in the modeling section. Integration of the sizing and subsystem models enables quantification of the coupling between the aircraft sizing and the subsystem architecture's impacts. The extent of the coupling can be explored by running test cases (architectures) through this environment and quantifying the covariance and correlations between architecture impact and TOGW. Recalling Observation 5, these values are likely to be positive.

Observation 5: The covariances and correlations between architecture impacts and aircraft size are likely to be positive.

The change in TOGW due to this coupling is probably significant due to the functional relationships between TOGW and subsystem impact previously described. For MEA, this assertion is also due to the continued existence of the MEA research and their preliminary findings of weight and power differences as well as the previously discussed interactions of TOGW and subsystem impacts. This leads to Hypothesis 1, which is listed below. The testing of Hypothesis 1 enables evaluation of the

importance of capturing the coupling of aircraft sizing and subsystem architecture impacts.

Hypothesis 1: If the impact of the coupling between aircraft sizing and architecture impacts is quantified, then this coupling will be found to be significant.

Observation 2: Variations in the subsystems architecture can lead to significant platform-level impacts.

Observation 3: Subsystem architecture platform-level impacts are coupled with the sizing of the aircraft.

In Observation 6 below, the significance of capturing this coupling may vary with passenger class. This fact leads to Research Question 2.

Observation 6: The magnitude of the impact of the coupling between the platform-level impacts of the subsystem architecture on the platform and aircraft sizing may vary with aircraft passenger class.

Research Question 2: What is the impact of varying aircraft passenger class on the magnitude of the coupling between the platform-level impacts of the subsystem architecture and aircraft sizing?

To examine this question, a review of Observations 7 and 5 is useful.

Observation 7: Aircraft subsystem weights are historically a function of the TOGW.

The coupling is still likely to be significant as the functional relationships between the parameters still exists.

Observation 5: The covariances and correlations between architecture impacts and aircraft size are likely to be positive.

The correlations and covariances are also likely to be positive. Further, the correlation is likely significant as discussed in Hypothesis 1. The change in TOGW due to this coupling is likely significant for different passenger classes due to the still existing functional relationships between TOGW and subsystem impact. The MEA

research and their preliminary findings again further reinforces this assertion. This leads to Hypothesis 2, which examines whether capturing this coupling is significant for different passenger classes of aircraft.

Hypothesis 2: If the aircraft class examined is varied, then the impact of the coupling between aircraft sizing and architecture platform-level impacts is still significant.

If this hypothesis is correct (which is shown to be the case), then this coupling must be captured for aircraft subsystem architecture selection for different passenger classes.

4.3.1 Aircraft Sizing Metrics

The metric selection to capture aircraft size is important for a demonstration of MAIA and is discussed in this subsection. As explained in Chapter 1, the impact of the selection of a subsystem architecture is coupled with aircraft sizing. There are many possible metrics that can be utilized to examine aircraft configuration, performance, and sizing. Metrics that can illustrate aircraft sizing characteristics include Thrust-to-Weight Ratio (TWR), wing loading (W/S), wing area (SW), wing span(b), aspect ratio(AR), and TOGW. Anderson [18] states that within conceptual design some important performance variables include maximum lift coefficient, lift to drag ratio, W/S, and TWR. These variables greatly impact the aircraft performance as discussed in [18]. Aircraft sizing commonly focuses on determining the design takeoff gross weight (TOGW or W0), the weight of the aircraft as it starts its design mission [115]. The design takeoff gross weight can be broken into various components as shown in equation (8) below [115] and [18] (and [67], [141], [106], [123], and [127] had similar formulations). It should be noted that other variations of this formula exist, in which the weight is separated into more detailed categories such as the weights of the propulsion systems, the fuselage, wings, and other components, or other means of

separating the TOGW [67] and [60]. The TOGW can be determined by estimating its components or by estimating TOGW from parameters such as payload and statistical trends (a simpler and possibly early estimate in the conceptual design process) [141].

According to [115] and [18]:

$$TOGW = W_{crew} + W_{payload} + W_{fuel} + W_{empty} \tag{8}$$

Another important aspect of the sized aircraft is its cost [115]. In a similar concept to several sizing methods in conceptual design, aircraft cost estimation is primarily statistical and is based on the costs of previous aircraft [115]. Although return on investment (ROI) is a very important parameter for determining the financial feasibility to the manufacturing company, there are some difficulties in using this parameter, difficulties which have led the industry to also perform life cycle cost analyses (the addition of all the cost elements of the aircraft during its life) [67]. Raymer [115], Howe [60], and Jenkinson, Simpkin, and Rhodes [67] have discussions concerning aircraft life cycle costs and estimation methods. Cost estimation during conceptual design is mostly statistical using parameters such as the aircraft weight [115]. Raymer [115] cites various different trends in aircraft cost as a function of weight. Raymer [115] also states that aircraft cost approximately 200 to 400 USD per pound. There are other cost estimating relationships and models which use inputs that include weight, production rate, and maximum velocity [115]. As can be seen, TOGW is a very important parameter, being both the driver of the cost [115], and the focus of aircraft sizing [115].

For the case studies utilized to examine subsystem architecting in this dissertation, the aircraft design mission and aircraft configuration are already fixed. This is because the baseline aircraft is based on existing civil aircraft, with the baseline being a generic current 150-passenger class aircraft, where the design mission and aircraft are already determined based on the existing aircraft in the examined passenger classes.

Specifically, the case studies are created utilizing baseline generic civil aircraft based on current traditional aircraft designs. The TWR, W/S, and AR are already fixed in the case study aircraft. As a result, the TOGW (and SW, which are related through W/S) shows the primary difference in aircraft sizing due to the examined trades in subsystem architectures in the case studies examined.

4.4 Design Knowledge Uncertainty Propagation

Step D of MAIA is Design Knowledge Uncertainty Propagation. This step attempts to capture the uncertainty mentioned in Observation 8. This implementation of this step raises Research Question 3a.

Observation 8: Subsystem architecture impacts have epistemic and aleatory uncertainty in various characteristics of the integrated components such as weight and efficiency.

Research Question 3a: How can the uncertainty inherent in the impacts of subsystem architectures be examined in subsystem architecture trades to inspect the robustness of the resulting designs?

Uncertainty plays an important role in many diverse areas of study including conceptual architecture trades. Possibly as a partial result of its widespread applicability and importance, many different ways of examining uncertainty exist.

Aleatory and epistemic uncertainties both appear in subsystem architecture trades. As previously discussed, a statistical treatment of aleatory uncertainty, such as using a sample variance [138], requires repeated measurements [100], which may not always be possible depending on the specific problem being studied. However, Bayesian probability and statistics can use all available information to asses probabilities and can handle aleatory and epistemic uncertainties [114]. In Bayesian probability and statistics, these uncertainties can be combined into single probability values or distributions [114].

As there is considerable epistemic uncertainty in subsystem architecture trades due to a lack of knowledge concerning requirements and the weight and efficiency of the integrated components, Bayesian distributions can be applied on parameters impacted by uncertainty within these trades. As a result, the creation and placement of probability distributions within the modeling environment is the first part of the selected application of this step. These subjective distributions are to be based on available information and expert opinion.

Once the uncertainty is captured by Bayesian (and/or frequentist) probability distributions of random variables, the impact of the uncertainty on the variables must be examined. To determine the impact of the uncertainty on the output variables of interest from the analysis, additional analyses must be performed. Different methods can be used for these analyses as discussed in the chapter on uncertainty. These include sensitivity analysis, which is one method for examining the impact of uncertainty [132], two-way sensitivity analysis, which is another common way to examine the impact of uncertainty, and Monte Carlo simulations. As the number of variables from which to examine the impact of uncertainty increases, the uncertainty impact analysis usually becomes a probabilistic uncertainty analysis, often using Monte Carlo simulations [132]. As discussed in the chapter on uncertainty, Monte Carlo simulations provide a means to examine the impact of the distributions of subsystem level uncertainty on the platform level. Monte Carlo methods are also widely and routinely used [38] and [56]. Although Monte Carlo simulations are one of the most commonly used methods within design (and will likely work well for subsystem conceptual architecting), there are several other approaches to characterizing and quantifying uncertainty [129] and [42]. For the reader's reference, some of these other methods were discussed in the chapter on uncertainty.

An examination of the methods discussed in order to find a suitable method for dealing with uncertainty in subsystem architecture impact analyses and trades reveals

that several methods are not applicable because of the defining characteristics of this problem and the uncertainty within. For example, the fact that epistemic uncertainty plays a potentially dominating role (and the fact the physical experiments may be expensive or impossible) rules out techniques such as characterizing data statistically from a set of experiments which is applicable for characterizing aleatory uncertainty. The fact that the change in the power required by the components and the change in their integrated weight and power required due to uncertainty can take on any of many different continuous values also makes intervals and sets not as applicable. Also, depending on the type of models of the subsystems used, derivatives or partial derivatives are not necessarily readily available. However, in some cases these could be estimated. The lack of available derivatives or other characteristics that may occur due to available models further limits the applicable techniques.

The approaches that previous subsystem related trade studies used to capture their uncertainty were examined previously in this work. This includes the POA program which applied distributions on the current (or flow/power) draw of the different components within the VIB modeling environment [25]. The Virtual Iron Bird (VIB) was an integrated modeling environment of aircraft system models to examine the power demands of systems and their architectures [25]. In the POA program, once the distributions were applied to the component current/power demands, Monte Carlo simulations were run, pulling values out of these distributions to capture the impact of uncertainty on the parameters of interest [25]. The Monte Carlo simulations were viewed as an enabler to allow the creation of the distributions on the metrics of interest [25]. Additionally, since the runs of the Monte Carlo simulations were independent of each other, the runs could be run on parallel computing clusters [25]. In the POA, distributions were placed on the power demand of components, and Monte Carlo simulation was used to aggregate the impact [25]. The use of Monte Carlo simulations enables parallelization of runs of the simulation environment which

enables the potential for more runs to be made, possibly allowing more subsystem architectures to be compared [25]. The use of these techniques and advantages shows that a similar method can be applied to the examination of the impact of uncertainty in this problem of comparing subsystem architectures. Despite the fact that many techniques cannot work for such a problem, the distributions of the component's parameters such as weight, efficiency, and required performance can be estimated (creating Bayesian distributions) as discussed in Observation 9. The placement of the distributions on physical parameters of individual components allow the experts to be able to evaluate a parameter on the device related to their expertise and not on some aggregated system variable on which they may have less experience. The resulting Bayesian distributions can be placed on the related variables within the modeling environment. Once the distributions are applied to these variables, an appropriate method must be used to aggregate their impact. Monte Carlo simulation is such a method. Monte Carlo simulation can thus be run on the modeling environment to try to capture the impact of the uncertainty.

Observation 9: Probability distributions can be created and applied on parameters within the modeling and simulation environment to capture uncertainty in those parameters.

The use of uncertainty distributions is selected along with MCS for the application of the MAIA step to subsystem architectures as discussed above. The noise parameters that these distributions can be placed upon include the values of the weight and efficiency of components within the aircraft subsystems. Such distributions are created as discussed in the section on Experiment 3a. These distributions are utilized to capture uncertainty on the noise parameters in the modeling environment. Once these distributions are placed in the modeling environment, MCS is then used to determine the resulting impacts of the distributions on the response (TOGW) as

discussed in the chapter on uncertainty. This analysis results in distributions of platform and system variables that could then be examined for their robustness utilizing metrics such as SNR [88], which is discussed in the last step of MAIA. This leads to Hypothesis 3a.

Hypothesis 3a: If distributions characterizing noise variables within aircraft subsystem architecture trades are utilized in the subsystem modeling and simulation environment, then a robust selection of the subsystem architecture design can be performed.

The integrated models must be capable of handling probabilistics to enable examination of the impact of uncertainty. In order to capture the impact of uncertainty, the models must shift from a deterministic analysis to the use of a stochastic design methodology that can account for uncertainty [84]. Mavris, DeLaurentis, Bandte, and Hale [84] present an approach which utilizes metamodels to enable this shift and reduce the computational time required to analyze the cases. These metamodels are often regression models of computer programs [84]. The approach specifically uses physics-based metamodels that are linked into an aircraft sizing and synthesis program [84]. The metamodels enable the use of more accurate higher order methods typically used later in design during earlier design phases [84]. This approach allows the inclusion of uncertainty and uses physics-based analysis and metamodels to replace historically based data, which the authors state is likely obsolete for current and future aircraft [84]. Due to the required number of cases and their associated computational time, metamodels are utilized in the application of this step as listed in the test plan for Hypothesis 3a.

There are different methods for creating these metamodels including the use of Artificial Neural Networks (ANNs) (which are utilized in Test 3a), fuzzy sets, and the Response Surface Methodology (RSM) [84]. According to Meyers and Montgomery

[88], "Response surface methodology (RSM) is a collection of statistical and mathematical techniques useful for developing, improving, and optimizing processes." The parameters or metrics that the user wishes to track are known as responses, which are treated as a function of the input variables (also called the independent variables) to the problem [88]. Successful application of RSM is dependent on the creation of a useful approximation for the response [88]. Typically, a first or second order polynomial is used for this approximating function [88]. The second order polynomial model is the most commonly used in RSM [88]. The use of polynomial approximating functions is based on the use of Taylor series expansion [88]. Surrogate models can be used in exploring architecture design spaces as an enabler for reducing the computational run time required to examine a given architecture.

Another concept that is useful within RSM is the use of experimental designs including the use of fractional factorial designs (which are utilized in Test 3a to generate the data needed to create the ANNs) [88]. If the higher order interaction terms within the approximating polynomial can be neglected, then a fraction of the number of experimental runs (as compared to run a full factorial design where all setting levels are tested) can be used to create the Response Surface Equation (RSE) [88]. This allows a potential reduction in the number of experiments (or runs of code) to create RSEs, which can make their creation more feasible. For reference, Meyers and Montgomery discuss experimental designs, including the creation of experimental designs, for the creation of second order RSEs, which includes the use of Central Composite Designs (CCDs) [88].

4.5 Architecture Selection

Step E of MAIA is the selection of the desired architecture. This selection should be based on the deterministic values of metrics such as TOGW for different architectures and their SNR to examine their robustness. In the experiments, the deterministic

results are used (as discussed in experiment 3a) to select the top three architectures. The robustness of these architectures is then examined in MAIA step D. The most robust out of these top candidates then becomes the selected design. The robustness was captured utilizing SNR as discussed in the section on robustness in the chapter on uncertainty. The specific definition of SNR utilized is shown in equation (9). The use of equation (9) was motivated by the concept of having to meet the target of the deterministic TOGW for that architecture due to the fact that deviation from the target would likely cause redesign, a delay in the schedule, and additional cost.

As discussed in [88], [111], [48], and [138]:

$$SNR = -10log((\mu^2)/\sigma^2) \tag{9}$$

Several other approaches to capturing the robustness of a design were not utilized. Some of these approaches for examining multiple responses are discussed in the section concerning robustness. This could happen in subsystem architecture trades, but the driving metric examined in the case study was TOGW, allowing SNR to be sufficient. In Abraham [13], two such approaches are discussed. In the first of these approaches, SNRs are calculated for each response and then combined into a desirability function [13]. The other approach discussed in [13] extended the first approach by adding weights on the desirability of the responses in the desirability function [13]. One disadvantage to the approaches discussed in [13] is the fact that these approaches distill comparing the designs to one metric whose values would change as these weights are varied. In Hui [63], a generalized multivariate distance from a multivariate target is used to examine robustness, using Hotelling's Tsquared as shown in equation (10). As shown in [63]:

$$Ti^2 = (x_i - x_t)(S^{-1})(x_i - x_t) \tag{10}$$

Another applicable robust design method is Robust Design Simulation (RDS) which is discussed in [87] and [85] and was motivated by the need for future aircraft

such as an economically viable supersonic transport. RDS applies probabilistics to design and examines the objective as a distribution caused by the effects of distributions on noise or uncertainty variables [87] and [85]. This method enables the capturing of the impact of uncertainty on parameters[87]. RDS examines the identification of a robust design [87] and [85] and is an alternative to Taguchi's approach for examining robustness of subsystem architectures by applying distributions to the noise variables which results in distributions of the design's responses.

Identified control variables in subsystem architecture selection include: the (hydraulic/electrical/other) system each component is connected to, the type of component used, the route network configuration, the number of each component, and the aircraft configuration. In the proposed methodology described later, the aircraft configuration is decided by the designer before trading the subsystems, so it can be considered to be fixed. The number of each component would be minimized to make the systems as small and as light as possible while remaining within the constraints of failure scenarios and therefore would be mostly fixed as well. The route network is also mostly fixed by the locations of the fuel tank and other compartments. Therefore, the primary control variables examined in the proposed methodology are the type of components used and which systems they are connected to. For the specific case study, these were limited to hydraulic actuators and EHAs on the aircraft control surfaces and landing gear. Identified noise variables include: the efficiency of each component, the efficiency of the integrated systems, the weight of each component, and the weight of the integrated systems. For the case study, the specific noise variables identified included: the electrical motor efficiency within the EHA, the electrical system's generator efficiency, uncertainty on the weight of the wiring, the weight of the EHAs, and the weight of the hydraulic actuators. The distribution of each of these variables would impact the distribution of platform-level variables such as TOGW and system-level variables such as power draw. After the proposed

methodology has been used to find the resulting distributions, the robustness of the subsystem architecture designs to uncertainty was compared using SNRs. The architecture that was in the top three deterministic cases (having the lowest TOGW) and was the most robust out of these candidates was selected is discussed in the chapter on the Experimental Results.

4.6 Sensitivity of Design to Uncertainty Determination

The final step of MAIA is the examination of the sensitivity of the design to the sources of uncertainty. This step examines the different sources of uncertainty to attempt to determine which of these sources has the largest impact on the selected design (specifically, on the TOGW distribution) from MAIA step E. The creation of this step is motivated by Observation 10.

Observation 10: Uncertainties on subsystem traits with the highest platform-level impacts should be identified.

This leads to Research Question 3b.

Research Question 3b: How can the primary sources of uncertainty in the platform-level impacts of the selected subsystem architecture be identified?

4.6.1 Capturing the Impact of Uncertainty

There are several different ways for capturing the impact of uncertainty. As discussed in the chapter on uncertainty, one such method for capturing the impact of the uncertainty on subsystem architectures is the use of Bayesian Networks. The selection of the use of Bayesian Networks over other methods is discussed in the chapter on uncertainty. Bayesian Networks (BN) are useful tools which can create predictive models utilizing available data[53] and [96]. Such a network can be fit to data coming from running cases within a modeling environment as is done in MAIA step D. An example of such a network structure could have the variables that have uncertainty on their values as nodes that are connected to a node representing the output(s) of

interest (such as TOGW). This network could then be used to quantify the strength of the links between variables (if the data are discretized) [41]. This concept of determining the strength of the links and how this strength is defined between variables in discrete Bayesian Networks is described in [41]. The links that were characterized as the strongest would then identify which uncertainty distributions were having the strongest impact on the output(s). A different network could be set up and then varying the arrangement of the network could also be performed to find the most accurate representation of the system [53] and [96]. The above described possible use of Bayesian Networks to examine the sensitivity of a design to uncertainty on subsystem architecture values leads to Observation 11.

Observation 11: Bayesian Networks can capture the sensitivity of a design to uncertainty.

There are other approaches that can be used to examine the impact of uncertainty on the design. However, such approaches are not the focus of the related proposed methodology step due to their disadvantages and the advantages of BN. For example, correlation values between the variables can also be used to examine which of the variables have impacts on the TOGW. There are limitations to this approach as correlations measure how linear the relationship is and not necessarily the strength of this connection [138]. A related parameter, covariance, also examines only if there is a linear relationship [138]. Examination of these parameters may be useful to cross-reference to see if utilizing the BN is selecting the correct link as the strongest.

Recalling Observation 11, Bayesian Networks (BN) are useful tools that can enable the capturing of this uncertainty. In the application of BN to MAIA, such a network could be fit to data coming from running cases within a modeling environment. This network could be used to quantify the strength of the links between variables as discussed in the chapter on uncertainty [41]. Varying the arrangement of the network could also then be performed to find the most accurate representation of the system

[53] and [96]. It should be noted that correlation values and covariance values between the variables can also be used to examine which of the variables have impacts on the TOGW. As mentioned above, there are limitations to this approach because these parameters measure how linear the relationship is, and not necessarily the strength of this connection [138]. However, as noted above, examination of these parameters may be useful to cross-reference to see if utilizing the BN is selecting the correct link as the strongest. The proposed use of a Bayesian Network leads to Hypothesis 3b.

Hypothesis 3b: If a Bayesian Network is created to represent the impact of the uncertainty in the subsystem architectures characteristics on aircraft sizing, then the variables with the largest impacts can be identified.

CHAPTER V

HYPOTHESIS TESTING

This chapter examines the corresponding test plan for each hypothesis and the development of the modeling and simulation environment. The subsequent chapter explores the application of these plans and results from running these experiments.

5.1 Overarching Hypothesis Experimental Plan

To review, the **Overarching Hypothesis** states the following: Capturing of the coupling between aircraft sizing and subsystem architecture impacts and exploring the architecture design space enables a significantly better architecture selection than a point-driven design.

To test this hypothesis requires the corresponding Overarching Experiment. The overall intended purpose of this test is to demonstrate that the application of the proposed methodology is better than a point-driven philosophy. To test this requires an examination of an architecture design space using the first few steps of MAIA while capturing the coupling between aircraft sizing and subsystem architecture impacts. This test has several required steps. The first step is to create the required modeling environment to perform the steps in MAIA to enable capturing this coupling. This requires the creation of physics-based modeling of aircraft internal subsystems for the selected example configuration of an aircraft. These models must be able to capture the impact of varying the selected subsystem architectures. This modeling environment must include a sizing calculation for the systems and their components. Then, these models must be integrated with a sizing and synthesis algorithm in order to capture the coupling between aircraft sizing and architecture impacts. The modeling environment is further described and explored in the section later in this

chapter on the modeling environment. For each design examined, the platform and system-level impacts should be demonstrated in the converged values of the outputs, such as the power extraction and TOGW.

Once this environment is created, the next step is to explore the architecture design space for the test case, using the proposed methodology. This design space exploration is performed utilizing the modeling environment and enables comparison of the best design found to a single point design. This exploration is done through a full factorial DOE varying each group of control surfaces (flaps, elevators, rudder, aileron, landing gear, for example) from being hydraulically powered to being powered by EHAs as described in the test case section. This DOE examines every possible architecture in the design space, assuming that all actuators on any given type of control surface will be powered by the same technology. This DOE examines every possible combination of each group of control surfaces (spoilers, flaps, rudder, elevator, for example) being powered by EHAs or hydraulic actuators. This DOE includes all hydraulic, all EHA, and hybrid architectures. Examples of examined architectures can be seen in Figures 25 (all hydraulic actuation), 26 (all EHAs), and 27 (an example hybrid architecture). It should be noted that these figures utilize an aircraft diagram from [31].

The DOE is run to determine how large a difference in TOGW there is between a selected point design (the worst case) and the best design. The magnitude of this range in pounds will demonstrate if the difference between a point design and the design space exploration including coupling is significantly better. This value needs to be examined in the context that only the flight control actuation system is being changed in the example architecture study. Given that Roskam [121] states that the range to expect for the total weight of the actuation system is approximately 0.6 to 1.2 percent of TOGW, the difference in converged TOGW by varying this system can be compared to this range in order to determine significance.

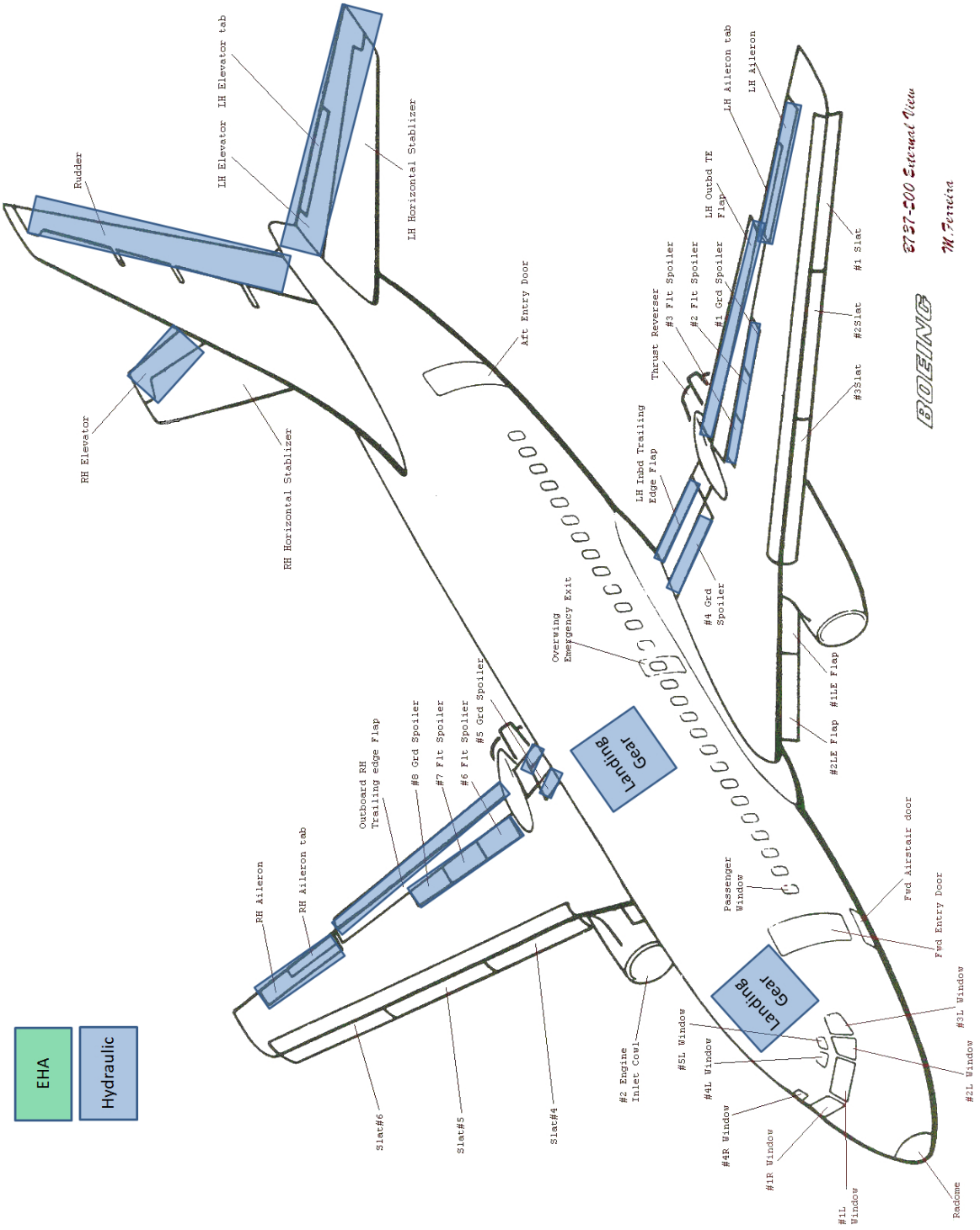

Figure 25: Hydraulic Actuation Architecture adapted from [31]

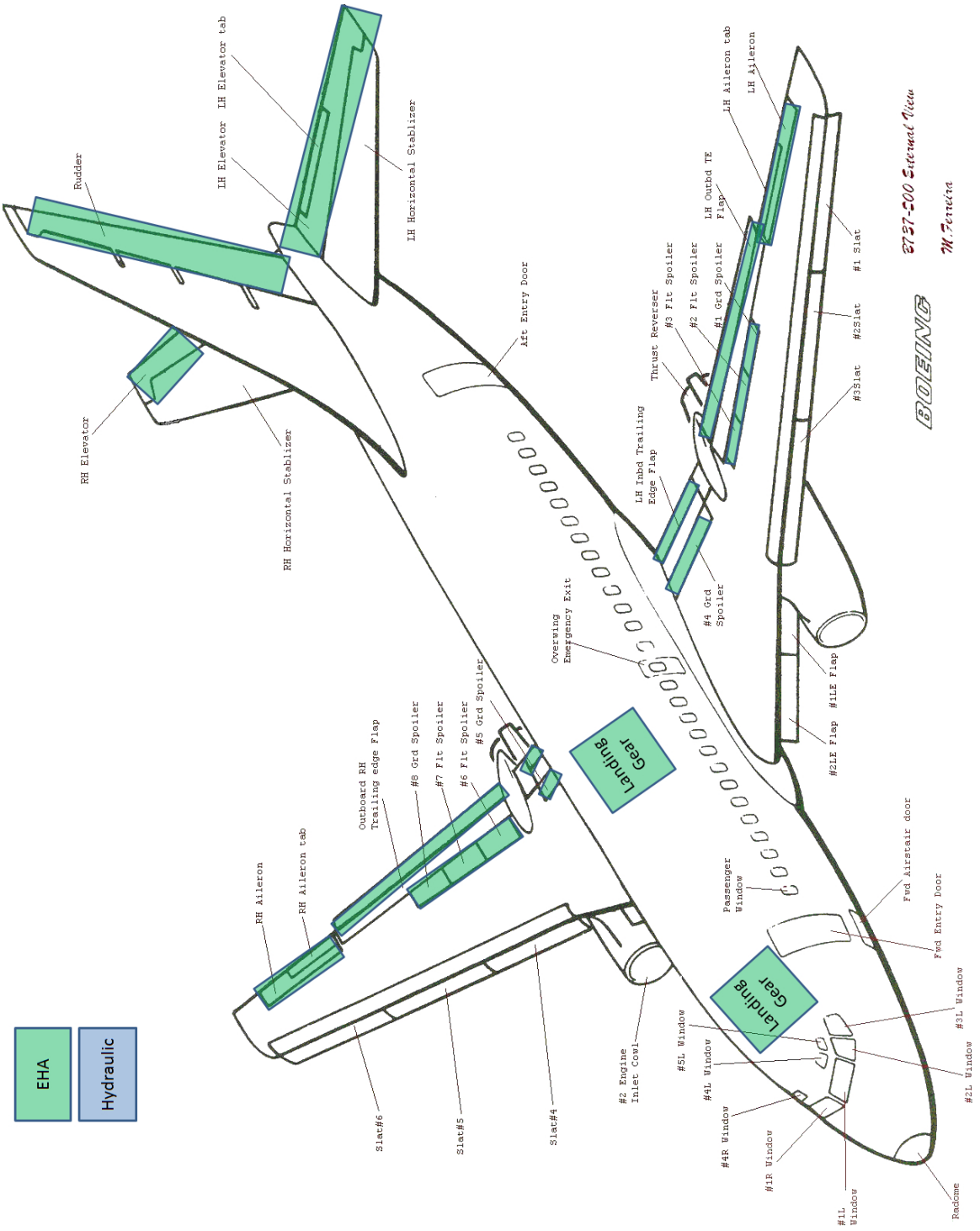

Figure 26: All EHA Architecture adapted from [31]

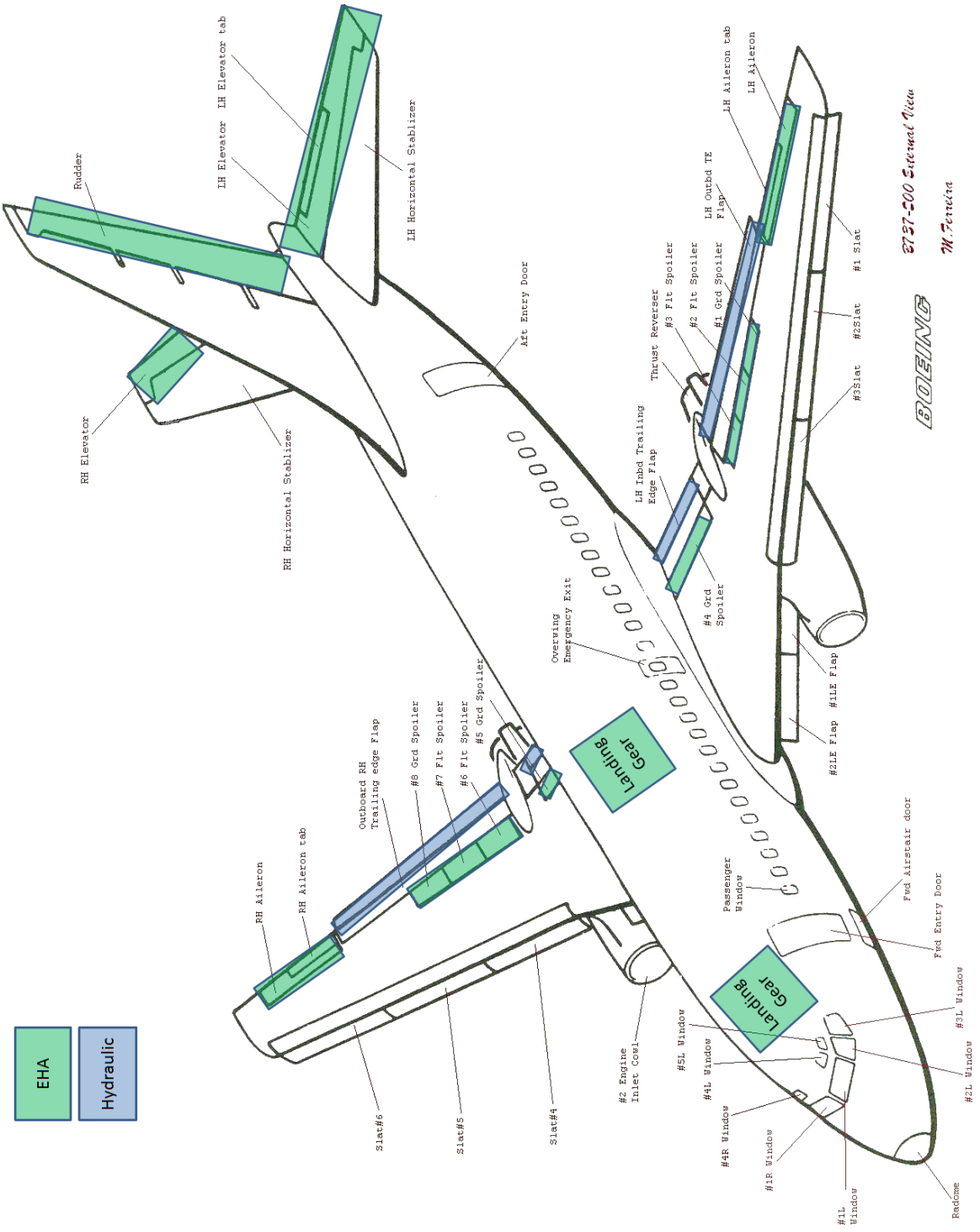

Figure 27: Example Hybrid Architecture adapted from [31]

5.2 Hypothesis 1 Experimental Plan

To review, **Hypothesis 1** states the following: If the impact of the coupling between aircraft sizing and architecture impacts is quantified, then this coupling will be found to be significant.

The primary purpose of Experiment 1 is to examine the significance of the impact of the coupling between aircraft sizing and architecture impacts. The quantification of this coupling requires an integrated modeling environment of aircraft sizing and aircraft subsystems. As a result, for Experiment 1, the models made for the Overarching Experiment can be leveraged to examine the extent of this coupling. The same modeling and simulation environment that the Overarching Experiment requires must be created. Then, the architecture design space must be explored utilizing the environment to generate the needed data to examine the coupling. The same architecture design space defined in the section on the test case is utilized. Then the same DOE run for the Overarching Experiment must be run as this DOE examines every possible architecture in the design space (assuming that all actuators on any given type of control surface will be powered by the same technology). Again, this DOE examines every possible combination of each group of control surfaces being powered by EHAs or hydraulic actuators. Figures 25 (all hydraulic actuation), 26 (all EHAs), and 27 (an example hybrid architecture) show examples of examined architectures. Again, it should be noted that these figures utilize an aircraft diagram from [31].

The metrics of maximum and average power extraction, subsystem weight, and TOGW can all be stored when running the DOE and then analyzed. Next, the results must be analyzed to examine the coupling. Covariances and correlations between the variables (especially the subsystem impacts such as subsystem weight and power extraction as well as TOGW) must be examined. These metrics can assist in examining the coupling by determining whether a linear relationship exists [138] and how strong this relationship may be. The closer to 1 or -1 the correlation is

from 0, the stronger the indication of a stronger linear relationship. Examination of a multivariate plot for trends and magnitudes can also assist in this examination, as a trend in the result indicates the existence of coupling between variables. The magnitude of the encountered range of TOGW demonstrates the magnitude of the impact of this coupling on TOGW, as otherwise TOGW would be determined utilizing only the historically based sizing aircraft weight. Given that Roskam [121] states that the range to expect for the total weight of the actuation system is approximately 0.6 to 1.2 percent of TOGW, the difference in converged TOGW by varying this system can be compared to this range to determine significance. Finally, the trends seen in plots of the results, the magnitude of the correlations, covariances, and the range in TOGW must be examined to determine the significance of the results.

5.3 Hypothesis 2 Experimental Plan

To review, **Hypothesis 2** states the following: If the aircraft class examined is varied, then the impact of the coupling between aircraft sizing and architecture platform-level impacts is still significant.

To test this hypothesis requires Experiment 2. The primary objective of Experiment 2 is to determine if the impact of the coupling between aircraft sizing and architecture platform-level impacts is still significant when different passenger classes of aircraft are examined. As a result, this test needs a similar modeling environment to Tests 0 and 1. The modeling environment must contain an aircraft sizing algorithm and models of the aircraft subsystems. As a result, this test can leverage the same modeling environment created for Tests 0 and 1. However, this modeling environment must then be updated, to be able to model other passenger classes of aircraft to examine the impact of this coupling on other aircraft sizes. Specifically, 210-passenger and 300-passenger aircraft are used for this test. These sizes are selected due to model and data availability. Once the modeling environment is created

and updated, it must be used to explore generate the data needed to explore the coupling.

Then, the same DOE run for Tests 0 and 1 must be run for each passenger class size as this DOE examines every possible architecture in the design space (assuming that all actuators on any given type of control surface are powered by the same technology) for the selected aircraft size. The same DOE is also used to enable direct comparison with the data generated in Experiment 1. This DOE again examines every possible combination of being powered by EHAs or hydraulic actuators for each group of control surfaces. This DOE again includes all hydraulic, all EHA, and hybrid architectures. For comparison to the experiment 1 results, these architectures contain the same control surfaces updated for the larger aircraft. For reference, examples of examined architectures can be seen in Figures 25 (all hydraulic actuation), 26 (all EHAs), and 27 (an example hybrid architecture). Again, it should be noted that these figures utilize an aircraft diagram from [31]. Such a DOE was constructed and run for both of the added aircraft passenger classes.

In a process similar to Experiment 1, the metrics of maximum and average power extraction, subsystem weight, and TOGW can all be stored when running the DOE and then analyzed for each passenger class size. After the DOE is run, analysis must be performed to examine the coupling. Covariances and correlations between the variables must be examined to determine if a linear relationship exists [138] and how strong this relationship may be. The larger the absolute value of the correlation, the higher the indication of a stronger relationship. An examination of a multivariate plot for trends that indicate the existence of coupling between variables would then be performed. The magnitude of the range of TOGW demonstrates the magnitude of the impact of this coupling on TOGW for each passenger class size. Given that Roskam [121] states that the range to expect for the total weight of the actuation system is approximately 0.6 to 1.2 percent of TOGW, the difference in converged TOGW by

varying this system can be compared to this range to determine significance for each passenger class. Finally, in a similar fashion to Experiment 1, the trends seen in plots of the results, the magnitude of the correlations, covariances, and the range in TOGW must be examined to determine significance of the results.

5.4 Hypothesis 3a Experimental Plan

To review, **Hypothesis 3a** states the following: If distributions characterizing noise variables within aircraft subsystem architecture trades are utilized in the subsystem modeling and simulation environment, then a robust selection of the subsystem architecture design can be performed.

To test Hypothesis 3a requires the corresponding Experiment 3a. The primary objective of Experiment 3a is to apply distributions in the modeling and simulation environment characterizing the noise variables and then quantify the robustness of the subsystem architecture designs. The utilized noise variables and their distributions will be further discussed in the section on the implementation and results for experiment 3a. To start this test requires the development of the needed modeling and simulation environment. This modeling and simulation environment must be able to capture subsystem architecture impacts and their coupling with aircraft sizing. Similar to Experiment 1, this test can leverage the physics-based modeling of aircraft internal subsystem architectures integrated with an aircraft sizing algorithm made for the Overarching Experiment. This test examines the probabilistic distributions using a method consistent with the proposed methodology, utilizing Monte Carlo Simulation (MCS) to sample the distributions. Due to computational time feasibility, the number of architectures to be examined in this test is limited to the top candidates from running the DOE on the modeling and simulation environment as described in Tests 0 and 1. The top candidate architectures selected will have

the lowest deterministic values of TOGW due to the impact of this metric as discussed in the chapter on MAIA. The different examined architectures is the design variable for the robust design study. This study attempts to find an architecture that results in the best SNR of the response, in this case TOGW. Then, to capture the uncertainty, probability distributions are applied on the noise parameters within the subsystem modeling environment. These parameters are parameters such as efficiencies of the motors and generators and weight per capacity (such as lb/kN output force for EHAs) for different components. The specific examined parameters are discussed in the Experiment 3a section. These probability distributions should be based on available data and expert opinion and placed on parameters such as component efficiencies and weights. Ranges on the parameters are determined by the creation of these distributions. These ranges should then be leveraged to create DOEs to explore the subsystem modeling environment and aircraft sizing algorithms for the purpose of generating metamodels of these environments to make the computational time feasible for a larger number of cases. If possible, ANNs or other metamodels should be created. ANNs could be utilized because of their previous use with the utilized aircraft and engine sizing algorithm [69] and [70] and the likely non-linearity of some of the data. These metamodels should make the run time of MCS cases feasible.

After creating metamodels, the distributions need to be applied on the noise variables. Then, MCS should be run on the integrated modeling environment, pulling variables out of the probability distributions but holding the architecture constant. Then the additional cases of other architectures should be run. The resulting data from running these cases then needs to be analyzed. The data can be utilized to create multivariate plots and correlation values to provide insight into relationships between the parameters. The resulting robustness of the different designs can be compared through the robustness of TOGW utilizing SNR as discussed in the section on proposed methodology. Finally, the robustness of these designs is used to select

the top architecture by comparing the SNR values. The determination of the SNR values of TOGW for the different designs demonstrates that the robustness of the designs can be quantified.

5.5 Hypothesis 3b Experimental Plan

To review, **Hypothesis 3b** states the following: If a Bayesian Network is created to represent the impact of the uncertainty in the subsystem architecture's characteristics on aircraft sizing, then the variables with the largest impacts can be identified.

To test Hypothesis 3b requires the corresponding Experiment 3b. The primary objective of Experiment 3b is to identify the variables with the largest impacts on aircraft sizing, utilizing a Bayesian Network to demonstrate that this can be done and to enable the use of Bayesian Networks for this analysis for aircraft subsystems due to the advantages of Bayesian Networks discussed in the chapter on uncertainty. This test studies the top architecture identified using SNR in Experiment 3a to attempt to identify which of the variables with uncertainty distributions is driving the response. Such an identification enables a designer to determine which variables to investigate further, in order to reduce the variability in the response. As Experiment 3b is using a Bayesian Network to study the top architecture from Experiment 3a, this test can leverage the modeling environment and data created from running the environment for the top architecture created for Experiment 3a. Then, a Bayesian Network must be created and fit to the resulting data from the MCS run in Experiment 3a of the modeling environment for the top architecture. This network should have nodes for each of the input variables connected to a node for the response (TOGW), to enable direct comparison of their link strengths as discussed in [41] and the chapter on uncertainty. An example of such a Bayesian Network structure is shown in Figure 28. To examine which variables have the largest impact, the strength of the resulting connections must be determined as discussed in [41]. The variables with the largest

impacts should be identified by having the strongest connections. Potentially, what network structure may fit the data best could also be explored to gain additional insight. Specifically, the connections between nodes can be explored to determine what structure fits the data best to identify if the best network structure gives any additional insight into which variables are driving the response. Finally, the results should be cross-referenced with the covariance/correlations between the variables, ANOVA results, and the trends seen in the multivariate plot of the MCS results to enable a validation of the results by comparison to the statistical parameters characterizing these relationships. As discussed in the chapter on uncertainty, such a use of Bayesian Networks is unusual, but if it can be validated, then this enables the use of Bayesian Networks for such an analysis. This is greatly desired due to the additional analysis enabled by the use of Bayesian Networks, such as predictive analysis during subsystem development.

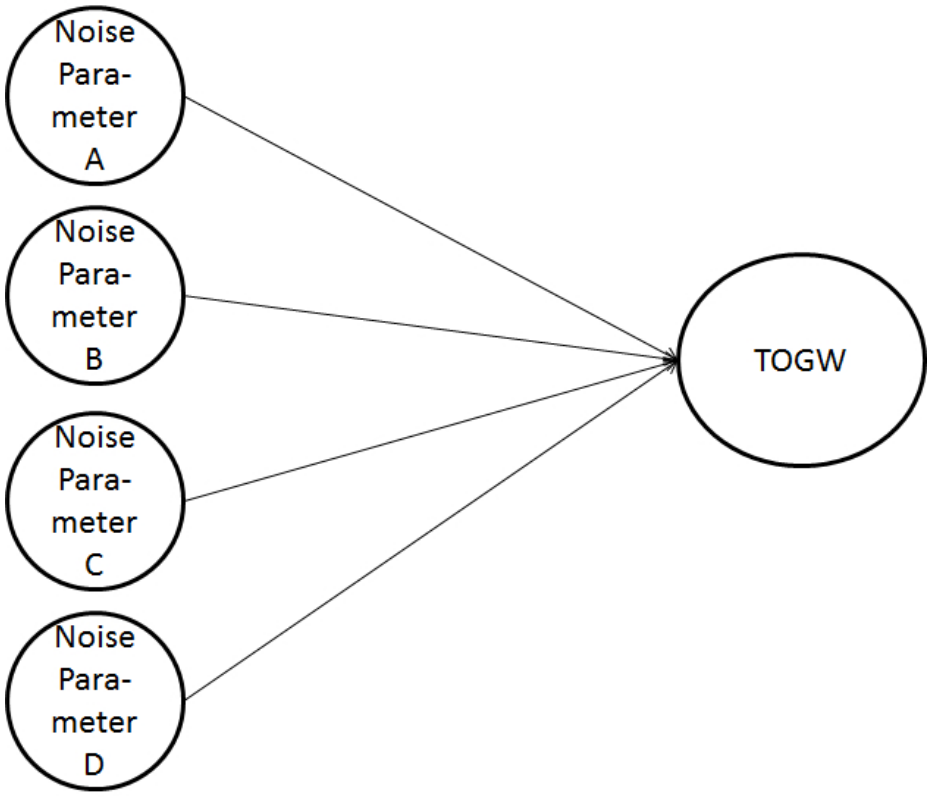

Figure 28: Experiment 3b Bayesian Network Structure

5.6 Modeling Environment

This section discusses the modeling environment created to test the hypotheses. First, the overall concept of the environment is described. Then, the primary elements of that environment are discussed. The creation of such an environment enables the experiments and use of MAIA.

5.6.1 Modeling Environment Concept

The concept of the modeling environment is illustrated in Figure 29. This environment was created to study the impact of different subsystem architectures and the coupling of subsystem impacts with aircraft sizing. The environment takes in a vector representing the subsystem architecture to be examined by the environment, the duty cycles for the aircraft control surfaces (as this study was limited in scope to varying the actuation systems), and the design mission profile for the current aircraft under examination. The outputs from this environment are the converged impacts of the architecture.

The environment consists of three main elements interacting together. These elements were selected based on the fact that, to perform the experiments, the modeling environment must capture the coupling of the subsystems impact and the aircraft (and engine core) sizing. Therefore, elements were chosen that enabled determination of the impact of the subsystems on aircraft sizing and, conversely, the impact of sizing on the subsystems. The first element contains physics-based models of the subsystems to determine their impacts on the engine and aircraft sizing (shaft power extraction). The second element is a function to determine the weight of the modeled subsystems (which also impacts the aircraft sizing). The third element contains an aircraft sizing environment integrated with an engine core sizing environment to capture the aircraft and engine size and the impacts of the subsystems on this. These elements pass the necessary data back and forth until they come to a converged solution. The overall

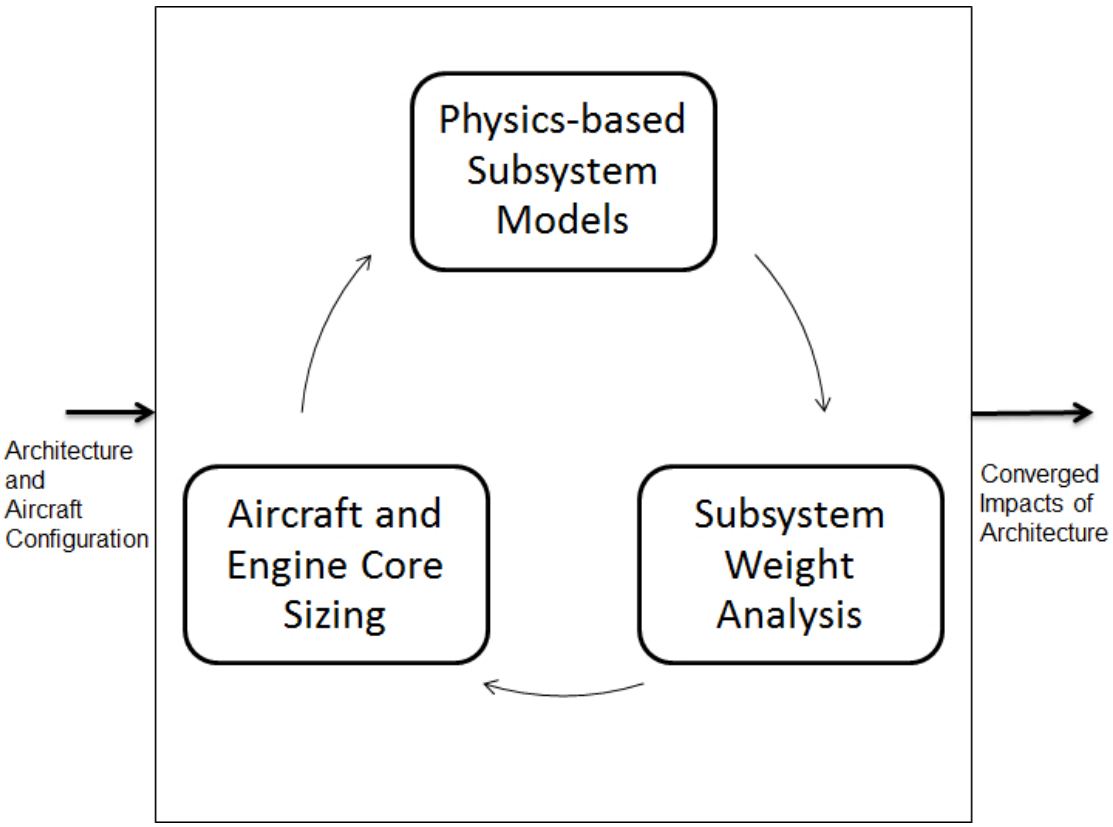

Figure 29: Modeling Environment Concept

concept of the data flow between the created and integrated modeling environment pieces is shown in Figure 30. This modeling environment utilized a subsystem modeling environment integrated with an aircraft and engine sizing algorithm to enable capturing the coupling between subsystem trades and aircraft sizing.

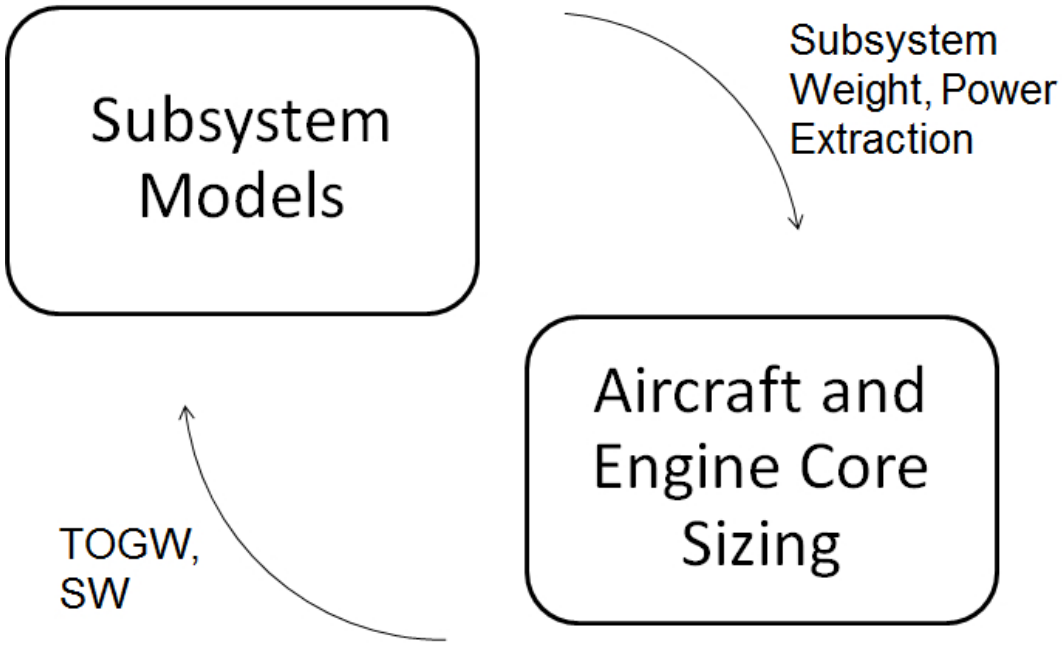

Figure 30: Modeling Environment Data Flow

5.6.2 Integrated Modeling Environment

An overview of the implementation of this modeling environment concept can be seen in Figure 31. The physics-based subsystem model was created in Simulink utilizing applicable physical relationships and available data. The Simulink model of the subsystems computes power extraction necessary to power the modeled subsystems. These values along with the weight of the architecture are passed to an integrated environment called the Environmental Design Space (EDS) (EDS is discussed in [77] and [76]). EDS calculates an aircraft and an engine core size and was utilized specifically because it captures the engine core sizing impacts and integrates this information

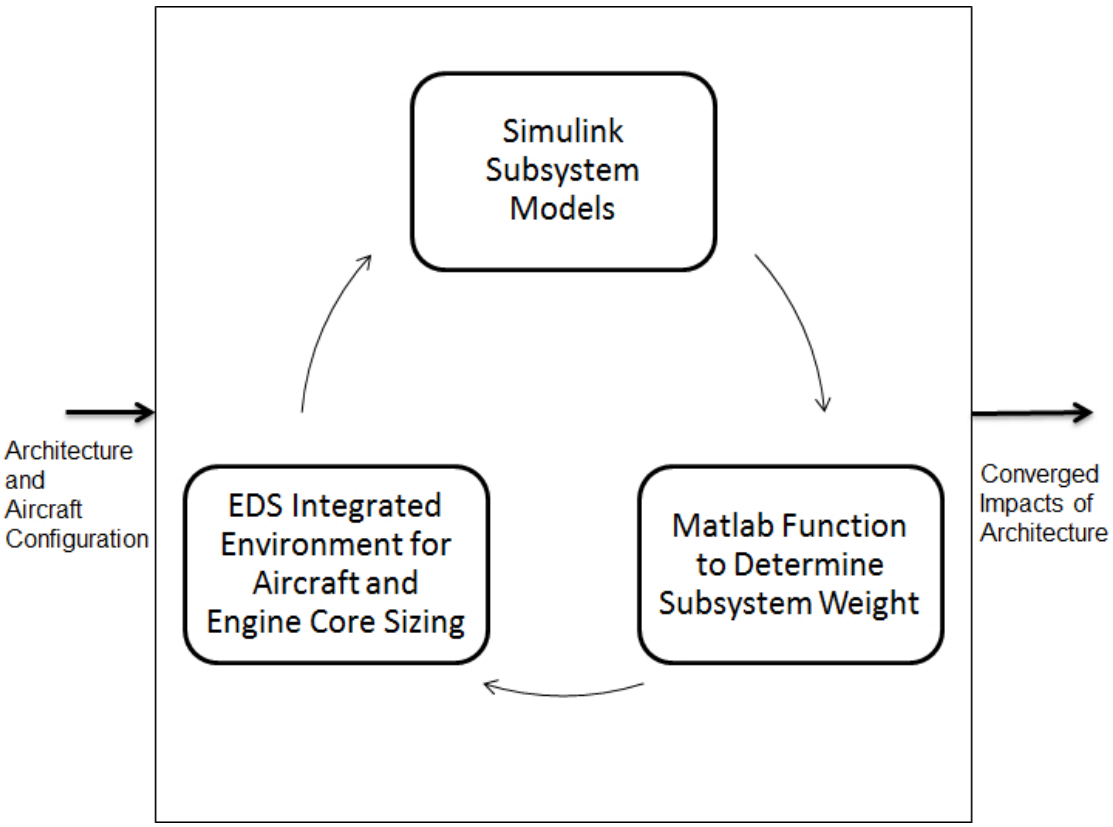

Figure 31: Overview of Modeling Environment

with aircraft sizing [77]. The aircraft characteristics are then passed back to Matlab/Simulink to size the actuators for the aircraft size calculated. This environment then runs until it converges.

These models and tools were integrated together in ModelCenter, which is a graphical integration and optimization tool [12]. ModelCenter calls the EDS environment and Matlab/Simulink. The wrapper that calls Matlab/Simulink takes in the TOGW, aircraft geometry, and the architecture selection. Matlab/Simulink then runs the Simulink model and additional Matlab code which determine the subsystem impacts (power extraction) and the subsystem weight. The power extraction and the subsystem weight are then passed into the EDS environment, which sizes the aircraft and engine core. EDS then passes TOGW to a converger, which passes an updated TOGW value to the Matlab Wrapper. EDS also passes aircraft geometric information

(fuselage length and wing span) to Matlab/Simulink.

5.6.3 Aircraft and Engine Sizing

The capturing of the aircraft and engine core sizing impacts of the subsystems are very important to the experiments. Therefore, Environmental Design Space provides a useful and calibrated tool to perform aircraft and engine core sizing [77] and [76]. Specifically, EDS has calibrated cases for existing transport aircraft [76]. The appropriate passenger class EDS model is used as a baseline for the sizing of that aircraft and engine. For the baseline aircraft size, the 150-passenger baseline model is utilized in EDS. This environment was adapted to capture the engine core and aircraft sizing impacts of the subsystem architectures. This core sizing impact is the reason that it was necessary to use EDS rather than merely an aircraft sizing code. Inputs to EDS include subsystem weight and power extraction maps. The outputs of TOGW, fuselage length, and wing span (or SW and AR) are then utilized by the integrated environment to iterate with the Simulink code and arrive at a converged solution. The integrated environment writes values of hydraulic system weight to capture the hydraulic weight and additional electrical weight due to adding EHAs and also two different power extraction variables (a baseline value and a variable turning on the power extraction map) to the Design of Experiments (DOE) input table in EDS. A power extraction map is then written to the MDP input file by the integrated environment, giving a power extraction vs altitude table to EDS. EDS then interpolates in this table based on the current altitude to determine the added power extraction above the constant baseline value (to capture the loads that were not modeled). The relationship used for power extraction by EDS is shown in equation (11).

$$P = (P_M \times 1) + P_B \tag{11}$$

The code in Matlab that runs the Simulink model post-processes the results of power extraction to find average values for different altitudes. The average is used instead of the maximum to minimize the impact of numerical spikes in the data caused by using larger simulation time steps. The baseline used for power extraction is determined as shown in equation (12) utilizing the original power extraction value used in EDS and the maximum power extraction value in the map (for the 150-passenger class aircraft) when all hydraulic actuation is utilized in order to account for loads and systems not modeled. It should be noted that the same value is utilized for the other passenger classes as they had the same previous baseline power extraction value in EDS.

The data from running the Matlab/Simulink model with the selection of all hydraulic was utilized to recalibrate the EDS model to ensure that the environment provides correct results. This calibration was performed for all three aircraft sizes using an existing EDS calibration code and capabilities to calibrate, utilizing the all-hydraulic actuation case. This calibration made the all-hydraulic case sized correctly to match the existing modeled aircraft within EDS.

$$P_B = P_{EDS} - \text{Max}(P_M) \tag{12}$$

5.6.4 Subsystem Modeling

The subsystem models were created to take in an architecture, aircraft geometry, and mission profile and determine the power extraction requirements of the subsystems to then be sent to the aircraft and engine sizing models. An overview of the algorithm used within this model is shown in Figure 32. This modeling concept was implemented in Simulink. The computations start with a hinge moment calculation for each control surface utilizing the mission profile and duty cycle (of deflection angle) for that surface. The hinge moments are then sent to models of actuators (a hydraulic

actuator and a EHA for each control surface). The hydraulic actuator calculates the hydraulic fluid flow rate needed for the actuator, and the EHA calculates the electrical power needed. The architecture is then enforced utilizing gains. Specifically, the power/flow for the non-utilized actuator is set to zero by multiplying by zero. The hydraulic flow rate and electrical power needed for the actuators are then propagated up through components such as electrical busses, electrical generators, hydraulic pumps, and the gear boxes, using conservation principles. While this power demand is being propagated upwards, additional electrical loads are added in to account for galley and IFE loads. The resulting value from propagating these power demands is the required shaft power extraction to power the modeled components.

Similar to the virtual iron bird from the POA study, this modeling environment uses inverse dynamics for modeling the aircraft systems [25]. Inverse dynamics switches the typical inputs and outputs to where the required movements of the control surfaces become inputs [25]. A screen shot of a sample inverse dynamics model is shown in Figure 33. The use of inverse dynamics in [25] enables the user to determine the power demand of aircraft subsystems. The model starts with a mission profile and desired control movement and calculates the energy demand for this control movement.

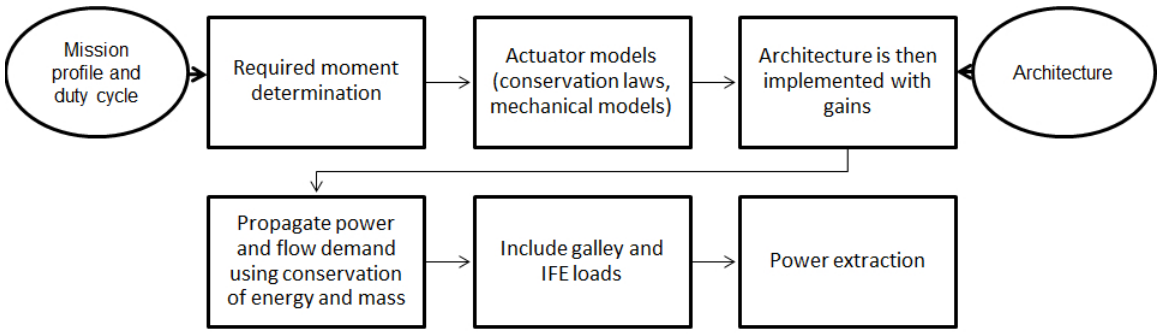

Figure 32: Subsystem Model Formulation

A screenshot of this modeling environment can be seen in Figure 34. The box on the left side labeled actuators contains the models and calculations for the mission

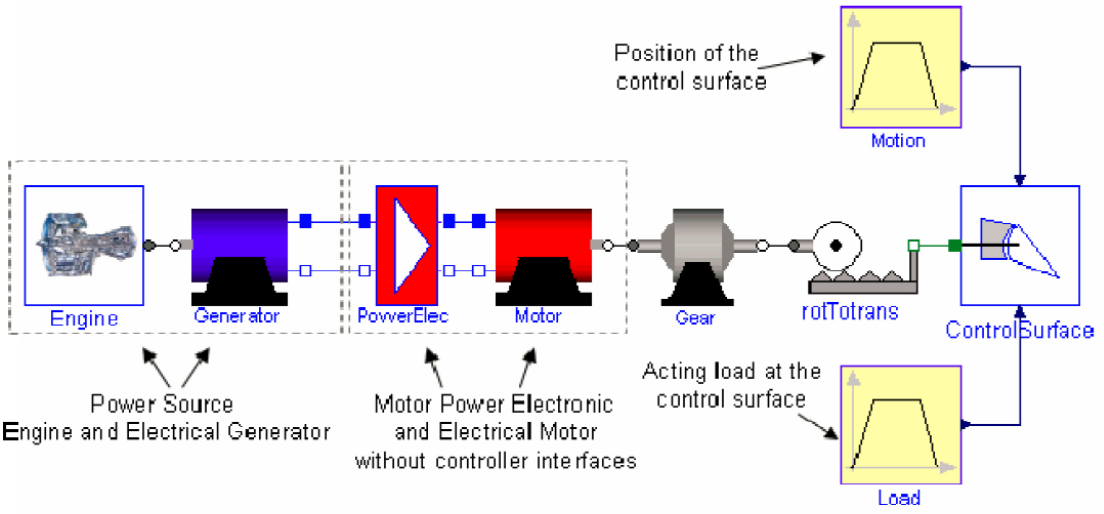

Figure 33: Example Inverse Dynamics Model [25]

profile, duty cycles, hinge moments, and actuators. The hydraulic flow demand from the actuators is then sent to the hydraulic pumps from the appropriate systems. These pumps are connected to the gearbox and to the electrical systems, as some pumps are electrically powered while others are powered from the shaft power extraction directly. The electrical power demand for all the EHAs is then sent to the electrical systems in which the efficiencies of the busses and generators are applied and the galley and IFE loads are included. The power demand from the engine driven hydraulic pumps is added to the demand from the electrical systems and passed through gearboxes to determine the shaft power extraction for the modeled systems.

5.6.4.1 Hinge Moment Determination

The box on the left side of Figure 34 labeled actuators contains the models and calculations for the mission profile, duty cycles, hinge moments, and actuators. The computations start with a lookup table containing the Mach Number and altitude as a function of time. The mission profile that is utilized is the design mission profile from Pace SysArc for the passenger class aircraft under consideration. Pace SysArc (Systems Architecture) is an aircraft preliminary design tool that allows the study of

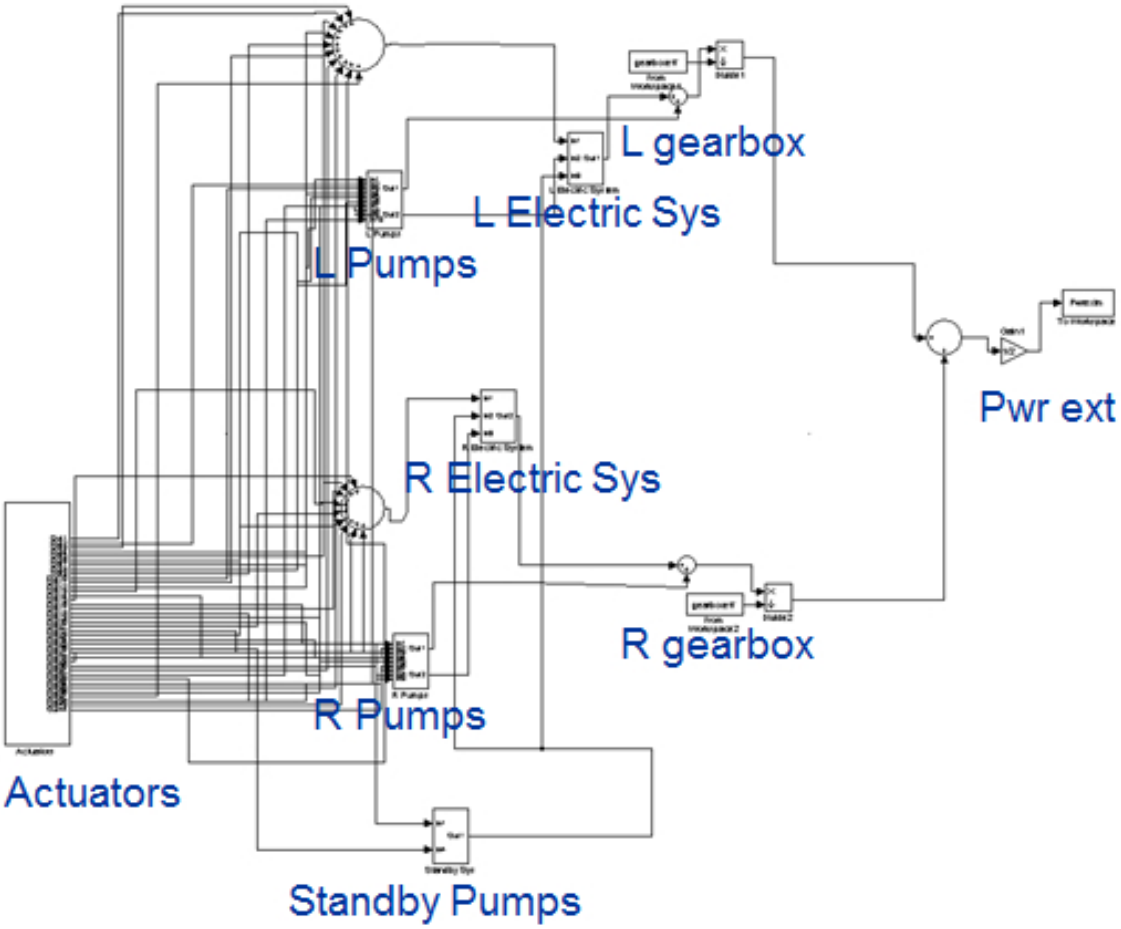

Figure 34: Subsystem Model

the internal systems [110]. This design mission for the 150-passenger class aircraft is illustrated in Figure 35. The duty cycle was created utilizing knowledge about the use of the different surfaces. The flaps and spoilers were made to deflect and stay deflected at maximum deflection towards the end of the flight, the landing gear was retracted once early in the flight, and the rest of the surfaces had duty cycles created based on data in the literature. Specifically, the duty cycles of the other surfaces were based on two sources. To determine accurate average power use, the use of an 80/20 duty cycle was found to be accurate in [78]. This duty cycle was 20 out of every 100 increments of time, the surface would be operating at the max and not operating the other 80 time increments [78]. This 80/20 approximation is captured using a pulse generator which is multiplied a sine wave function that used as its amplitude an assumed range of motion for the control surfaces which was based on the operating range of deflection angles for the surfaces on the Boeing 777 [9]. This sine wave also had a frequency corresponding to one deflection/second which was approximated from [124]. An illustration of such a duty cycle is shown in Figure 36. The Mach Number, altitude, and deflection angle are then sent to an embedded Matlab function that determines the current and maximum hinge moments. For the spoilers, the embedded Matlab function is written utilizing two different formulas for the hinge moment depending on whether the surface is deflected or not from [124] as seen in equation (13) and equation (14) from [124]. For the other control surfaces, the hinge moments are calculated utilizing codes that use Roskam's [122] formulation and data for trailing edge surface hinge moments. This code was adapted from code originally made for aircraft control surface modeling as discussed in [32] and [54]. For these calculations, the geometry of the control surfaces was estimated based on available data from Boeing [11] and Pace [110]. It should be noted that the contribution of angle of attack to the hinge moment was neglected when applying this formulation. To account for changing aircraft size, as this is integrated with a sizing

algorithm, the moment and maximum moment are scaled by the ratio of the aircraft size to a baseline size. The current size of the baseline aircraft is defined utilizing TOGW as the scaling parameter, which is related to wing area through W/S, which is held constant.

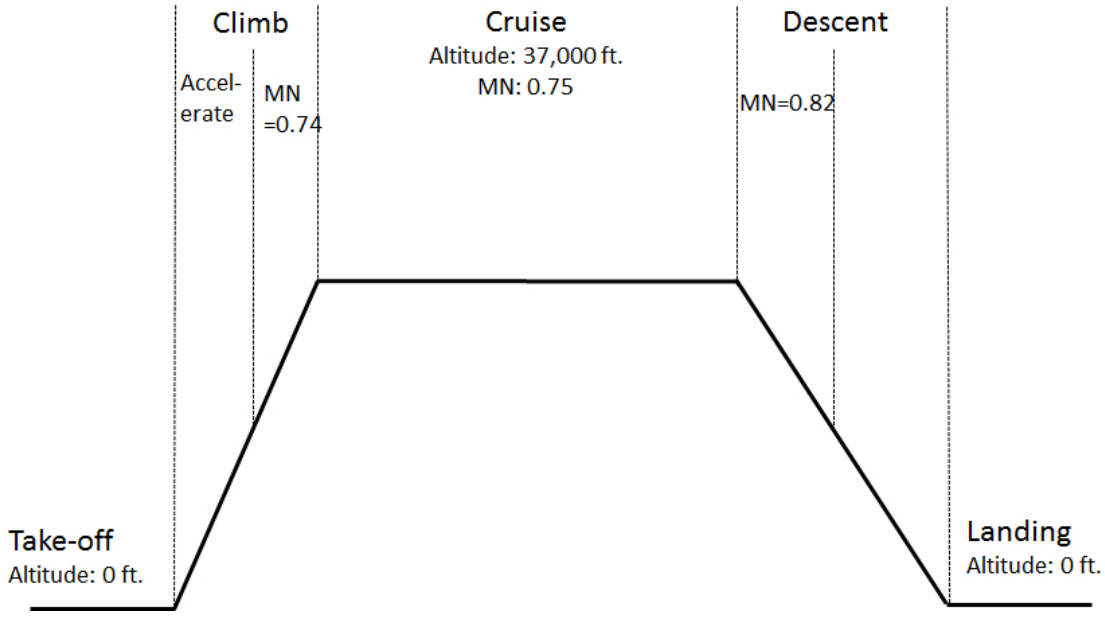

Figure 35: 150-Passenger Class Design Mission

When the spoiler is extended [124]:

$$M = C_D \times S_{sp} \times ((\sin(\delta))^2) \times (\rho \div 2) \times ((V)^2) \times (c \div 2) \tag{13}$$

When the spoiler is retracted [124]:

$$M = ((c \times S_{sp} \times W_N \times n \times 1.5) \div (c_{wsp} \times b \times \text{pi})) \times (1 - (2 \times y_{sp} \div b)^{2^{(}}0.5)) \tag{14}$$

The hinge moment, maximum hinge moment, and surface deflection angle then are utilized in models of a hydraulic actuator and an EHA for the control surface. The hydraulic actuator calculates the hydraulic fluid flow rate needed for the actuator, and the EHA calculates the electrical power needed. After the actuator models are run,

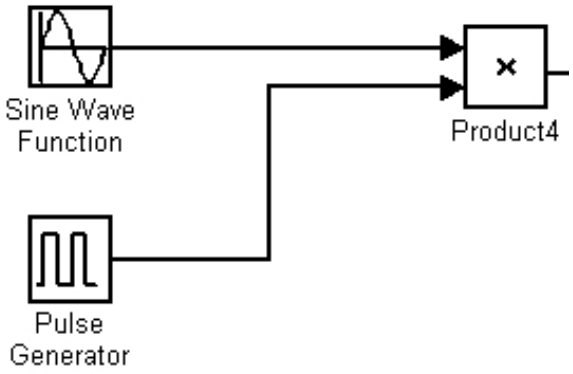

Figure 36: Example Duty Cycle

the architecture is then enforced, utilizing gains. Specifically, the power/flow for the non-utilized actuators are set to zero by multiplying by zero. Both the hydraulic and EHA models were created utilizing a parameter called a gearing ratio from [32]. As can be seen in equation (15) and equation (16), the gearing ratio (G) accounts for the mechanism between the actuator and the control surface and its geometry (formulas adapted from [32]). To enable accurate analysis, the value of the location of the hinge line on the control surfaces (except the spoilers, which use a different formulation) was then calibrated to bring the max force required from each actuator to be similar to A-320 control surface max force from [78], as seen in Table 3. For all the surfaces except the spoilers, the determined value of G was determined by the approximation of the surface angular velocity in [124] and the max piston velocity from the A-320 data [78], as seen in Table 3. It should be noted that one common value was used for G for these surfaces as they had similar angular and piston velocities. The value of G was then calibrated for the spoilers to the max actuator output force data from the A-320 [78].

$$G = \dot{\delta} \div (V_p) \tag{15}$$

Table 3: A-320 Actuator Characteristics [78]

Characteristic	Aileron	Spoiler	Elevator	Rudder
ActuatorStroke(mm)	44	84	60	110
NoLoadRate(mm/s)	90	100	60	110
Max.ExtendForce(kN)	48.0	44.9	27.7	44.3
Max.RetractForce(kN)	48.0	36.6	27.7	44.3

$$F_{req} = G \times M \tag{16}$$

5.6.4.2 Hydraulic Actuator Model

The hydraulic actuator model starts by determining the required piston area using the definition of gearing ratio and the fact that pressure is force per area as seen in equation (17) and equation (18). The maximum pressure is determined by assuming a 3000 psi hydraulic system.

$$G \times M = F_{req} = Pr \times A \tag{17}$$

$$A = (G \times (M_{\text{Max}})) \div (Pr_{\text{Max}}) \tag{18}$$

The piston velocity is then calculated by utilizing the definition of G and the duty cycle as shown in equation (19). This value is then limited by a maximum placed on this variable to make the value physical when the duty cycle has a discontinuity. This discontinuity arises from starting or stopping surface movement abruptly, which causes a large derivative in deflection angle at that point. This is a result of having the surface not continually deflecting and not having a smooth curve starting the deflection. To capture a smooth curve would require a small time step in the simulation, to have several points inside this start of deflection, which then significantly increases the simulation runtime to a value which is unfeasible for exploring

the architecture design space. To deal with this difficulty, non-smooth duty cycles are used. Then the values of the velocity and acceleration are limited at the discontinuities, and the power extraction values utilized are averages for different altitudes. This has the impact of averaging out these instantaneous transients. The values are limited by assuming a maximum velocity of approximately one range of deflection per second for the control surface based on [124]. The acceleration values are limited to achieving the maximum velocity in 0.5 second for all surfaces except the spoilers, which assumed 1 second instead. The mass and acceleration of the piston is seen to have a negligible impact. An assumed value of 2 kg is used for the piston mass.

$$V_p = \dot{\delta} \div G \tag{19}$$

The hydraulic flow rate is then determined by equations (20), (21), and (22) where the leakage is calculated utilizing [79] (this source contains the formulation utilized, where the leakage due to the pressure difference is considered with the coefficient of $2 * 10^{-}13m^3/(Pa * s)$ also from the source, and the leakage to the exterior is neglected),[31] (this source contains data on the B-737 hydraulic system including the system pressure), and [116] (this source contains a figure of pressure drops in the hydraulic system that was used to estimate deltaP in the hydraulic cylinder). This total flow rate is then sent to the appropriate hydraulic pumps in the Simulink model. It should be noted that the landing gear utilizes a different formulation from the rest of the actuators, and for the hydraulic landing gear actuation, this uses 10 GPM per actuator [1] (plus leakage) while the gear is being retracted and leakage alone when the gear is not being moved.

$$Q_{\text{surf}} = A \times V_p \tag{20}$$

$$Q_{\text{total}} = Q_{\text{surf}} + Q_{\text{leakage}} \tag{21}$$

$$Q_{\text{leakage}} = k \times Pr_{\text{loss}} \tag{22}$$

5.6.4.3 EHA Model

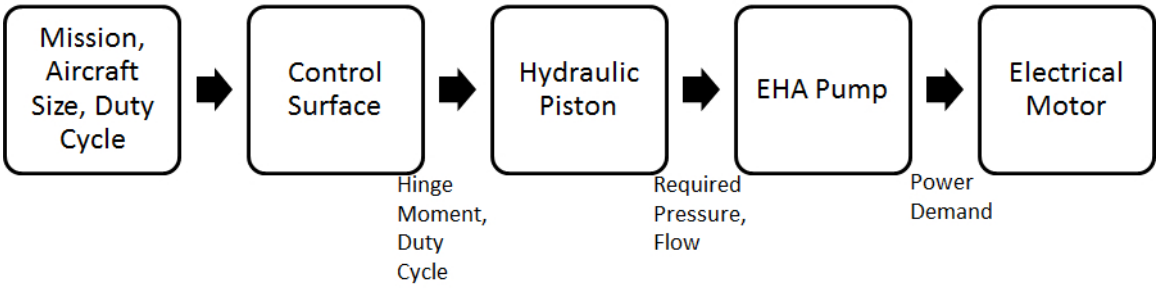

Figure 37: EHA Model

The overall flow of the EHA model is shown in Figure 37. The EHA utilizes the same force balance to find piston area, piston velocity, and flowrate calculations as the hydraulic actuator with one exception. Specifically, the pressure utilized for the leakage which is calculated as shown below. The same max velocity and acceleration limits are utilized to limit any numerical issues while having a runtime that enables architecture trades. The cylinder pressure is calculated as shown in equation (23). The mass and acceleration of the piston is seen to have a negligible impact. An assumed value of 2 kg is used for the piston mass. This cylinder pressure is then utilized to determine the pump output power (pressure*flowrate) as shown in equation (24). The input power to the pump is then calculated utilizing the output power and an

efficiency curve based on [137], as shown in equation (25). Specifically, this source [137], contains plots of overall efficiency for different pumps against flow rate, generally being at 0 at 0 GPM and maximum of around 0.9 at maximum flow rate. This trend is approximated in the model by a linear relationship between the percent of maximum flow and the efficiency. This relationship utilized 0.05 at 0 flow and 0.9 at maximum flow as the end points of this curve based off of the source [137]. This power is then scaled by an efficiency value to account for the motor efficiency [3]. The efficiency value used for the electrical motors is a constant of 0.9. The electrical motor efficiency is approximated based on tables in [3] containing efficiency for different motor speeds, sizes, and load levels. In this data, most of the efficiency values are approximately 0.9 [3]. This electrical power demand is then sent to the appropriate electrical system. It should be noted that the landing gear utilizes a different formulation from the rest of the actuators, for the landing gear EHA this formulation uses a flow rate of 10 GPM per actuator [1] (plus leakage) while the gear is being retracted and just leakage when the gear is not being moved and the pressure in the actuator is always 3000 psi (and the pump is assumed to be operating at its max efficiency for the landing gear).

$$Pr_{\text{cyl}} = (G \times M + (m_p) \times \alpha) \div A \tag{23}$$

$$P_{\text{out}} = Pr_{\text{cyl}} \times Q_{\text{total}} \tag{24}$$

$$P_{\text{in}} = P_{\text{out}} \div \eta \tag{25}$$

5.6.4.4 Hydraulic Pump Model

The hydraulic flow rates are propagated up to the pumps that power the hydraulic system that the individual surfaces are attached to. These flows are combined utilizing the conservation of mass to give the flow rate that the pumps from that system must provide. The flow is then divided between the two (or one in the case of the standby system) pumps on the system by the ratio of their capacities. The pump output power is calculated from the system pressure and flow as listed in equation (26). This output power is then converted into pump input power by utilizing the pump efficiency curve based on [137] that is utilized for the EHA pumps, as shown in equation (27). The pump efficiency is a function of flow rate as can be seen in Figure 52 [137]. The power demand from the engine-driven pump is sent to the gearbox. The power demand for the electrical powered pump is then scaled by an efficiency for the electrical motor based on [3]. Figure 38 shows a motor efficiency curve from [3]. The selected efficiency value came from this curve, the typical operating range, and the tabulated efficiency values from the same source [3]. This electrical demand is then sent to the appropriate electrical system.

$$P_{\text{out}} = Pr \times Q \tag{26}$$

$$P_{\text{in}} = P_{\text{out}} \div \eta \tag{27}$$

5.6.4.5 Power Demand Propagation

The overall power extraction in the case of EHAs is determined as shown in Figure 39 and for the case of hydraulic actuation as shown in Figure 40. The power required for the EHAs connected to each electrical system is combined with the electrical demand from the electrical pumps connected to that electrical system. This is then combined with an IFE load of 100 W/pax, scaled by the number of pax, which is based off data

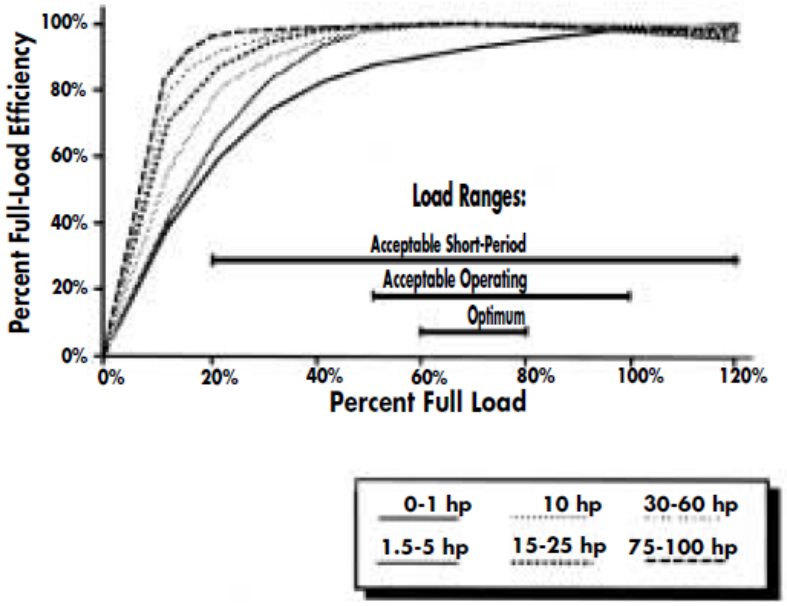

Figure 38: Electric Motor Efficiency [3]

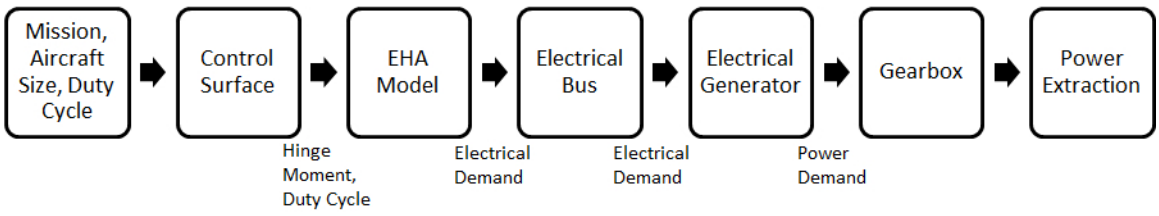

Figure 39: EHA Data Flow

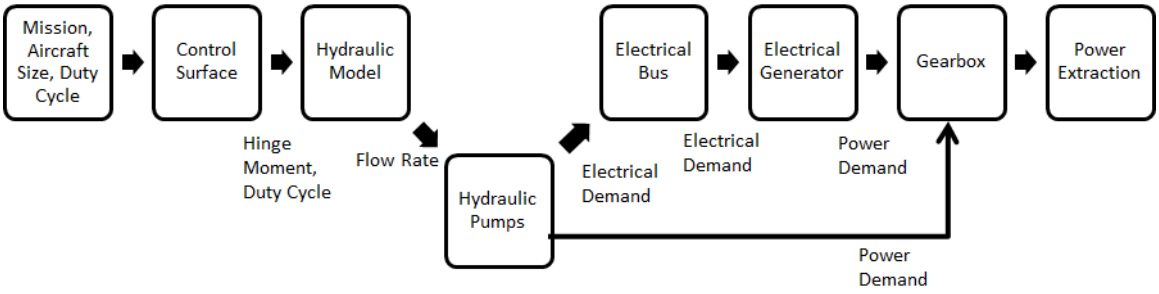

Figure 40: Hydraulic Actuation Data Flow

in [93]. Specifically, Moir [93] states that on the modern Airbus A-380, IFE loads are approximately 100 Watts per passenger seat. This power demand is also combined with a galley load [58] as a function of simulation time, which is also scaled by the number of passengers. This galley load schedule, seen in Figure 41, came from [58], and was created for a more electrical aircraft study. The resulting electrical power demand from the system is then scaled by efficiencies of the busses [36] and [21] and generators [21]. The bus efficiency is based on Armstrong's [21] and de Tenorio's [36] dissertations. Armstrong utilized a constant bus efficiency of 0.98 [21]. de Tenorio's [36] work utilized constant bus efficiencies of between 0.97 and 0.99, depending on the type of bus. Based on these sources, a constant bus efficiency of 0.98 is utilized in the model. Armstrong also had data in his dissertation for generator efficiency [21]. Specifically, Armstrong [21] had a generator efficiency relationship of efficiency as a function of the percent of max load and speed that the generator is operating at. (The load can be seen to have a dominating effect in his data [21]). As seen in Figure 42, the generator efficiency varies between 0.95 and 0.8 [21]. As the efficiency

depends on the transients of electrical loads that are not modeled and captured in this analysis, the conservative value of the lowest efficiency of 0.8 from Armstrong's work is utilized in the modeling as the generator efficiency [21].

The generator power demands from each engine are then combined with the engine-driven hydraulic pump power demands. This gives the power drawn off of the gearbox for each engine for the systems modeled. These values are then scaled up by an efficiency to account for the efficiency of the gearboxes [19] to get the shaft power extraction from each engine. The gearbox efficiency is treated as a constant of 0.98 based on data in [19] in which the plotted data showed the efficiency to be close to 0.98. This data can be seen in Figure 43 (the gearbox efficiency as a function of oil and oil temperature) and Figure 44. The values of total power extraction are calculated for each engine and so are then averaged for the given time step. The resulting value of power extraction is the output for a given time step from the Simulink model. An example of this output can be seen in Figure 45 for the case of all hydraulic actuation for a 150-passenger class aircraft.

Load category	Flight phase											
	Loading		Engine start[a]		Taxi		Takeoff and climb		Cruise		Descent, hold, and land	
	kVA	Power factor	kVA	Power factor	kVA	Power factor	kVA	Power factor	kVA	Power factor	kVA	Power factor
Essential (includes main bus and flight controls)	29.7	0.92	38.1	0.91	56.5	0.91	80.3	0.91	80.3	0.91	74.9	0.91
Utility (includes environmental control system)	133.5	.85	----	-----	129.1	.85	130.4	.85	87.2	.85	87.8	.85
Galley	37.0	1.0	----	-----	50.8	.99	47.8	.99	57.8	.99	13.2	.95
Total	195.7	.91	38.1	.91	233.3	.91	254.7	.91	222.4	.92	175.3	.89

Figure 41: More Electric Aircraft Loads [58]

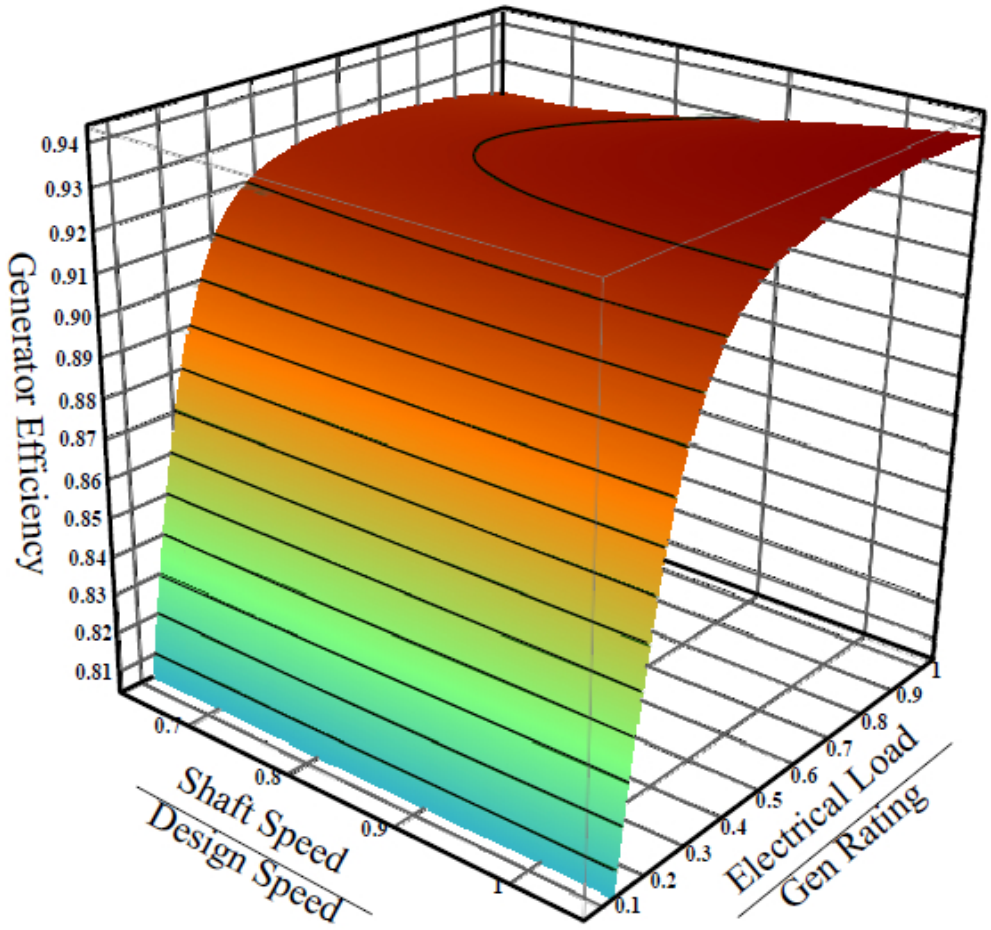

Figure 42: Generator Efficiency [21]

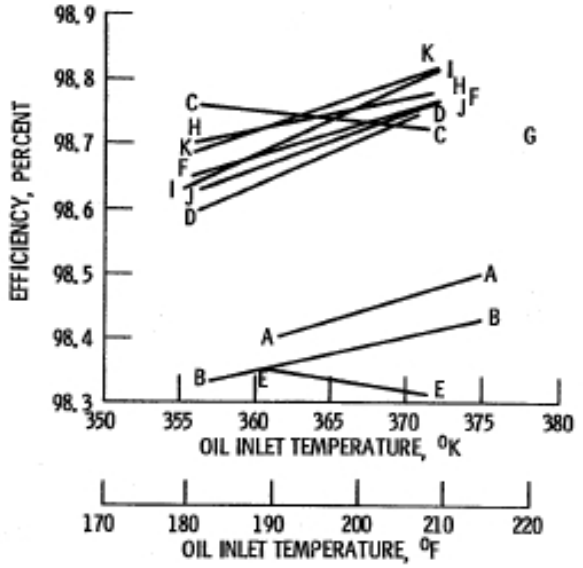

Figure 43: Gearbox Efficiency Data [19]

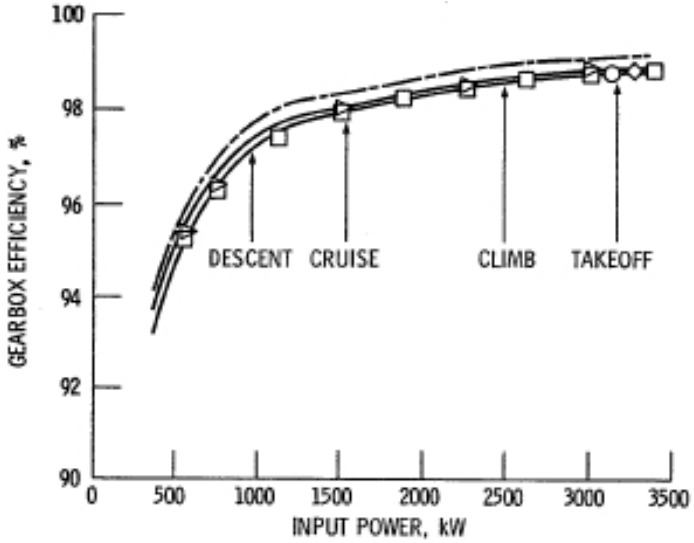

Figure 44: Gearbox Power Efficiency [19]

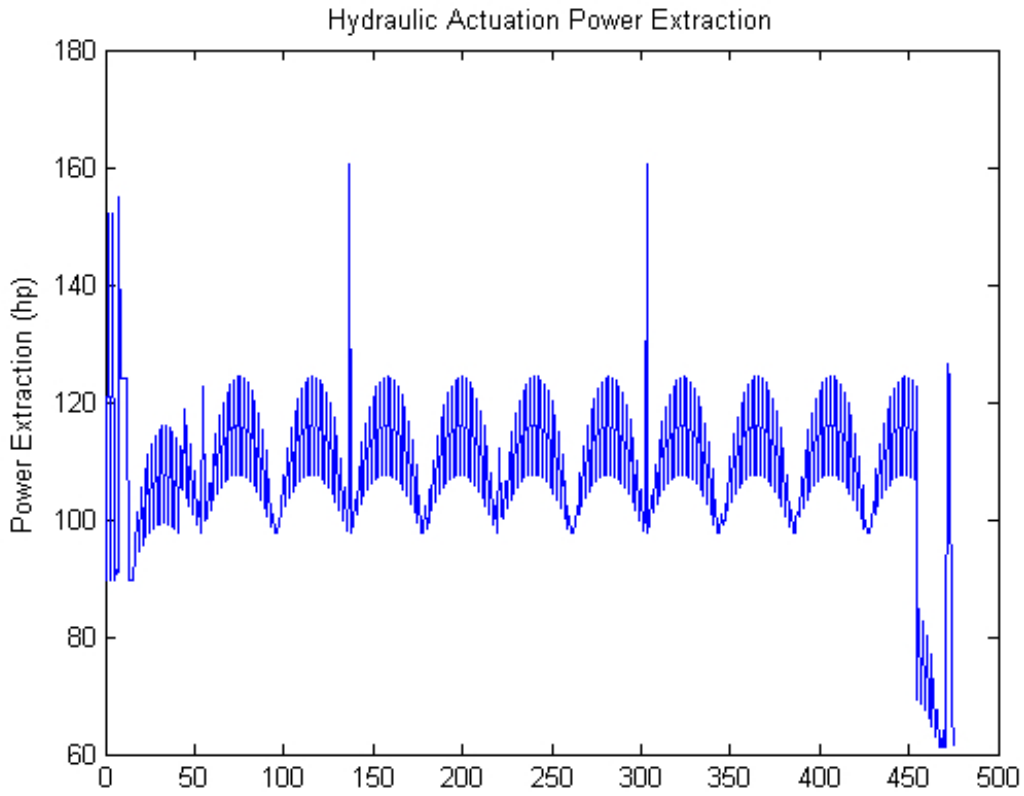

Figure 45: Example Power Extraction Output

5.6.4.6 Subsystem Weight Analysis

The weights of the modeled subsystems are calculated by combining the weights of the examined components and distribution systems required by the architecture under study. For the distribution weight, functions were created to size the different required wires and pipes. These algorithms take in the length of the line and the required capacity (power or hydraulic flow rate) and determine the weight of each individual wire and pipe.

5.6.4.7 Electrical Distribution Weight

The electrical wire sizing is based off [7] which had a table of the current capacity of different wire gauges as shown in Table 4. The needed current is calculated from the required power and the system voltage. This leads to a current value that is used to look up in this table the necessary wire size. This wire size combined with the length and the density of the wire gives the weight of the wires. The wire density was derived from [33] assuming TKT wire, the determined value was updated to account for insulation utilizing insulation density data from [39]. The wire lengths are approximated by measuring an 3-view CAD drawing from Boeing for the baseline class craft under study and then the wire lengths are scaled with fuselage length and/or wing span depending on the location [11]). The wire sizing algorithm is applied to wires for each EHA in the architecture currently being examined. These wires are run from electrical busses in the avionics bay to the EHAs at the control surfaces. The weight of these is combined with the increase in wire weight between the electrical buses and the generators to give the increase in wire weight due to utilizing EHAs. This increased wire weight is calculated by sizing the wire with a baseline generator size and with the added power demand for the EHAs and taking the delta in weight. The baseline generator size is 125 kVA for the baseline aircraft, and for the other aircraft sizes this value is updated based on data in [91].

Table 4: Wire Capacity Data [7]

Wire size(AWG)	Maximum Current (amps)	Resistance (ohms/ft)
24	4	0.03
22	5	0.016
20	7	0.01
18	9	0.006
16	11	0.005
14	14	0.003
12	19	0.002
10	26	0.0012
8	57	0.0007
6	76	0.0004

5.6.4.8 Hydraulic Distribution Weight

The hydraulic pipe sizing algorithm is based on [116] which includes formulas for the inner diameter of the pipe as a function of the acceptable pressure loss across the pipe (which was approximated from another figure in that paper, seen in Figure 46, and the aircraft geometry of the 737-800 [11]), the length of the lines (which were approximated by measuring a 3-view CAD drawing from Boeing for the baseline class craft under study and then the pipe lengths are scaled with fuselage length and/or wing span [11]), the amount of laminar flow (it is assumed to be turbulent flow in the pipe for this work), and the properties of the fluid which are from the assumed fluid in [126]. The formula utilized to determine the diameter can be seen in equation (28) and came from [116]. The required inner diameter is rounded up to the next biggest size of pipe used in the 737-800 as is documented in [4] as seen in Figure 47. The density of the materials listed in [4] combined with the pipe size and length gives its weight [22], [23]. The dry and wet weights of the pipes are calculated based off of the architecture and max flow for the hydraulic actuators. The hydraulic piping weight is the total pipe wet weight plus a factor which is from [116] to account for other things such as fittings. Specifically, there is a factor of 10 percent of the wet weight of the pipes for support clamps and 20 percent of the dry weight of the pipes for end

fittings and tube nuts [116].

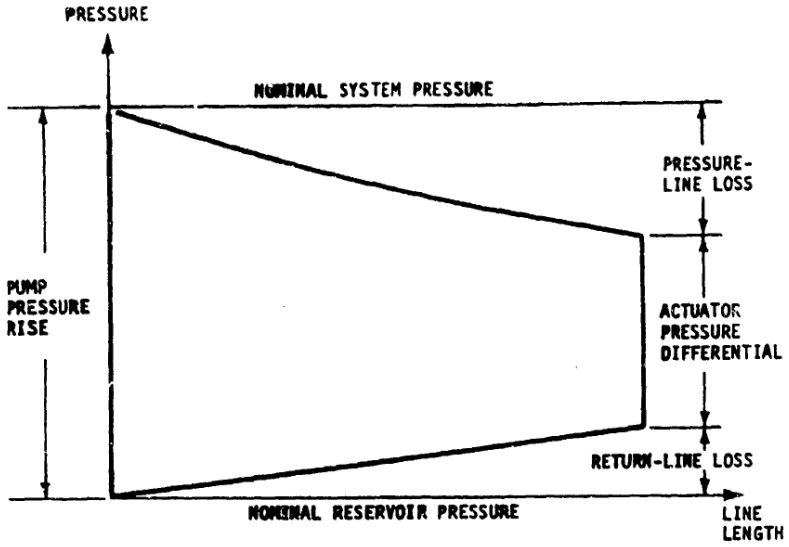

Figure 46: Hydraulic System Pressure Cycle [116]

$$\Delta Pr = 0.0135 \times l \times f \times SG \times (Q_{GPM})^2 \div ((D)^5) \tag{28}$$

High Pressure
Material Specification: Ti 3Al 2.5V Titanium alloy per AMS4945
Diameters/Wall Thicknesses: 0.25/0.016 in (6.35/0.406 mm), 0.375/0.020 in (9.53/0.508 mm), 0.50/0.026 in (12.7/0.660 mm), 0.625/0.033 in (15.875/0.838 mm), 0.75/0.039 in (19.05/0.991 mm), 1.00/0.052 in (25.4/1.321 mm)

Low Pressure Lines
Material Specification: 6061-T6 Aluminum alloy per AMS4083
Diameters/Wall Thicknesses: 0.25/0.035 in (6.35/0.889 mm), 0.375/0.035 in (9.53/0.889 mm), 0.50/0.035 in (12.7/0.889 mm), 0.625/0.035 in (15.875/0.889 mm), 0.75/0.035 in (19.05/0.889 mm), 1.00/0.035 in (25.4/0.889 mm)

Figure 47: Boeing 737 Hydraulic Line Data [4]

5.6.5 Subsystem Component Weights

The component weights are calculated primarily from their required capacity and using a value for capacity/wt derived from literature. The actuator capacities are determined by running the model and processing saved data from the model. The capacity per weight for the hydraulic actuators are based on the ratio of 7 lb/kN

for two hydraulic actuators in [93] (which had values of 6.65 and 7.2). The capacity per weight for the EHAs are based on the ratio of 3 kN/lb for the actuator in [99]. This value is also in the range of other EHAs examined: 3.9 [112] and 2.2 [47]. The pump capacities are created by subtracting deltas in flow rate based on the selected architecture from the pump capacities listed in [4]. Specifically, the pump capacity is determined by the baseline size (from [4]) for the current aircraft and reducing the size by the sizing flow rates of actuators that are switched to EHAs in a given architecture, while ensuring that the pump capacity is above the required amount for the remaining actuators. For engine driven pumps, the pump weight per capacity is based on [4], which contains the pump capacities for the Boeing 737 in GPM, and [137], which contains weight and capacity in GPM data for different engine driven pumps used to find an approximate constant value of 0.37 lb/GPM for pumps around the capacity of the B-737. The electrically powered pump weight per capacity is based on [136], which had the electrically powered pump for the Boeing 737 and is used to determine a value of 6.3 lb/GPM. The reservoir capacity is determined by [4]. The reservoir weight per capacity is based on the assumed fluid density in [126]. The delta in generator capacity is determined by the amount of power required from the EHA's. The generator weight per capacity is based on [16], which contains, as shown in Figure 48, the weight per capacity as a function of capacity, which combined with the chosen baseline capacity from [91] gives an approximate value of 0.55 lb/kVA, a value which is used for all aircraft. Again, the baseline aircraft generator capacity is approximated at 125 kVA for the baseline aircraft, and, for the other aircraft sizes, this value is updated based on data in [91].

The weight of any hydraulic components and distribution is combined with additional weight added from adding EHAs to the electrical system, and this value is sent to the hydraulic weight input parameter in the aircraft sizing environment.

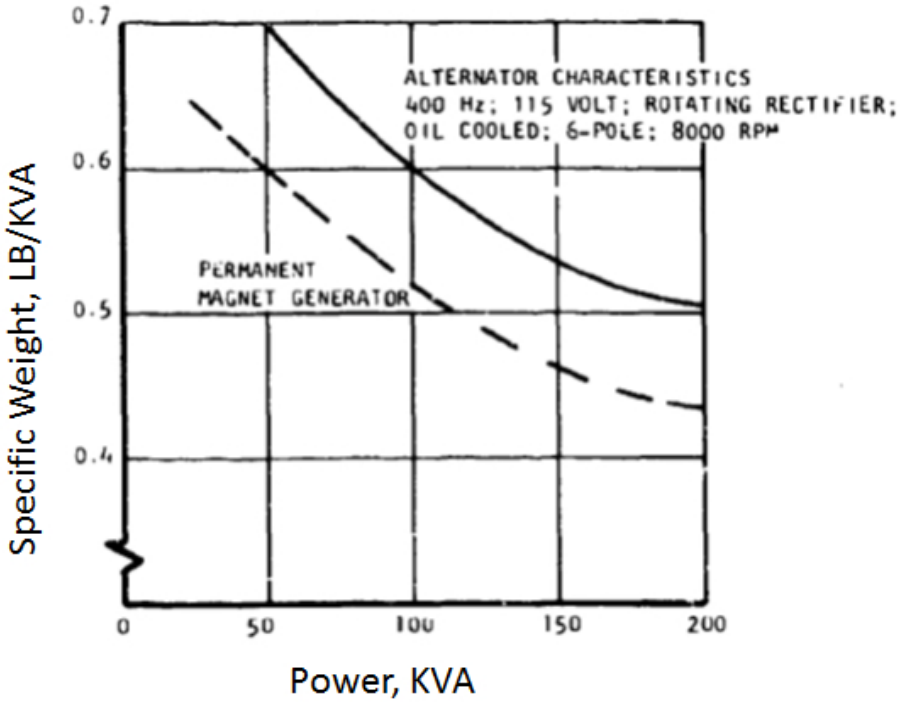

Figure 48: Generator Weight Data adapted from [16]

CHAPTER VI

ANALYSIS RESULTS AND HYPOTHESIS VALIDATION

6.1 Experiment 1

To review, **Hypothesis 1** states the following: If the impact of the coupling between aircraft sizing and architecture impacts is quantified, then this coupling will be found to be significant.

For Experiment 1, the modeling environment discussed in the previous chapter was leveraged to examine the extent of this coupling. This environment for Experiment 1 was created based on a 150-passenger class aircraft as was discussed in the section on the model. This passenger class was selected as the test aircraft configuration as described in the test aircraft configuration selection section. The Matlab/Simulink modeling environment was run to determine the all-hydraulic actuation subsystem weight and power extraction values. The 150-passenger class EDS model was recalibrated utilizing these values. This was done utilizing the existing calibration codes and capabilities within EDS. Then, the newly calibrated and integrated environment of EDS and Matlab/Simulink, which is discussed in the section on the modeling, was utilized to examine the extent of the coupling between aircraft sizing and architecture impacts. This exploration was done utilizing a full factorial DOE varying each group of control surfaces (including flaps, elevators, rudder, aileron, and landing gear) from being hydraulically powered to being powered by EHAs as described in the test case section. The converged values of metrics of interest, such as TOGW, for each architecture were then saved for analysis. Finally, the results were analyzed to examine the coupling.

The converged values of subsystem weight are plotted against TOGW in Figure 49.

There appears to be a definite trend in this data, an almost linear relationship between TOGW and subsystem weight. This appears to indicate that there may be significant coupling between these two variables. The lowest TOGW values for the converged cases led to the determination of the top three candidates for the subsystem architecture for the selected configuration. These top three candidates were further explored in Experiment 3a. These candidates were the use of all EHAs, the use of all hydraulic actuation, and a hybrid system, in which the elevators were powered by EHAs and the rest of the control surfaces were powered by hydraulic actuators. The difference between the top and bottom architectures in TOGW was 2627 pounds, or approximately 1.51 percent of the TOGW. Given that Roskam [121] states that the range to expect for the total weight of the actuation system is approximately 0.6 to 1.2 percent of TOGW, the difference in converged TOGW by varying this system is significant. It should be noted that the all-EHA case was slightly outside the approximate linear trend, which is to be expected as it is a different technology. Also, the highlighted cases that had hydraulic actuators on the ailerons, spoilers, and rudder were slightly below the overall trend; this is likely due partially to the fact that the hydraulic actuators were lighter than the EHAs for the modeled surfaces.

The converged values of maximum power extraction from inside the power extraction map are plotted against TOGW in Figure 50. There appears to be a trend in this data, a slightly negative relationship between TOGW and maximum power extraction. This outcome may not be what engineering judgment at first glance would indicate. However, this trend does exist and is determined by the particular architectures examined. Within these architectures, the lower power extraction values are at higher subsystem weights as can be seen in Figure 51. As was already suggested in Figure 49, it will be shown that significant coupling exists between TOGW and subsystem weight which, for the ranges of data explored with these architectures, appears to dominate the power extraction impact on TOGW, leading to this slightly

negative trend. This trend can be further seen in some of the results in Experiment 3a for selected architectures and in the correlation and covariance values for this experiment, which are shown later in this section. It should be noted that there was one point that did not appear to fit the overall trend; this point was the use of all EHAs, as it was based entirely on the use of a different technology. The impact of the weight of the subsystem dominating the impact of the power use implies that the less efficient lighter architectures lead to the minimum TOGW, which is an interesting finding.

The fact that, within the examined architectures, the more efficient architectures are heavier is logical as these architectures are hybrid architectures. The hybrid architectures still have the weight of hydraulic pumps, pipes, and the added electrical weights associated with the use of EHAs, making these architectures heavier. The hybrid architectures are also more energy efficient because of the difference in the hydraulic pump sizing and, therefore, the efficiency. The hydraulic architectures are often operating at the lower values of pump efficiency as they are not all operating at maximum flow rate. This situation occurs because the pump efficiency is a function of flow rate as can be seen in Figure 52 [137]. When the pump is made smaller because some actuators are electrically powered, it increases the corresponding efficiency at which lower flow rates operate. Also, the EHA has a low maximum overall efficiency as modeled due to losses within the generator, busses, and EHA motor. As a result, the hybrid architectures are more efficient but heavier.

The converged values of average power extraction from inside the power extraction map are plotted against TOGW in Figure 53. As with the maximum power extraction, there appears to be a modest trend in this data, with a slightly negative relationship between TOGW and average power extraction. This may be counter-intuitive; however, this trend is again due to the particular architectures examined.

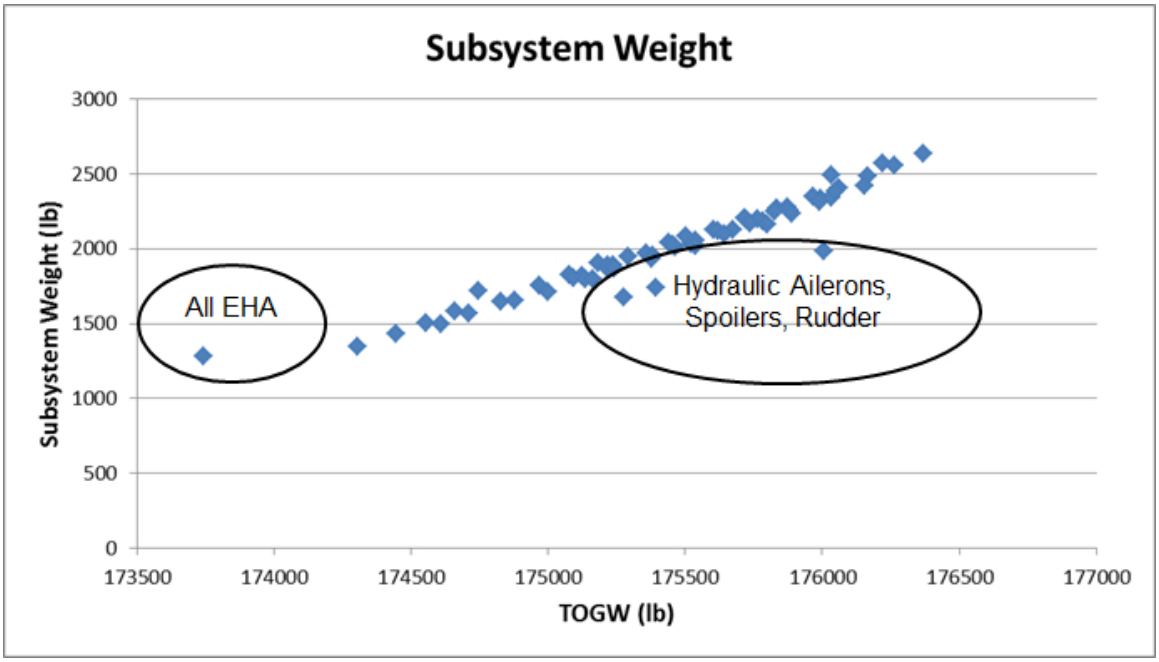

Figure 49: 150-Passenger Class Subsystem Weight

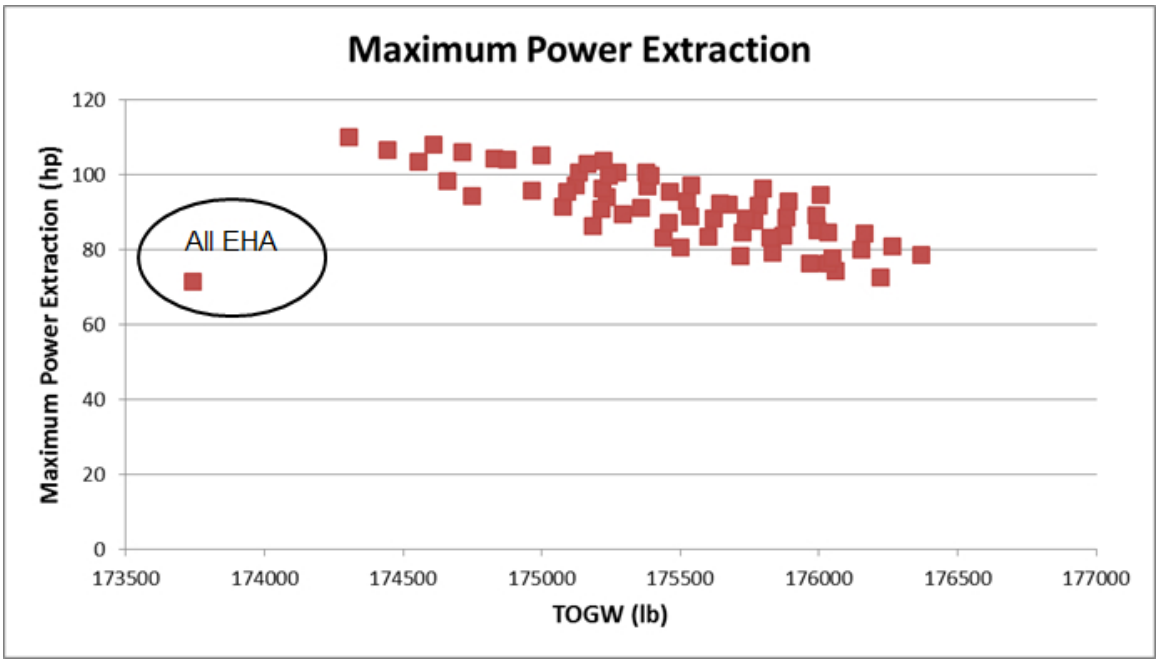

Figure 50: 150-Passenger Class Maximum Power Extraction

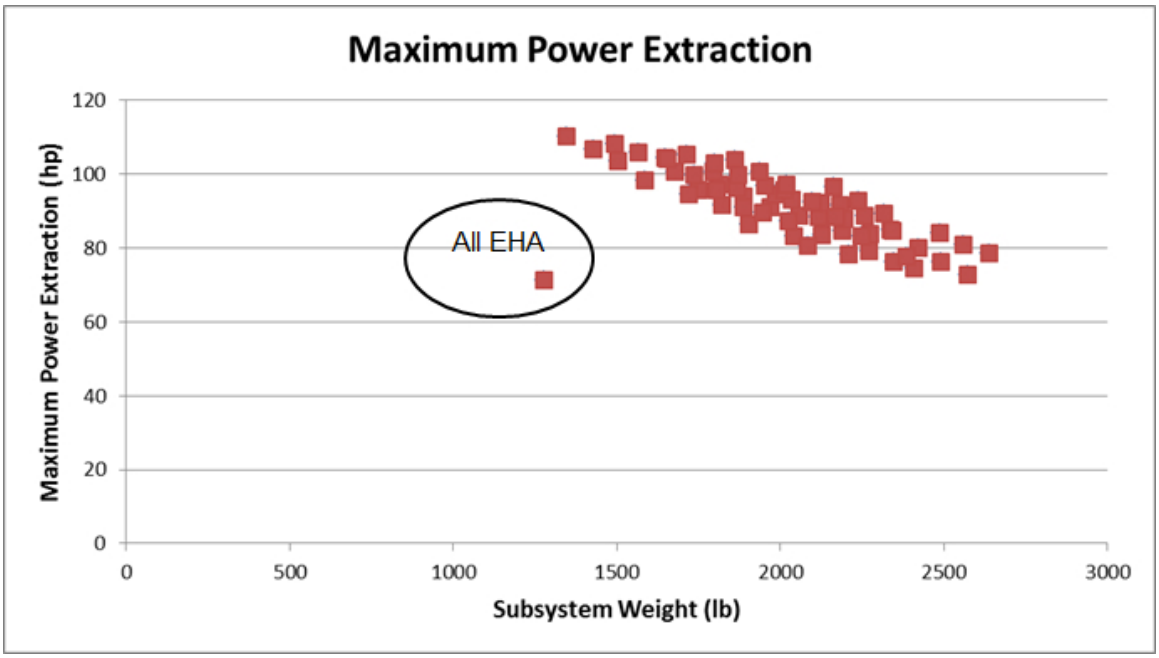

Figure 51: 150-Passenger Class Maximum Power Extraction vs Subsystem Weight

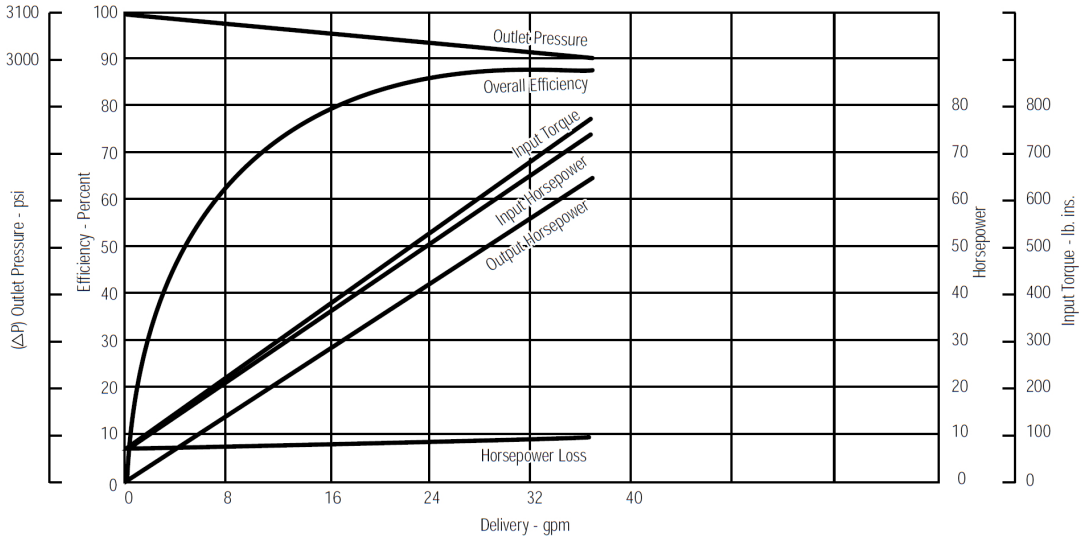

Figure 52: Pump Efficiency [137]

Within these architectures, the lower power extraction values are at higher subsystem weights as can be seen in Figure 54. As was already suggested in Figure 49, it will be shown that significant coupling exists between TOGW and subsystem weight which, for the ranges of data explored with these architectures, appears to dominate the power extraction impact on TOGW, leading to this slightly negative trend. This trend can be further seen in the results of Experiment 3a for the selected architectures and in the correlation and covariance values for this experiment. One point did not again fit the overall trend, the all-EHAs case as it was based entirely on a different technology.

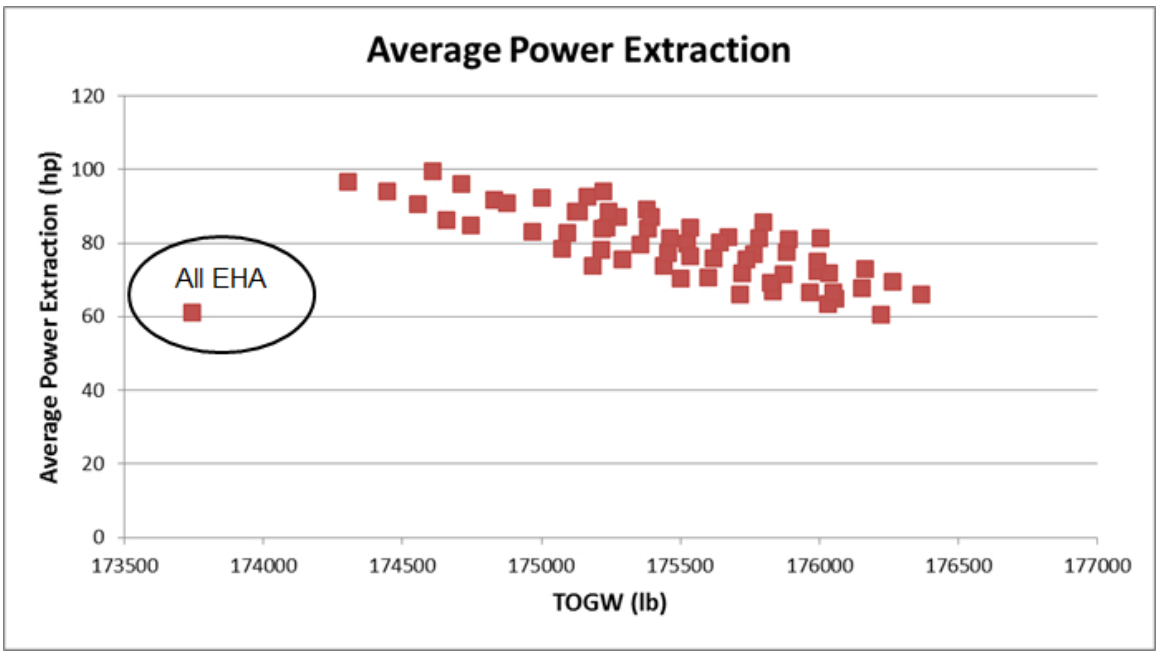

Figure 53: 150-Passenger Class Average Power Extraction

Figure 55 shows a contour plot of the examined design space in Experiment 1 and illustrates further the point that the heavier aircraft can be seen to have better power extraction. This point is better illustrated by the removal of the all EHA case (as it is outside the examined trends because it is a different technology) from the diagram as shown in Figure 56. It should be further noted that Figures 55 and 56 illustrate the design space examined and possibly some of the internal trades and

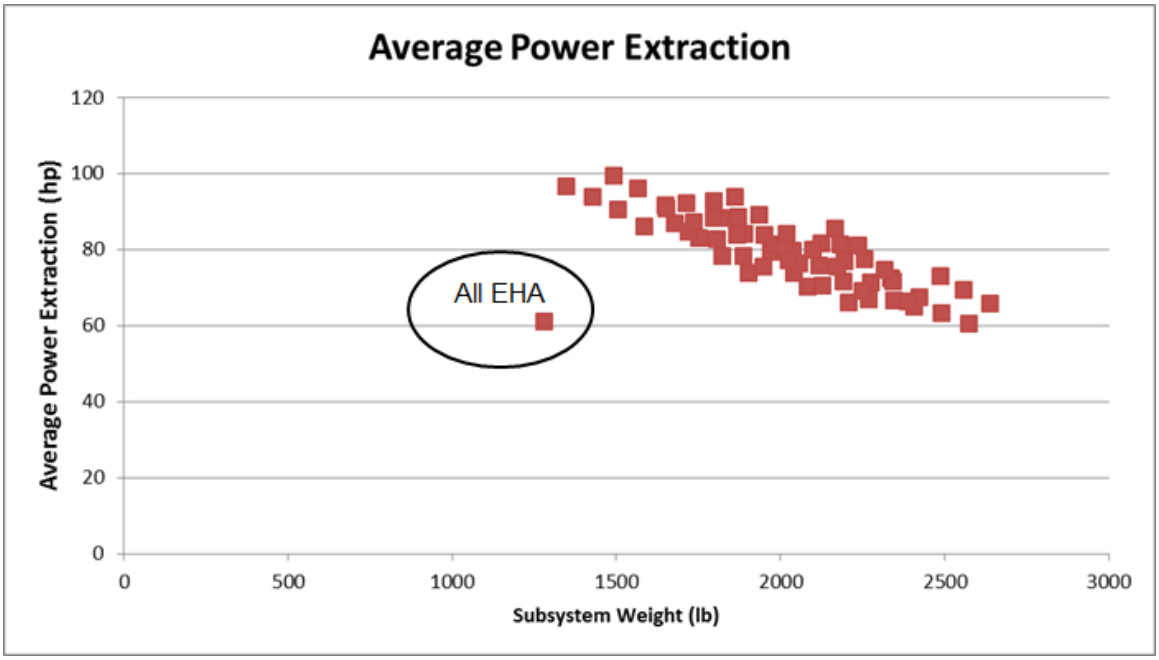

Figure 54: 150-Passenger Class Average Power Extraction vs Subsystem Weight

possible constraints within this design space.

Another way to visualize trends in the Experiment 1 data is to utilize a multivariate scatter plot such as the plot shown in Figure 57. This plot shows many of the same trends previously discussed in this section, such as TOGW increasing with subsystem weight and power extraction decreasing with subsystem weight. The designs within this plot were then filtered to include only the lower TOGW (175,000 lb or less) designs. The filtered designs are plotted in Figure 58, showing that the lowest TOGW designs have the lowest subsystem weight values, which can be seen to dominate the impact of the power extraction.

To further examine and characterize the relationships between aircraft size and subsystem parameters, Response Surface Equations (RSEs) were fit to the data. As discussed in the chapter on MAIA, Mavris, DeLaurentis, Bandte, and Hale [84] presented an approach that utilizes metamodels (regression models of computer programs [84]). Also, as discussed in the Chapter on MAIA, RSM is a method that can be utilized in the creation of such metamodels [88]. The parameters or metrics that the

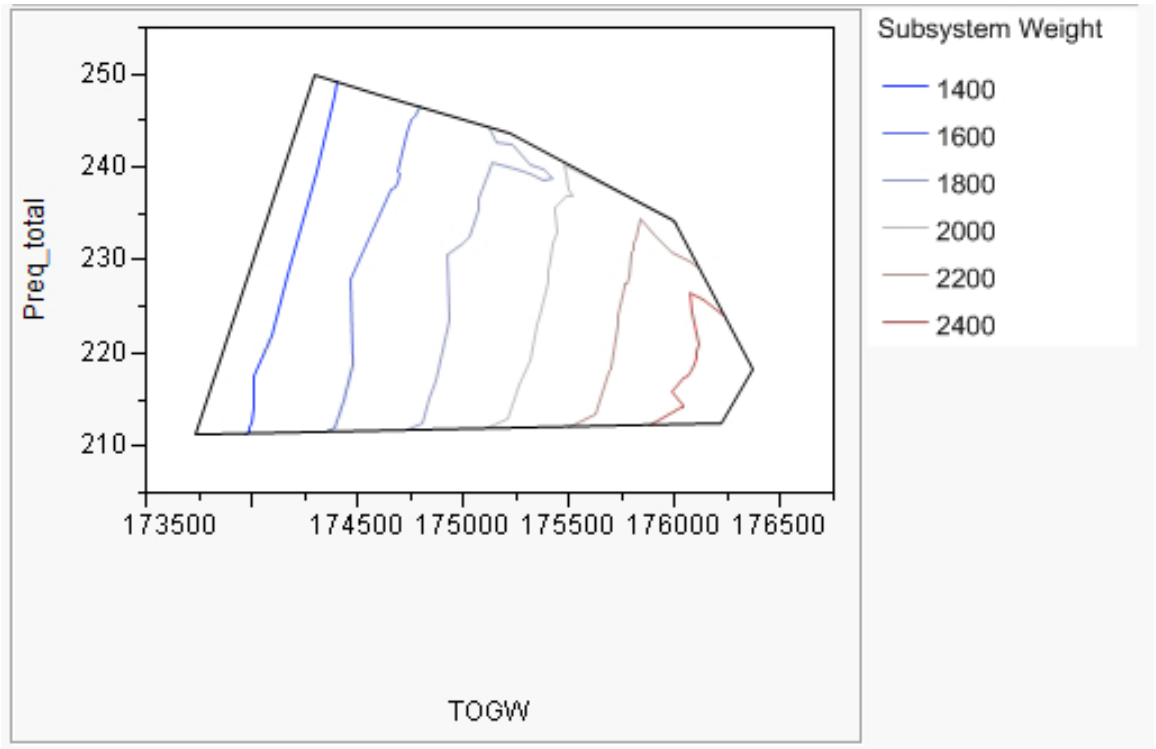

Figure 55: Subsystem Design Space

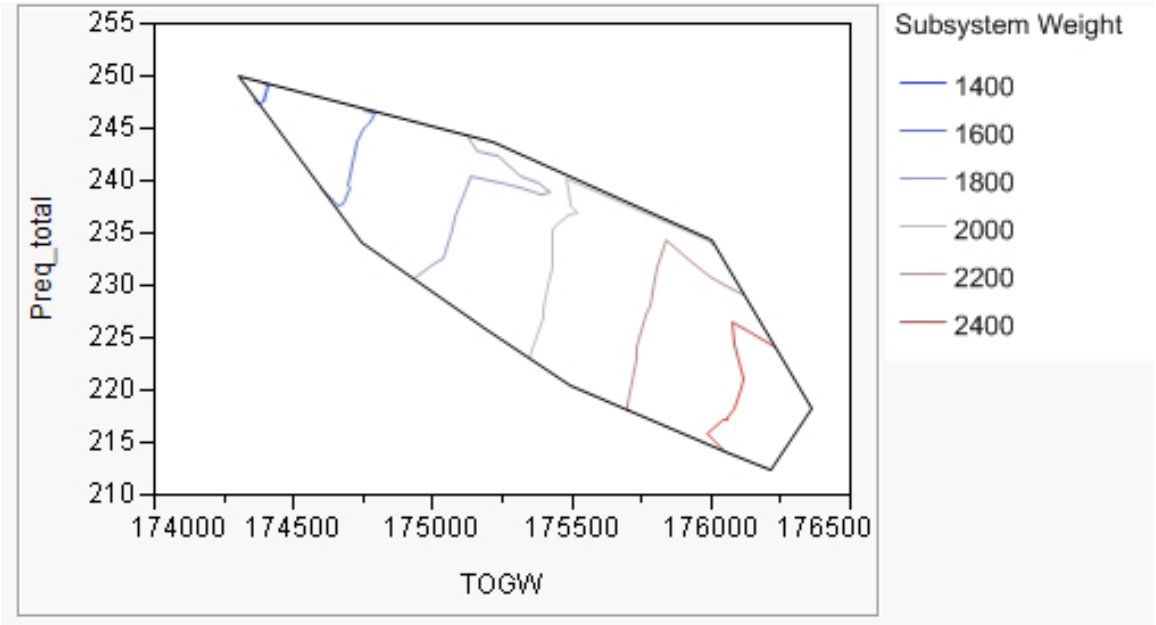

Figure 56: Hydraulic and Hybrid Design Space

user wishes to track are known as responses (in this case TOGW and SW), which are treated as a function of the input variables (in this case subsystem weight and power extraction) to the problem [88]. A second order polynomial model was utilized as the form of the RSE because it is the most commonly used form in RSM [88]. Figure 59 shows an interactive sensitivity analysis environment illustrating the RSEs that were fit. Such a plot displays the partial derivatives of the different variables and therefore their local relationships. Similar trends to those already observed can be seen, such as the strong almost linear relationship between TOGW and subsystem weight. Such an interactive analysis environment enables the visualization of these partial derivitatives as the values are changed as seen in Figure 60 in which the value of TOGW was lowered, showing the partial derivatives at this different value of TOGW, which contians similar relationships. The quality of the fit data for the RSEs is shown in Appendix D.

Covariances and correlations between the variables, especially the subsystem impacts and TOGW, must be examined. These metrics can assist in examining the coupling by examining whether a linear relationship exists [138]. The covariances and correlations from the 150-passenger class data are shown in Tables 5 and 6. As can be seen, the subsystem weight and TOGW appear to be highly positively correlated. It should be noted that a smaller negative correlation is shown between TOGW and the power extraction; this is likely due to the negative coupling of the subsystem weight and power demand for the modeled architectures as shown in Tables 5 and 6. This relationship is due to a trade, and Pareto frontier in the architectures explored where more energy efficient architectures seem to be heavier due to being hybrid architectures which have the added weight from utilizing both technologies.

Finally, the data in this experiment leads to the conclusion that the coupling between aircraft sizing and subsystem impact exists and is significant, thus validating Hypothesis 1. This is supported by all of the resulting trends, correlation values, and

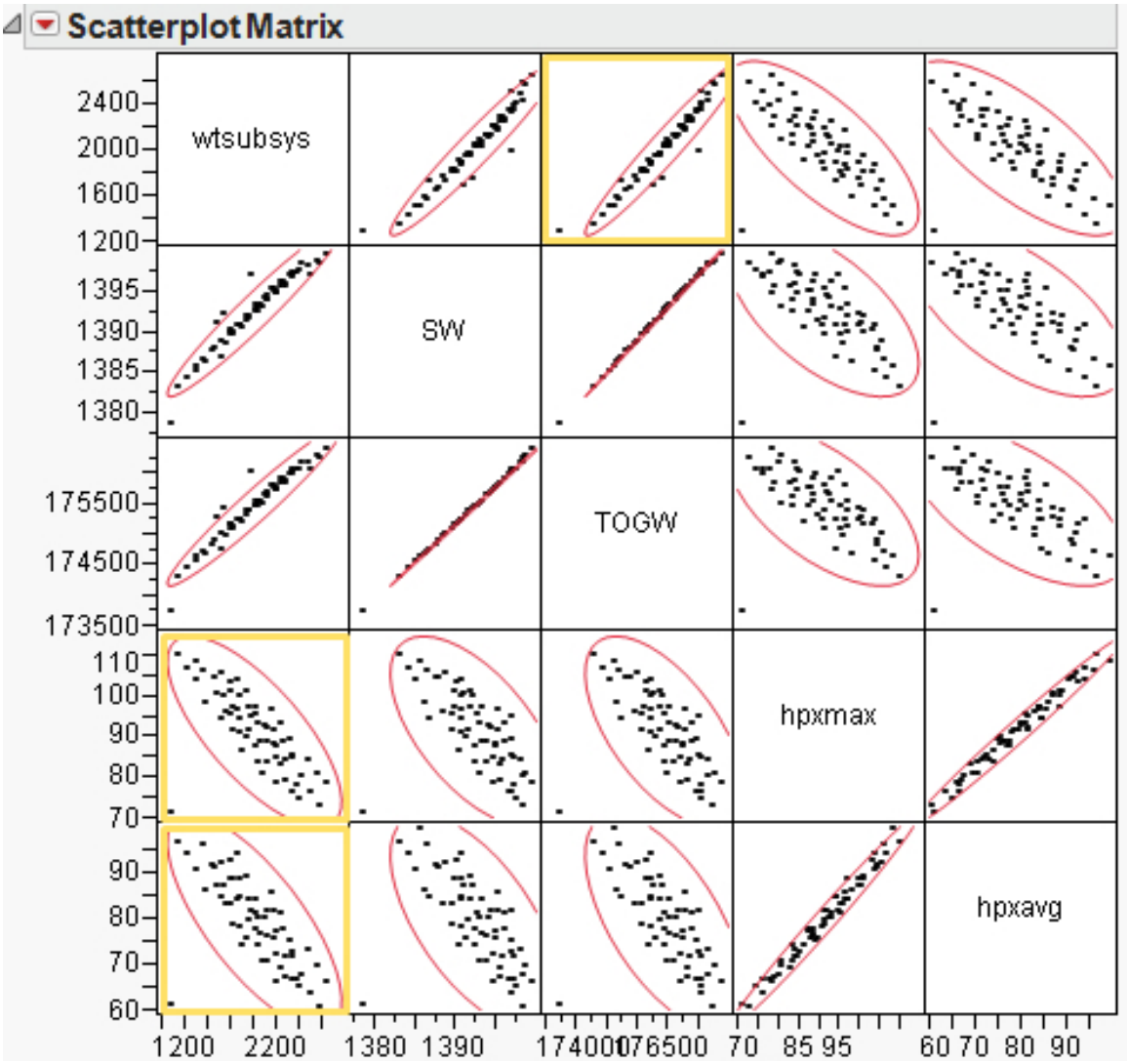

Figure 57: 150-Passenger Class Multivariate Plot

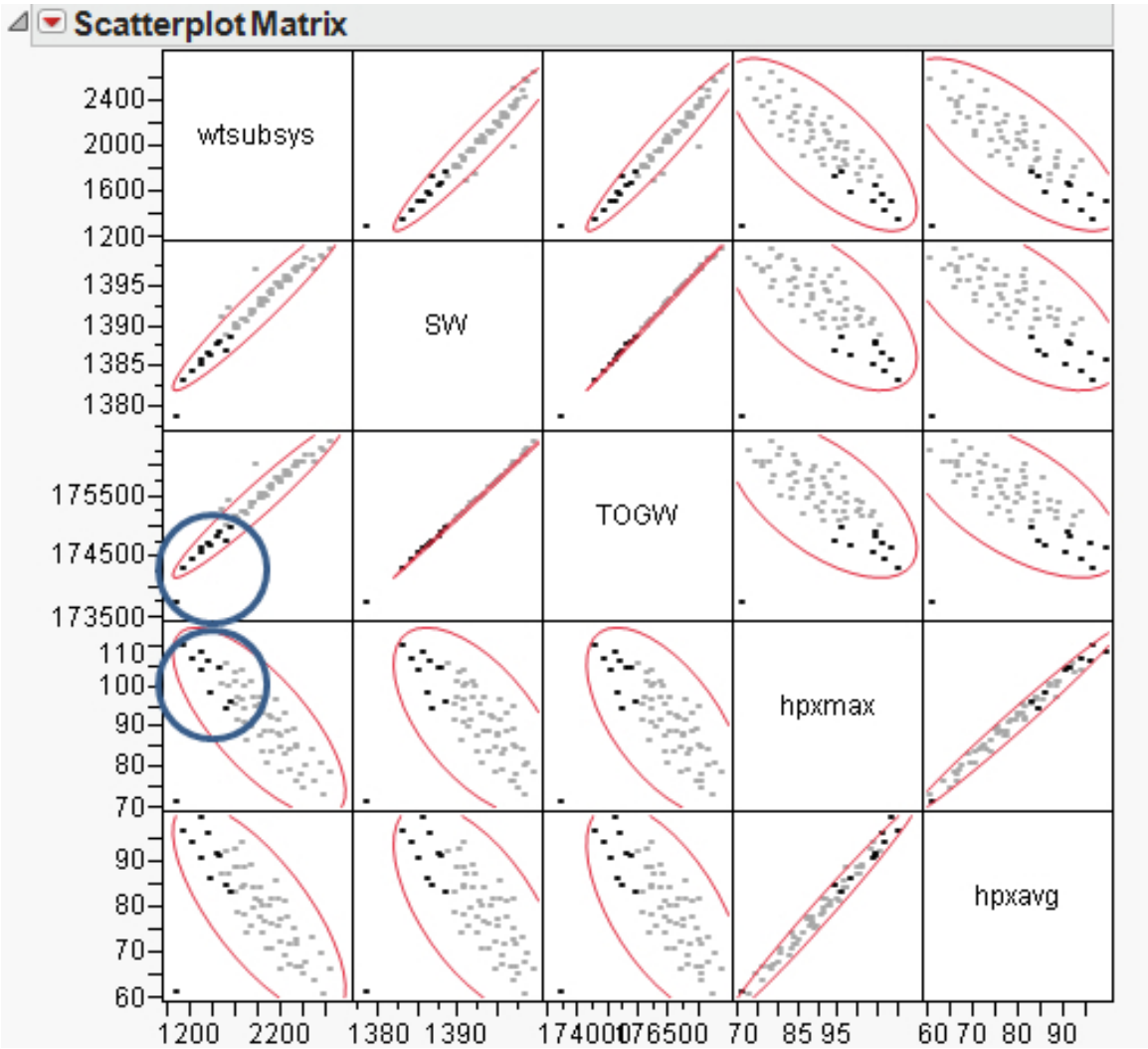

Figure 58: Lower TOGW 150 Pax Designs

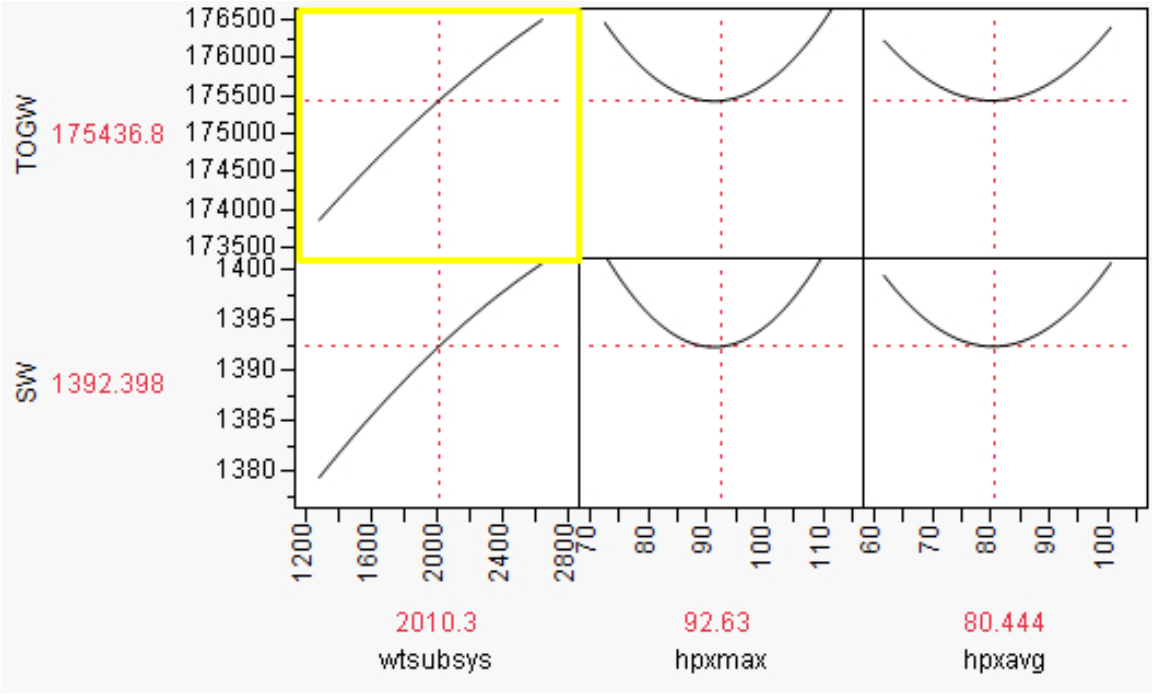

Figure 59: 150-Passenger Class Interactive Sensitivity Analysis Environment

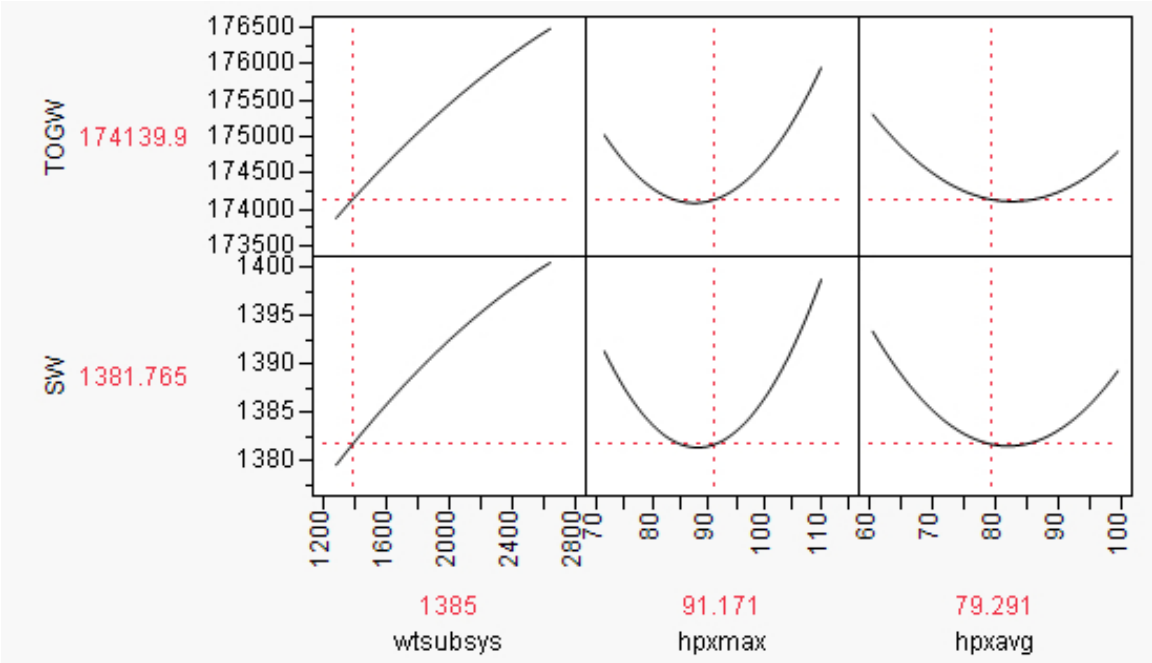

Figure 60: 150-Passenger Class Interactive Sensitivity Analysis

Table 5: 150-Passenger Class Correlations

	Subsystem Wt	SW	TOGW	hpx max	hpx avg
Subsystem Wt	1	0.96452	0.96712	-0.73426	-0.73815
SW	0.96452	1	0.99974	-0.60780	-0.61929
TOGW	0.96712	0.99974	1	-0.61088	-0.62224
hpx max	-0.73426	-0.60780	-0.61088	1	0.98910
hpx avg	-0.73815	-0.61929	-0.62225	0.98910	1

Table 6: 150-Passenger Class Covariance Matrix

	Subsystem Wt	SW	TOGW	hpx max	hpx avg
Subsystem Wt	97298.6	1282.9	160178	-2193.1	-2203.9
SW	1282.9	18.2	2263.5	-24.8	-25.3
TOGW	160178	2263.5	281925.4	-3105.9	-3162.4
hpx max	-2193.1	-24.8	-3105.9	91.7	90.7
hpx avg	-2203.9	-25.3	-3162.4	90.7	91.6

range encountered in TOGW. As discussed above, the magnitude of the correlations and covariances show a strong coupling between subsystem impacts and aircraft size, especially subsystem weight and TOGW. The range in TOGW seen for the different architectures establishes the significance of this coupling.

The significance of capturing this coupling is demonstrated in this experiment and in the validation of Hypothesis 1. The capturing of this coupling within MAIA, as demonstrated within Experiments 1 and 2, enables subsystem architecture trades during conceptual design. Specifically, the architectures that would lead to the smallest aircraft size can be identified.

6.1.1 Constraint Analysis

This subsection analyzes the constraints on subsystem architecture design and their impact on the non-dimensional aircraft sizing utilizing the results from Experiment 1. Specifically, the impact of power extraction constraints on engine and aircraft sizing is examined. Such an analysis is motivated by capturing the impact of subsystem trades on engine core sizing and aircraft non-dimensional sizing. If the subsystems demand

more power than is available, the engine must be resized which, as shown in this section, would also change the non-dimensional sizing of the aircraft. Specifically, this would increase the T/W ratio while not impacting W/S, shifting the selected non-dimensional design point up on a constraint diagram as shown in Figure 64. The determination of the impact on this design point could be utilized to update the conceptual design of the aircraft, making it more accurate and reducing unexpected weight gains during aircraft development. The overall steps in the determination of the subsystem power constraints and their impact on aircraft non-dimensional sizing is shown in Figure 61.

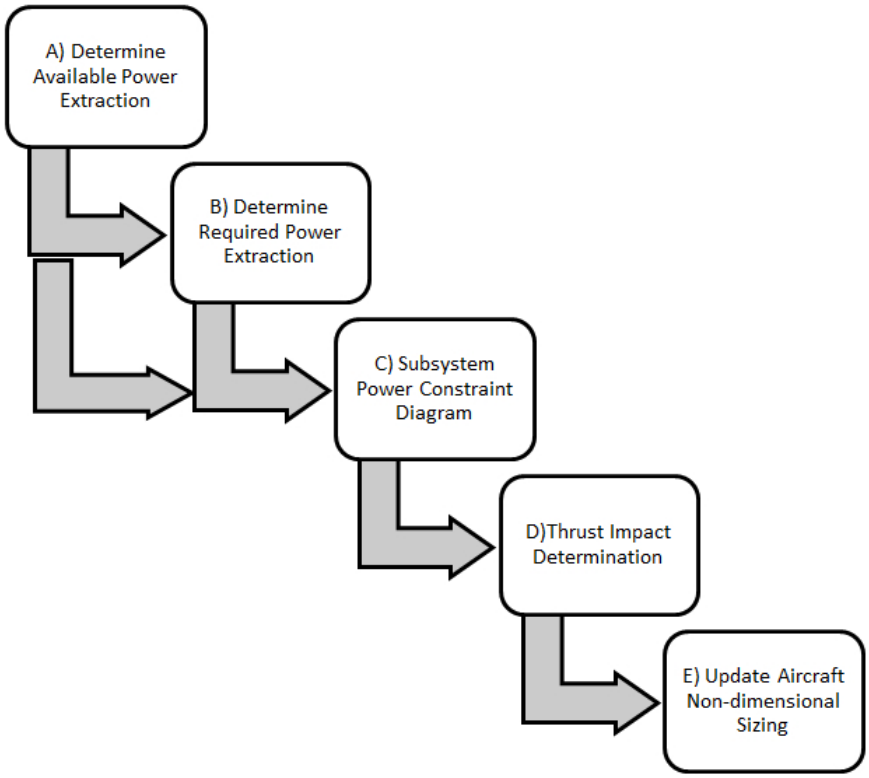

Figure 61: Subsystem Constraint Analysis Process

The first step in examining the power extraction constraints is to determine the available power assumed when sizing the engine. This determines the power available line in a subsystem power constraint plot as shown in Figure 62. Then, the power needed by the subsystems must be determined, utilizing available data and models.

This enables determination of the power required curve, which can then be placed on the power constraint plot as shown in Figure 62. The Subsystem Power Constraint Diagram in Figure 62 is an example that utilizes the data from experiment 1. This figure shows the different power extraction loads compared to the available value for different aircraft sizes. As discussed in the section on the modeling environment, some modeled loads, such as IFE and galley loads are determined by the number of passengers, and therefore do not vary with TOGW (or actuation architecture). These loads are displayed along with the actuation loads which vary with TOGW in the modeled systems power required line. It should be noted that the variability in this data comes from the fact that this curve was made utilizing Experiment 1 results, which include different architectures that impact the power extraction. There is a constant line that contains the value utilized to account for unmodeled loads as discussed in the section in the modeling environment. These combined values determine the total required power extraction which is plotted in Figure 62. The distance between this and the available power shows the available margin. If the required power exceeds the available, then the engine core may need to be resized to enable the use of the subsystems. Therefore, Figure 62 shows if and when engine core resizing due to power extraction may be required. The margin between the required and actual shown in Figure 62 is also a function of the selected architecture (as some architectures demand more power than others), the TOGW (as this impacts the required power), and subsystem noise parameters (discussed in Experiment 3a).

If the power extraction is larger than the assumed value during engine sizing, the engine core may need to be resized to account for a reduction in thrust due to a higher power extraction, as the required thrust would still be the same. To examine how much additional thrust must be provided, engine analysis such as that done in the Masters thesis by Faidi [45] could be performed. Faidi utilized NPSS modeling to determine the impact of power extraction and bleed loads as shown in

Figure 63 [45]. Alternatively, similar analysis could be performed as done in the modeling environment, where the engine and aircraft were resized due to subsystem power demands and weight. Such an analysis could be performed to determine the thrust loss due to the additional power extraction as shown in Figure 63 [45]. This would enable the determination of the increase of the amount of additional thrust that the engines would have to be resized in order to accommodate the needed power extraction. This increase in engine size would occur for the same W/S that was previously determined by the non-dimensional sizing of the aircraft as discussed in Mattingly [83] and shown in Figure 64.

The non-dimensional aircraft sizing could then be updated to account for this engine core size increase. Specifically, as shown in Figure 64, the T/W ratio would be increased at the selected W/S. This increase is a result of the change in power extraction increases the needed T/W ratio slightly (as the thrust would increase by the determined amount while TOGW would be approximately the same). The amount of increase in T/W could be determined by utilizing the updated thrust rating of the engine and the TOGW. Such an analysis enables updating the non-dimensional size of the aircraft, enabling more accurate aircraft sizing during conceptual design. This could increase the accuracy of conceptual design and reduce unexpected weight gains.

6.2 Experiment 2

To review, **Hypothesis 2** states the following: If the aircraft class examined is varied, then the impact of the coupling between aircraft sizing and architecture platform-level impacts is still significant.

For Experiment 2, the modeling environment discussed in the previous chapter was leveraged to examine the extent of this coupling. In addition, the environment for Experiment 1 was updated to capture 210-passenger and 300-passenger aircraft

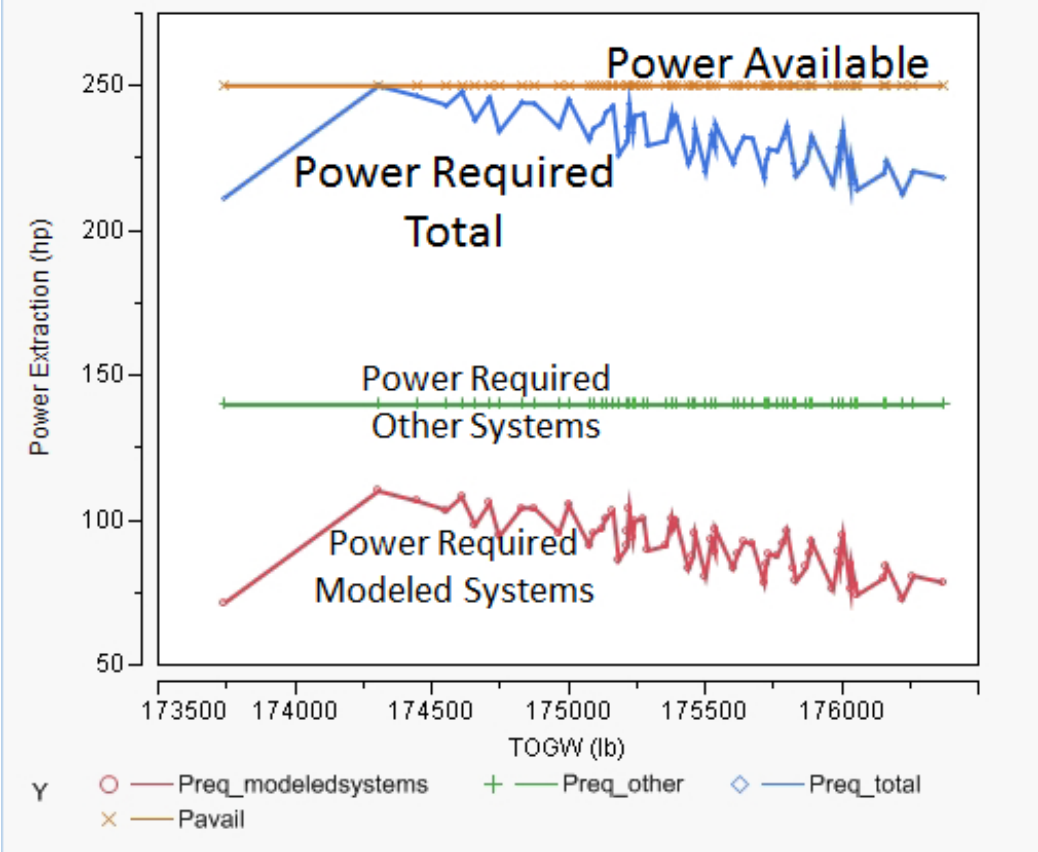

Figure 62: Subsystem Power Constraint Diagram

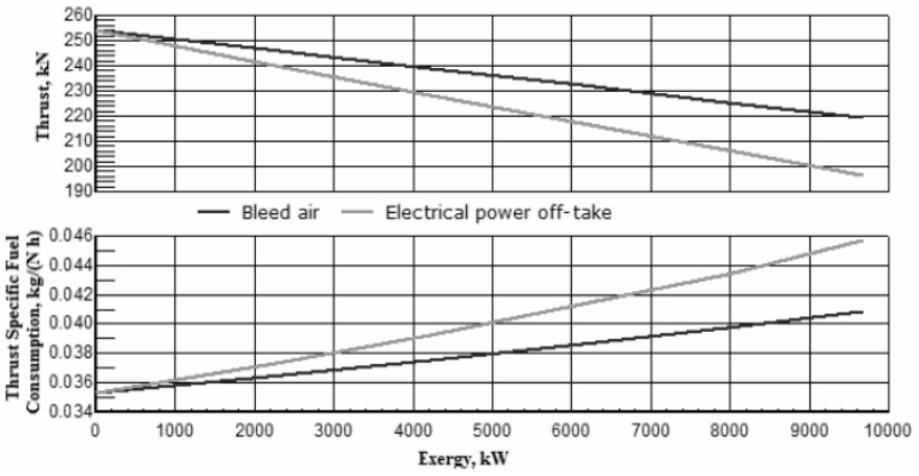

Figure 63: Thrust Impact of Power Extraction [45]

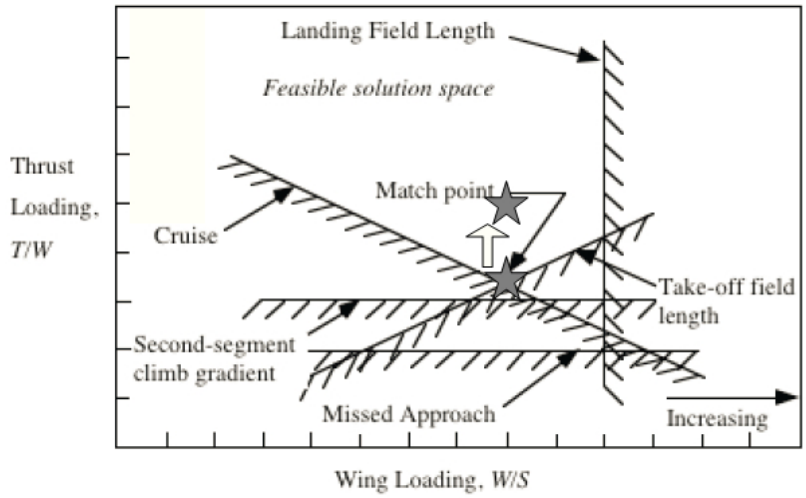

Figure 64: Example Aircraft Constraint Diagram Adapted From [82] and [80]

in order to examine the impact of this coupling on other aircraft sizes. The Matlab/Simulink modeling environment was run to determine the all hydraulic actuation subsystem weight and power extraction values for both new aircraft sizes. The 210- and 300-passenger classes EDS models were recalibrated utilizing these values. This was done utilizing the existing calibration codes and capabilities within EDS. Then, the newly calibrated and integrated environment of EDS and Matlab/Simulink was utilized to examine the extent of the coupling between aircraft sizing and architecture impacts for both of these passenger classes. This exploration was done utilizing the same full factorial DOE varying each group of control surfaces (such as flaps, elevators, rudder, aileron, and landing gear) from being hydraulically powered to being powered by EHAs utilized in Experiment 1. This DOE was run twice in Experiment 2, once for each passenger class. The converged values of metrics of interest, such as TOGW, for each architecture and passenger class were then saved for analysis. Finally, the results were analyzed to examine the coupling for these other passenger class sizes.

For the 210-passenger class aircraft, Figure 65 plots the converged values of subsystem weight against TOGW. There still appears to be an almost positive linear

relationship between TOGW and subsystem weight. This still implies that significant coupling exists between TOGW and subsystem weight. The difference between the top and bottom architecture was approximately 1.4 percent of the TOGW, or 5773.1 pounds. Given that Roskam [121] states that the range to expect for the total weight of the actuation system is approximately 0.6 to 1.2 percent of TOGW, the difference in converged TOGW by varying this system is still significant for a 210-passenger class aircraft. The all EHA architecture appears to be slightly outside the overall trend as this uses a different technology.

For the 210-passenger class aircraft in Figure 67, the converged values of maximum power extraction are plotted against TOGW. There still appears to be a slightly negative relationship between TOGW and power extraction. This trend again exists and is due to the particular architectures examined. Within these architectures, the lower power extraction values occur at higher subsystem weights, as can be seen in Figure 66. Again, the all EHA architecture seems to be outside the overall trend in the data. Similar to the results in Experiment 1, the impact of the weight of the subsystem dominating the impact of the power extraction creates a situation in which lighter architectures lead to the minimum TOGW. The more efficient architectures are hybrids, as discussed in the Experiment 1 results. It makes sense that hybrid architectures are heavier as they have added weight from still having the hydraulic systems and the added electrical weight from having EHAs. As discussed in the Experiment 1 results, hybrid architectures are also more efficient, partially due to a smaller hydraulic pump size, shifting the operating point of these systems to a higher efficiency value as seen in Figure 52.

For the 210-passenger class aircraft, in Figure 68, the converged values of average power extraction (inside of the power extraction map) are plotted against TOGW. Similar to the maximum power extraction, there still appears to be somewhat of a negative trend in this data. Lower power extraction values are at higher subsystem

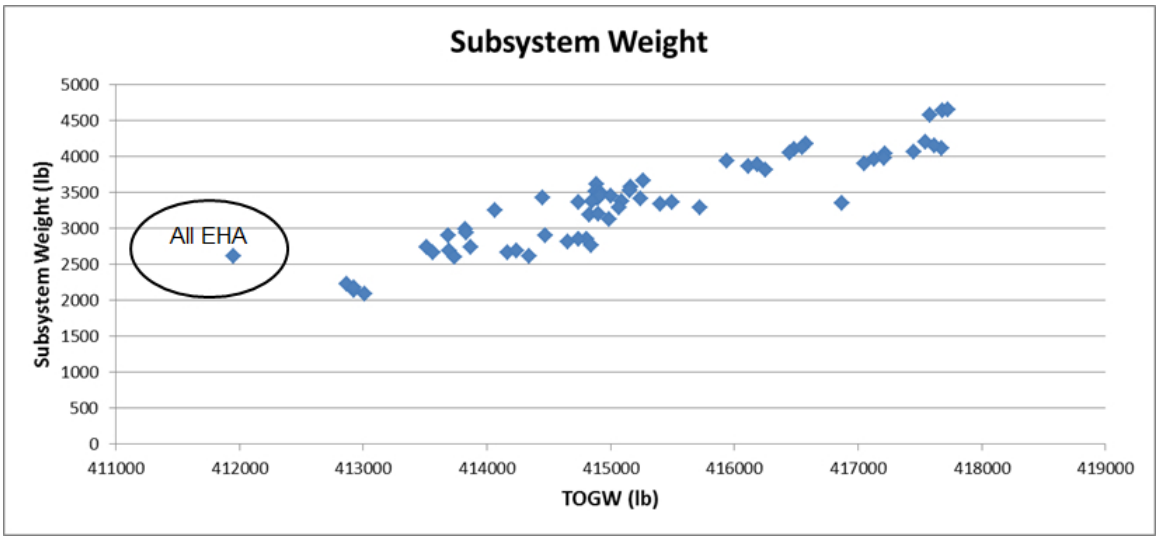

Figure 65: 210-Passenger Class Subsystem Weight

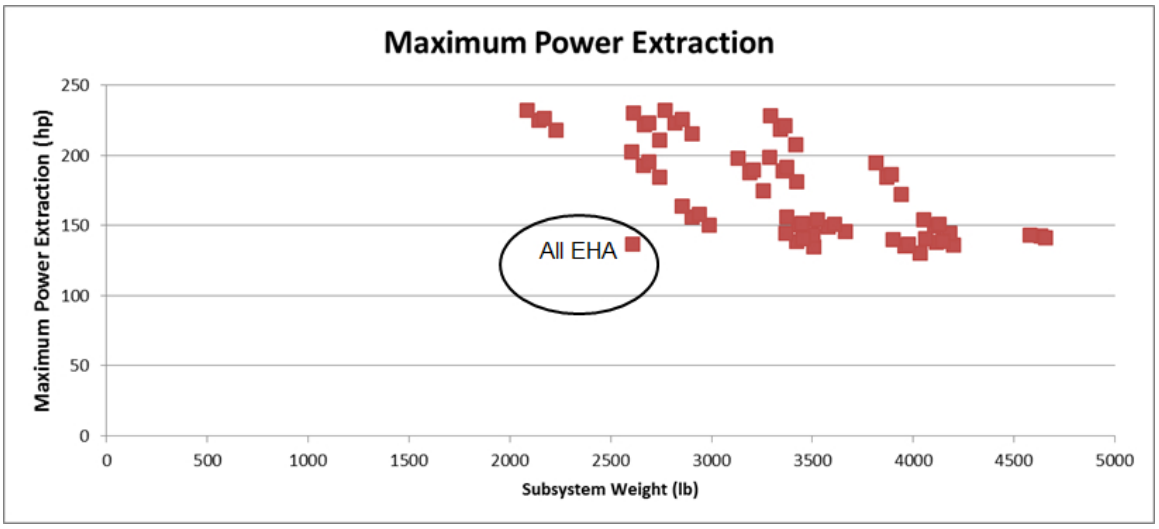

Figure 66: 210-Passenger Class Maximum Power Extraction vs Subsystem Weight

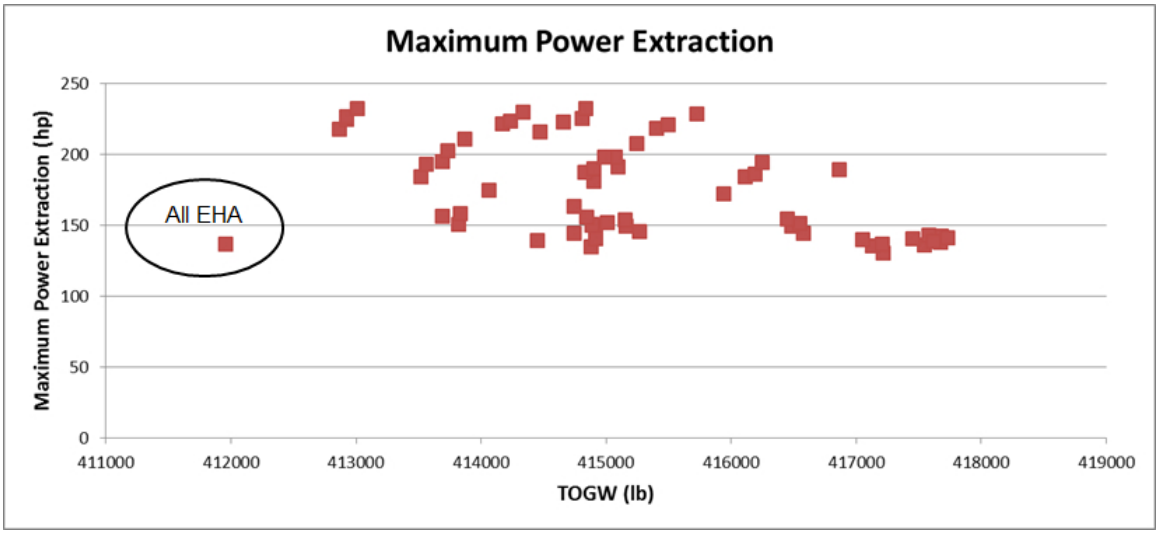

Figure 67: 210-Passenger Class Maximum Power Extraction

weights for the examined architectures as can be seen in Figure 69. The use of all EHAs seems to be again outside the trends of the data slightly.

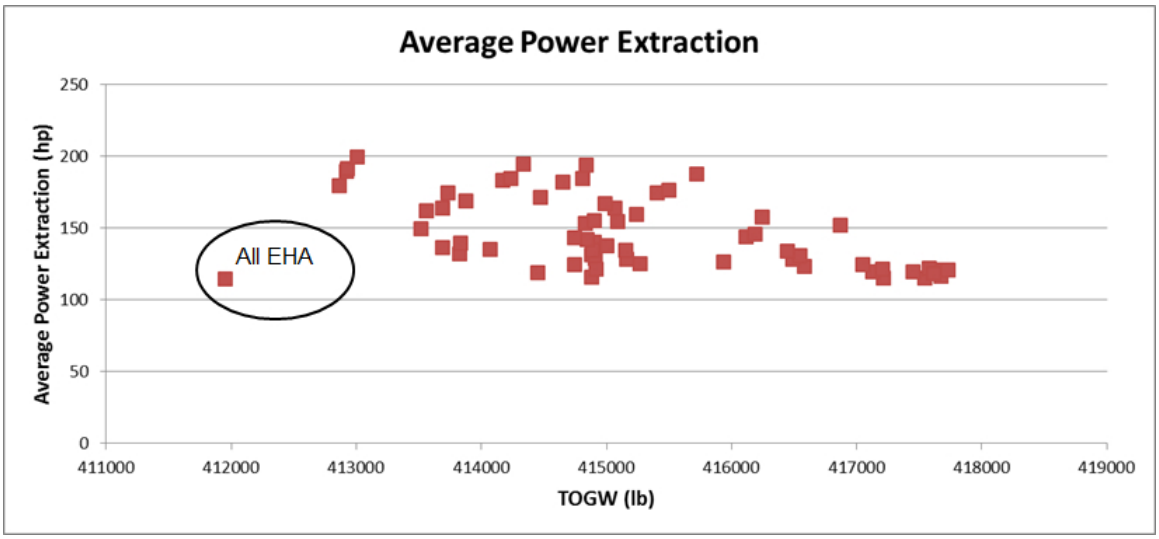

Figure 68: 210-Passenger Class Average Power Extraction

Similar to the data in Experiment 1, a multivariate scatter plot is another way to visualize these trends. Such a plot is shown in Figure 70. This plot shows trends such as TOGW increasing with subsystem weight and power extraction decreasing with subsystem weight. The designs shown were then filtered to the lower TOGW designs (at or lower than 415000 lb). The filtered designs are shown in Figure 71.

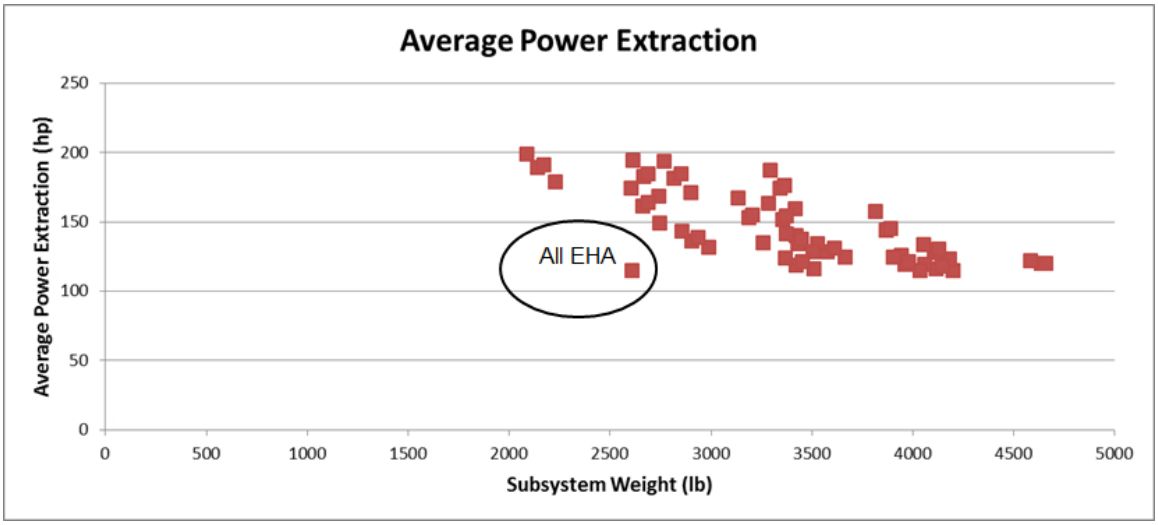

Figure 69: 210-Passenger Class Average Power Extraction vs Subsystem Weight

In Figure 71, it can be seen that the lower TOGW designs have lower subsystem weights.

Response Surface Equations (RSEs) were fit to the data, in order to further examine and characterize the relationships between aircraft size and subsystem parameters. As discussed in Experiment 1 Results and the Chapter on MAIA, RSM is a method that can be utilized in the creation of such metamodels [88]. The examined responses were again TOGW and SW, which were treated as a function of the input variables which were again in this case subsystem weight and power extraction [88]. Similar to Experiment 1, a second order polynomial model was utilized as the form of the RSE because it is the most commonly used form in RSM [88]. An interactive sensitivity analysis environment illustrating the RSEs is shown in Figure 72. To review, such a plot displays the partial derivatives of the different variables. Similar trends to those already observed can be seen, such as the strong almost linear relationship between TOGW and subsystem weight. As shown in the summary of fit data in Appendix D, the RSEs and trends shown in the interactive sensitivity analysis environment are valid. However, because the subsystem weight has a dominating impact on TOGW over the power extraction, its relationship is lilkely better within the RSEs, which

the reason that the curves for power extraction appear more linear than for the 150-passenger class aircraft. However, the primary observed trend of TOGW with subsystem weight can be seen and is consistent with the results.

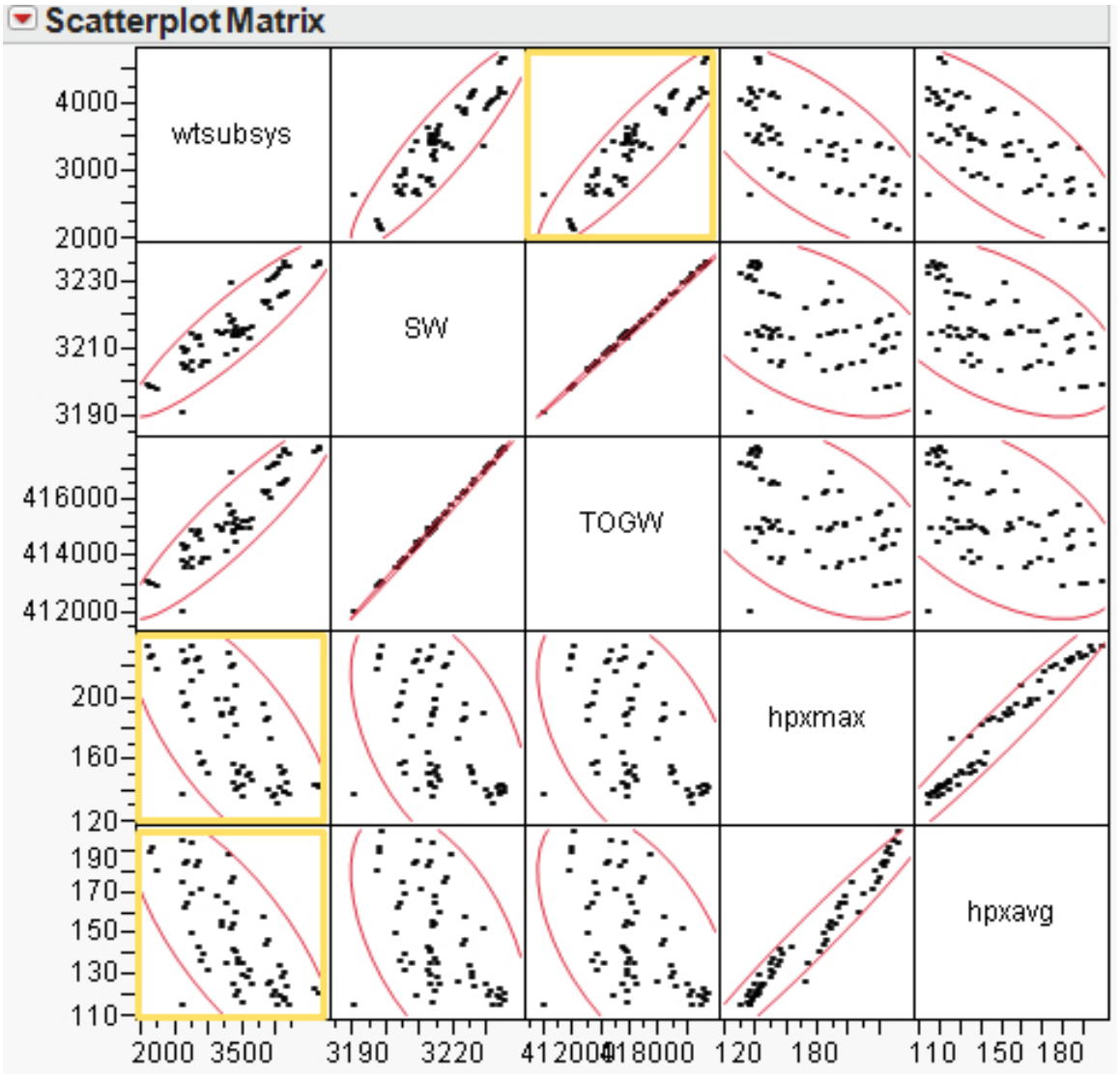

Figure 70: 210-Passenger Class Multivariate Plot

Covariances and correlations between the variables must again be examined. Tables 7 and 8 shows the covariances and correlations from the 210-passenger class data. As can be seen, the subsystem weight and TOGW again appear to be highly positively correlated. A smaller negative correlation is shown again between TOGW and the power extraction, again likely due to the negative coupling of subsystem weight

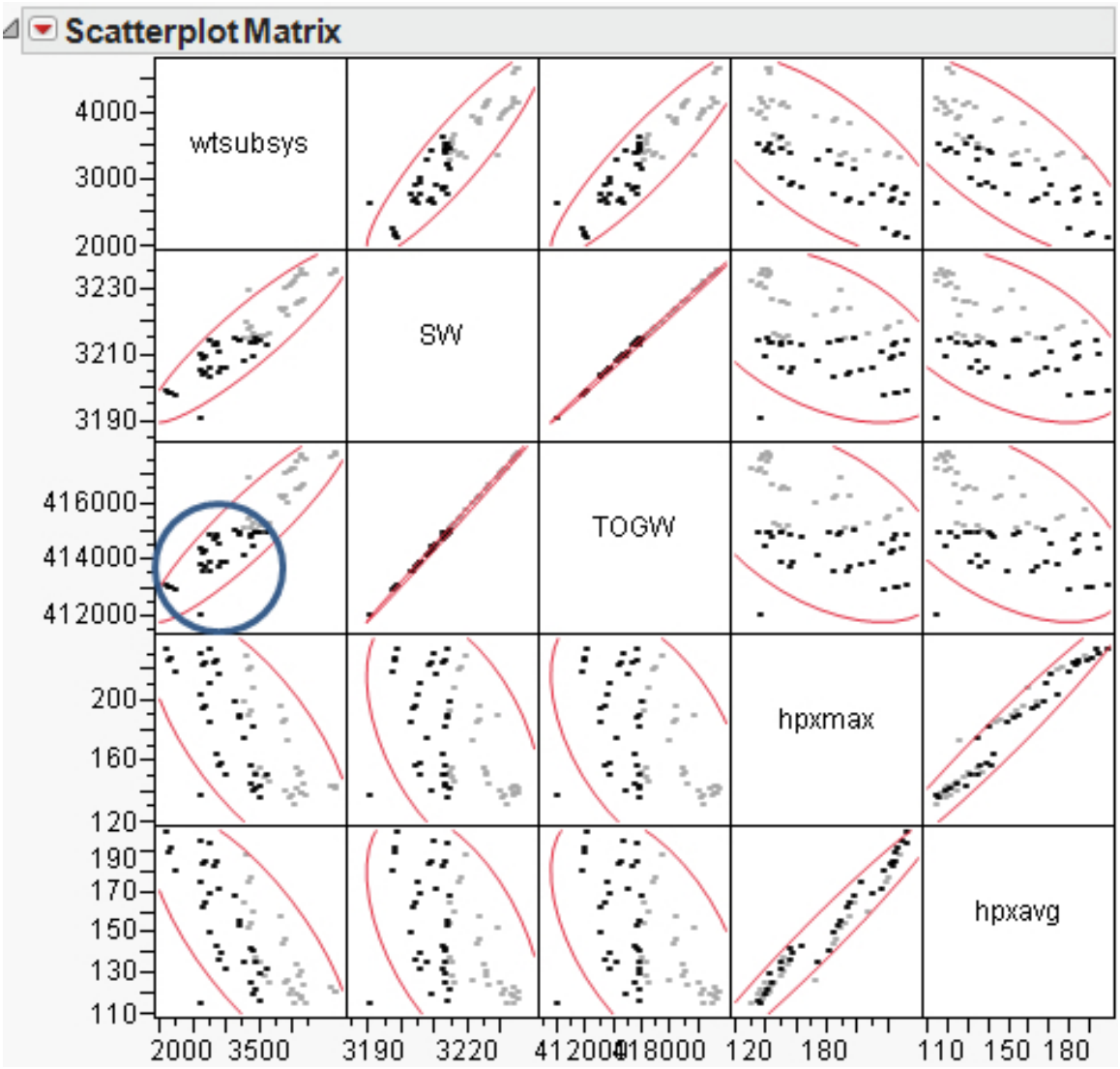

Figure 71: Lower TOGW 210 Pax Designs

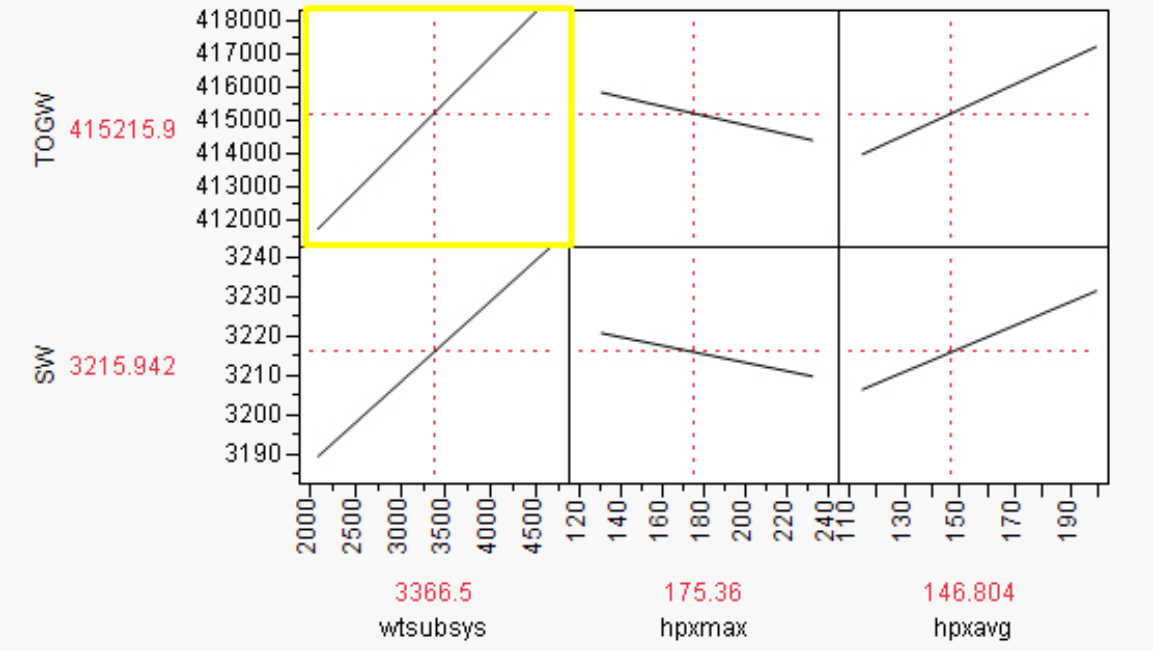

Figure 72: 210-Passenger Class Interactive Sensitivity Analysis Environment

and power demand for the modeled architectures.

Table 7: 210-Passenger Class Correlations

	Subsystem Wt	SW	TOGW	hpx max	hpx avg
Subsystem Wt	1.0000	0.9093	0.9152	-0.6959	-0.7495
SW	0.9093	1.0000	0.9995	-0.4881	-0.5291
TOGW	0.9152	0.9995	1.0000	-0.4957	-0.5369
hpx max	-0.6959	-0.4881	-0.4957	1.0000	0.9775
hpx avg	-0.7495	-0.5291	-0.5369	0.9775	1.0000

Table 8: 210-Passenger Class Covariance Matrix

	Subsystem Wt	SW	TOGW	hpx max	hpx avg
Subsystem Wt	388728.7	6121.6	805551.8	-14607.1	-11886.3
SW	6121.6	116.6	15235.1	-177.5	-145.3
TOGW	805551.8	15235.1	1992897.4	-23560.7	-19277.9
hpx max	-14607.1	-177.5	-23560.7	1133.5	837.1
hpx avg	-11886.3	-145.3	-19277.9	837.1	647.0

The data for the 210 passenger aircraft from this experiment leads to the conclusion that: the coupling between aircraft sizing and subsystem impact exists and

still is significant for this passenger class of aircraft. This helps in the validation of Hypothesis 2. As discussed above, the magnitude of the correlations and covariances (especially the subsystem weight and TOGW), along with the trends in their data demonstrate a strong coupling between subsystem impacts (especially weight) and TOGW. The significance of this coupling for the 210-passenger class aircraft is established by the range in TOGW seen for the different architectures.

Figure 73 contains the converged values of subsystem weight plotted against TOGW, for the 300-passenger class aircraft. There is again an almost linear relationship between TOGW and subsystem weight. However, the all EHA architecture appears to be outside the trend because of the use of a new technology along with the use of EHAs on the ailerons, flaps, and landing gear likely due to the impact of the loads on these surfaces and the fact that EHAs are heavier actuators. The difference between the top and bottom architecture in TOGW is 8688.1 pounds, or approximately 1.32 percent of the TOGW. The difference in converged TOGW by varying this system is still significant for a 300-passenger class aircraft due to the fact that, as Roskam [121] states, the range to expect for the total weight of the actuation system is approximately 0.6 to 1.2 percent of TOGW.

The converged values of maximum power extraction are plotted against TOGW in Figure 74, for the 300-passenger class aircraft. There still appears to be a modest trend in this data (although this pattern is not as noticeable), and this seems to be a slightly negative relationship between TOGW and maximum power extraction. This may not be what engineering judgment would indicate at first glance. However, this trend still exists and is again due to the particular architectures examined. Within these architectures, the lower power extraction values are still at higher subsystem weights as can be seen in Figure 75. This trend can be further be seen to be implied in some of the results in Experiments 1 and in the correlation and covariance values for this experiment. It should again be noted that there is one point that does not

appear to fit the overall trend; this point is the use of all EHAs as it is based entirely on the use of a different technology.

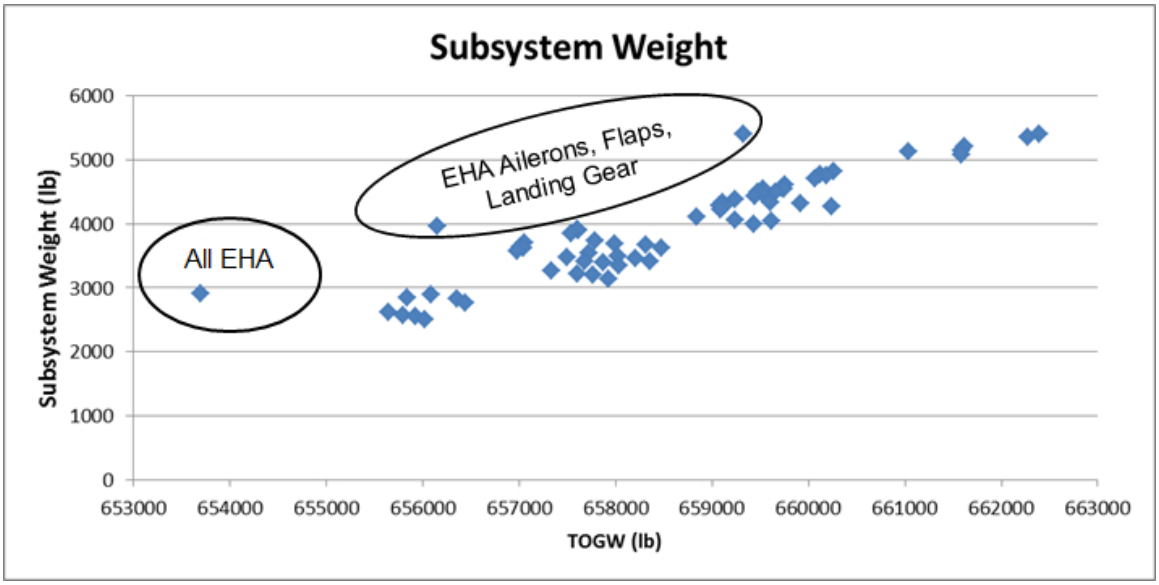

Figure 73: 300-Passenger Class Subsystem Weight

The converged values of the average power extraction within the power extraction map are plotted against TOGW in Figure 76 for the 300-passenger class aircraft. There appears to be a slight trend in this data (which again is more difficult to discern), specifically a slightly negative relationship between TOGW and average power extraction. Within the particular architectures examined, the lower average power extraction values are at higher subsystem weights as can be seen in Figure 77. There is again one point that did not appear to fit the overall trend; this point is the use of all EHAs as it is based entirely on the use of a different technology. It should be noted that in the larger aircraft sizes there appears to be a larger scatter in the plotted data. This is likely due to the slightly reduced coupling as a percent of TOGW and correlation values for larger aircraft. However, even these slightly reduced values are still seen to be significant in this experiment.

Similar to Experiment 1 and the 210-passenger aircraft, another way to visualize trends in the data is to utilize a multivariate scatter plot. Such a plot is shown in

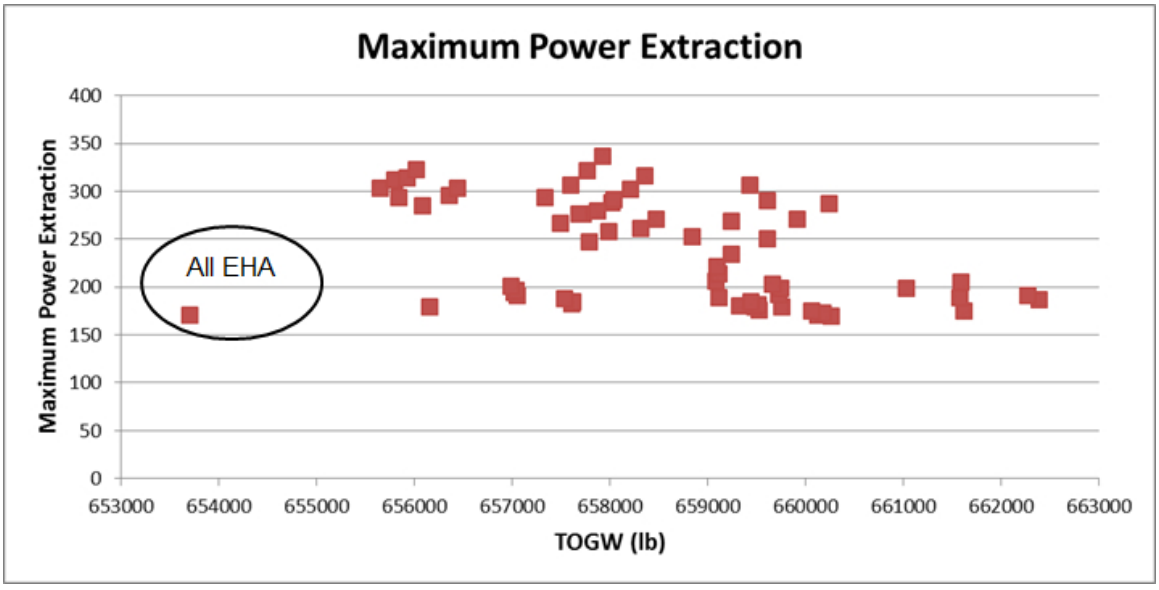

Figure 74: 300-Passenger Class Maximum Power Extraction

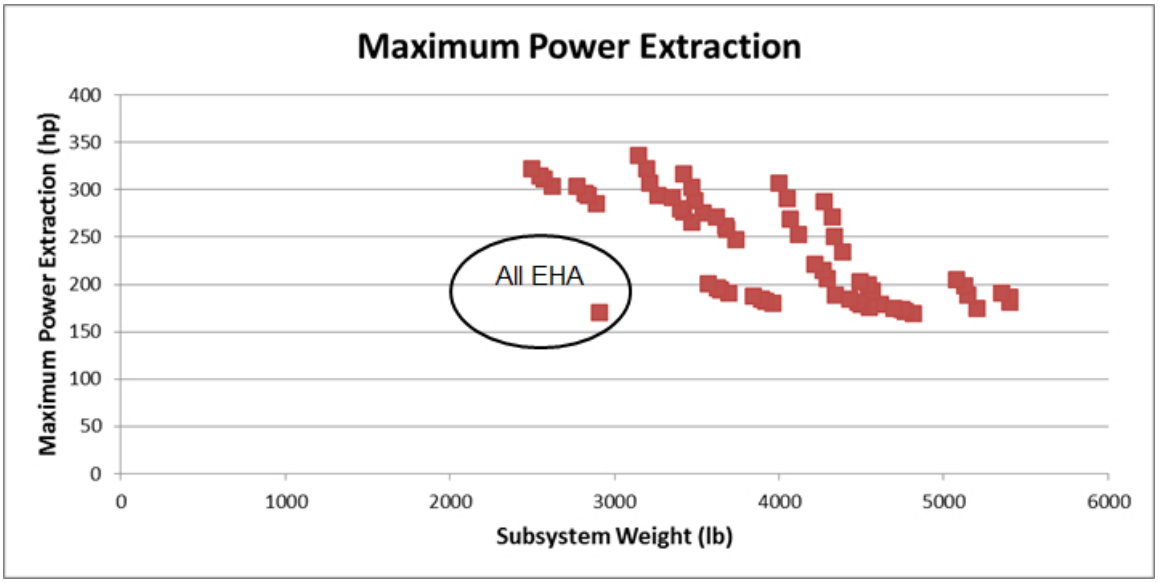

Figure 75: 300-Passenger Class Maximum Power Extraction vs Subsystem Weight

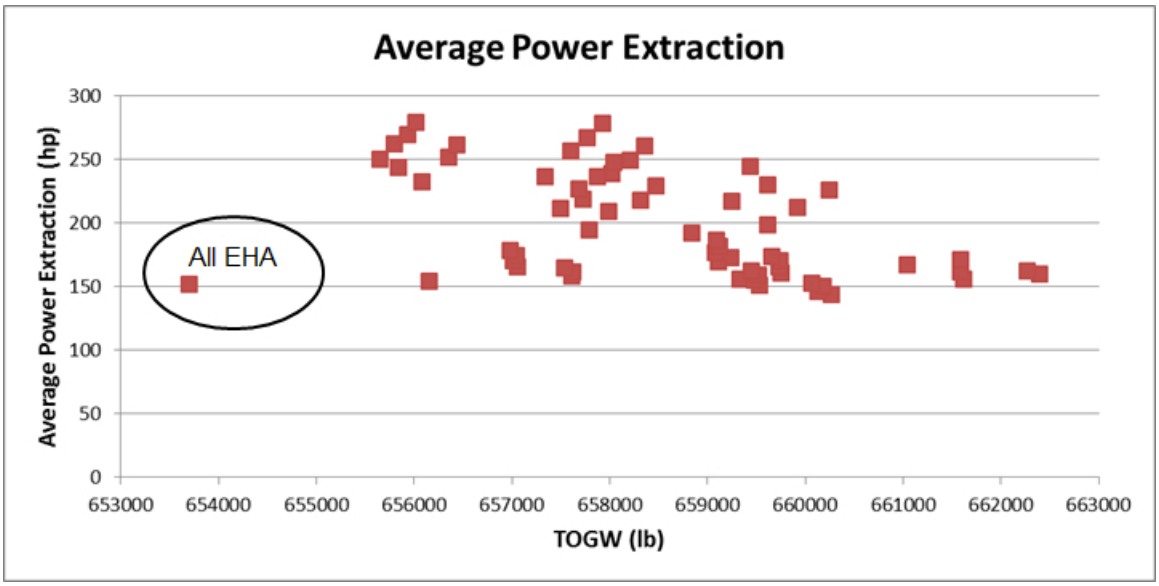

Figure 76: 300-Passenger Class Average Power Extraction

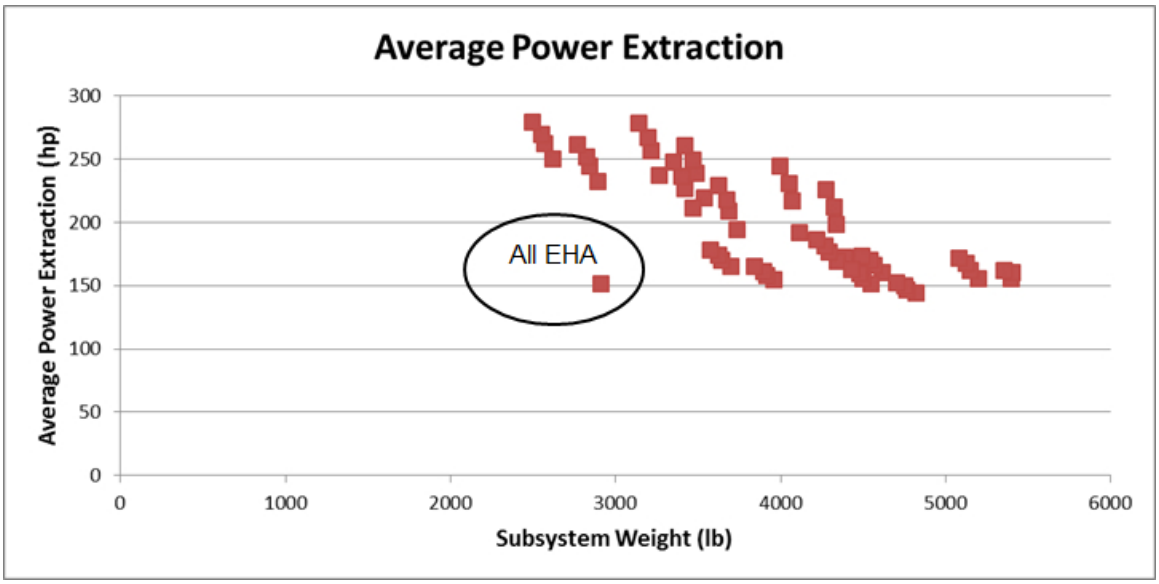

Figure 77: 300-Passenger Class Average Power Extraction vs Subsystem Weight

Figure 78 for the 300-passenger aircraft. This plot shows the same trends previously discussed in this section for this aircraft, such as TOGW increasing with subsystem weight and power extraction decreasing with subsystem weight. The designs within the multivariate plot are filtered to only the designs with the lower TOGW (at or below 657000 lb). The filtered designs are plotted in Figure 79. It can be observed from Figure 79 that only the designs with lower subsystem weights have the lowest TOGW values and that this is somewhat dominating the impact of power demand on aircraft size.

Response Surface Equations (RSEs) are again fit to the data to further examine and characterize the relationships between aircraft size and subsystem parameters. TOGW and SW are again the examined responses which are treated as a function of the input variables. Similar to the other aircraft sizes, second order polynomial models are again utilized as the form of the RSEs. The RSEs are illustrated in the interactive sensitivity analysis environment shown in Figure 80, displaying the partial derivatives of the different variables. The linear relationship between TOGW and subsystem weight can be seen. As seen in Appendix D, the RSEs and trends shown in the interactive sensitivity analysis environments are valid.

The covariances and correlations from the 300-passenger class data is shown in Tables 9 and 10. Subsystem weight and TOGW appear to be highly positively correlated. A smaller negative correlation is shown again between TOGW and the power extraction; this is again likely due to the negative coupling of subsystem weight and power demand for the modeled architectures.

The data for the 300-passenger aircraft from this experiment leads to the conclusion that the coupling between aircraft sizing and subsystem impact exists and is still significant for this passenger class of aircraft (helping to validate Hypothesis 2). The magnitude of the correlations and covariances show a strong coupling between subsystem impacts (especially weight) and TOGW. The range in TOGW seen for the

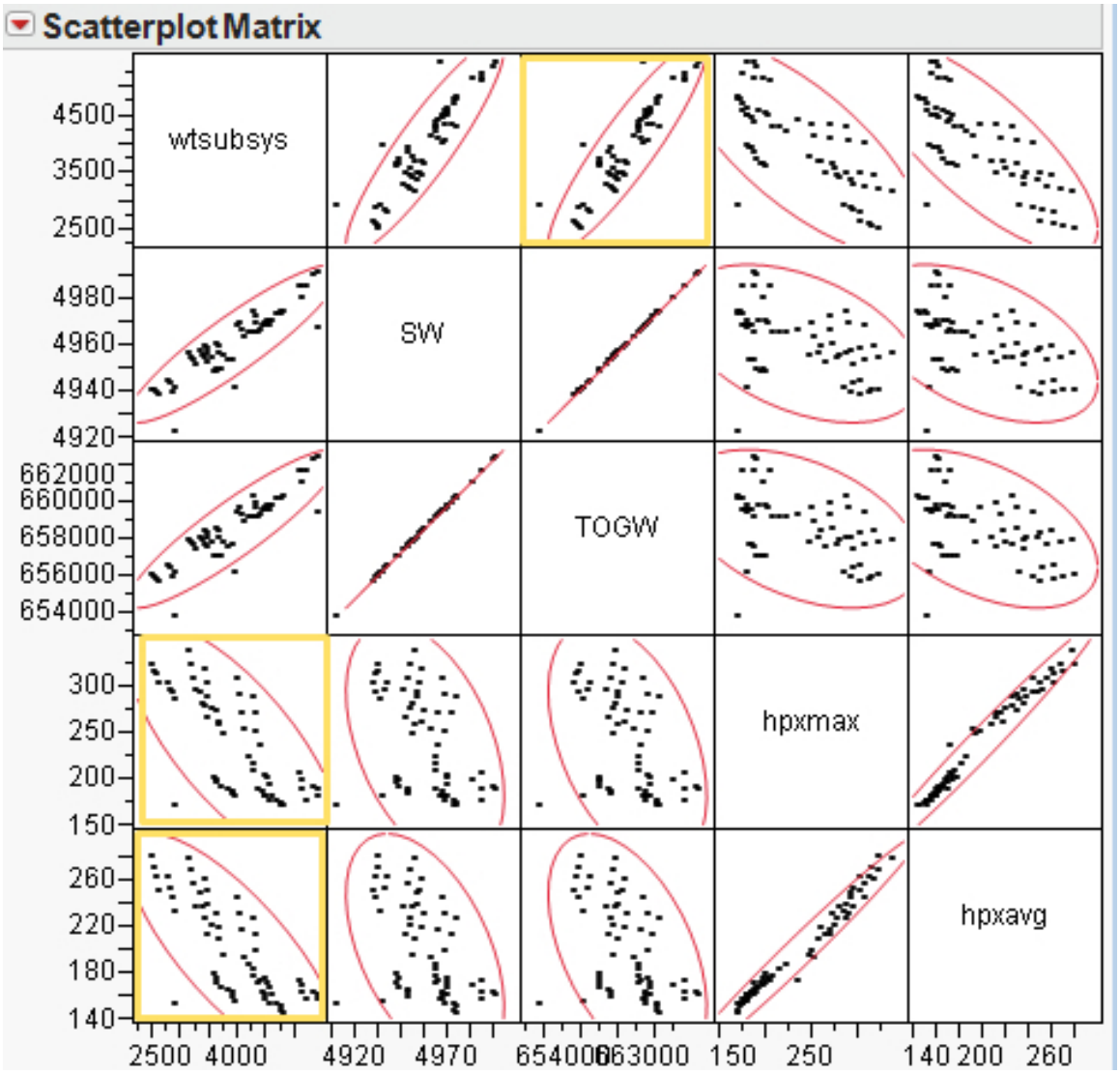

Figure 78: 300-Passenger Class Multivariate Plot

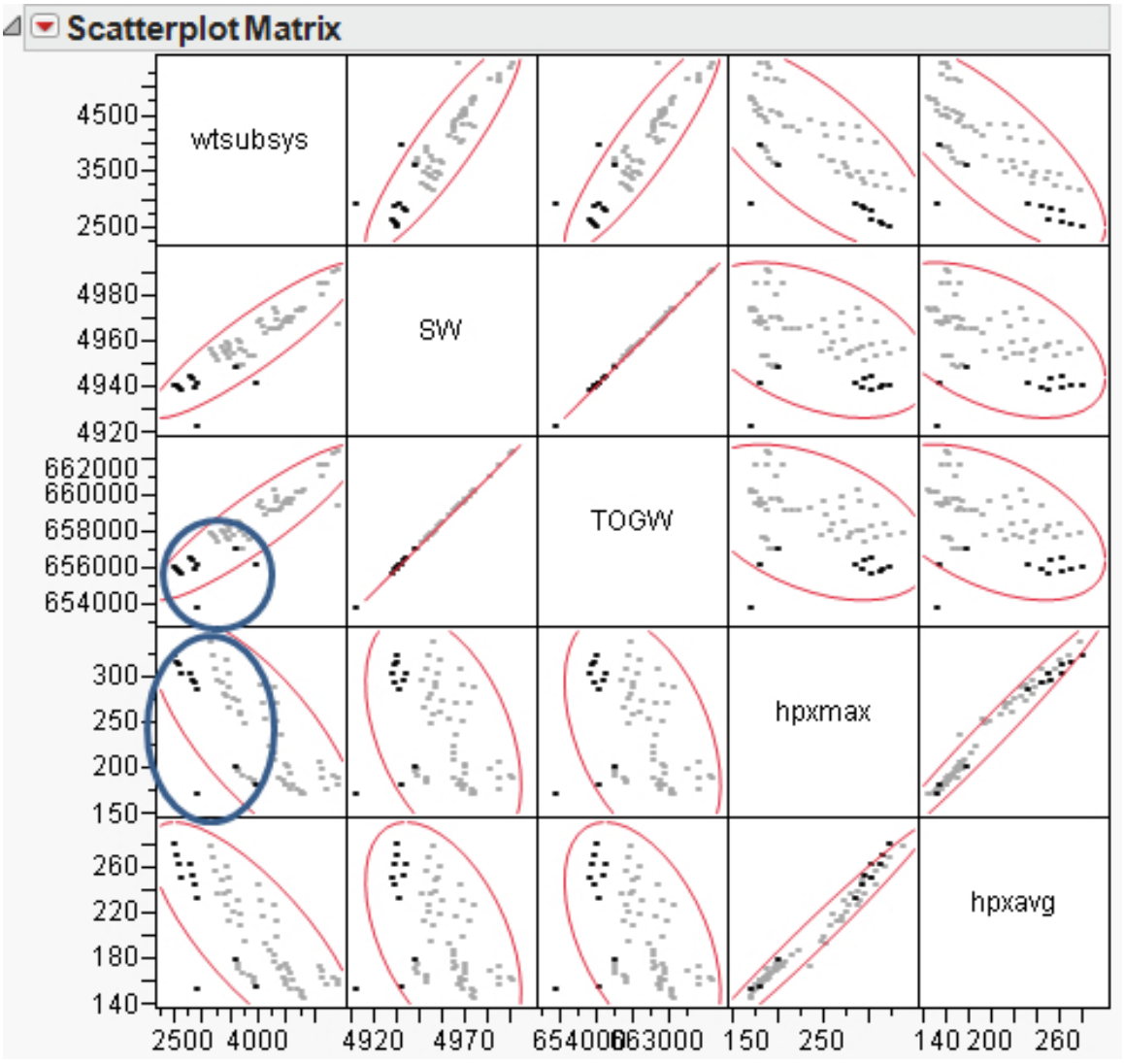

Figure 79: Lower TOGW 300 Pax Designs

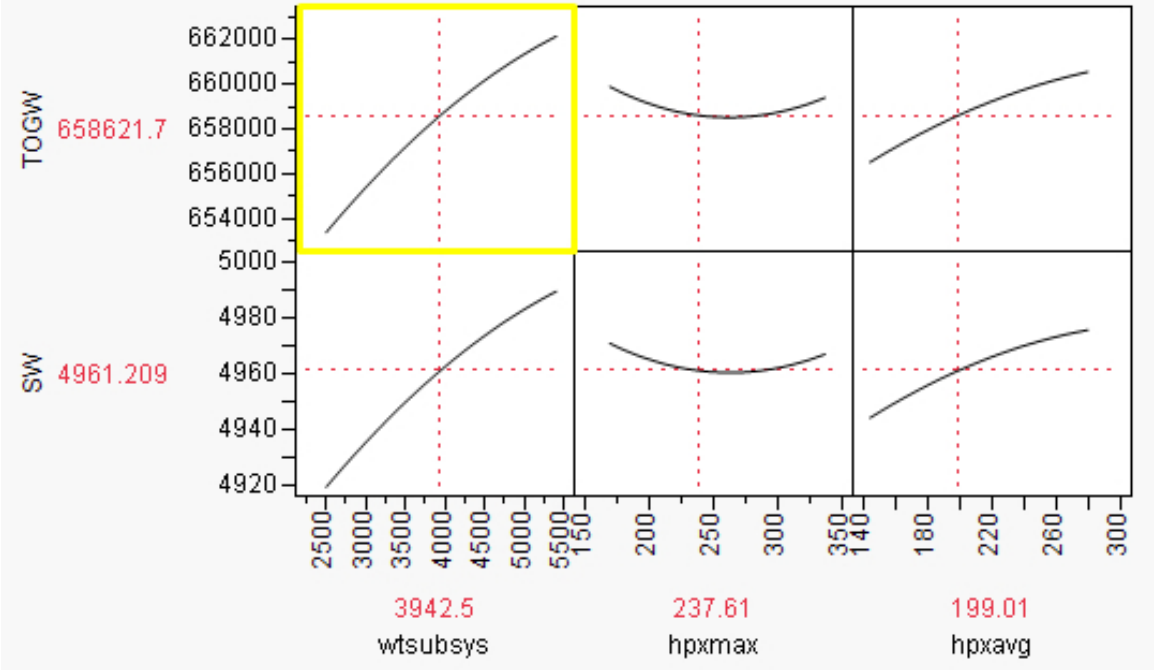

Figure 80: 300-Passenger Class Interactive Sensitivity Analysis Environment

Table 9: 300-Passenger Class Correlations

	Subsystem Wt	SW	TOGW	hpx max	hpx avg
Subsystem Wt	1.00000	0.90669	0.90660	-0.73004	-0.77406
SW	0.90669	1.00000	0.99999	-0.43247	-0.48111
TOGW	0.90660	0.99999	1.00000	-0.43243	-0.48099
hpx max	-0.73004	-0.43247	-0.43243	1.00000	0.98580
hpx avg	-0.77406	-0.48111	-0.48099	0.98580	1.00000

Table 10: 300-Passenger Class Covariance Matrix

	Subsystem Wt	SW	TOGW	hpx max	hpx avg
Subsystem Wt	587743.6	9739.5	1219344.2	-29924.7	-24537.9
SW	9739.5	196.3	24581.0	-324.0	-278.7
TOGW	1219344.2	24581.0	3077750.8	-40562.0	-34891.5
hpx max	-29924.7	-324.0	-40562.0	2858.8	2179.4
hpx avg	-24537.9	-278.7	-34891.5	2179.4	1709.8

different architectures as discussed establishes the significance of this coupling for the 300-passenger class aircraft.

As previously discussed in this section, the data for the 210 and 300 passenger aircraft from this experiment leads to the conclusion that the coupling between aircraft sizing and subsystem impact exists and is still significant for these additional passenger classes of aircraft (validating Hypothesis 2). Experiments 1 and 2 demonstrate the significance of this coupling and the capturing of this coupling.

It should be noted that the all EHA architecture is found to be deterministically the best architecture for all three aircraft sizes. However, this architecture is unlikely to be the most robust of the top architectures for any of the aircraft sizes as hydraulics have been much more widely utilized than have EHAs. In fact, the all-EHA case is seen to be the least robust of the top architectures for the baseline aircraft size in the next experiment.

6.3 Experiment 3a

To review, **Hypothesis 3a** states the following: If distributions characterizing noise variables within aircraft subsystem architecture trades are utilized in the subsystem modeling and simulation environment, then a robust selection of the subsystem architecture design can be performed.

Experiment 3a utilized the physics-based modeling of aircraft internal subsystem architectures for the selected test configuration of an aircraft integrated with a sizing and synthesis algorithm made for Experiment 1. In experiment 3a, this modeling and simulation environment is used to quantify the robustness of the resulting designs when the top three subsystem architectures are utilized. As this experiments characterizes robustness, a discussion of the design and noise variables is necessary before discussing the results of the analysis.

This experiment is examines the determination of which subsystem architecture leads to the most robust design, in this case, where the most robust design has the best SNR of TOGW (the response). The selection of the architecture is the design

variable in the robust design study that attempts to find an architecture that leads to the most robust system design to sources of uncertainty. Due to the computational expense of the probabilistic analysis, this examination was limited to the top three candidate architectures. The architectures selected within this test were identified as the top candidates from running the DOE on the modeling and simulation environment as described in Experiment 1. These top candidate architectures have the lowest deterministic values of TOGW due to the impact of this metric. These candidates were the use of all EHAs (shown in Figure 26), the use of all hydraulic actuation (shown in Figure 25), and a hybrid system in which the elevators were powered by EHAs and the rest of the flight control system was powered by hydraulic actuators as seen in Figure 81. (It should be noted that these figures utilize an aircraft diagram from [31].)

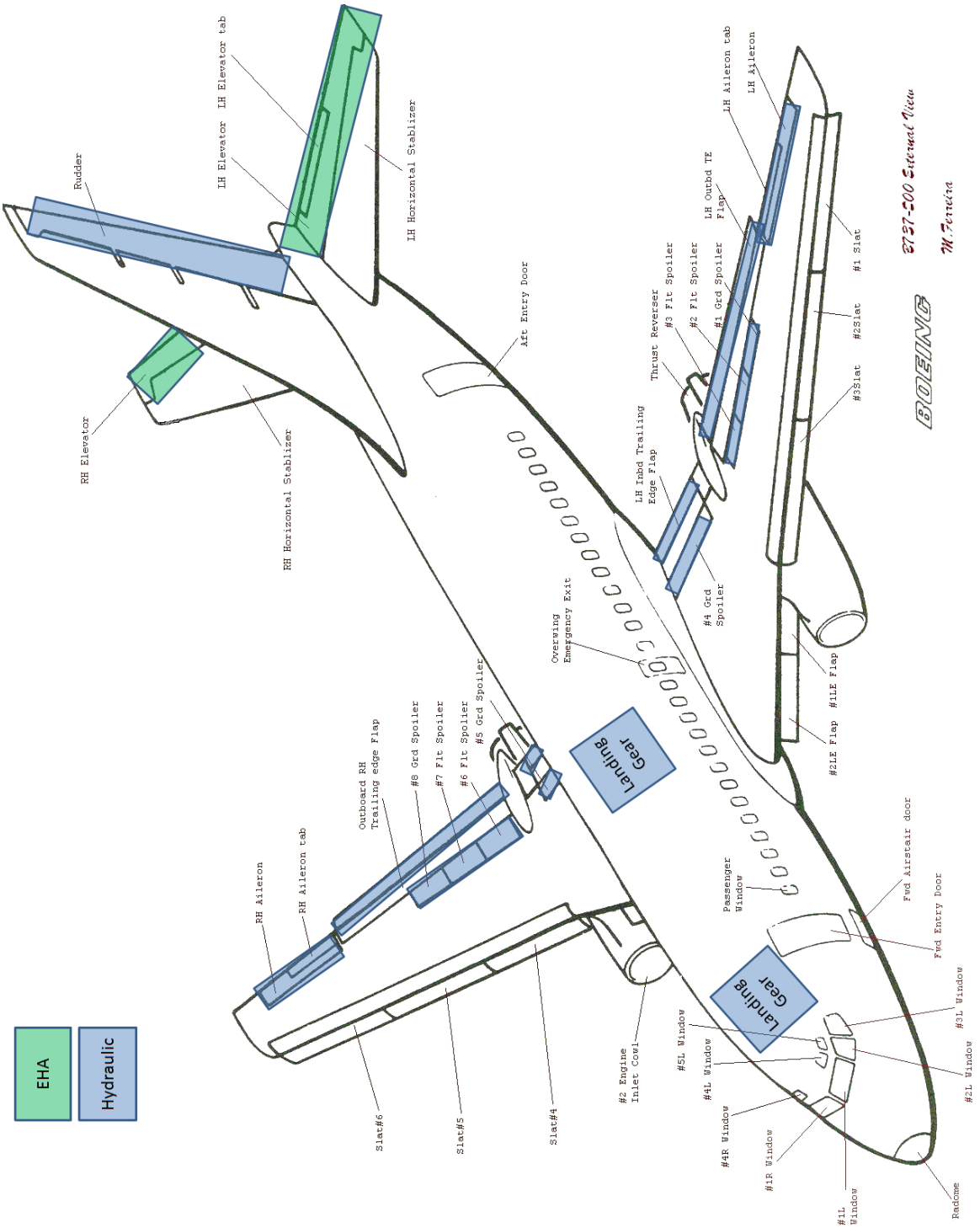

Figure 81: Top Hybrid Architecture adapted from [31]

To capture the uncertainty, probability distributions were applied on noise parameters within the subsystem modeling environment, such as the exact values of

efficiencies and weights. Specifically, Bayesian (subjective) distributions were utilized because such distributions can capture more than one type of uncertainty (including epistemic and aleatory) [114]. Distributions were created based on available information in literature, expert opinion, and engineering judgment. These distributions were determined for specific selected parameters and applied to these parameters in the modeling and simulation environment to enable determination of the impact of these distributions on the response of TOGW. The parameters were selected by engineering judgment after examining the available parameters in the modeling and simulation environment, their uncertainty, and system impacts. The selected variables can be seen in Table 11. EHA actuator weight was selected because of epistemic uncertainty in this parameter, partially due to technological uncertainty as EHAs are not widely utilized. The hydraulic actuator weight was selected due to epistemic uncertainty on the exact value of this parameter because of the fact this analysis is being performed during an early design phase. The motor and generator efficiencies were also selected as these parameters were treated as constants in the modeling environment with the exact true values of these efficiencies having epistemic uncertainty on this value due to the fact that these values are unknown in an early design phase and the impact on this efficiency (within its range) of varying the size of the motor and generator is not captured. Uncertainty in the wire weight was examined due to epistemic uncertainty coming from the determination of the exact impact of utilizing EHAs on this value and neglected certain contributions to this value such as fittings. The engine driven pump weight was also treated as a noise parameter due to epistemic uncertainty in this value for hybrid architectures, where there is uncertainty on the impact of the pump re-sizing due to switching some surfaces to being powered by EHAs on this parameter.

The selected Bayesian distributions can be seen in Table 12. The distributions

were created based on the cited sources and engineering judgment with the exception of the actuator weight ranges. The actuator weight distributions were determined based on the noted sources, data supplied by experts from the Parker Hannifin Corporation Aerospace Group, and engineering judgment. Specifically, the expert-supplied actuator weight ranges were increased to account for technological uncertainty (especially on the EHAs as the use of EHAs is much less developed than hydraulic actuators). It should be noted that these distributions were placed only on the architecture applicable to them. For example, the hydraulic actuator weight distribution was not placed on the all-EHA architecture. Specifically, the following noise parameters were utilized in the all EHA-architecture: wire weight, generator efficiency, EHA weight, and motor efficiency. The following noise parameters were used for the all-hydraulic architecture: generator efficiency, hydraulic actuator weight, and motor efficiency. Finally, the following noise parameters were captured for the hybrid architecture: wire weight, generator efficiency, hydraulic actuator weight, EHA weight, engine driven pump weight, and motor efficiency.

These Bayesian distributions capture technological uncertainty, epistemic uncertainty due to the design phase and available data, and uncertainty in the true exact value of some parameters treated as constants in the modeling environment. The engine-driven pump weight was treated as a weight per capacity of lb/gpm and was examined due to uncertainty in knowledge of the value of this parameter as the pump was varying in size. A Bayesian distribution for this value was created based on the range in this value encountered in engine-driven pumps in [137] and engineering judgment to capture this uncertainty. The weight of the EHA and hydraulic actuators were modeled as a mass per capacity in terms of kg/KN. The values of the EHA and hydraulic weight were examined as noise variables due to uncertainty in knowledge of the exact value of the weight, as discussed above. The possible range for these parameters used to define the Bayesian distribution was based on data supplied by experts

from the Parker Hannifin Corporation Aerospace Group. For the EHA, the range of this distribution was widened to account for technological uncertainty utilizing engineering judgment, as this was a less developed and less frequently utilized technology. As discussed above, the generator efficiency is treated as a constant within the modeling environment, and there is epistemic uncertainty on this parameter. The range for the selected Bayesian distribution to capture the epistemic uncertainty on this parameter was based on the range encountered within a generator efficiency curve in Armstrong's dissertation [21] and engineering judgment. The electric motor efficiency was also treated as a constant within the model and had epistemic uncertainty, as discussed above. As a result of a lack of knowledge of the exact value of the motor efficiency, this was also treated as a noise parameter with its range based on operating ranges of electric motors within [3] and on engineering judgment. As discussed above, due to uncertainty in its exact value and neglected contributions such as fittings, the wire weight was also treated as a noise parameter. The range for this parameter was based on engineering judgment and the factor found in [116] to account for neglected components such as fittings for hydraulic lines.

Table 11: Selected Variables

Variable	Reason
wire weight factor	neglected contributions, uncertainty in knowledge
electric motor efficiency	treated as constant in model
generator efficiency	treated as constant in model
hydraulic actuator weight	uncertainty in knowledge
EHA weight	uncertainty in knowledge
engine driven pump weight	uncertainty in knowledge

Ranges on the selected parameters were determined by the creation of these distributions. These ranges were then leveraged to create a DOE to explore the subsystem modeling environment. This DOE had a full factorial of all the end points of the defined ranges applicable to each architecture. The ranges came from the distributions

Table 12: Selected Distributions

Variable	Distribution and Source for Values
wire weight factor	uniform, 1 to 1.2 [116]
electric motor efficiency	uniform, 0.8 to 0.98 [3]
generator efficiency	uniform, 0.8 to 0.95 [21]
hydraulic actuator weight	uniform, 0.0976 Kg/kN to 0.45 [93]
EHA weight	uniform, 0.16 to 1.34 Kg/KN [99] and [112] and [47]
engine driven pump weight	uniform, 0.34 to 0.73 lb/gpm [137]

except TOGW and SW ranges, which were defined by taking the range seen in Experiment 1 and increasing it as needed to ensure a valid range, and a latin hypercube to capture the interior points. Such a DOE was run for each candidate architecture. The resulting data was used for two purposes: first, to define ranges to make a similar DOE for EDS, and second to attempt to fit surrogate models to the data to enable the number of runs required. Due to the successful previous use of ANNs on EDS [69] and [70] and the likely non-linearity of the data, ANNs were utilized to attempt to create surrogate models. ANNs were fit to the subsystem weight (used in EDS), the power extraction map (used in EDS), the average power extraction map value (not used in EDS), the maximum power extraction value (not used in EDS), and the minimum power extraction value (not used in EDS). The summary of fit data for these ANNs can be seen in Appendices A,B, and C. It can be seen that these fits are are reasonable. These metamodels made the run time of MCS cases feasible as it was determined that the runtime to utilize the integrated environment without surrogates was infeasible.

Utilizing the ranges of the data obtained from running the DOEs on Matlab/Simulink, ranges were determined for the inputs to EDS. These ranges were utilized to create a DOE that was run on EDS. Then, the resulting data was utilized to create ANNs of EDS. The summary of fit data is shown in Figures 82 and 83. In the summary of fit data, it is desirable to have a R-squared as close to 1 as possible, a close to linear actual by predicted plot, a random scatter of the residual, and small values for MFE

and MRE. The plots below utilize the residual as the definition of error and are fits of the natural logarithm of the responses as this transformation was seen to improve the quality of the fit. As can be seen, the quality of this fits appears sufficient for use, enabling MCS runs of the modeling environment.

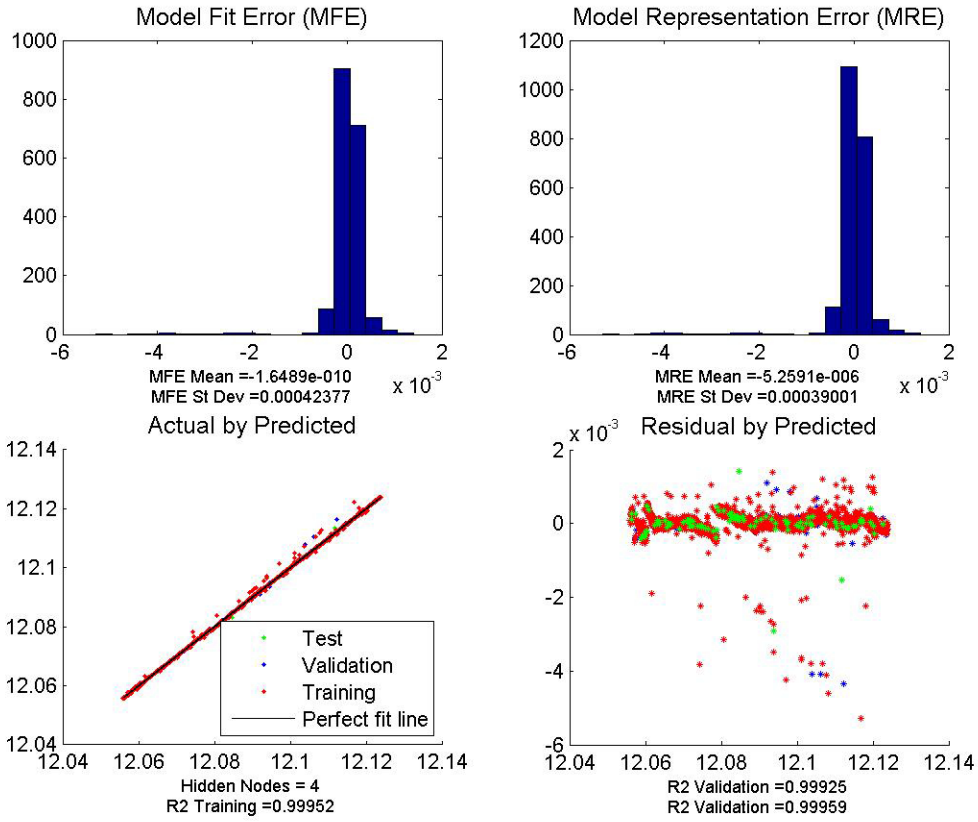

Figure 82: EDS ANN fit Data for TOGW

After applying the distributions and creating metamodels, Monte Carlo Simulation (MCS) was run on the metamodels of the integrated modeling environment, pulling variables out of the probability distributions but holding the architecture constant for 10000 cases per architecture. Then, the additional cases of other architectures were run. Multivariate plots of the resulting data and the correlation values are shown in Figures 84 and 85, respectively, for the all-EHA architecture. The designs within the multivariate plot were then filtered to include only designs that had a TOGW less than 175,000 lb. The filtered data is shown in Figure 86. It can be seen from this

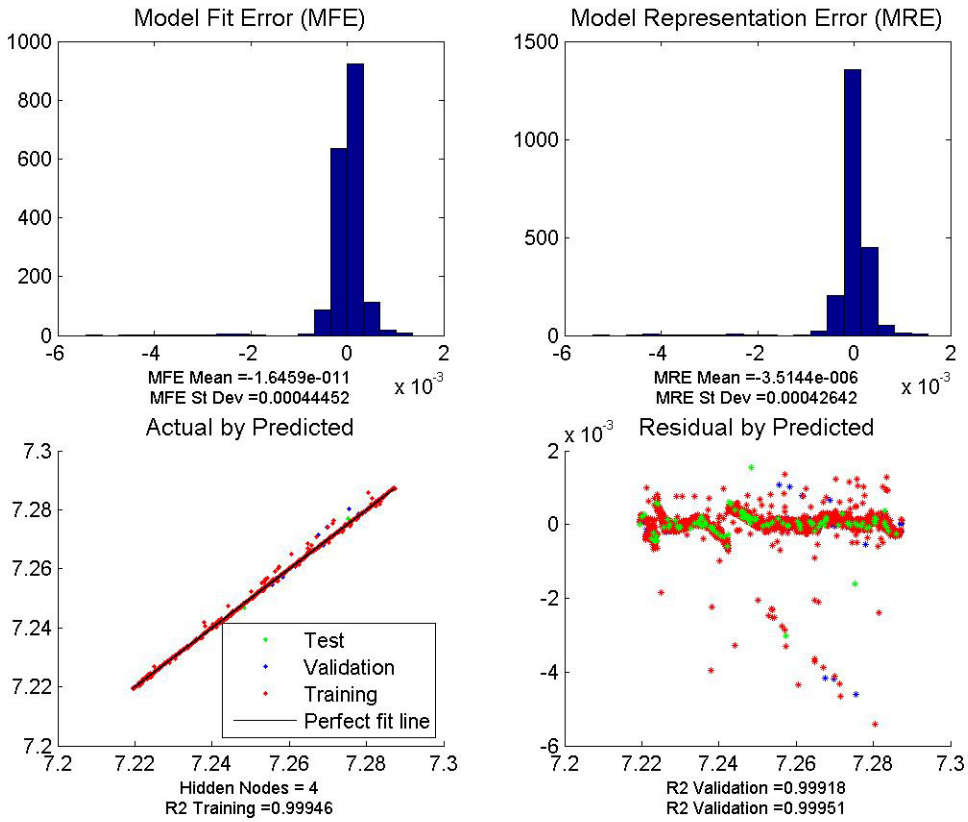

Figure 83: EDS ANN fit Data for Wing Area

figure that to achieve the lower TOGW values, the lower EHA and subsystem weights must be achieved. Multivariate plots of the resulting data and the correlation values can be seen in Figures 87 and 88, respectively, for all hydraulic actuation. The designs within this multivariate plot were again filtered to only include designs with a TOGW less than 175,000 lb. The filtered designs can be seen in Figure 89 where it can be observed that for the lower TOGW designs to be achievable for this architecture, the lower values of actuator weight must be achieved. Multivariate plots of the resulting data and the correlation values can be seen in Figures 90 and 91, respectively, for the case in which the elevator is powered by EHAs. Again, the designs within the multivariate plot were filtered to contain only designs with TOGW values lower than 175,000 lb. These filtered designs are shown in Figure 92, in which it can be observed that there are fewer designs left after the filtering because this architecture has a higher deterministic TOGW. It can be also observed that the lower TOGW designs again have the lower values for their weight-related parameters. By examining all of the architectures, it can be seen that the parameters related to subsystem weight (especially the actuator weights) are highly correlated with the TOGW, and those parameters may have the largest impact on the distribution of TOGW. This concept is explored further in Experiment 3b. It can also be seen in the results that the generator efficiency is negatively correlated with power extraction. This trend is logical as a more efficient system would demand less power. The data points from all 30000 cases were next used to determine the robustness of the architectures using SNR as described in the next subsection.

To further examine and characterize the relationships between the response(s) and the noise variables, Response Surface Equations (RSEs) were fit to the data for the different architectures. A second order polynomial model was again utilized as this is the form of the RSE as it is the most commonly used form in RSM [88]. Figures 93, 94, and 95 show interactive sensitivity analysis environments illustrating the RSEs that

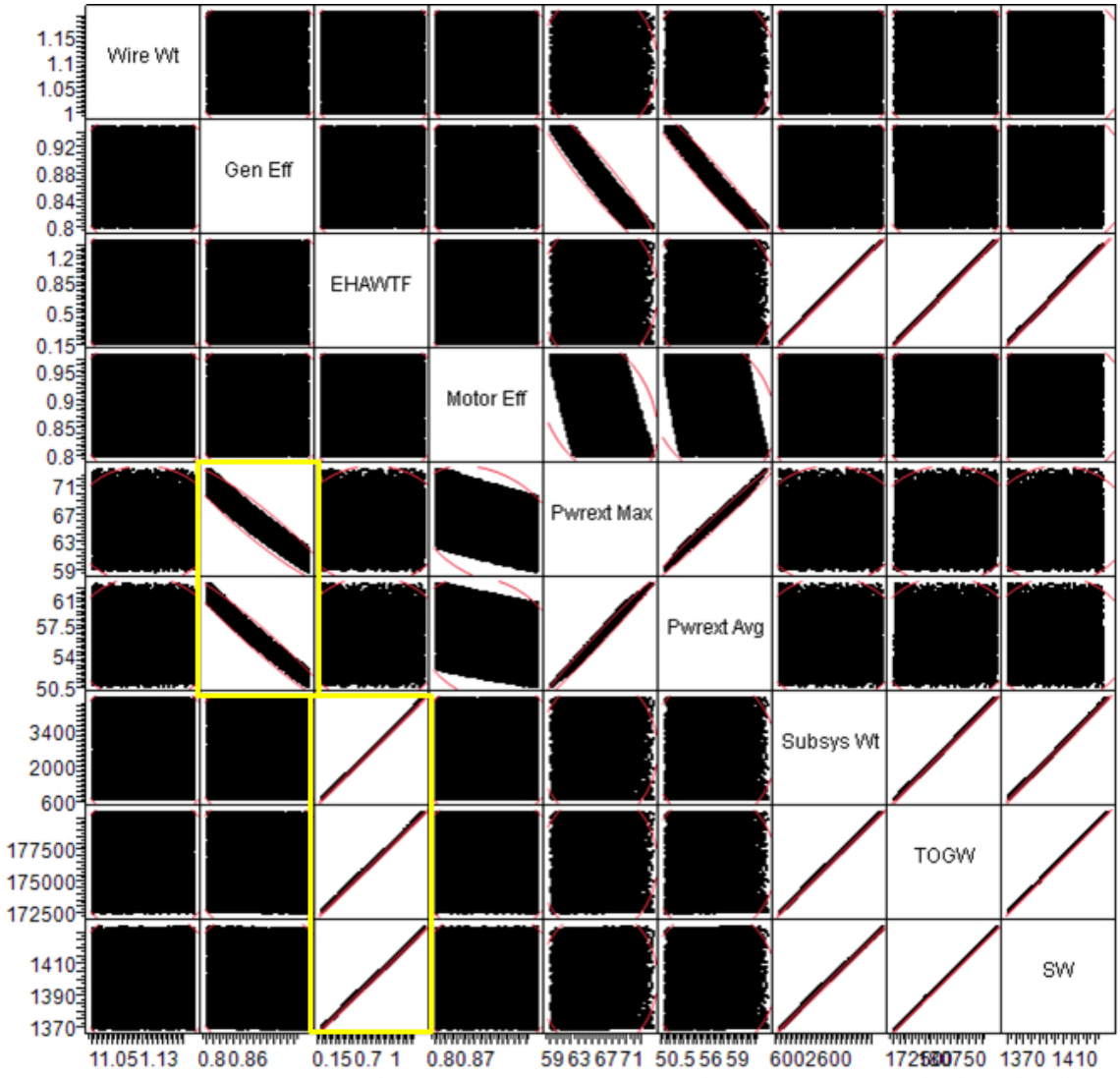

Figure 84: EHA Multivariate Plot

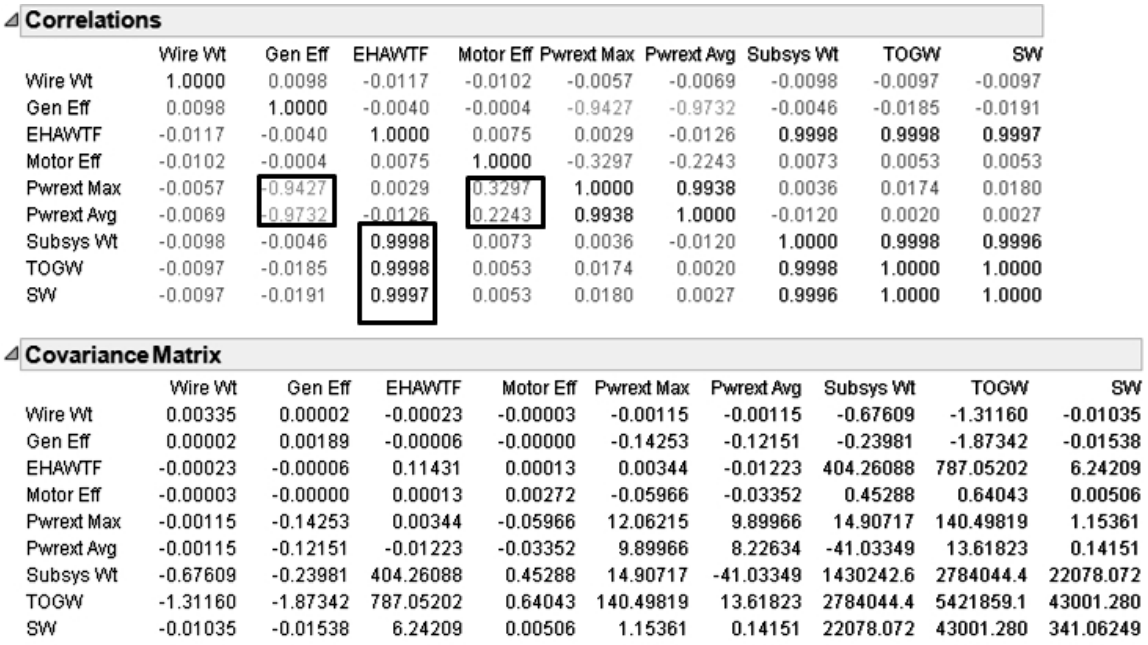

Correlations

	Wire Wt	Gen Eff	EHAWTF	Motor Eff	Pwrext Max	Pwrext Avg	Subsys Wt	TOGW	SW
Wire Wt	1.0000	0.0098	-0.0117	-0.0102	-0.0057	-0.0069	-0.0098	-0.0097	-0.0097
Gen Eff	0.0098	1.0000	-0.0040	-0.0004	-0.9427	-0.9732	-0.0046	-0.0185	-0.0191
EHAWTF	-0.0117	-0.0040	1.0000	0.0075	0.0029	-0.0126	0.9998	0.9998	0.9997
Motor Eff	-0.0102	-0.0004	0.0075	1.0000	-0.3297	-0.2243	0.0073	0.0053	0.0053
Pwrext Max	-0.0057	-0.9427	0.0029	0.3297	1.0000	0.9938	0.0036	0.0174	0.0180
Pwrext Avg	-0.0069	-0.9732	-0.0126	0.2243	0.9938	1.0000	-0.0120	0.0020	0.0027
Subsys Wt	-0.0098	-0.0046	0.9998	0.0073	0.0036	-0.0120	1.0000	0.9998	0.9996
TOGW	-0.0097	-0.0185	0.9998	0.0053	0.0174	0.0020	0.9998	1.0000	1.0000
SW	-0.0097	-0.0191	0.9997	0.0053	0.0180	0.0027	0.9996	1.0000	1.0000

Covariance Matrix

	Wire Wt	Gen Eff	EHAWTF	Motor Eff	Pwrext Max	Pwrext Avg	Subsys Wt	TOGW	SW
Wire Wt	0.00335	0.00002	-0.00023	-0.00003	-0.00115	-0.00115	-0.67609	-1.31160	-0.01035
Gen Eff	0.00002	0.00189	-0.00006	-0.00000	-0.14253	-0.12151	-0.23981	-1.87342	-0.01538
EHAWTF	-0.00023	-0.00006	0.11431	0.00013	0.00344	-0.01223	404.26088	787.05202	6.24209
Motor Eff	-0.00003	-0.00000	0.00013	0.00272	-0.05966	-0.03352	0.45288	0.64043	0.00506
Pwrext Max	-0.00115	-0.14253	0.00344	-0.05966	12.06215	9.89966	14.90717	140.49819	1.15361
Pwrext Avg	-0.00115	-0.12151	-0.01223	-0.03352	9.89966	8.22634	-41.03349	13.61823	0.14151
Subsys Wt	-0.67609	-0.23981	404.26088	0.45288	14.90717	-41.03349	1430242.6	2784044.4	22078.072
TOGW	-1.31160	-1.87342	787.05202	0.64043	140.49819	13.61823	2784044.4	5421859.1	43001.280
SW	-0.01035	-0.01538	6.24209	0.00506	1.15361	0.14151	22078.072	43001.280	341.06249

Figure 85: EHA Correlations

were fit for the hybrid, hydraulic, and EHA architectures respectively. As a reminder, such a plot displays the partial derivatives of the different variables. Similar trends to those already observed can be seen in these figures such as the strong, almost linear, relationship between TOGW and subsystem weight. It can be seen in these plots that the weight-related parameters, especially of the dominant actuator within the examined architecture, have a strong impact on aircraft size (TOGW). Generator efficiency can also be seen to have a strong impact on power extraction. As seen in Appendix D, which contains information illustrating the quality of these fits for the different responses, the quality of these fits is acceptable for analysis. The figures shown in Appendix D demonstrate that the RSEs and trends shown in the interactive sensitivity analysis environments are valid.

Then, the robustness of the different designs were compared, using the robustness of different parameters such as TOGW, utilizing a metric such as SNR. Finally, the robustness of these designs were then used to select the top architecture as discussed in the next subsection. The determination of the SNR for parameters, such as TOGW,

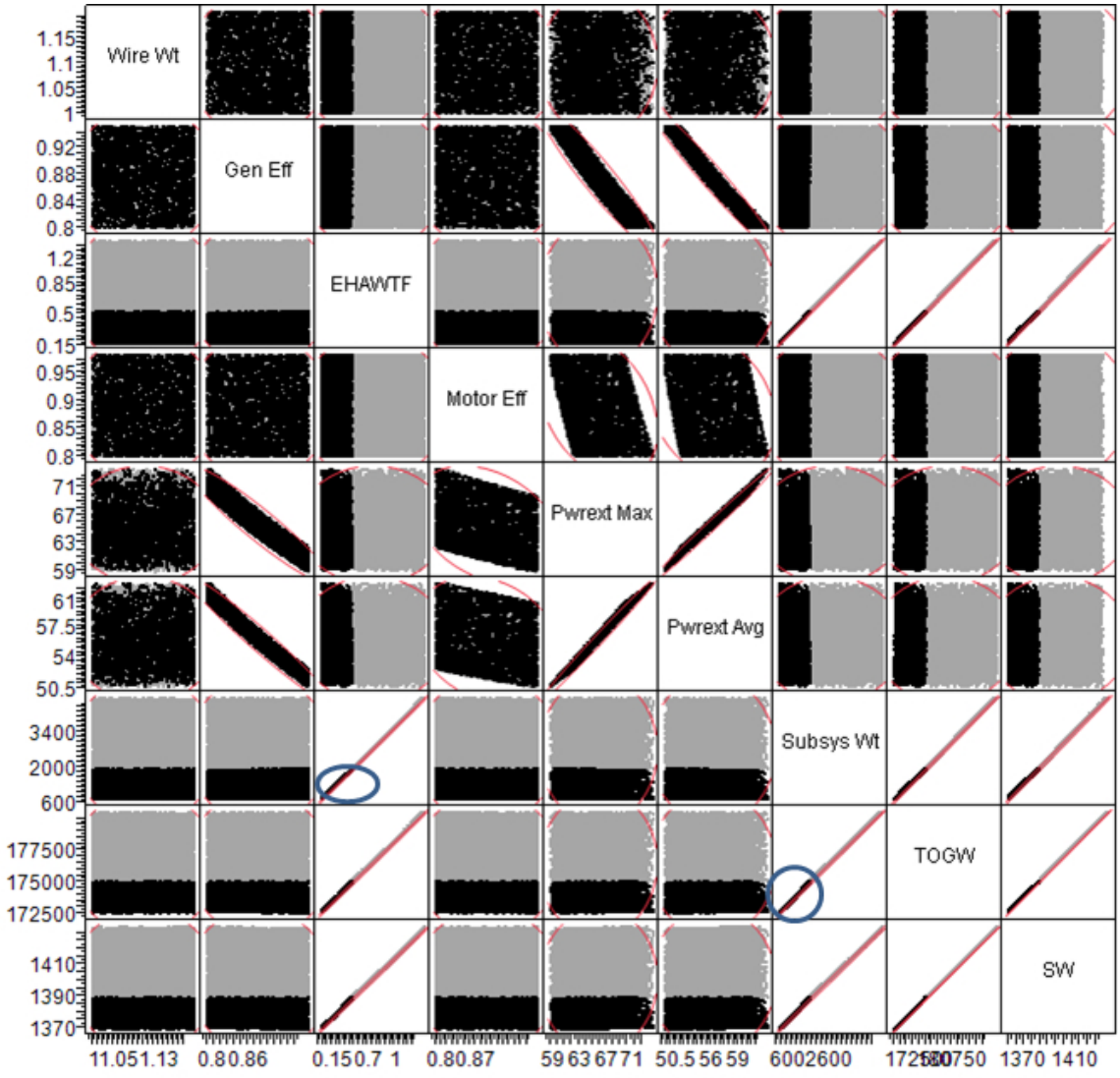

Figure 86: Lower TOGW EHA Designs

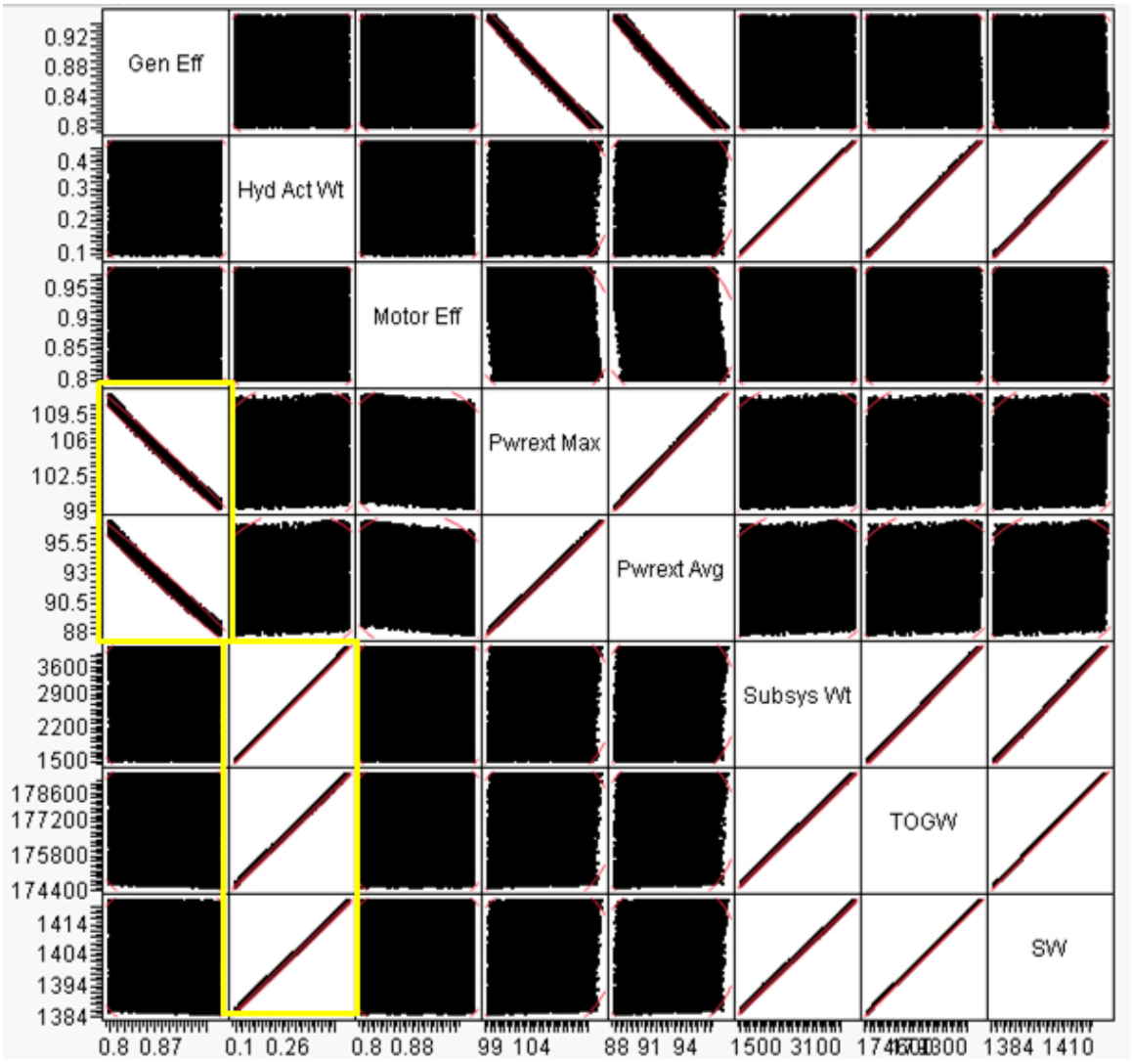

Figure 87: Hydraulic Multivariate Plot

Correlations

	Gen Eff	Hyd Act Wt	Motor Eff	Pwrext Max	Pwrext Avg	Subsys Wt	TOGW	SW
Gen Eff	1.0000	0.0015	0.0031	-0.9954	-0.9923	0.0008	-0.0213	-0.0209
Hyd Act Wt	0.0015	1.0000	0.0057	0.0401	0.0461	0.9999	0.9997	0.9996
Motor Eff	0.0031	0.0057	1.0000	-0.0769	-0.1080	0.0055	0.0033	0.0033
Pwrext Max	-0.9954	0.0401	-0.0769	1.0000	0.9995	0.0409	0.0630	0.0627
Pwrext Avg	-0.9923	0.0461	-0.1080	0.9995	1.0000	0.0469	0.0691	0.0687
Subsys Wt	0.0008	0.9999	0.0055	0.0409	0.0469	1.0000	0.9997	0.9997
TOGW	-0.0213	0.9997	0.0033	0.0630	0.0691	0.9997	1.0000	1.0000
SW	-0.0209	0.9996	0.0033	0.0627	0.0687	0.9997	1.0000	1.0000

Covariance Matrix

	Gen Eff	Hyd Act Wt	Motor Eff	Pwrext Max	Pwrext Avg	Subsys Wt	TOGW	SW
Gen Eff	0.00187	0.00001	0.00001	-0.13508	-0.10632	0.02371	-1.23654	-0.00955
Hyd Act Wt	0.00001	0.01017	0.00003	0.01268	0.01152	71.26448	135.26963	1.06268
Motor Eff	0.00001	0.00003	0.00269	-0.01250	-0.01388	0.20225	0.23244	0.00183
Pwrext Max	-0.13508	0.01268	-0.01250	9.82425	7.75300	90.53185	264.97900	2.06972
Pwrext Avg	-0.10632	0.01152	-0.01388	7.75300	6.12472	82.03948	229.25615	1.79162
Subsys Wt	0.02371	71.26448	0.20225	90.53185	82.03948	499269.82	947648.72	7444.7317
TOGW	-1.23654	135.26963	0.23244	264.97900	229.25615	947648.72	1799818.0	14139.680
SW	-0.00955	1.06268	0.00183	2.06972	1.79162	7444.7317	14139.680	111.08497

Figure 88: Hydraulic Correlations

demonstrates that the robustness of the designs can be quantified.

6.4 Architecture Selection

The top three architectures were examined in Experiment 3a. They were selected as top candidates based on their having the best deterministic TOGW. TOGW was utilized due to the importance of this metric. In Experiment 3a, the uncertainty of top architectures was examined to determine the robustness of their resulting designs. The metric SNR was utilized to quantify their robustness on TOGW due to the impact of this metric. As was discussed in the MAIA description of this step, the SNR definition shown in equation (29) was utilized because of the desire to minimize redesign work due to deviation from the deterministic TOGW target.

According to [88], [111], [48], and [138]:

$$SNR = -10log((\mu^2)/\sigma^2) \tag{29}$$

The resulting SNRs can be seen in Table 13. The design with the best SNR was the use of a hybrid architecture with almost all hydraulic actuation and EHAs utilized

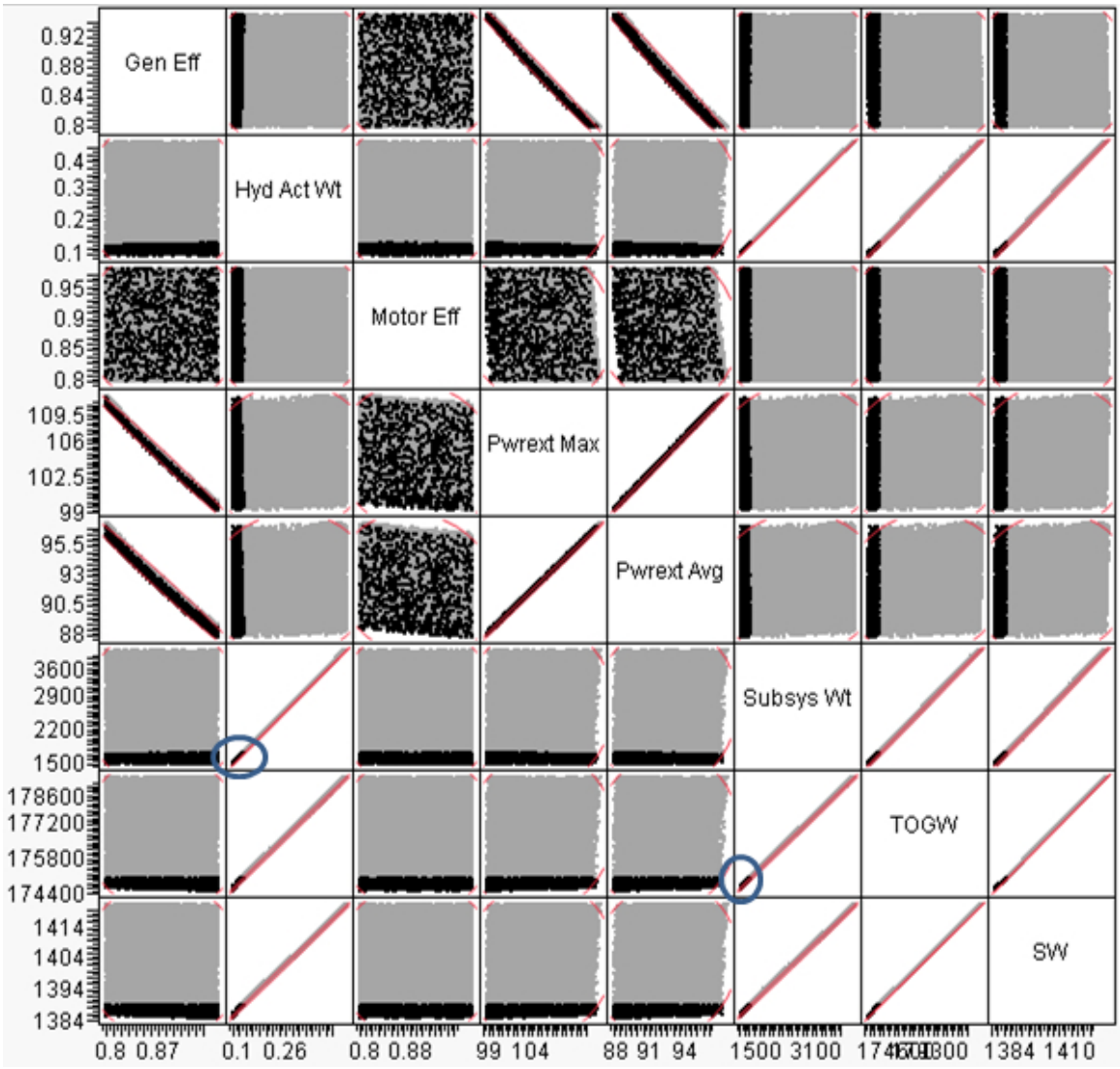

Figure 89: Lower TOGW Hydraulic Designs

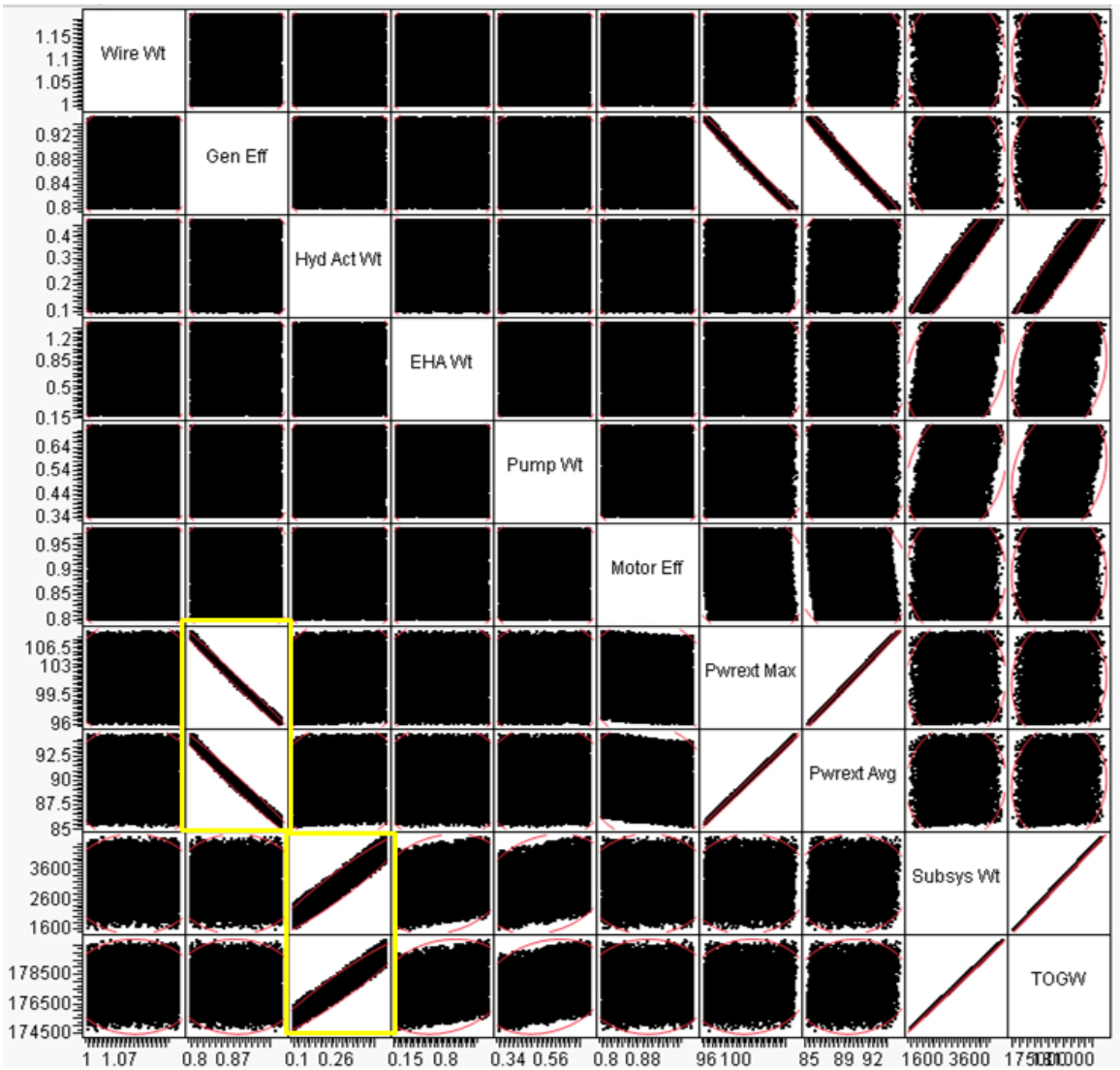

Figure 90: Hybrid Multivariate Plot

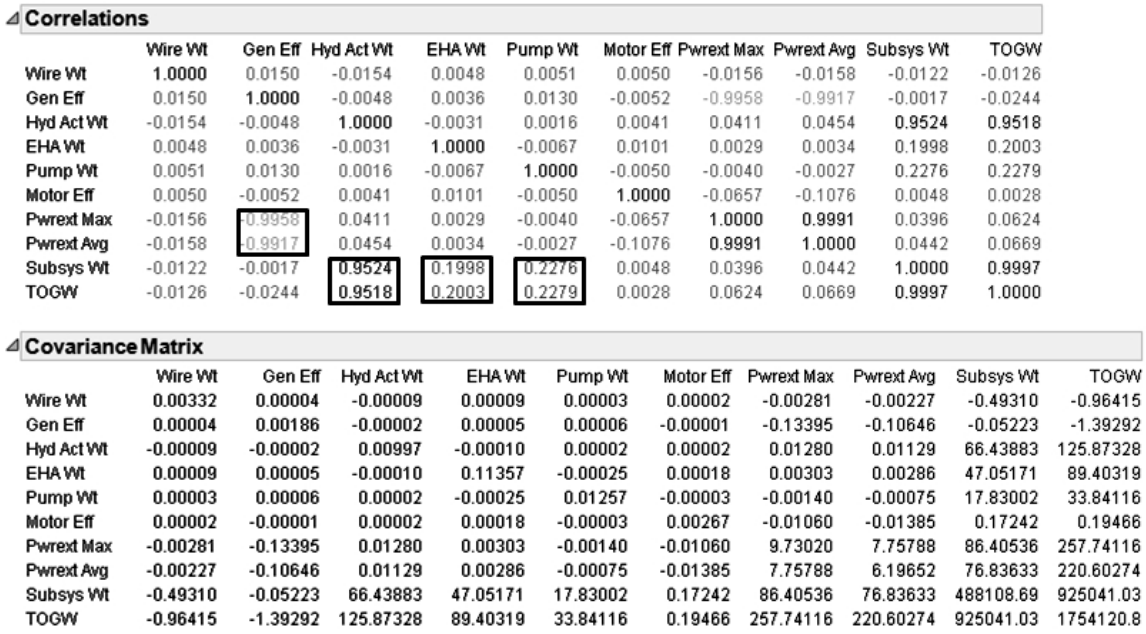

Correlations

	Wire Wt	Gen Eff	Hyd Act Wt	EHA Wt	Pump Wt	Motor Eff	Pwrext Max	Pwrext Avg	Subsys Wt	TOGW
Wire Wt	1.0000	0.0150	-0.0154	0.0048	0.0051	0.0050	-0.0156	-0.0158	-0.0122	-0.0126
Gen Eff	0.0150	1.0000	-0.0048	0.0036	0.0130	-0.0052	-0.9958	-0.9917	-0.0017	-0.0244
Hyd Act Wt	-0.0154	-0.0048	1.0000	-0.0031	0.0016	0.0041	0.0411	0.0454	0.9524	0.9518
EHA Wt	0.0048	0.0036	-0.0031	1.0000	-0.0067	0.0101	0.0029	0.0034	0.1998	0.2003
Pump Wt	0.0051	0.0130	0.0016	-0.0067	1.0000	-0.0050	-0.0040	-0.0027	0.2276	0.2279
Motor Eff	0.0050	-0.0052	0.0041	0.0101	-0.0050	1.0000	-0.0657	-0.1076	0.0048	0.0028
Pwrext Max	-0.0156	-0.9958	0.0411	0.0029	-0.0040	-0.0657	1.0000	0.9991	0.0396	0.0624
Pwrext Avg	-0.0158	-0.9917	0.0454	0.0034	-0.0027	-0.1076	0.9991	1.0000	0.0442	0.0669
Subsys Wt	-0.0122	-0.0017	0.9524	0.1998	0.2276	0.0048	0.0396	0.0442	1.0000	0.9997
TOGW	-0.0126	-0.0244	0.9518	0.2003	0.2279	0.0028	0.0624	0.0669	0.9997	1.0000

Covariance Matrix

	Wire Wt	Gen Eff	Hyd Act Wt	EHA Wt	Pump Wt	Motor Eff	Pwrext Max	Pwrext Avg	Subsys Wt	TOGW
Wire Wt	0.00332	0.00004	-0.00009	0.00009	0.00003	0.00002	-0.00281	-0.00227	-0.49310	-0.96415
Gen Eff	0.00004	0.00186	-0.00002	0.00005	0.00006	-0.00001	-0.13395	-0.10646	-0.05223	-1.39292
Hyd Act Wt	-0.00009	-0.00002	0.00997	-0.00010	0.00002	0.00002	0.01280	0.01129	66.43883	125.87328
EHA Wt	0.00009	0.00005	-0.00010	0.11357	-0.00025	0.00018	0.00303	0.00286	47.05171	89.40319
Pump Wt	0.00003	0.00006	0.00002	-0.00025	0.01257	-0.00003	-0.00140	-0.00075	17.83002	33.84116
Motor Eff	0.00002	-0.00001	0.00002	0.00018	-0.00003	0.00267	-0.01060	-0.01385	0.17242	0.19466
Pwrext Max	-0.00281	-0.13395	0.01280	0.00303	-0.00140	-0.01060	9.73020	7.75788	86.40536	257.74116
Pwrext Avg	-0.00227	-0.10646	0.01129	0.00286	-0.00075	-0.01385	7.75788	6.19652	76.83633	220.60274
Subsys Wt	-0.49310	-0.05223	66.43883	47.05171	17.83002	0.17242	86.40536	76.83633	488108.69	925041.03
TOGW	-0.96415	-1.39292	125.87328	89.40319	33.84116	0.19466	257.74116	220.60274	925041.03	1754120.8

Figure 91: Hybrid Correlations

on the elevator. This result is probably due to the fact that it utilizes mostly hydraulic actuation, a currently existing and utilized technology instead of a new technology, and the fact that it was one of the top three candidates that had the lowest TOGW. As a result, for this case study it is recommended to utilize the hybrid architecture that contains EHAs on the elevator only for the most robust actuation system design. It should be noted that the all-EHA architecture is seen to be the least robust. This is to be expected as it is a less utilized and less developed technology than hydraulic actuation, with more uncertainty in its weight and performance.

Table 13: Design Robustness

Design	SNR
Hydraulic	-4.240
EHA	-3.759
Hybrid	-4.255

Experiment 3a demonstrated examination of the robustness of the different architectures and robust architecture selection utilizing MAIA. This shows that inherent

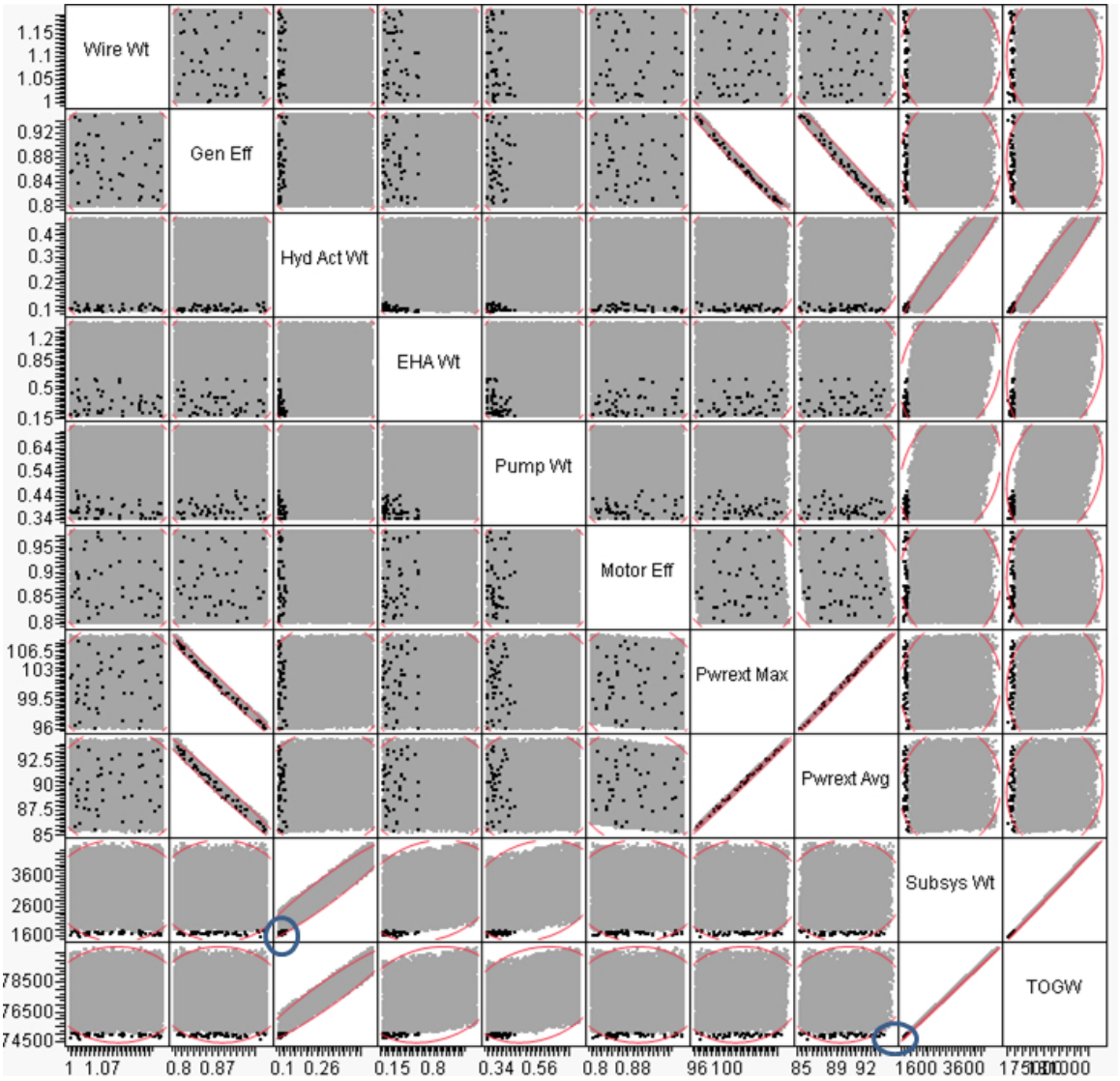

Figure 92: Low TOGW Hybrid Designs

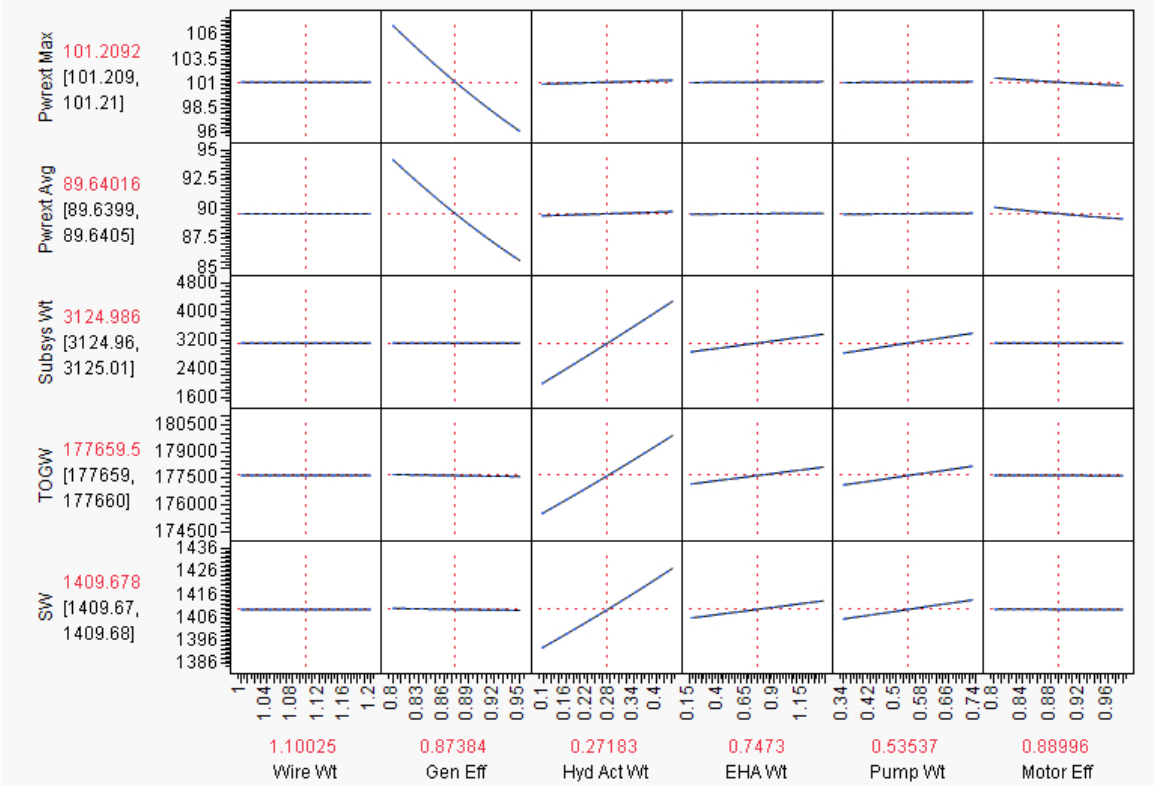

Figure 93: Hybrid Architecture Interactive Sensitivity Analysis Environment

uncertainty can be captured in subsystem architecture trades using probability distributions on the noise variables and Monte Carlo simulation. The examination of design robustness within MAIA enables the selection of robust subsystem designs that may reduce unexpected weight gains.

6.5 Experiment 3b

To review, **Hypothesis 3b** states the following: If a Bayesian Network is created to represent the impact of the uncertainty in the subsystem architectures characteristics on aircraft sizing, then the variables with the largest impacts can be identified.

Experiment 3b leveraged the data created from running the modeling environment for the top architecture(s) created for Experiment 3a. A Bayesian Network was created that had nodes for each source of uncertainty and TOGW and one connection from each source to TOGW in the BNT toolbox for Matlab [96]. The Bayesian

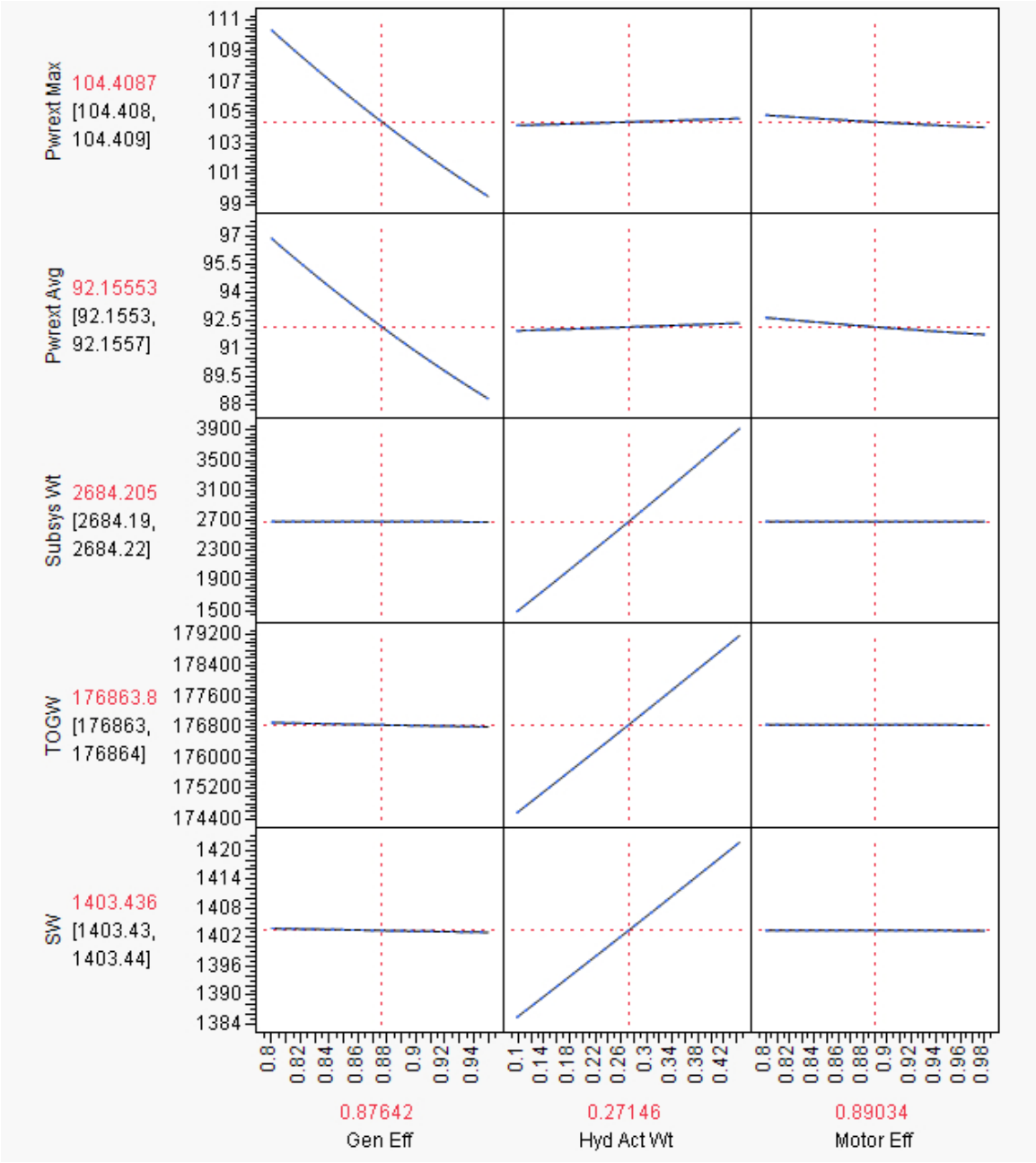

Figure 94: Hydraulic Architecture Interactive Sensitivity Analysis Environment

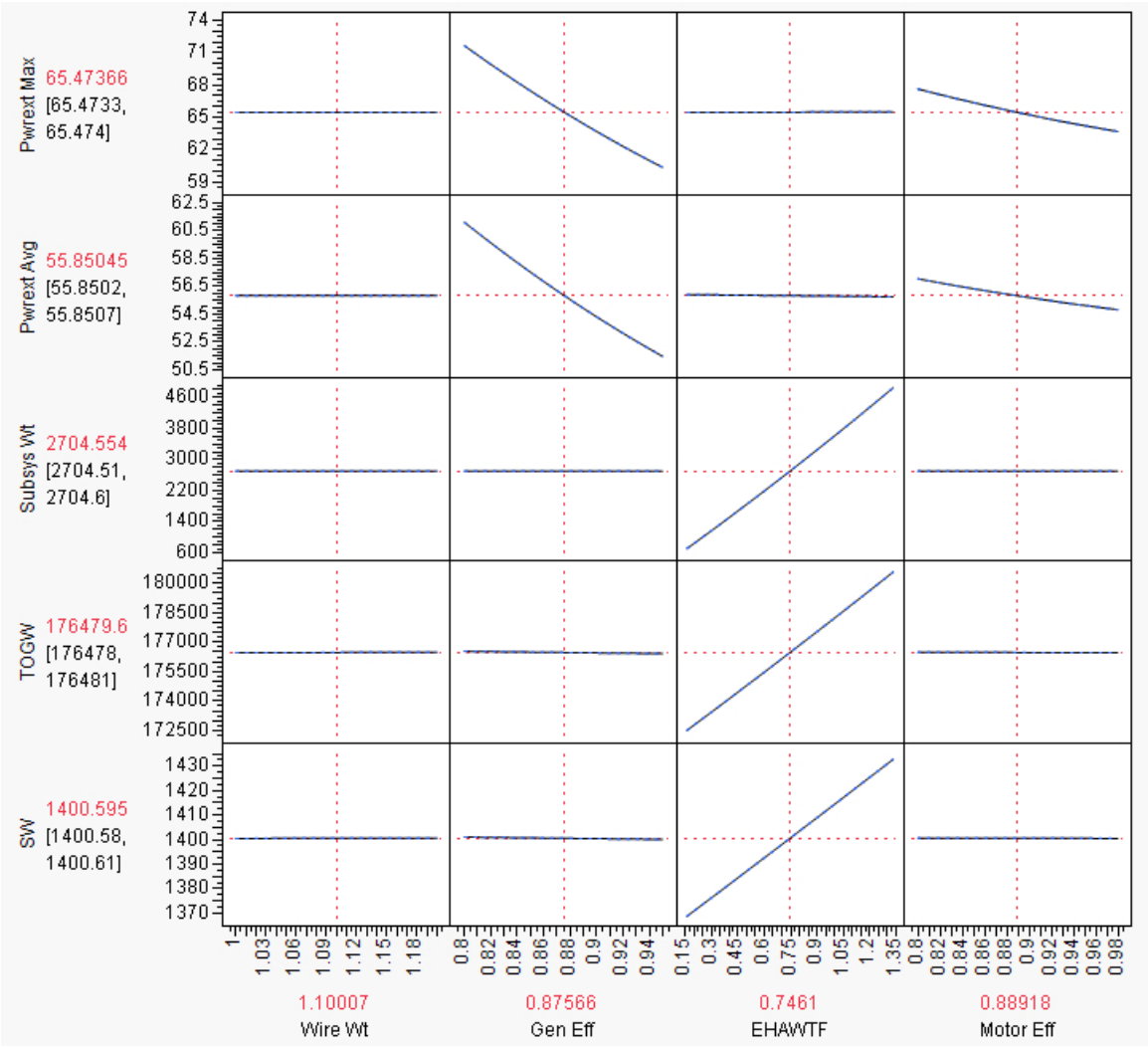

Figure 95: EHA Architecture Interactive Sensitivity Analysis Environment

Network was fit to a discretized form of the data from Experiment 3a for the top architecture. The utilized Bayesian Network structure can be seen in Figure 96. The strength of the connections were determined as discussed in [41]. The strengths of the links can be seen in Table 14. There are two strengths calculated and shown as discussed in [41]. The variables with the largest impacts are those that should have the strongest connections. It can be seen that there is a meaningful link strength in all the connections, a result which is to be expected, and that the strongest links are the weight related links which is consistent with the covariance/correlations between the variables and trends in the Monte Carlo data as shown in Experiment 3a. This is also compared to the use of an ANOVA as shown in Figure 98. Figure 98 shows that the weight-related parameters, especially the weight of hydraulic actuators have a significant impact on TOGW. This cross-referencing enables a validation of the results, which, in turn, validate the hypothesis. The identification of the larger correlation values match fairly closely the variables determined by examining the strength of the links, validating the result. The fact that the result is equivalent to other current methods makes the use of Bayesian Networks for such an analysis feasible and desirable due to additional predictive analysis during development of the subsystems. The network structure that may best fit the data was explored to gain additional insight using a Markov Chain Monte Carlo algorithm contained within the BNT toolbox [96]. The resulting structure has only one link that connects the variable with the largest impact (hydraulic actuator weight) and TOGW. This Bayesian Network structure is shown in Figure 97. The variable with the largest impact is hydraulic actuator weight, and if this architecture is to be developed, this variable should be investigated further to minimize the variance of TOGW. The results that determine, which parameters are the driving parameters are also consistent with the ANOVA results. Experiment 3b demonstrated that, utilizing Bayesian Networks, the designer can identify which of the noise variables had the strongest connection with the response. The demonstrated

feasibility of the use of Bayesian Networks for examining the connections between the noise and response variables enables their creation and use for such a purpose. This enables a possible reduction of the impact of the uncertainty for a selected design. As discussed in the chapter on uncertainty, these Bayesian Networks can then be utilized within the design process for useful additional analysis, including predictive analysis, which is enabled by the creation and use of these Bayesian Networks which is demonstrated to be feasible by this experiment.

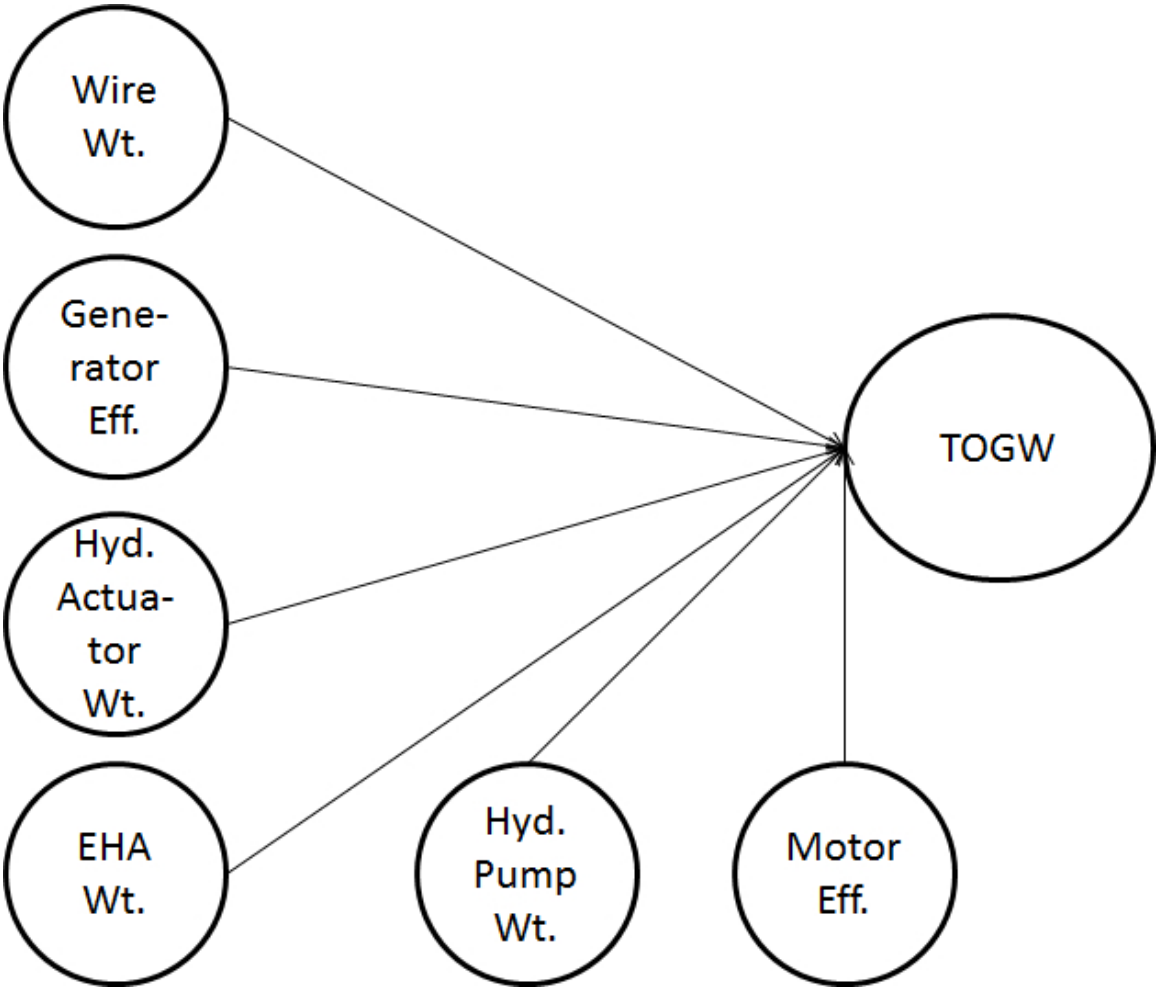

Figure 96: Hybrid Bayesian Network Structure

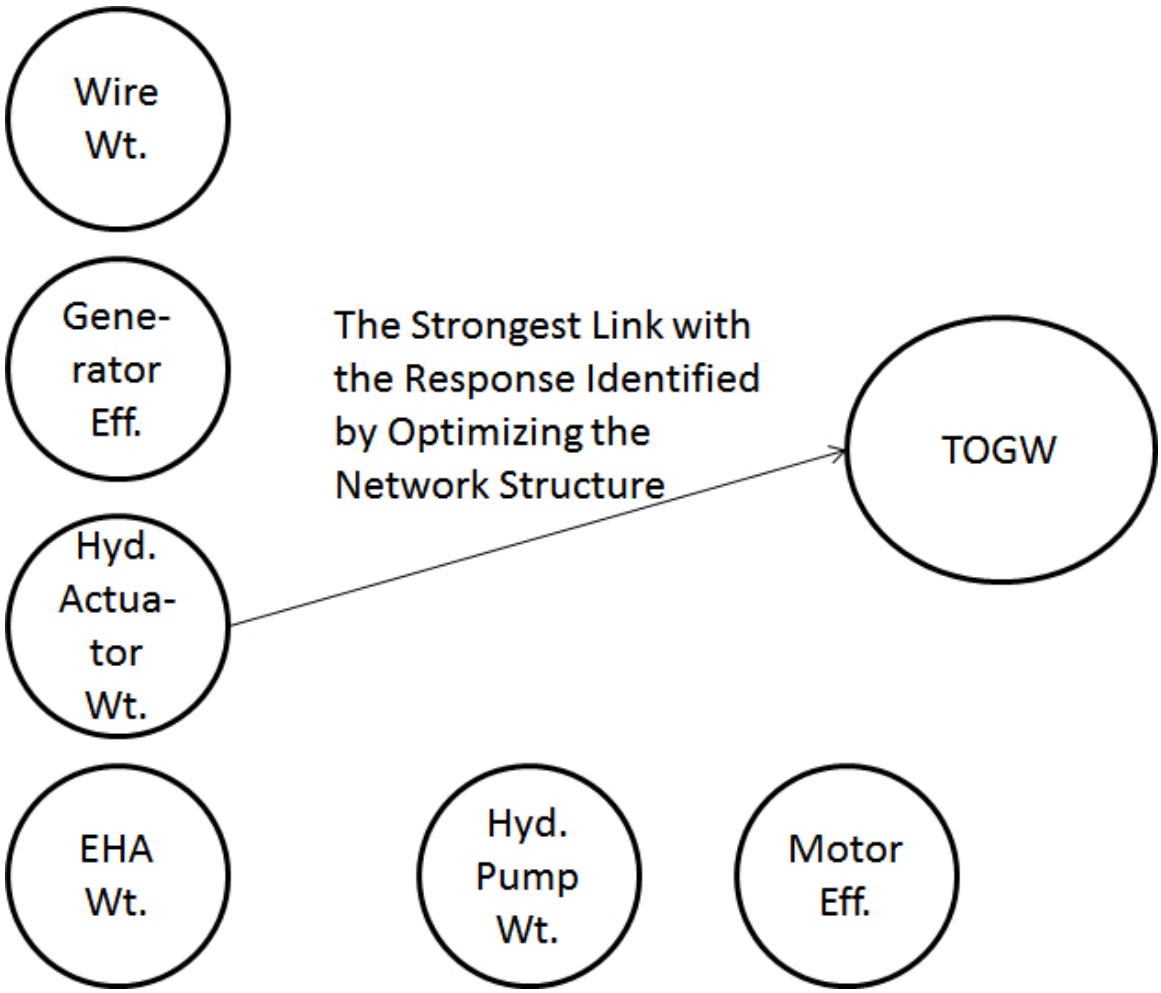

Figure 97: Optimized Hybrid Bayesian Network Structure

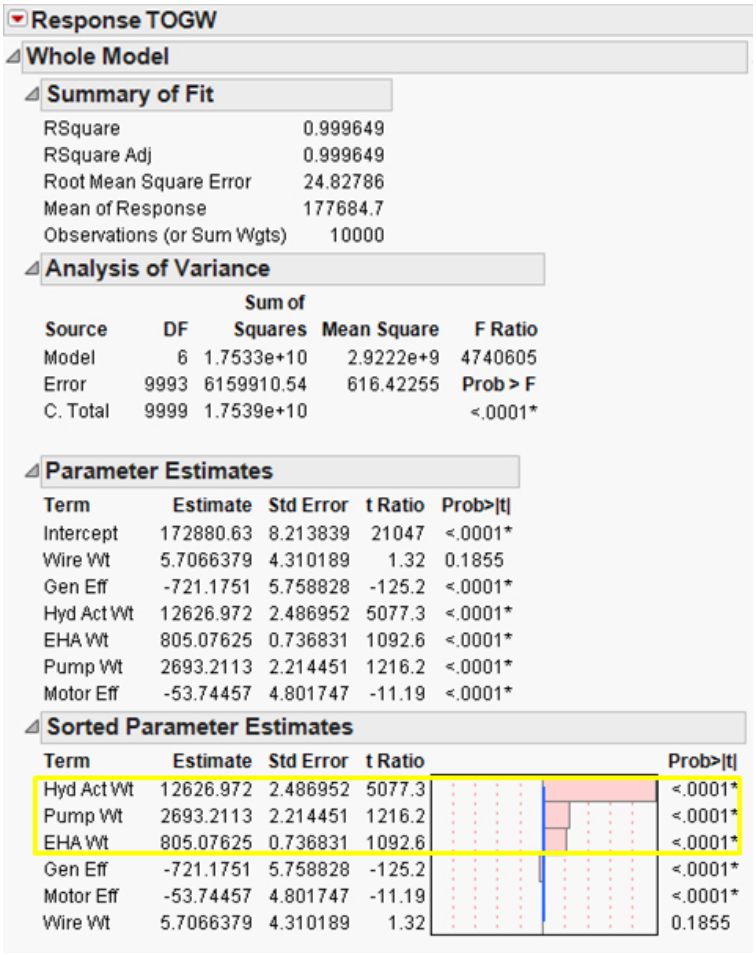

Response TOGW

Whole Model

Summary of Fit

RSquare	0.999649
RSquare Adj	0.999649
Root Mean Square Error	24.82786
Mean of Response	177684.7
Observations (or Sum Wgts)	10000

Analysis of Variance

Source	DF	Sum of Squares	Mean Square	F Ratio
Model	6	1.7533e+10	2.9222e+9	4740605
Error	9993	6159910.54	616.42255	Prob > F
C. Total	9999	1.7539e+10		<.0001*

Parameter Estimates

Term	Estimate	Std Error	t Ratio	Prob>|t|
Intercept	172880.63	8.213839	21047	<.0001*
Wire Wt	5.7066379	4.310189	1.32	0.1855
Gen Eff	-721.1751	5.758828	-125.2	<.0001*
Hyd Act Wt	12626.972	2.486952	5077.3	<.0001*
EHA Wt	805.07625	0.736831	1092.6	<.0001*
Pump Wt	2693.2113	2.214451	1216.2	<.0001*
Motor Eff	-53.74457	4.801747	-11.19	<.0001*

Sorted Parameter Estimates

Term	Estimate	Std Error	t Ratio	Prob>|t|
Hyd Act Wt	12626.972	2.486952	5077.3	<.0001*
Pump Wt	2693.2113	2.214451	1216.2	<.0001*
EHA Wt	805.07625	0.736831	1092.6	<.0001*
Gen Eff	-721.1751	5.758828	-125.2	<.0001*
Motor Eff	-53.74457	4.801747	-11.19	<.0001*
Wire Wt	5.7066379	4.310189	1.32	0.1855

Figure 98: Hybrid ANOVA

Table 14: Bayesian Network Link Strengths

Noise Variable	Strength True Average	Strength Blind Average
Wire Wt	59.3	68.6
Generator Eff	60.5	69.2
Hydraulic Wt	62.8	70.0
EHA Wt	62.9	68.6
Pump Wt	60.9	68.9
Motor Eff	59.9	68.3

6.6 The Overarching Experiment

To review, the **Overarching Hypothesis** states the following: Capturing of the coupling between aircraft sizing and subsystem architecture impacts and exploring the architecture design space enables a significantly better architecture selection than a point-driven design.

The first step of the Overarching Experiment was to create the required modeling environment to perform the steps in MAIA. This required the creation of physics-based models of aircraft internal subsystems for the selected example configuration of an aircraft. These models were made able to capture the impact of varying the selected subsystem architectures. This modeling environment includes a sizing calculation for the systems and their components. Then these models were integrated with a sizing and synthesis algorithm. For each design examined, the platform and system-level impacts were demonstrated in the converged values of the outputs such as the power extraction and TOGW. Once this environment was created, the next step was to explore the architecture design space for the test case utilizing the proposed methodology. This exploration was done utilizing a full factorial DOE, varying each group of control surfaces (flaps, elevators, rudder, aileron, landing gear, for example) from being hydraulically powered to being powered by EHAs as described in the test case section. This DOE was also utilized in Experiment 1. After the DOE was run, the significance of the use of MAIA over a point design was then explored.

It was seen in Experiments 1 and 2 that the coupling between aircraft sizing and subsystem architecture impacts was significant and necessary to capture. Examining the range in TOGW between the top and bottom architecture as in Experiment 1 shows that this coupling is important to capture and that the worst point design encountered in merely varying the actuation systems has a TOGW that is 2627 pounds heavier than the best architecture, or approximately 1.51 percent of the TOGW. Given that Roskam [121] states that the range to expect for the total weight of the actuation system is approximately 0.6 to 1.2 percent of TOGW, the difference in converged TOGW by varying this system is significant, and therefore the selection of a point design without exploration of the design space can be significantly inferior to one that is selected by exploring the design space while capturing the coupling between aircraft sizing and subsystem architecture impacts. This demonstrates the Overarching Hypothesis.

The existence of the coupling between aircraft sizing and subsystem architecture impacts and the significance of this coupling was demonstrated in Experiments 0, 1, and 2. Capturing of this coupling and exploration of the subsystem architecture design space utilizing MAIA was demonstrated in the experiments including the Overarching Experiment. Such design space exploration, which utilizes MAIA while capturing this coupling, was shown to represent a significant improvement over the use of a point design selected without exploring the design space or capturing this coupling between aircraft sizing and subsystem architecture impacts.

CHAPTER VII

CONCLUSIONS

7.1 Summary of Results

Experiment 1 examined the existence and the significance of the coupling between aircraft sizing and subsystem architecture platform-level impacts as discussed in Research Question 1 and Hypothesis 1, which are repeated below.

Research Question 1: What is the magnitude of the coupling between the subsystem architectures platform-level impacts and aircraft size?

Hypothesis 1: If the impact of the coupling between aircraft sizing and architecture impacts is quantified, then this coupling will be found to be significant.

To determine the significance of the coupling, it was first necessary to create the integrated modeling and simulation environment that could capture this coupling. This environment utilized the subsystem models integrated with aircraft sizing and synthesis algorithms as discussed in the section discussing the modeling environment.

Experiment 1 demonstrated that the coupling between aircraft sizing and architecture impacts exists and is significant for the baseline aircraft size, validating Hypothesis 1. This could be seen in the examined trends within the results, the magnitude of the impact on TOGW, and correlation values characterizing the coupling, especially between subsystem weight and TOGW. In fact, it can be seen that within the examined ranges, subsystem weight has a dominating impact over power extraction on TOGW. This implies that the use of lighter but less efficient subsystems would lead to a smaller aircraft size.

Experiment 2 examined the coupling between aircraft sizing and subsystem platform-level impacts for other aircraft passenger class sizes as discussed in Research Question

2 and Hypothesis 2.

Research Question 2: What is the impact of varying aircraft passenger class on the magnitude of the coupling between the platform-level impacts of the subsystem architecture and aircraft sizing?

Hypothesis 2: If the aircraft class examined is varied, then the impact of the coupling between aircraft sizing and architecture platform-level impacts is still significant.

Experiment 2 showed that the coupling is still significant for other aircraft passenger classes, validating Hypothesis 2. This can be seen in the observed trends, correlation values characterizing this coupling, and the impact on TOGW. It can be observed that the coupling and impact of the coupling is still significant for other passenger classes, and the subsystem weight again seems to have more impact on TOGW than power extraction within the examined variable ranges.

Experiment 3a examined Research Question 3a and Hypothesis 3a. Specifically, Experiment 3a examined the identification of a subsystem architecture that would lead to a robust design the sources of uncertainty.

Research Question 3a: How can the uncertainty inherent in the impacts of subsystem architectures be examined in subsystem architecture trades to inspect the robustness of the resulting designs?

Hypothesis 3a: If distributions characterizing noise variables within aircraft subsystem architecture trades are utilized in the subsystem modeling and simulation environment, then a robust selection of the subsystem architecture design can be performed.

Experiment 3a demonstrated the capturing of noise variables, utilizing Bayesian distributions, placed on the variables within the modeling and simulation environment. Monte Carlo simulation was then utilized to propagate the impact of the noise variables to the distribution of TOGW for each architecture examined. This enabled

the computation of SNR of TOGW, for each of the examined architectures, which was then utilized to select the desired robust architecture, validating Hypothesis 3a.

Experiment 3b examined the determination of the noise variables with the largest impact on the response (TOGW) utilizing Bayesian Networks as discussed in Research Question 3b and Hypothesis 3b. Bayesian Networks were examined due to the additional analysis enabled during development of the subsystems by the creation of such networks.

Research Question 3b: How can the primary sources of uncertainty in the platform-level impacts of the selected subsystem architecture be identified?

Hypothesis 3b: If a Bayesian Network is created to represent the impact of the uncertainty in the subsystem architecture's characteristics on aircraft sizing, then the variables with the largest impacts can be identified.

A Bayesian Network was fit to the probabilistic data created in Experiment 3a for the top candidate architecture in order to identify which sources of uncertainty were driving the TOGW, for the selected architecture. Such an identification would enable further analysis that could reduce unexpected weight gains during development. The link strength between nodes representing the noise variables and the response were determined and cross-referenced with other analyses. The network structure that best fit the data was explored for further insight. By examining this analysis and the link strength values, it was identified that weight related parameters especially the actuator weight had the largest impact on TOGW. The identification of which noise variables were driving the variability of the response validated Hypothesis 3b and enabled the use of Bayesian Networks for such an analysis.

The Overarching Research Question and the Overarching Experiment are derived from the desire to create a methodology that improves the current State of the Art (SOA).

Overarching Research Question: How does the proposed Methodology compare to the current SOA?

Overarching Hypothesis: Capturing of the coupling between aircraft sizing and subsystem architecture impacts and exploring the architecture design space enables a significantly better architecture selection than a point-driven design.

The Overarching Experiment examined the use of MAIA on the baseline aircraft size to explore the architecture design space and to capture the coupling between subsystem impacts and aircraft sizing. The coupling and design space exploration were found to provide a significant improvement in TOGW over the selection of a point design, validating Hypothesis 0.

As a reminder to the reader, the Research Objective was to create a methodology for subsystem architecture trades as described below. The related Motivating Research Question asked how such an objective could be achieved, as listed below.

Research Objective: To create and examine a methodology for capturing subsystem architecture trades and their coupling with aircraft sizing.

Motivating Research Question: How can the objective of creating and examining a methodology for capturing subsystem architecture trades and their coupling with aircraft sizing be achieved?

As was demonstrated by the analysis of the first two experiments, MAIA captured subsystem architecture trades and their coupling with aircraft sizing. The importance of capturing this coupling is also demonstrated in Experiments 1 and 2. Experiment 3a demonstrates that MAIA not only captures coupling between aircraft sizing and subsystem architecture platform-level impacts but also enables a robust selection of the design. MAIA represents a significant step forward in aircraft subsystem conceptual architecting. Because MAIA enables subsystem architecture trades while capturing the coupling, creation and examination of MAIA meets the Research Objective.

7.2 Impacts of Findings

MAIA represents a significant improvement over current industry practices of subsystem architecture selection, as industry currently utilizes a traditional point design of the architecture without exploring other possible architectures, as examined in the Overarching Experiment. MAIA captures coupling of the impact of this architecture and aircraft sizing and explores the subsystem architecture design space. The capturing of this coupling enables subsystem architecture trades during conceptual design. The first experiment demonstrated that the coupling between aircraft sizing and subsystem architecture impacts exists and is significant to capture for the baseline aircraft. This was seen in the examined trends, correlation values, and the magnitude of the impact on TOGW. This coupling was seen to be still significant for other passenger classes of aircraft in the second experiment. The continued importance of capturing this coupling for other aircraft sizes was seen in the correlations characterizing this coupling and the magnitude of the impact on TOGW. This leads to the conclusion that for all aircraft sizes examined, this coupling is significant and must be captured to enable aircraft subsystem conceptual architecting. In further examining this coupling, for the ranges considered, the subsystem weight seemed to have a dominating impact over the power extraction on the TOGW. This can be seen in the correlation values and trends of subsystem weight, power extraction, and TOGW examined in Experiments 1 and 2. It was also seen by the plots of subsystem weight against power extraction that within the examined architectures, the more energy efficient architectures were heavier overall in all of the examined aircraft sizes. For the examined architectures overall, use of the lighter architectures that were less efficient may lead to a lower TOGW. The strong and significant coupling of aircraft sizing and subsystem architecture impacts was demonstrated along with a method utilizing modeling and simulation to capture this coupling, enabling subsystem conceptual architecting trades.

Examination of the robustness of the different architectures and robust architecture selection was demonstrated in Experiment 3a. The probabilistic analysis in the third experiment demonstrated that the inherent uncertainty can be captured in subsystem architecture trades by the creation and use of the Bayesian distributions. This capturing enables a robust selection of the desired architecture as was demonstrated by selection of an architecture utilizing SNR of TOGW in Experiment 3a. It should be noted that the heavier architectures out of the top three considered (due to having the lowest deterministic TOGW) had the best SNR for TOGW. This was due to the use of hydraulic actuation primarily and not EHAs which have more uncertain characteristics because they are a newer and a less frequently used technology. The determination of SNR for the top architectures enabled the selection of a robust subsystem architecture design. This enables the selection of robust subsystem designs that may reduce unexpected weight gains.

The use of Bayesian Networks in Experiment 3b enabled the identification of which of the noise variables had the strongest connection with the response as was seen by the use of such an analysis within the experiment. This enables the designer to identify which noise variables are driving the response, as was demonstrated by such a determination within Experiment 3b. This, in turn, enables the identification and investigation of noise parameters in order to reduce the variability of the response. As discussed, in the Chapter on uncertainty, the use of Bayesian Networks enables additional analysis over the use of traditional techniques, including predictive analysis during subsystem development. All of these experiments were demonstrations of parts of MAIA, going from generating and evaluating architectures to a robust architecture selection.

MAIA represents a significant improvement over current industry practices of subsystem architecture selection as seen in the Overarching Experiment. MAIA enables the capturing of the coupling of the impact of this architecture and aircraft sizing,

which was seen to have a significant impact in Experiments 1 and 2. This coupling was shown to be important to capture for different aircraft passenger classes. As a result, this coupling must be captured to enable true energy optimized aircraft subsystem architectures. MAIA represents a significant step towards the development of robust aircraft subsystem conceptual architecting. The ability to examine the robustness of the different architectures and robust architecture selection was demonstrated in Experiment 3a. In addition, the ability to determine which sources of uncertainty are having the largest impact was demonstrated in Experiment 3b. This enables the identification of specific sources of uncertainty that should be further explored for the development of a design.

7.3 Future Work

The explored architecture design space represents only a portion of the total architecture design space. In the future, models can be developed and added to those created for this work to enable exploration of the entire architecture design space. This would enable a truly energy optimized aircraft and enable even greater improvements than those seen due to the additional impact of examining different subsystems. Also, the route network used for routing the wires and hydraulic lines along with some of the other possible changes to the subsystem architecture were held fixed during the proof of concept study. Further study should be done into route network and component placement optimization as part of subsystem architecture analysis.

Exploration of a larger design space would require a narrowing down of that design space to a feasible number of alternatives to evaluate. There are several ways such a design space reduction can be achieved. Further research into the best means of achieving this design space reduction for aircraft subsystems should be considered. Some alternatives to help with narrowing the design space include the use of MADM different techniques, expert opinion, and constraints to filter out any architecture that

does not meet the given set of requirements.

The impacts of requirements on the subsystem architecture design space and alternatives need to be examined further. Such requirements may only be partially known at even the platform level during a conceptual stage. All of the available requirements need to be identified and brought down to the system level, perhaps using concepts from Armstrong's Master's thesis [20]. The process of identification of these requirements and their impacts earlier in design needs to be studied further to enable better identification of the feasible design space.

The reliability of these subsystem architectures is a possible metric not considered in this work. Accurate means of determining this reliability and its relative importance to the aircraft sizing impacts should be examined in the future.

Other types of correlation values, such as Browning Distance Covariance [128], should be further evaluated to determine when they may be useful for considering the relative contributions of different noise variables to the SNR of TOGW. Perhaps these types of correlation values could be utilized along with the Bayesian Network analysis examined in this dissertation to provide additional insight to the designer.

Finally, the subsystem modeling environment utilized duty cycles for the control surfaces with sharp corners, as smooth curves could only be captured with a small time step which would have made the computational time infeasible. To account for this, limits were placed on the piston velocity and acceleration and average power extraction values for different altitudes were utilized. In the future, it is desirable to make the subsystem models more accurate by using smooth duty cycles captured by a smaller time step. To accomplish this, ways must be found to significantly reduce the computational time required by a smaller time step.

7.4 Concluding Thoughts

This dissertation demonstrated the need for a new methodology for conceptual aircraft subsystem architecture trades. Different approaches for previous examinations of this problem and related issues were discussed and found to traditionally rely on the use of a point design for the subsystem architecture that is selected without exploring other architectures. In this dissertation, a new approach in the form of MAIA was recommended and explored. MAIA enables subsystem architecture trades during conceptual design. MAIA utilizes conceptual physics-based modeling of the subsystem architecture impacts on the system and platform levels and integrates these impacts with a sizing and synthesis code. This enables capturing of the coupling between aircraft sizing and subsystem architecture impacts. The significance of these impacts was studied and demonstrated to be important to capture for different aircraft sizes. This coupling is not currently studied or captured in development and selection of aircraft subsystems. The capturing of this coupling enables essential subsystem architecture trades that have a significant impact on aircraft TOGW.

MAIA also captures uncertainty on parameters within the subsystem architecture trades. This enables determination of the robustness of the designs to these sources of uncertainty. The quantification of this robustness enables robust aircraft subsystem architecture selection. Such a selection enables selection of architectures that are less prone to weight changes further down the design process. A robust selection of architectures should help reduce occurrences of weight growth while developing and integrating subsystems as was seen in the Boeing 787 [6]. This could enable faster and cheaper development of aircraft due to a reduction in redesign work due to the weight growth of subsystems.

The importance of capturing the coupling between subsystem architecture impacts and aircraft sizing was explored and found to be significant. The importance of subsystem architecture trades especially early in design was also established. MAIA

demonstrated a methodology for exploring the subsystem architecture design space, identifying the architectures that would lead to the smallest aircraft size, and selection and analysis of the most robust of the lighter architectures. Such an analysis and selection enables more accurate and desirable aircraft subsystem architecture selections.

APPENDIX A

SUMMARY OF FIT DATA FOR EHA ANN

Summaries of fit data for the ANNs of the Matlab/Simulink environment for the all EHA architecture are shown in Figures 99, 100, 101, 102, 103, 104, 105, 106, 107, and 108. In the summary of fit data, it is desirable to have an R-squared as close to 1 as possible, a close to linear actual by predicted plot, a random scatter of the residual, relatively small residual values, and small values for MFE and MRE. The below plots utilize the residual as the definition of error. It can be seen that these fits are very good fits. The actual by predicted plots are almost linear, the magnitudes of the mean and standard deviations were small, the magnitude of the residuals was very small, and the R-squared values were close to 1. Any patterns in the residual that exist were determined to be insignificant because the magnitude of the residual was very small. As a result, these ANNs were utilized as surrogate models for the Matlab/Simulink EHA model to enable probabilistic analysis. It should be noted that these ANNs were used with ANNs of EDS for the probabilistic analysis. The ANNs of EDS were also seen to be reasonable fits as shown in the discussion of the implementation of Experiment 3a.

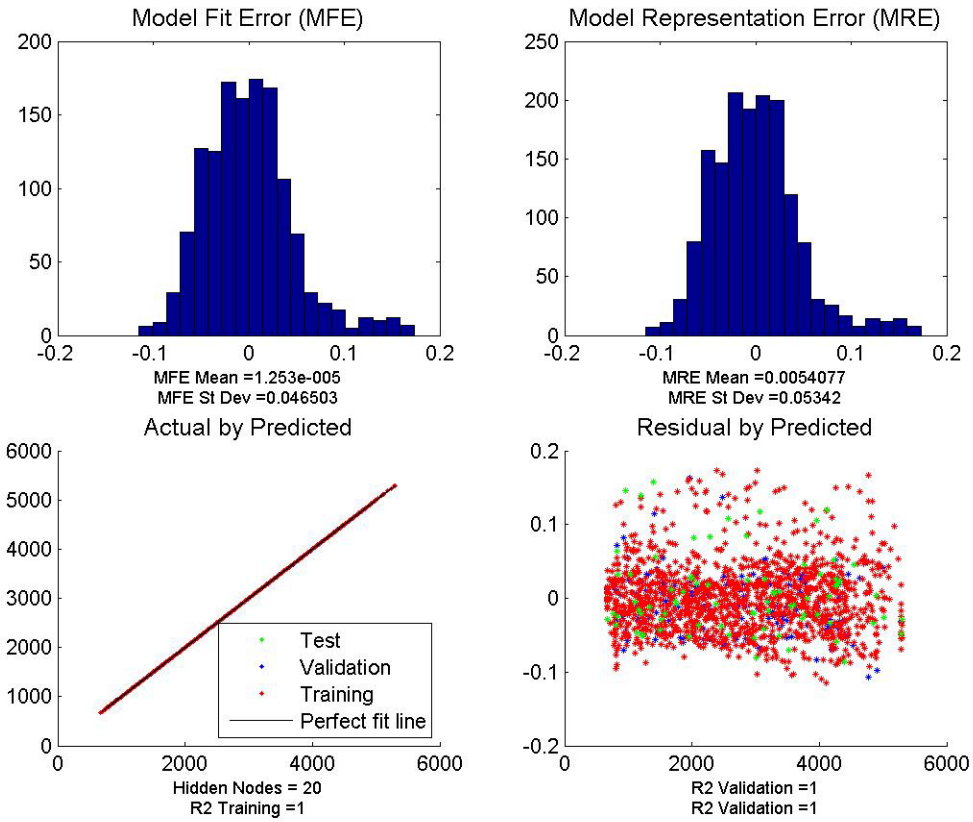

Figure 99: ANN fit Data for Subsystem Weight

Figure 99 shows the summary of fit data for the subsystem weight. Specifically, this subsystem weight value is one of the outputs of the Matlab/Simulink environment and in this case is the weight of the EHAs and the increased wiring and generator weight due to switching to EHAs. This can be seen to be a very good fit, with R-squared values of 1.

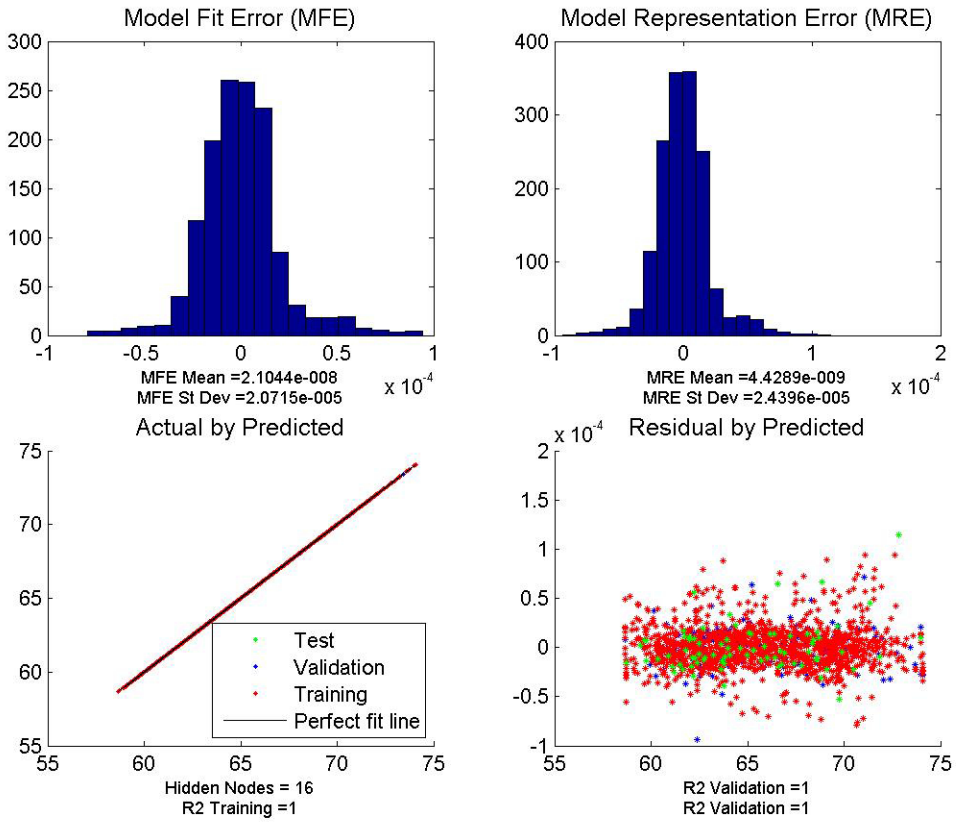

Figure 100: ANN fit Data for Maximum Power Extraction

The power extraction map is an important output of the Matlab/Simulink environment. This map captures the required power extraction to power the modeled systems. Figure 100 shows the quality of fit data for an ANN of the maximum value of this power extraction. This again is a good fit, with R-squared values of 1.

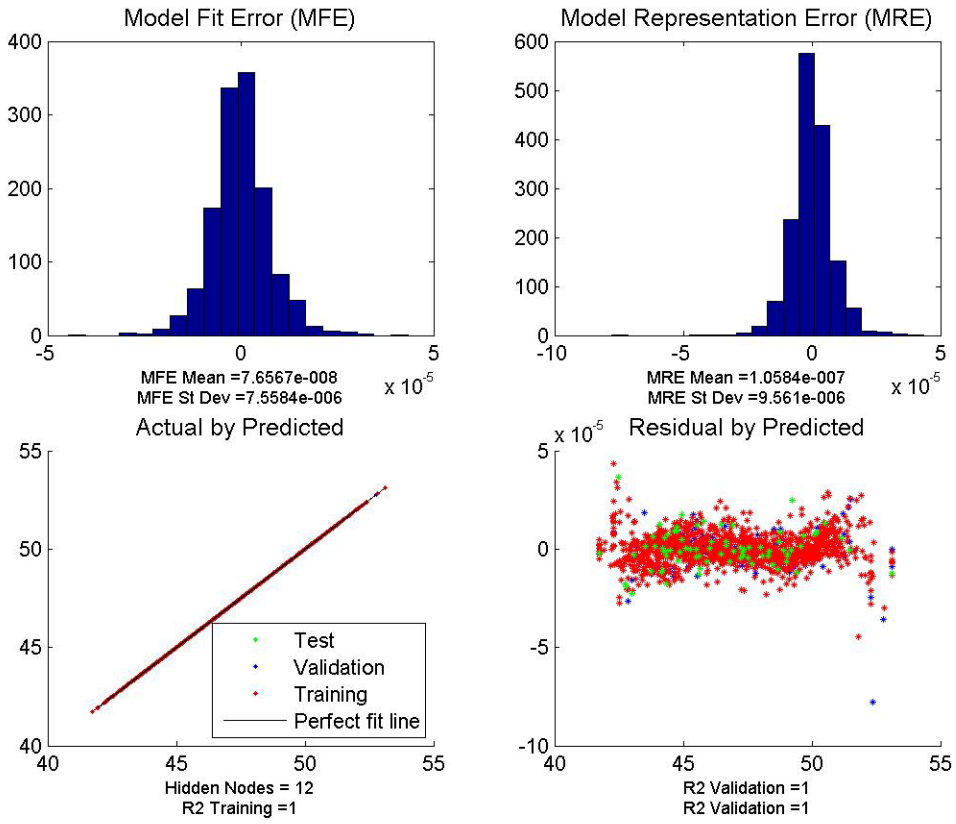

Figure 101: ANN fit Data for Minimum Power Extraction

Figure 101 shows the quality of fit information for an ANN fit of the minimum power extraction from the calculated power extraction map. This ANN can be seen to again be a very good fit, with an R-squared of 1.

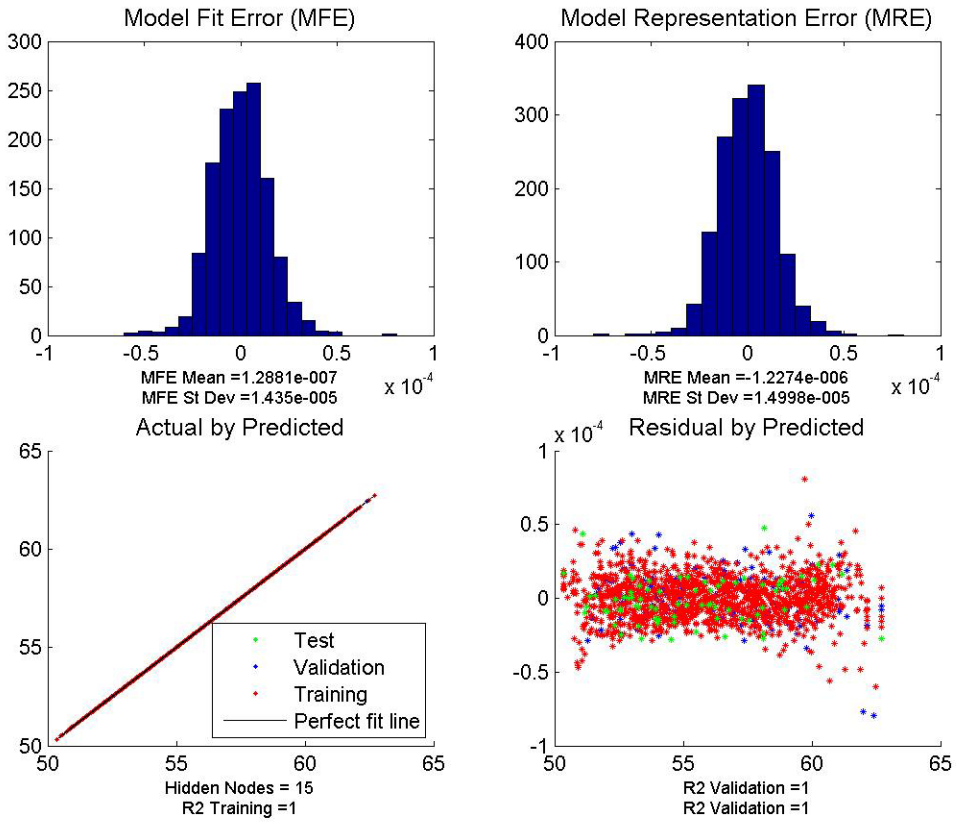

Figure 102: ANN fit Data for Average Power Extraction

The summary of the ANN fit of the average power extraction within the power extraction map can be found in Figure 102. This ANN is not used directly to create a value for EDS as EDS utilizes only the power extraction map itself, not its average. This parameter just provides additional information to the designer. The quality of the fit can be seen to be almost perfect for this parameter.

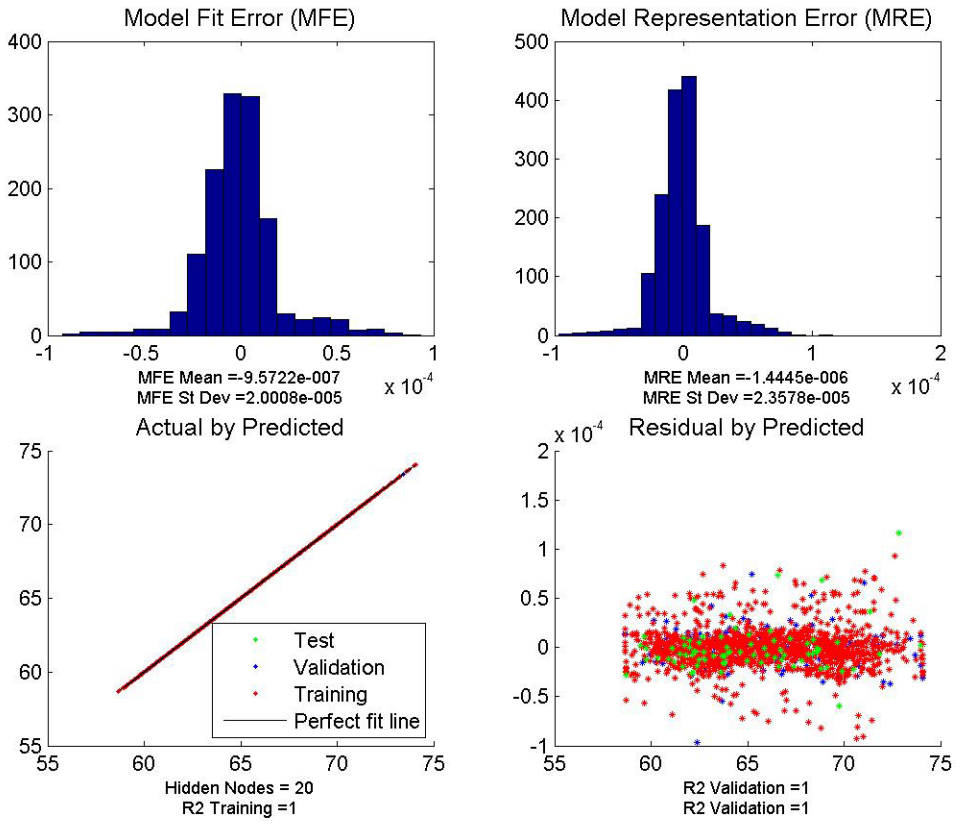

Figure 103: ANN fit Data for Power Extraction Map First Value

The power extraction map utilized a constant baseline value to account for systems not captured by the modeling and a table of power extraction against altitude (in order from lowest altitude to highest). The quality of the ANN fit for the first of these power extraction map values is shown in Figure 103. This fit again can be seen to be almost perfect.

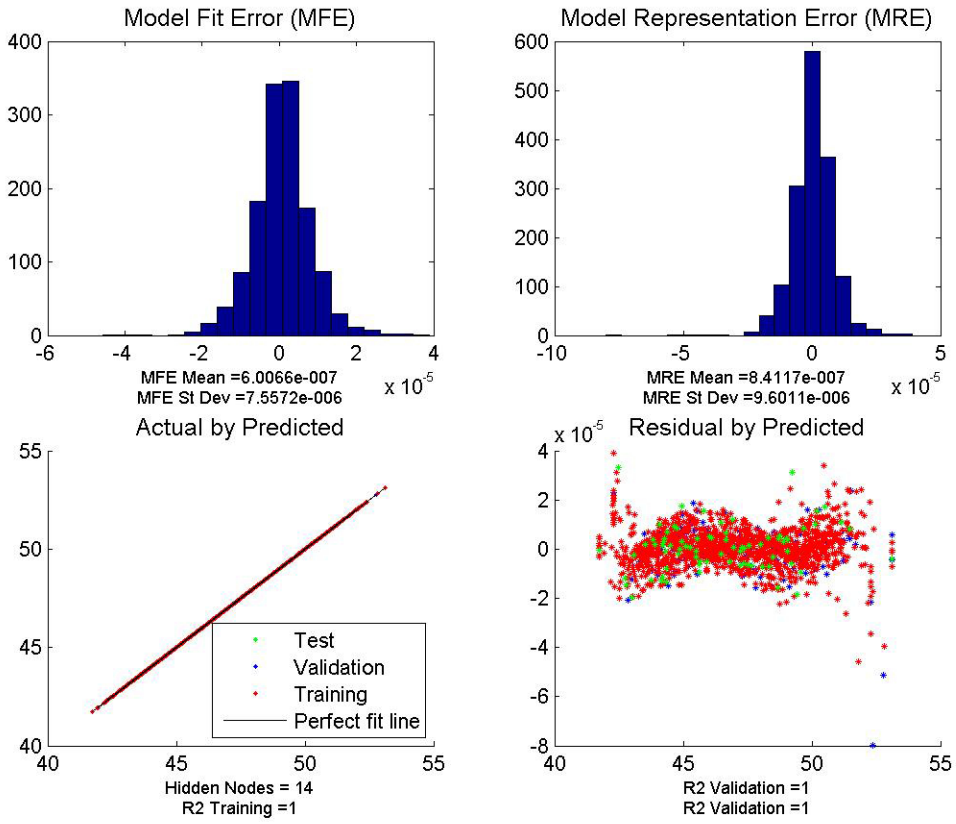

Figure 104: ANN fit Data for Power Extraction Map Second Value

The summary of fit data for the second entry of power extraction within the power extraction map of power extraction against altitude is shown in Figure 104. This fit is overall good, despite the slight pattern in the residual due to the very small magnitude of the residual.

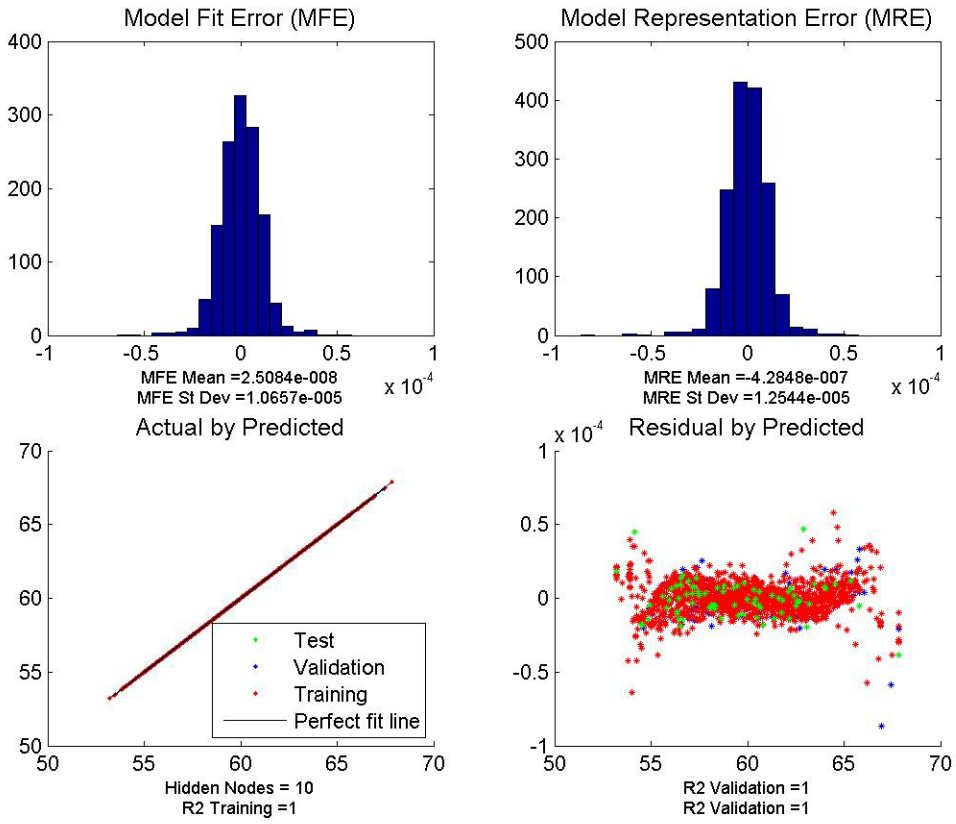

Figure 105: ANN fit Data for Power Extraction Map Third Value

Figure 105 shows the summary of fit data for the third value of power extraction within the calculated map. Overall, this fit appears acceptable for use, with R-squared values of 1 and small errors and residual values.

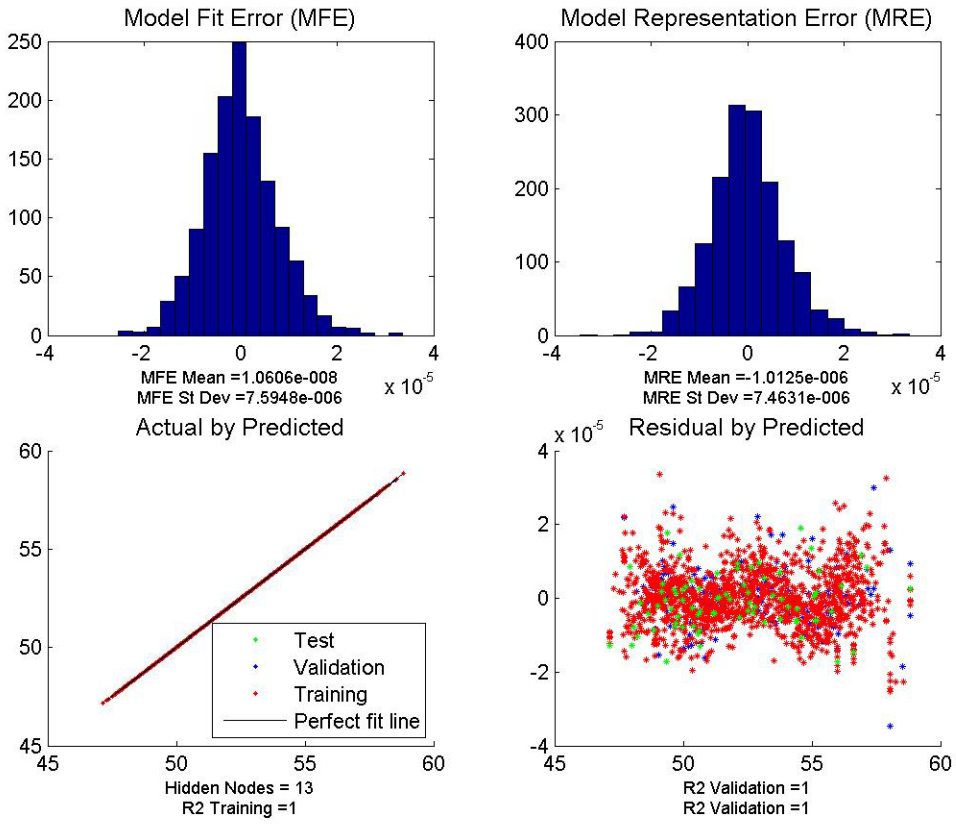

Figure 106: ANN fit Data for Power Extraction Map Fourth Value

Figure 106 shows the summary of fit data for the fourth entry in the power extraction map. A slight pattern can be seen in the residual values. However, due to the very small magnitude of the residuals, this fit is determined to be acceptable.

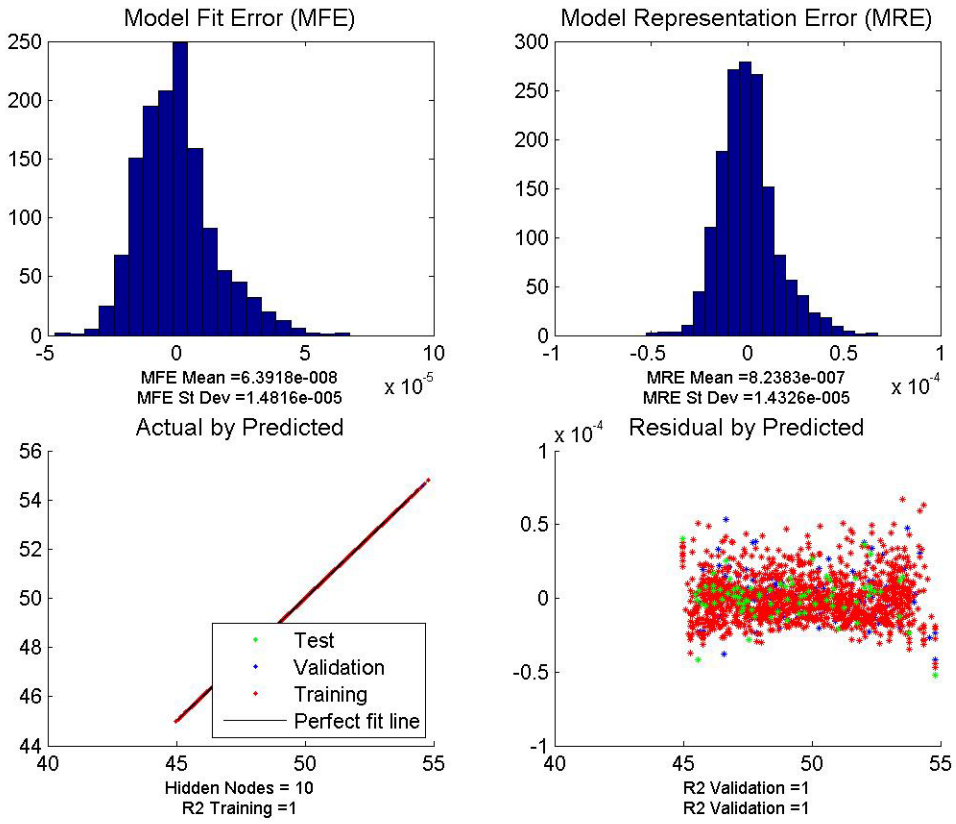

Figure 107: ANN fit Data for Power Extraction Map Fifth Value

The summary of fit data for the fifth entry of power extraction in the power extraction map is shown in Figure 107. Despite a slight skewness in the Model Fit Error (MFE), this is seen to have a good fit overall, partially due to the very small magnitude of the MFE.

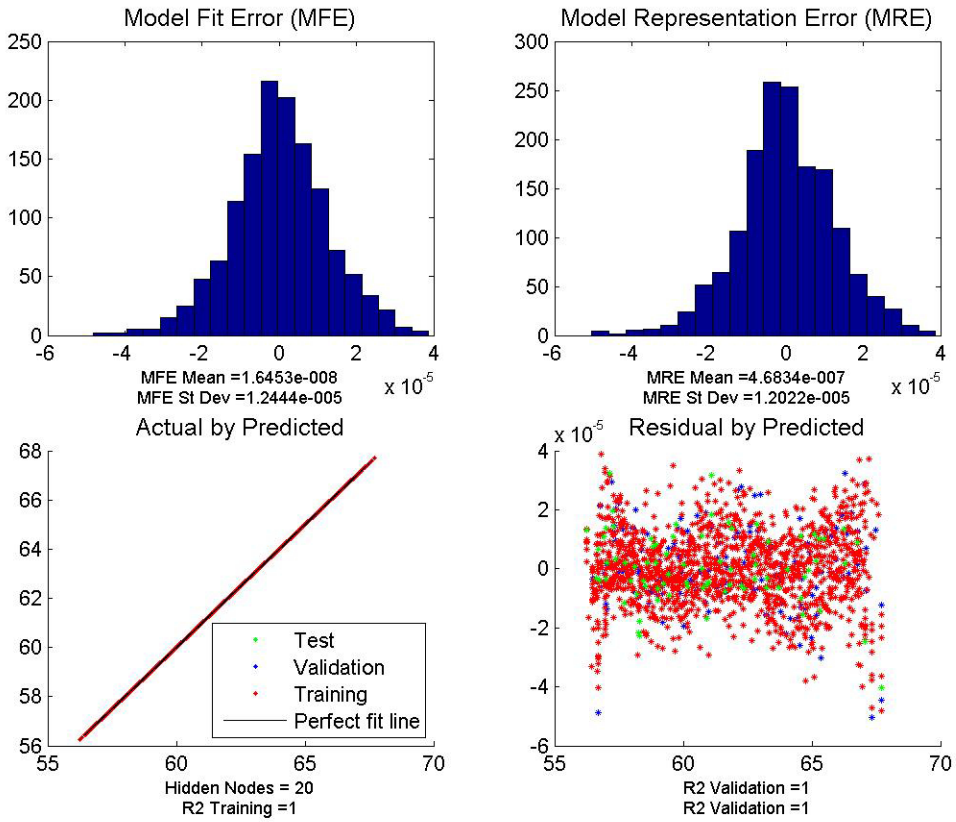

Figure 108: ANN fit Data for Power Extraction Map Sixth Value

Figure 108 shows the quality of fit data for the last power extraction value within the power extraction map. Overall, the quality of this fit is acceptable. There is a slight pattern in the residual that can be neglected due to the very small magnitude of the residual.

APPENDIX B

SUMMARY OF FIT DATA FOR HYDRAULIC ANN

Summaries of fit data for the ANNs of the Matlab/Simulink environment for the all hydraulic architecture are shown in Figures 109, 110, 111, 112, 113, 114, 115, 116, 117, and 118. To remind the reader, in the summary of fit data, it is desirable to have an R-squared as close to 1 as possible, a close to linear actual by predicted plot, a random scatter of the residual, relatively small residual values, and small values for MFE and MRE. Again, the below plots utilize the residual as the definition of error. It can be seen that these fits are not perfect but are very good fits. The actual by predicted plots are almost linear, the magnitudes of the mean and standard deviations were small, the magnitude of the residuals was very small, and the R-squared values were close to 1. Any patterns in the residual that exist were determined to be insignificant given that the magnitude of the residual was very small. Again, as a result, these ANNs were utilized as surrogate models for the Matlab/Simulink hydraulic model along with ANNs of EDS to enable probabilistic analysis. The ANNs of EDS were also seen to be reasonable fits as discussed in the implementation of Experiment 3a.

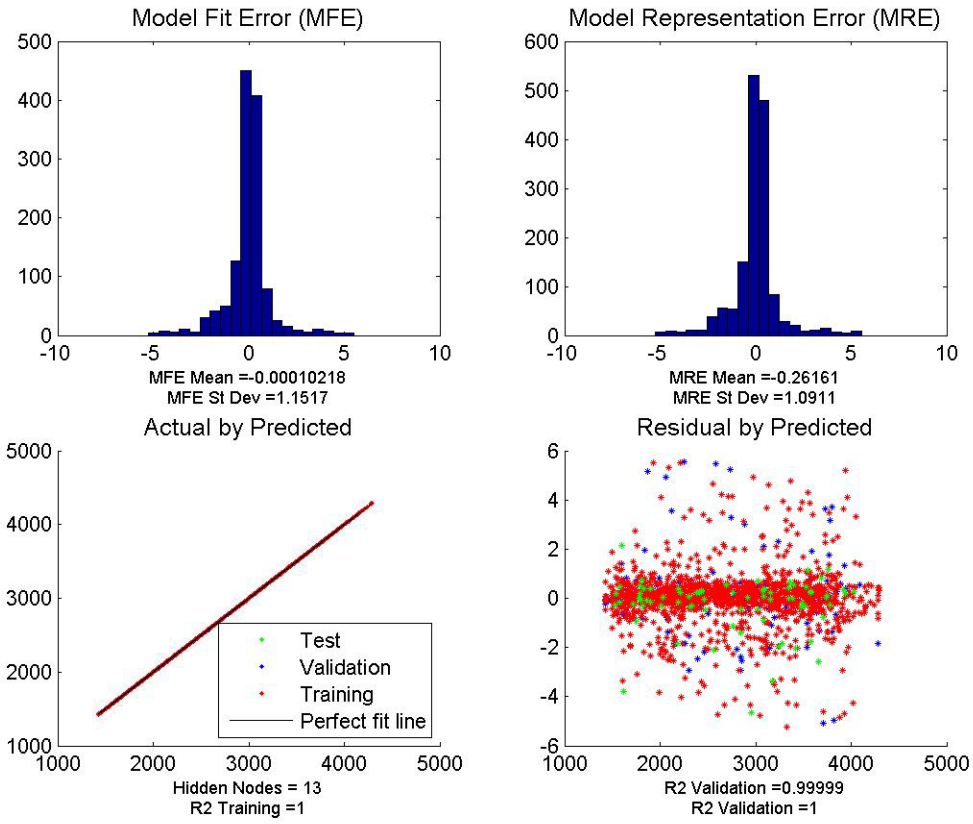

Figure 109: ANN fit Data for Subsystem Weight

Figure 109 shows the summary of fit data for the subsystem weight for the case of all hydraulic actuation. In this case, this value is the weight of the modeled hydraulic system. It can be seen that the quality of the fit is acceptable for use, with R-squared values of approximately 1.

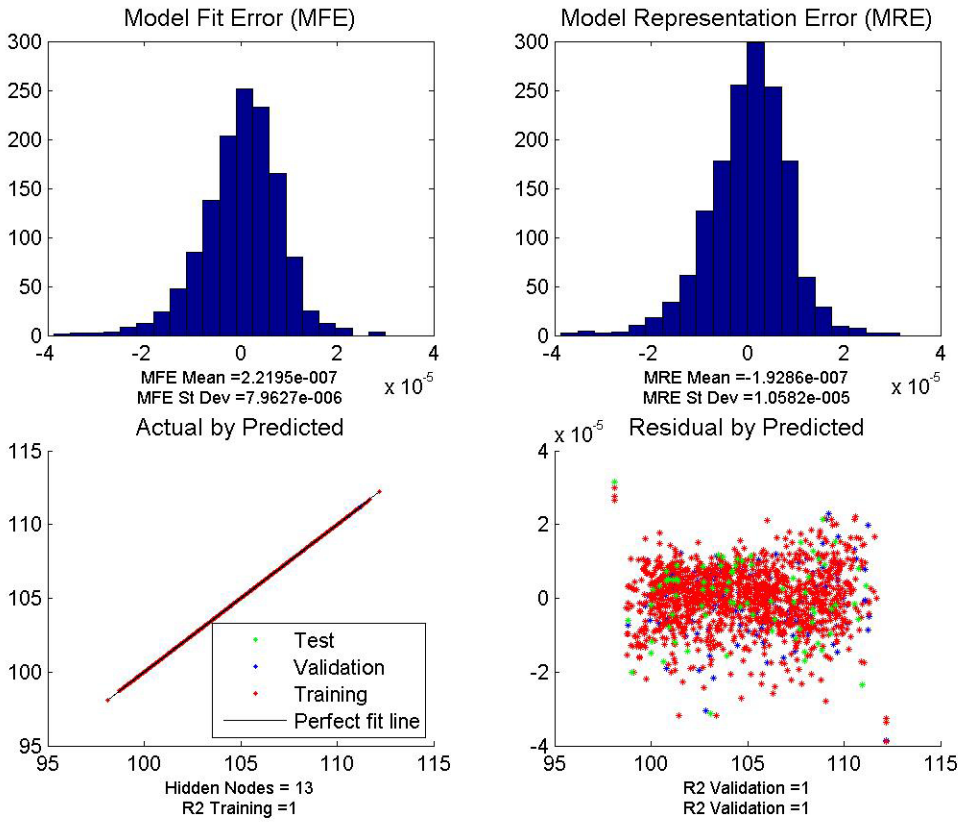

Figure 110: ANN fit Data for Maximum Power Extraction

The maximum power extraction value from within the power extraction map of power extraction against altitude to power the modeled subsystems was also fit with an ANN. The quality of fit for this parameter can be seen in Figure 110. It is clear that this is a good fit of the data, with small residual values and R-squared values of 1.

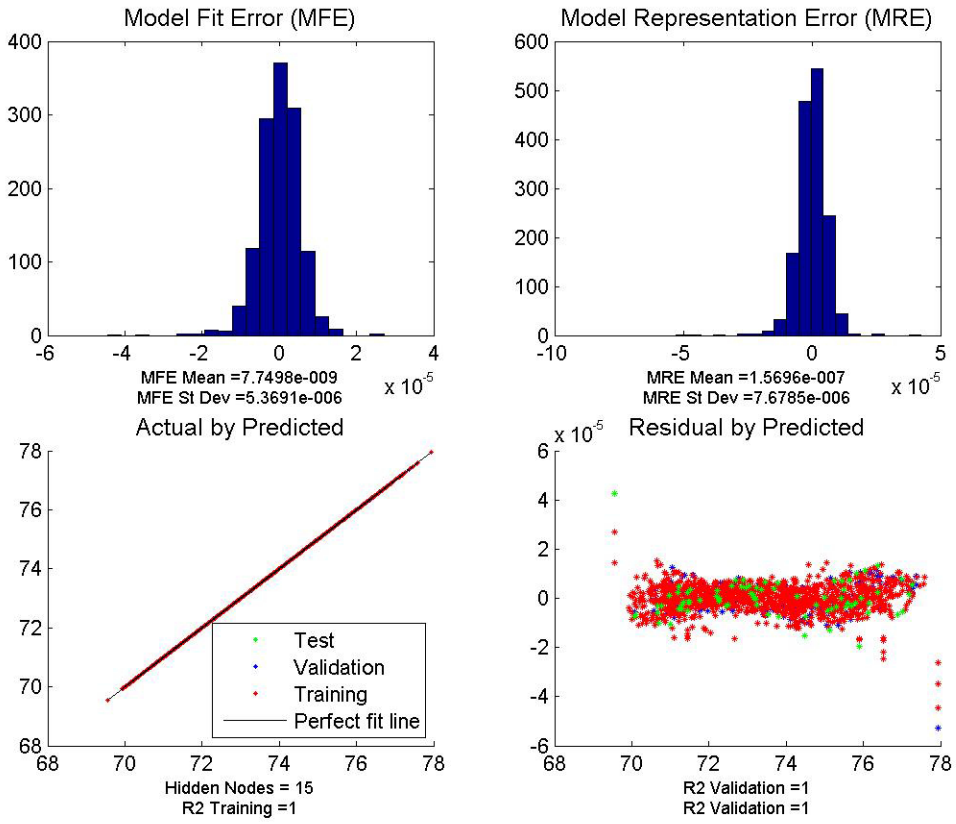

Figure 111: ANN fit Data for Minimum Power Extraction

The summary of fit data for the minimum power extraction from this map can be seen in Figure 111. This again is a good fit with R-squared values of 1 and a very small magnitude of the residuals.

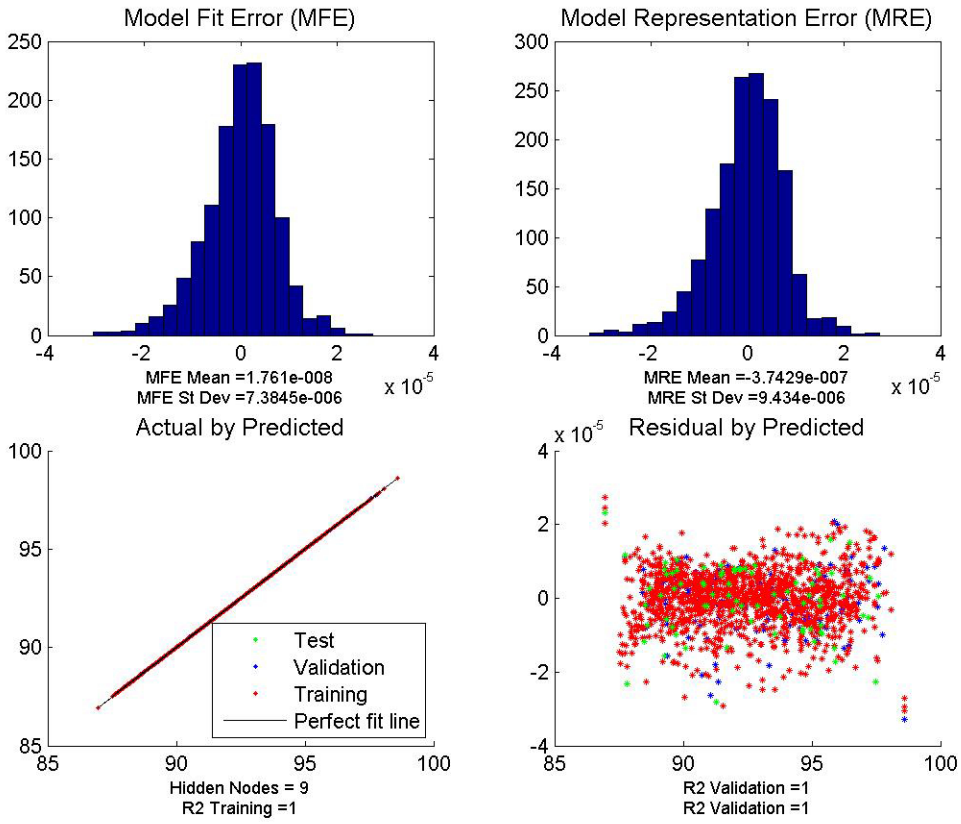

Figure 112: ANN fit Data for Average Power Extraction

Figure 112 shows the summary of fit data for the average value from this power extraction map. The R-squared values for this fit are 1, and the fit appears to be a good fit with small magnitudes of residuals and errors.

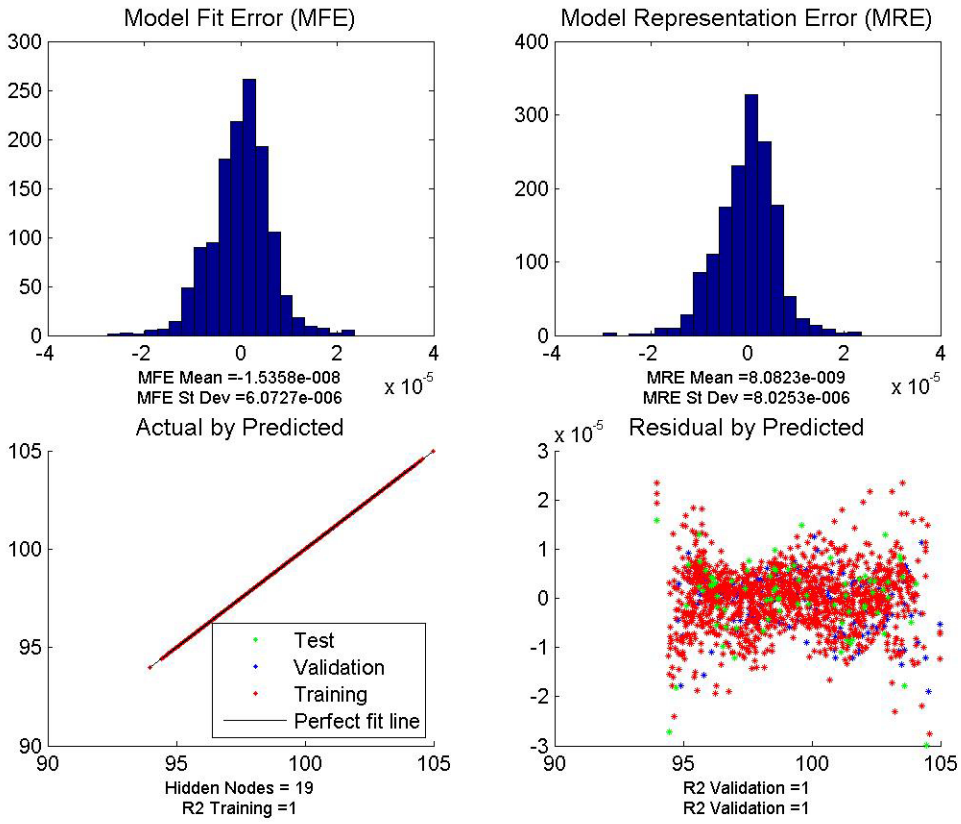

Figure 113: ANN fit Data for Power Extraction Map First Value

The power extraction map contains values of power extraction required to power the modeled subsystems. This power extraction map takes the form of a matrix containing power extraction values for different altitudes. The summary of fit data for the first value in the map can be seen in Figure 113. Overall, the fit appears to be acceptable, despite a slight pattern in the residual, due to the very small magnitude of the residuals.

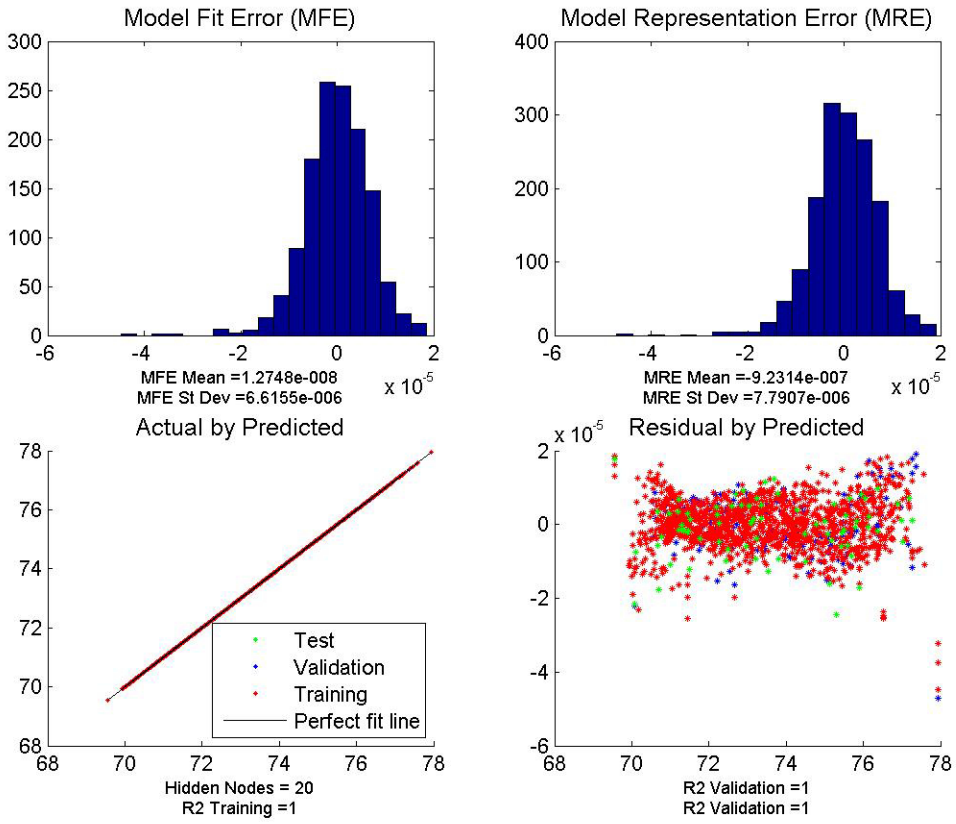

Figure 114: ANN fit Data for Power Extraction Map Second Value

The quality of fit data for the second value of power extraction within the power extraction map is shown in Figure 114. Overall the fit seems acceptable despite slight skewness and patterns in the residuals and errors due to the very small magnitude of these values.

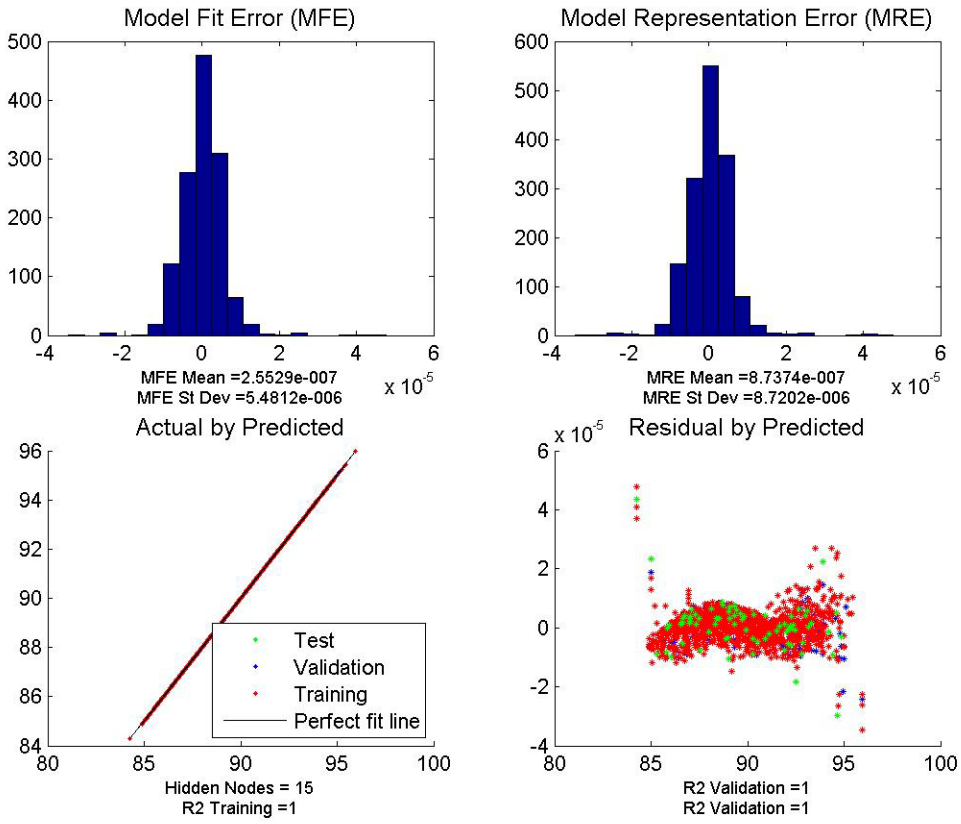

Figure 115: ANN fit Data for Power Extraction Map Third Value

Figure 115 shows the summary of fit data for the third entry of power extraction within the power extraction map. This fit appears to be very good except for a slight residual pattern which, given the very small magnitude of the residual, is acceptable to neglect.

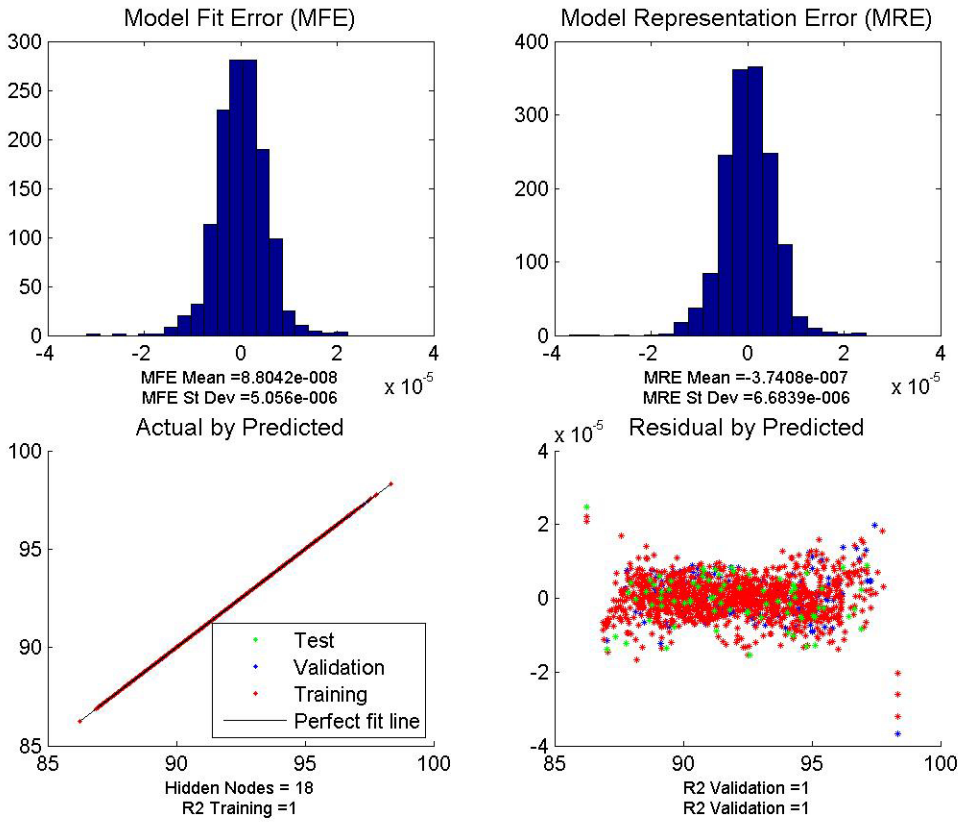

Figure 116: ANN fit Data for Power Extraction Map Fourth Value

Figure 116 contains the quality of fit data for the fourth value within the power extraction map. Overall, the fit appears acceptable, with R-squared values of 1 and a small magnitude of the error and residuals.

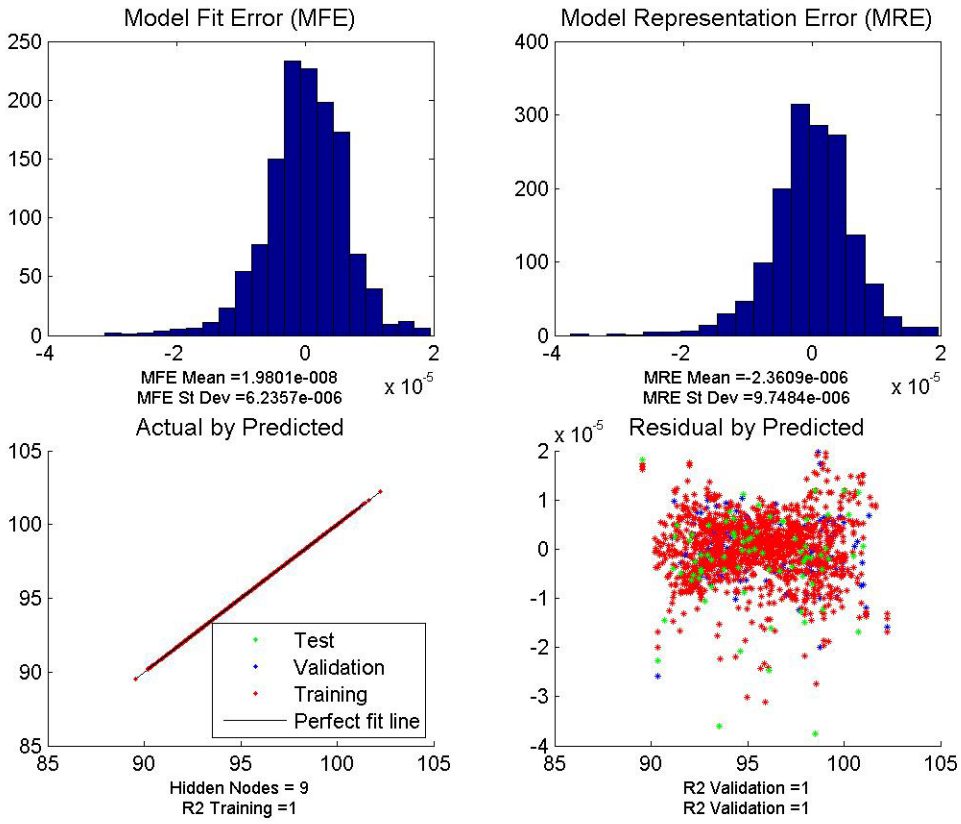

Figure 117: ANN fit Data for Power Extraction Map Fifth Value

The quality of fit data for the fifth power extraction value within the power extraction map is shown in Figure 117. This fit seems quite acceptable with small errors and residuals and R-squared values of 1.

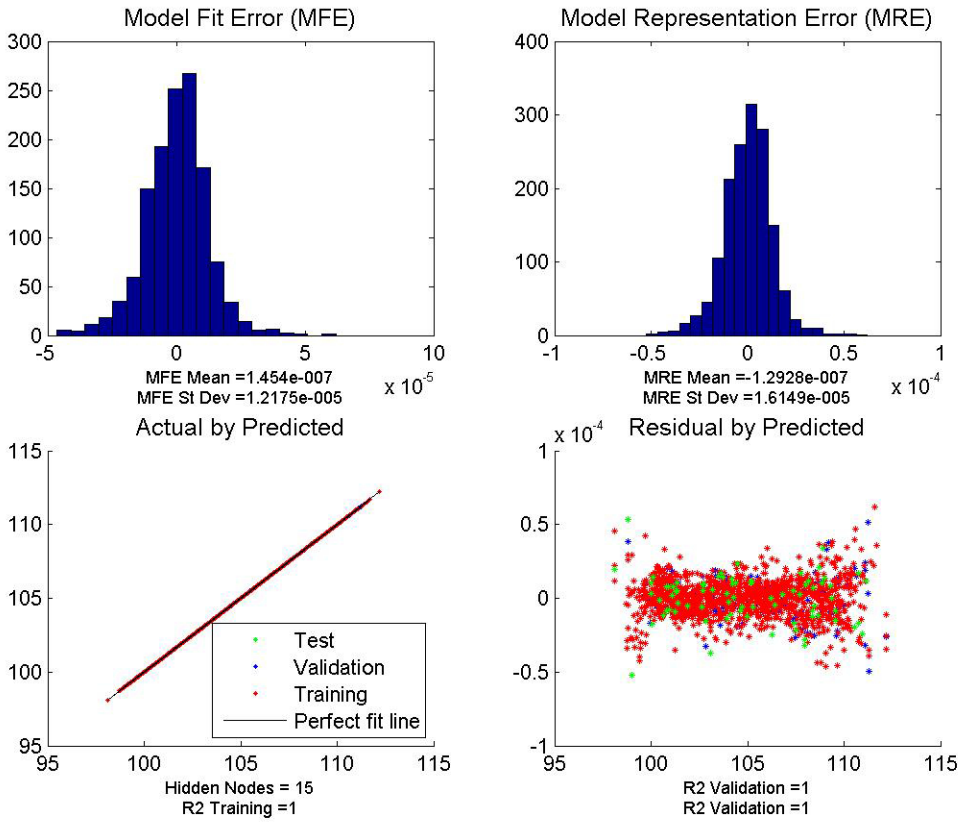

Figure 118: ANN fit Data for Power Extraction Map Sixth Value

Figure 118 contains the summary of the fit quality data for the ANN of the last value of power extraction contained within the power extraction map. The R-squared values of this fit are 1. Due to this fact, along with small magnitudes of errors and residuals, this fit is seen to be acceptable.

APPENDIX C

SUMMARY OF FIT DATA FOR HYBRID ANN

Summaries of fit data for the ANNs of the Matlab/Simulink environment for the hybrid architecture are shown in Figures 119, 120, 121, 122, 123, 124, 125, 126, 127, and 128. Again, to remind the reader, in the summary of fit data, it is desirable to have an R-squared as close to 1 as possible, a close to linear actual by predicted plot, a random scatter of the residual, relatively small residual values, and small values for MFE and MRE. The below plots again utilize the residual as the definition of error. It can be seen that these fits are not perfect but are very good fits. The actual by predicted plots are almost linear, the magnitudes of the mean and standard deviations were small, the magnitude of the residuals was very small, and the R-squared values were close to 1. Any patterns in the residual that exist were determined to be insignificant given that the magnitude of the residual was very small. Finally, these ANNs were again utilized as surrogate models for the Matlab/Simulink hybrid model to enable probabilistic analysis. These ANNs were used with ANNs of EDS to enable the probabilistic analysis. The quality of fit of the ANNs of EDS was also seen to be acceptable as shown in the discussion of the implementation of experiment 3a.

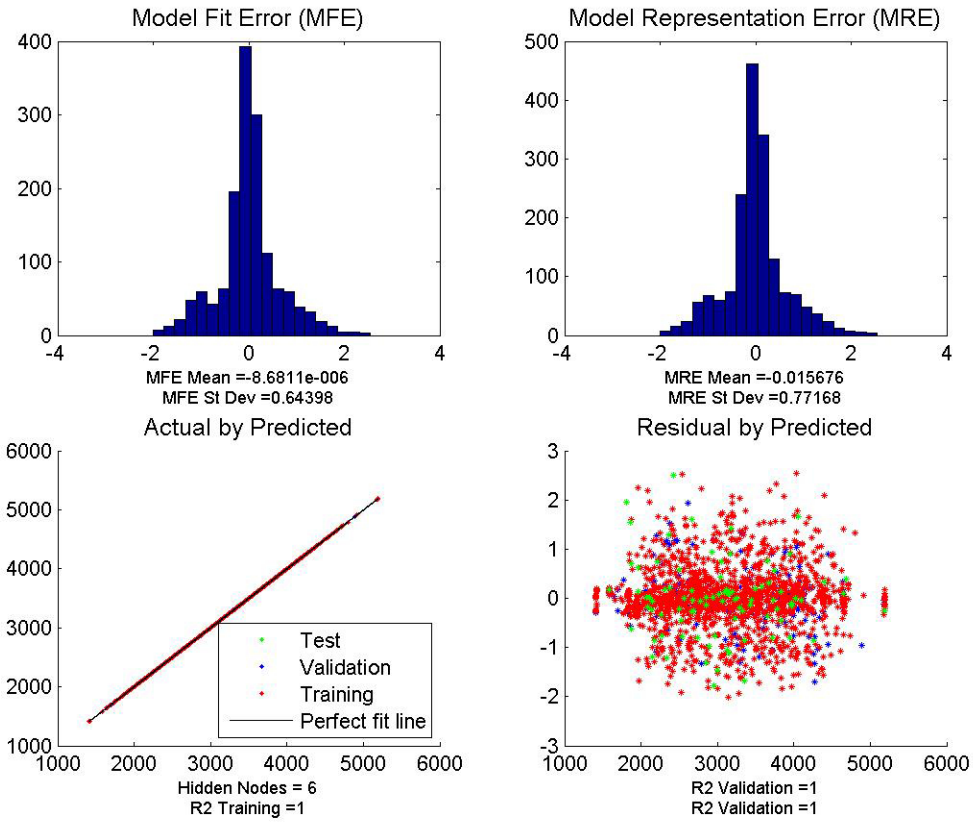

Figure 119: ANN fit Data for Subsystem Weight

Figure 119 shows the summary of fit data for the subsystem weight for the hybrid architecture. This subsystem weight includes the weight of the hydraulic system and any additional weight from utilizing EHAs. The quality of the fit can be seen to be very good with R-squared values of 1.

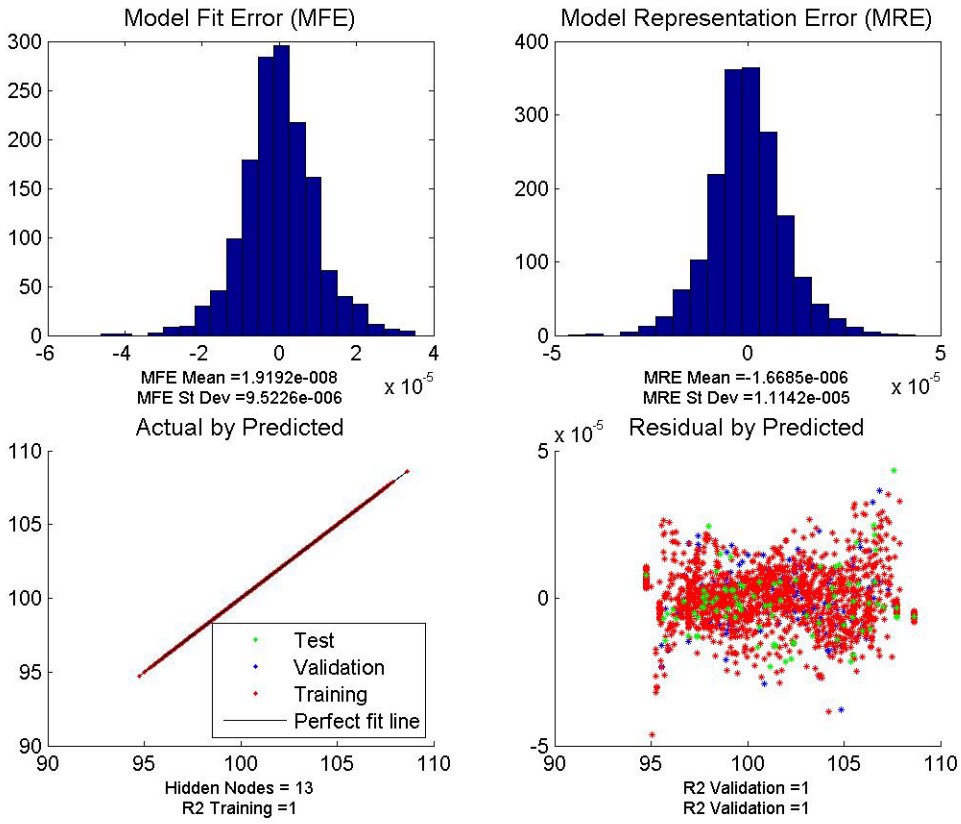

Figure 120: ANN fit Data for Maximum Power Extraction

The quality of fit data for the ANN for the maximum value of power extraction from the power extraction map is shown in Figure 120. This is the maximum value from the power extraction vs altitude map determined by Matlab/Simulink as the necessary power for the modeled subsystems. The quality of the fit appears acceptable, despite a slight pattern in the residual, due to the small magnitude of the residual values.

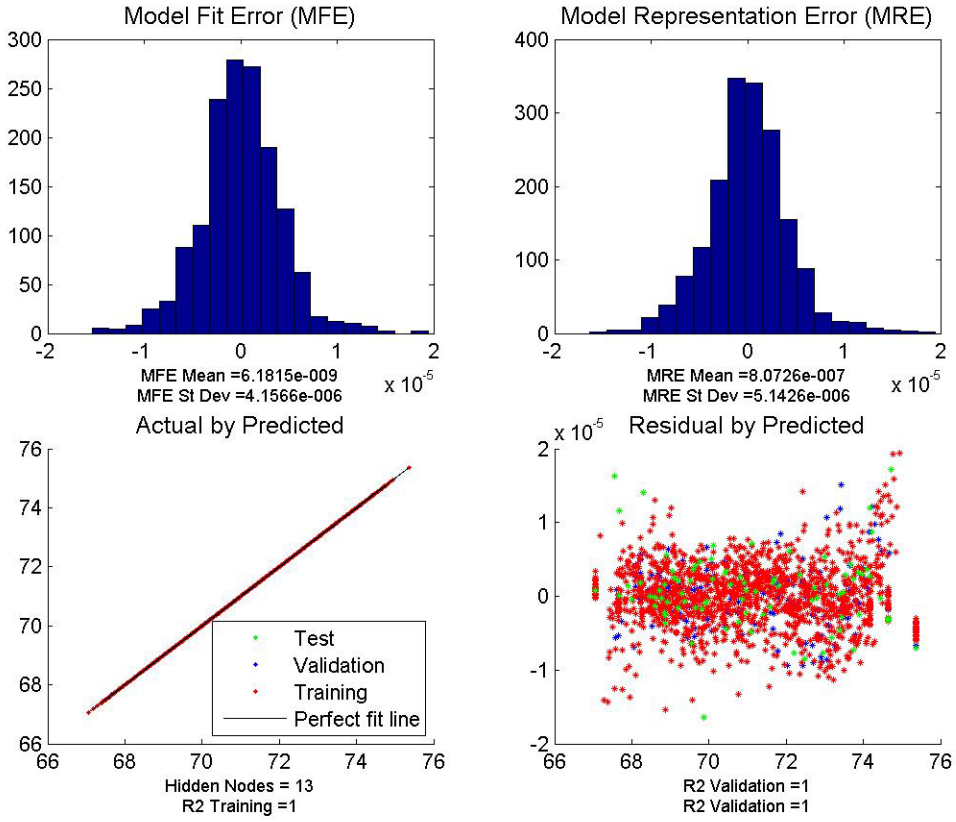

Figure 121: ANN fit Data for Minimum Power Extraction

Figure 121 shows the quality of fit information for the ANN fit to the minimum power extraction value from the power extraction map. It can be seen that the quality of the fit is very good, with R-squared values of 1.

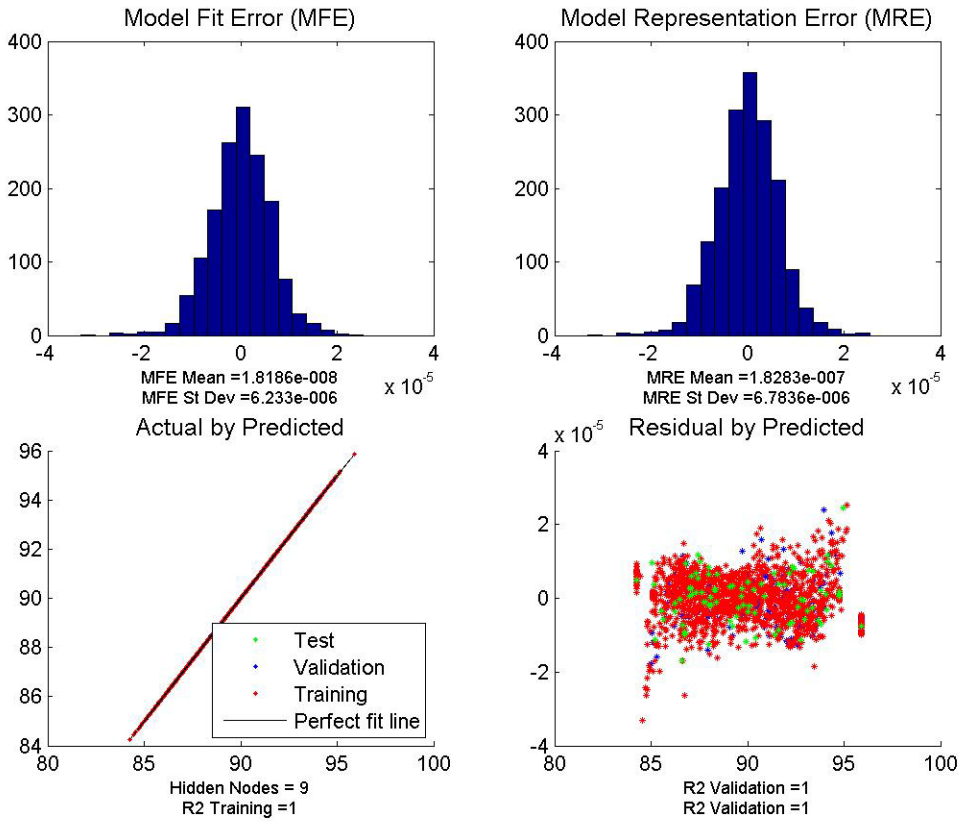

Figure 122: ANN fit Data for Average Power Extraction

Figure 122 shows the quality of fit data for the ANN of the average power extraction from the power extraction map. It can be seen that, despite a slight pattern in the residual, this fit is good. This is due to the very small magnitudes of the error and residual and the R-squared values of 1.

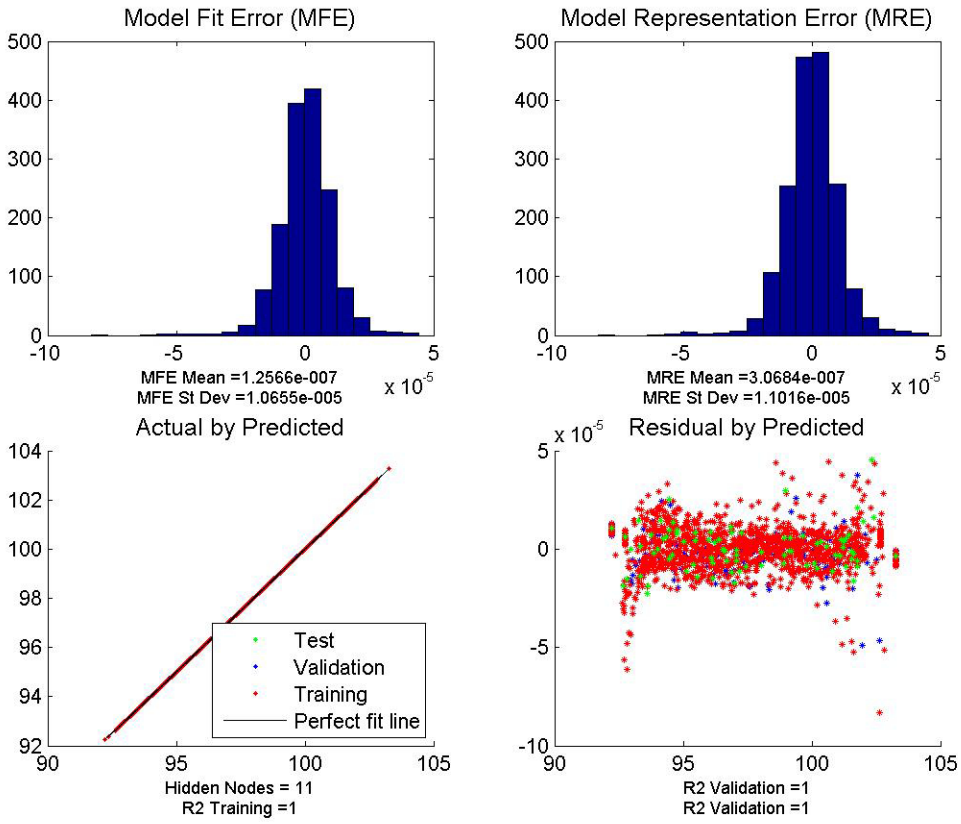

Figure 123: ANN fit Data for Power Extraction Map First Value

The summary of fit data for the first power extraction value contained within the power extraction map can be seen in Figure 123. This fit appears to be a very good fit as well because of the R-squared values of 1, the small magnitude of the residuals and errors, and the linear actual by predicted plot.

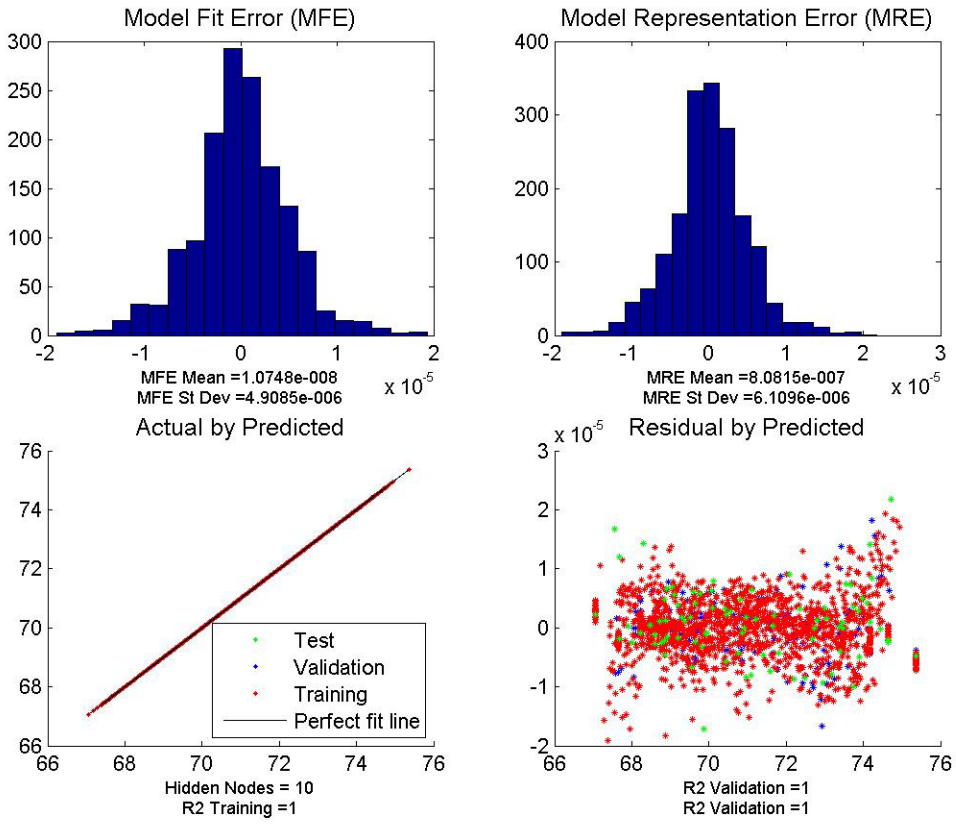

Figure 124: ANN fit Data for Power Extraction Map Second Value

Figure 124 shows the quality of fit information for the second value of power extraction from the power extraction map. The R-squared values are 1, the actual by predicted plot is linear, and the magnitude of the errors and residuals are very small, making the fit acceptable despite the slight pattern in the residual.

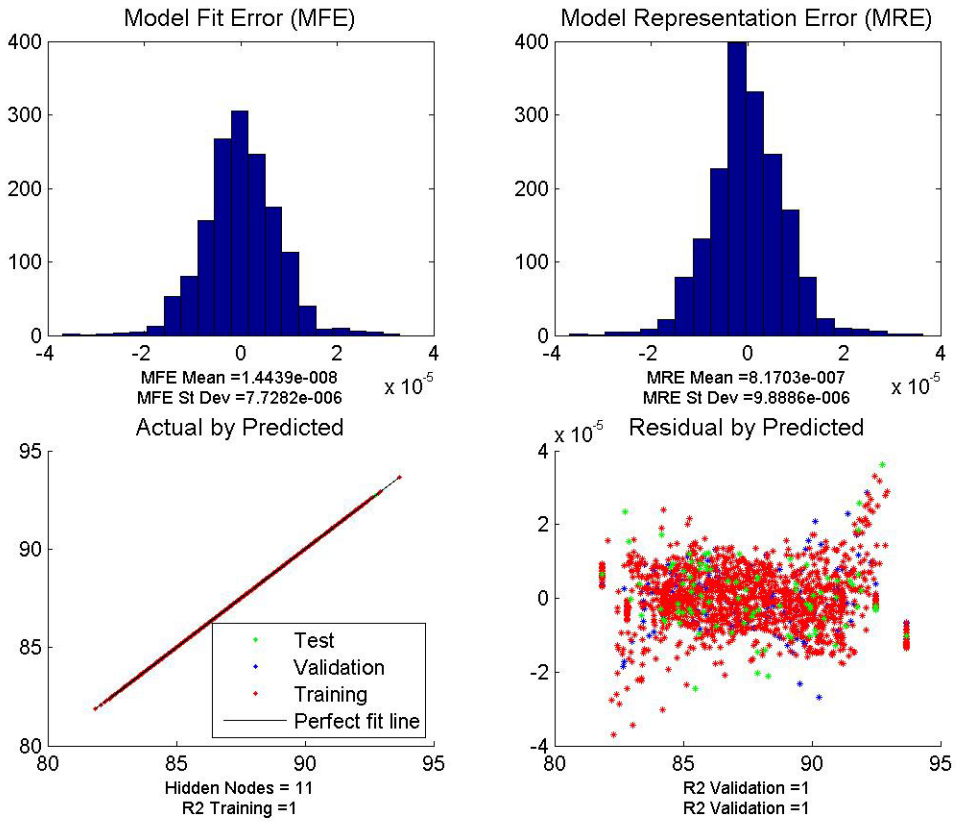

Figure 125: ANN fit Data for Power Extraction Map Third Value

Figure 125 contains the summary of the quality of fit data for the ANN for the third value of power extraction contained within the power extraction map. This fit is also seen to be acceptable. The actual by predicted plot is linear as desired, and the R-squared values are 1. The magnitude of the errors and residual are very small, enabling the use of this fit despite a slight pattern in the residual.

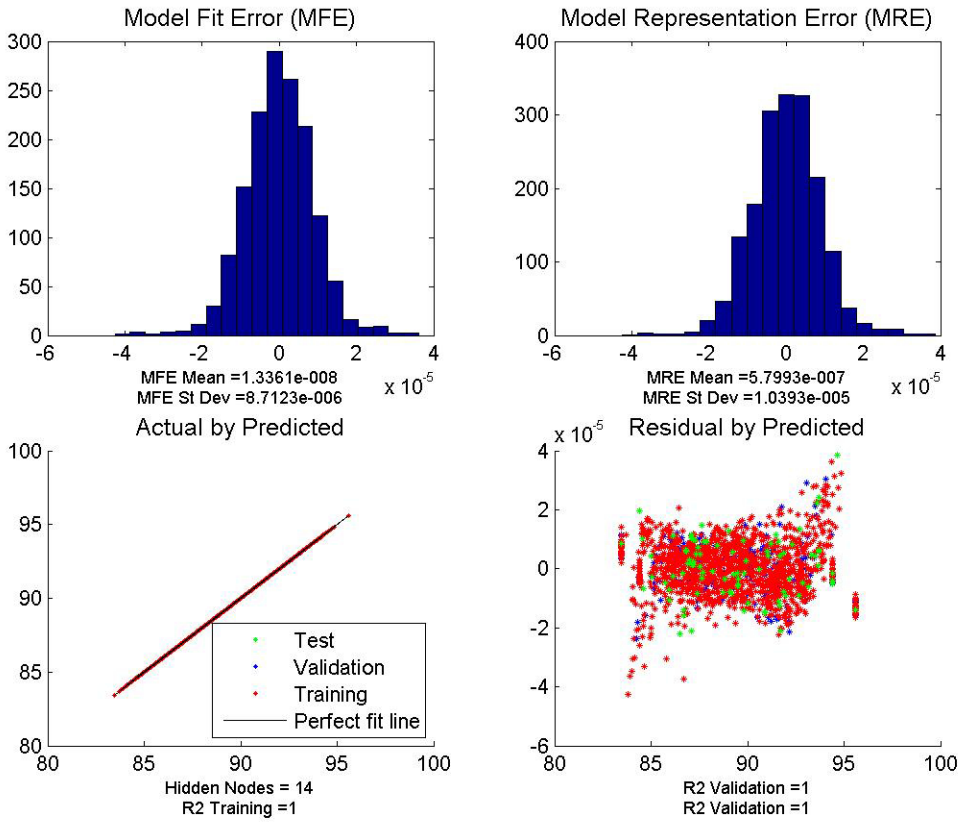

Figure 126: ANN fit Data for Power Extraction Map Fourth Value

The summary of fit data for the ANN of the fourth value of power extraction within the power extraction map output from Matlab/Simulink is shown in Figure 126. The R-squared values are 1, the actual by predicted plot is linear, and the magnitudes of the residual and error values are very small enabling use of this fit, despite a slight pattern in the residual.

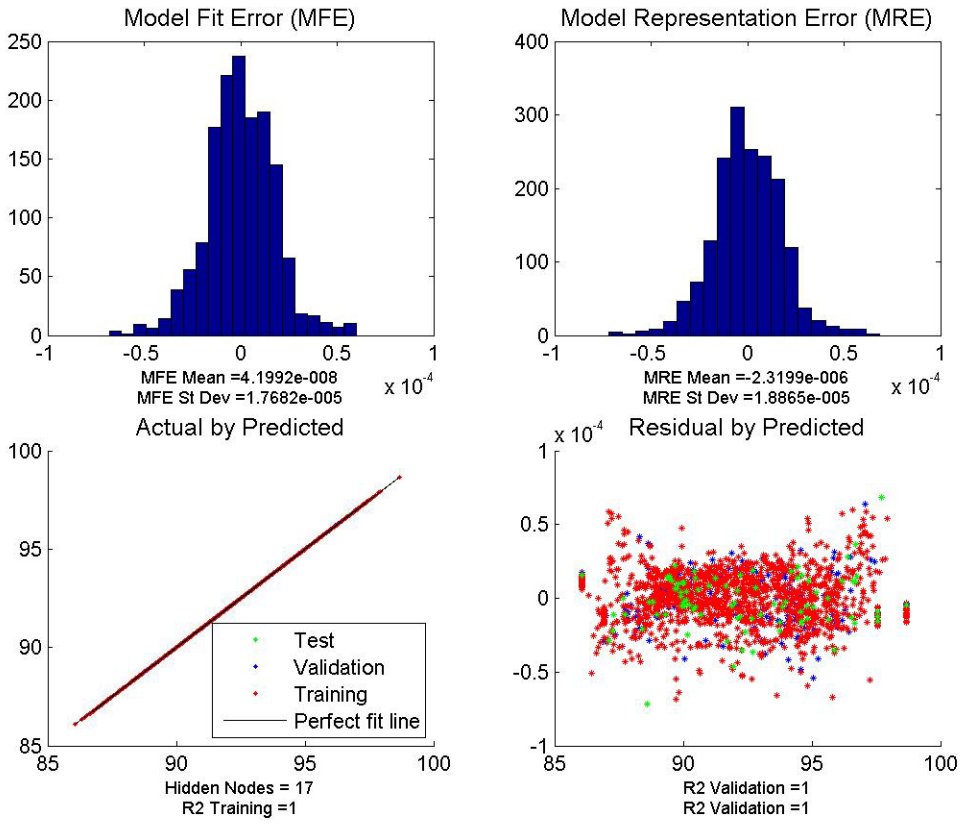

Figure 127: ANN fit Data for Power Extraction Map Fifth Value

Figure 127 contains the summary of fit data for the ANN fit for the fifth value within the power extraction map. The quality of this fit can be seen to be very good with a linear actual by predicted plot, R-squared values of 1, and very small magnitudes of error and residual values.

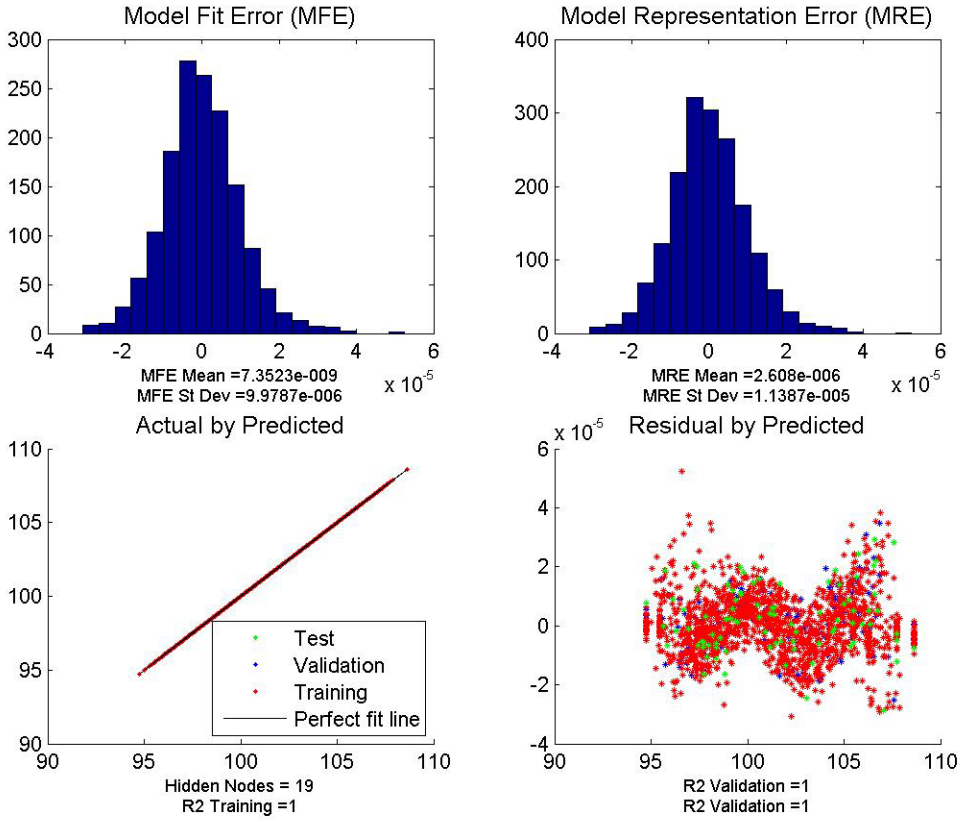

Figure 128: ANN fit Data for Power Extraction Map Sixth Value

Figure 128 contains the quality of fit data for the last value of power extraction within the power extraction map. This fit is seen to be acceptable despite a pattern in the residual due to the very small magnitude of the residual values. Also, the R-squared values are all 1, and the actual by predicted plot can be seen to be linear.

APPENDIX D

SUMMARY OF FIT DATA FOR RESPONSE SURFACE EQUATIONS

Summaries of fit data for the Response Surface Equations (RSEs) of the results shown in the interactive sensitivity analysis environments for the results of the different experiments are shown in the figures below. Similar to the summary of fit information for the ANNs in the previous appendices, in the summary of fit data, it is desirable to have R-squared values as close to 1 as possible, a linear actual by predicted plot, a random scatter of the residual, and a small magnitude residual values. It can be seen that these fits are not perfect but are useable fits. The actual by predicted plots are linear, the magnitude of the residuals are very small, and the R-squared values are close to 1. Any patterns in the residuals that exist are determined to be insignificant given that the magnitude of the residuals are very small. Finally, as these fits are acceptable, these RSEs are used to gain further insight into the experimental results.

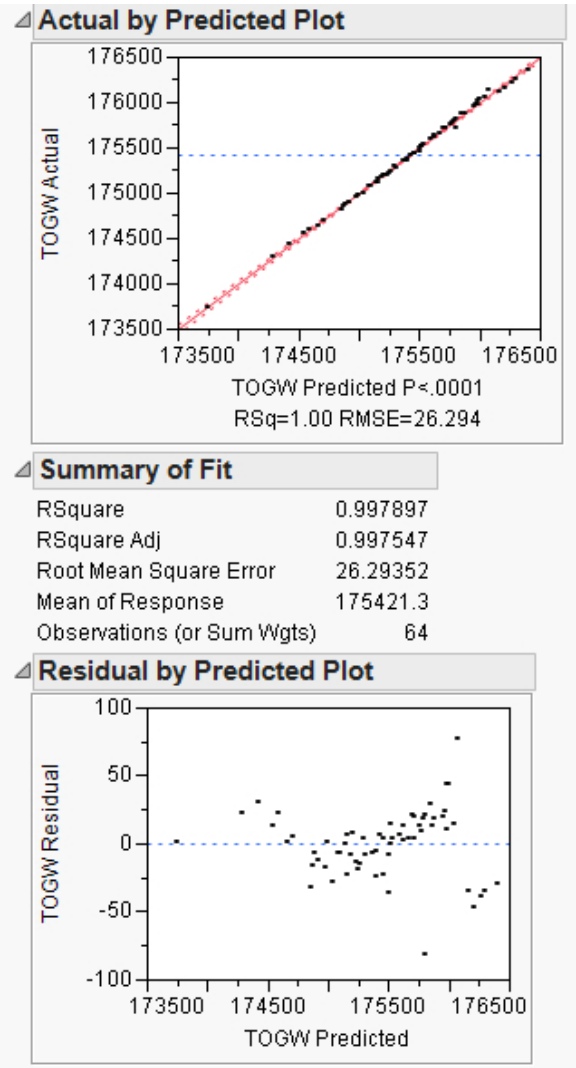

Figure 129: 150-Passenger Class TOGW Quality of Fit

Figure 129 and Figure 130 show the summary of fit information for the RSEs for TOGW and SW for the 150-passenger class aircraft. In the quality of fit, it is desired to have a linear actual by predicted plot, a small magnitude residual that is randomly scattered, and R-squared values close to 1. It can be seen that the fits of TOGW and SW in Figure 129 and Figure 130 are good fits. (The only negative is patterns in the residual, which is acceptable as the magnitude of the residual is small.) These figures show that the RSEs and trends shown in the interactive sensitivity analysis environments are valid.

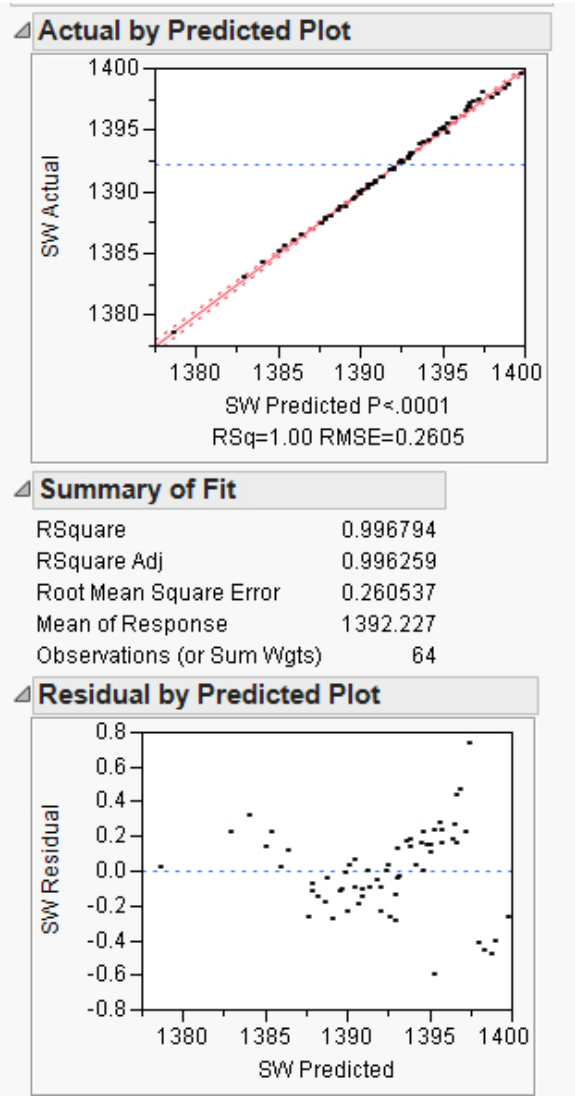

Figure 130: 150-Passenger Class SW Quality of Fit

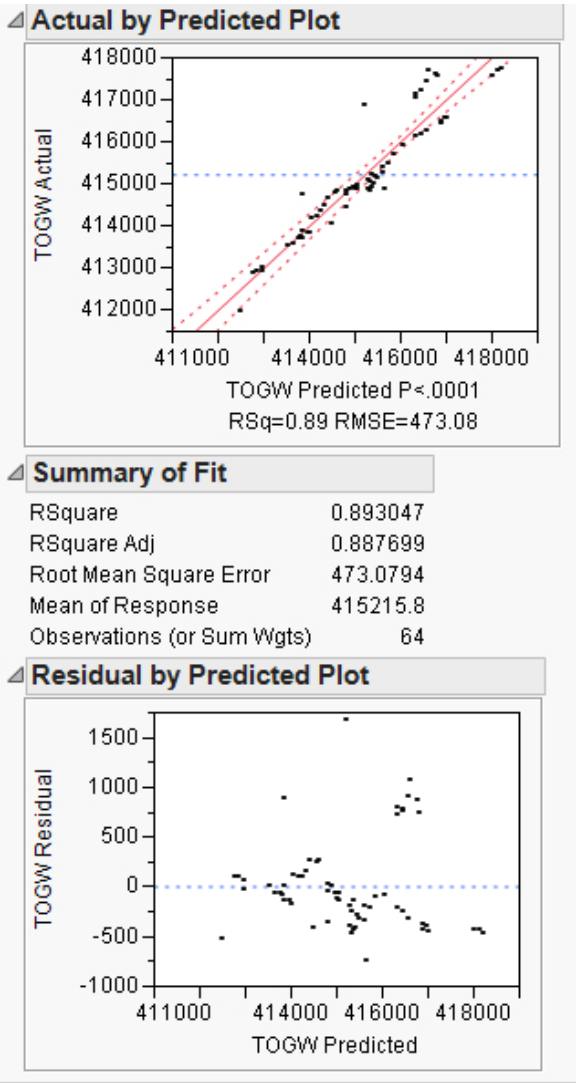

Figure 131: 210-Passenger Class TOGW Quality of Fit

For the 210-passenger class Aircraft, Figure 131 show the information illustrating the quality of the fit of TOGW. As the TOGW is related to SW through W/S which is held as constant in this analysis (as the aircraft is already non-dimensionally sized), the fit for SW is similar to TOGW. For reference, the quality of fit information for SW is seen in Figure 132. Again, in the quality of fit, it is desired to have a linear actual by predicted plot, a small magnitude residual that is randomly scattered, and R-squared values close to 1. It can be seen that the fits of TOGW and SW in Figure 131 and Figure 132 are usable, but not perfect fits.

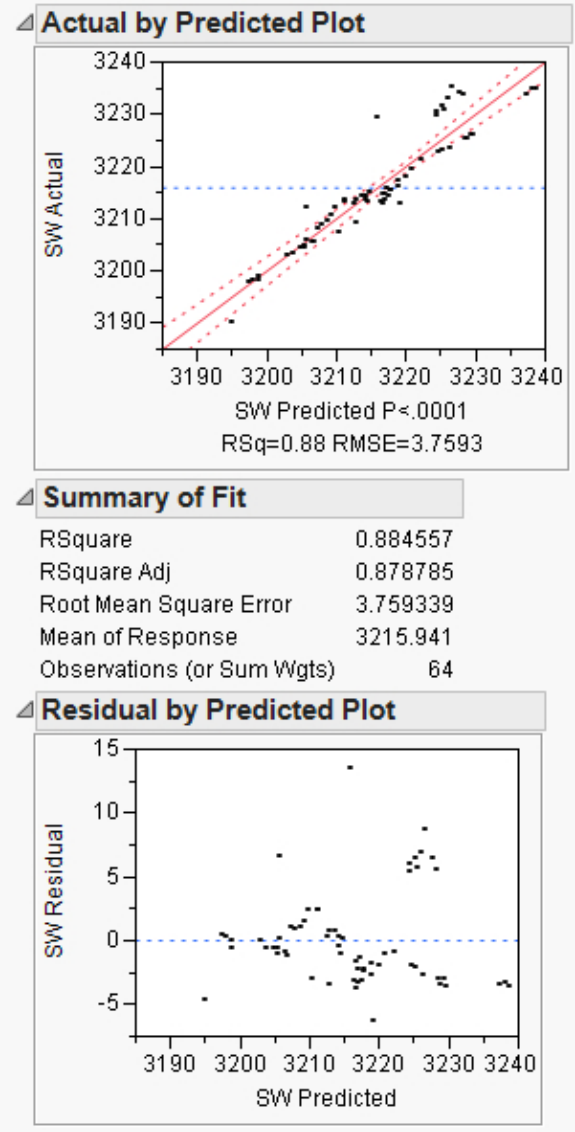

Figure 132: 210-Passenger Class SW Quality of Fit

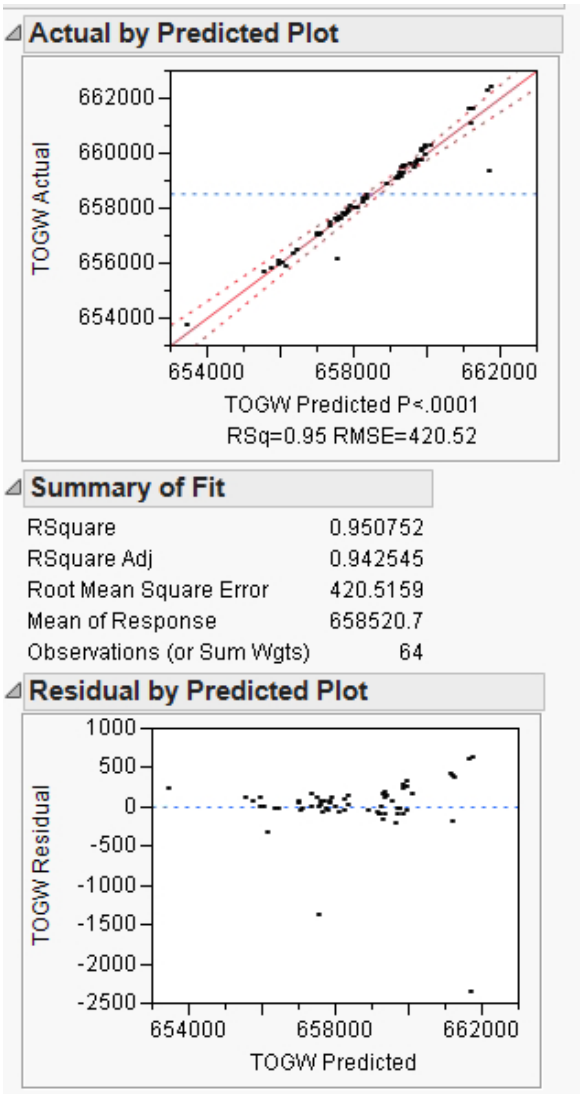

Figure 133: 300-Passenger Class TOGW Quality of Fit

For the 300-passenger class aircraft, Figure 133 shows information illustrating the quality of the RSE of TOGW. The quality of fit information for SW is also seen in Figure 134. Again, in the quality of fit, it is desired to have a linear actual by predicted plot, a small magnitude residual that is randomly scattered, and R-squared values close to 1. It can be seen that the fits of TOGW and SW in Figure 133 and Figure 134 are reasonable fits overall.

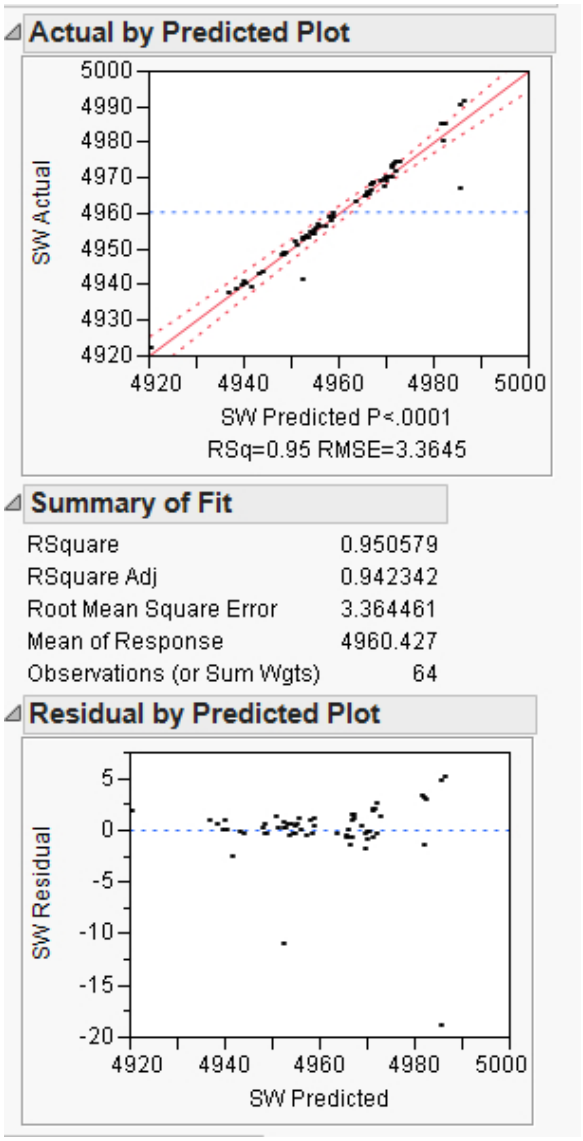

Figure 134: 300-Passenger Class SW Quality of Fit

The remaining quality of fit information within this appendix examines the quality of the fit of the RSEs generated within Experiment 3a, validating the use of the interactive sensitivity analysis environments created for the top architectures examined in this experiment. It can be seen that the fit of TOGW in Figure 135 is a reasonable fit. (The only negative is patterns in the residual, which is acceptable as the magnitude of the residual is small.) This would enable the use of this RSE. Figure 136 contains the RSE for TOGW which is, as was previously discussed, the

driving response within this study.

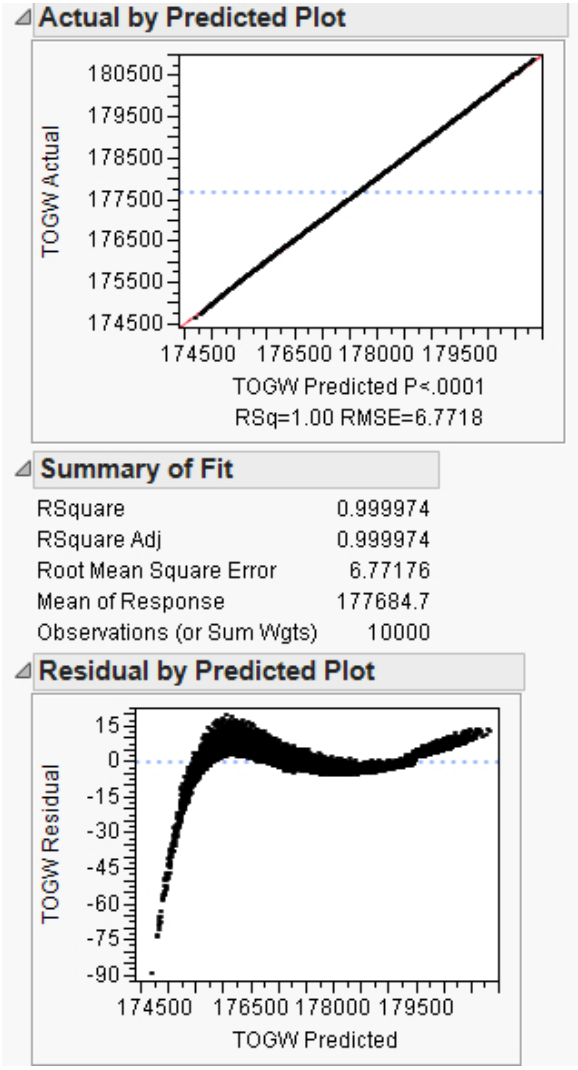

Figure 135: Hybrid Architecture TOGW RSE Fit Quality

Coef

	lnwtfactor	ingeneff	HYDACTWTF	EHAWTF	PUMPWTF	inmotoreff	TOGW
lnwtfactor	-71.69739	23.783881	4.5254272	-3.47314	14.952449	26.696417	115.49939
ingeneff	.	748.00016	-366.0813	-18.44944	-34.10823	74.046421	-1991.34
HYDACTWTF	.	.	2332.6814	291.74845	575.84316	-56.95347	11201.512
EHAWTF	.	.	.	7.4468835	23.221873	-7.467932	728.99214
PUMPWTF	.	.	.	.	-11.46868	-9.760792	2556.7281
inmotoreff	.	.	.	.	.	70.111747	-249.0453

Figure 136: Hybrid Architecture TOGW RSE

Figure 137 shows that the RSE of SW is an acceptable fit. (The only negative

is patterns in the residual, which is acceptable as the magnitude of the residual is small.) It should be noted that this fit is similar to the TOGW fit, which is logical as the two are directly related through W/S.

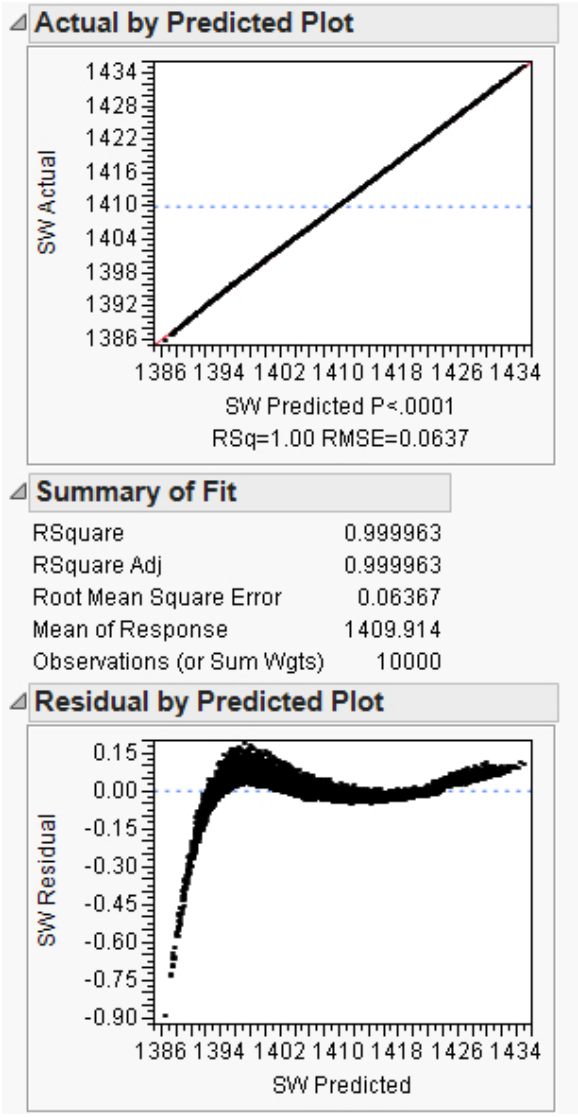

Figure 137: Hybrid Architecture SW RSE Fit Quality

Figure 138 contains the summary of fit data for subsystem weight for the hybrid architecture and shows that the RSE is a reasonable fit. (Again, the only negative is patterns in the residual, which is acceptable as the magnitude of the residual is small.)

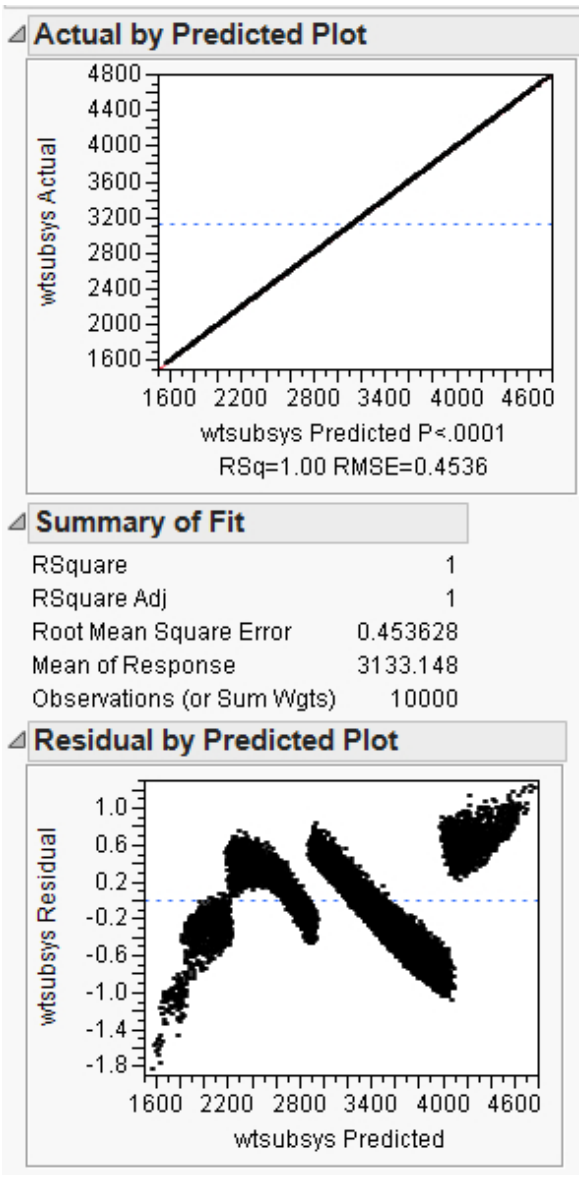

Figure 138: Hybrid Architecture Subsystem Weight RSE Fit Quality

Figures 139 and 140 contains the summary of fit data for average and maximum power extraction for the hybrid architecture and shows that the RSEs are a reasonable fit despite patterns in the residual, which is acceptable as the magnitude of the residual is small.

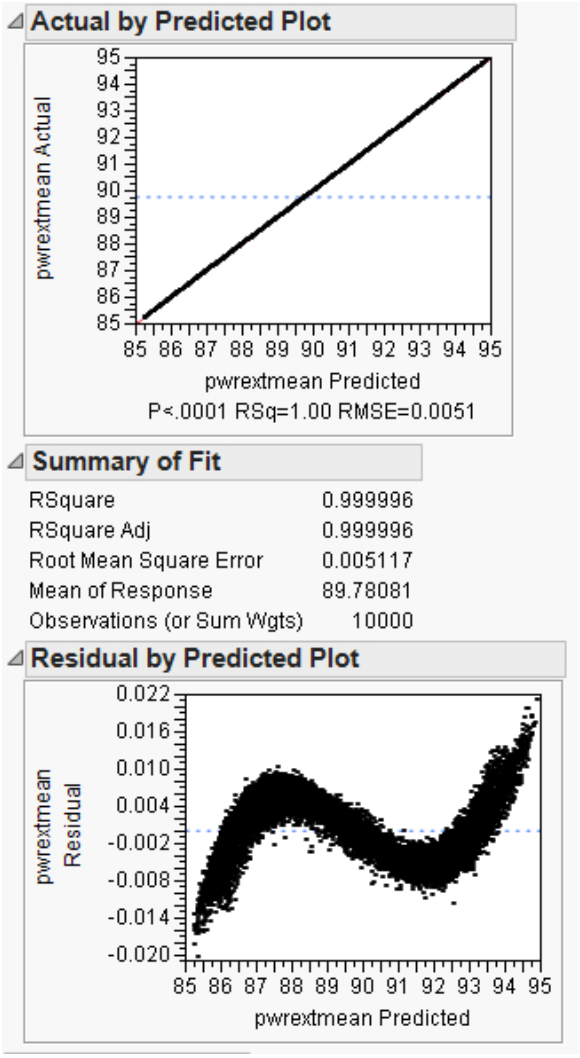

Figure 139: Hybrid Architecture Average Power Extraction RSE Fit Quality

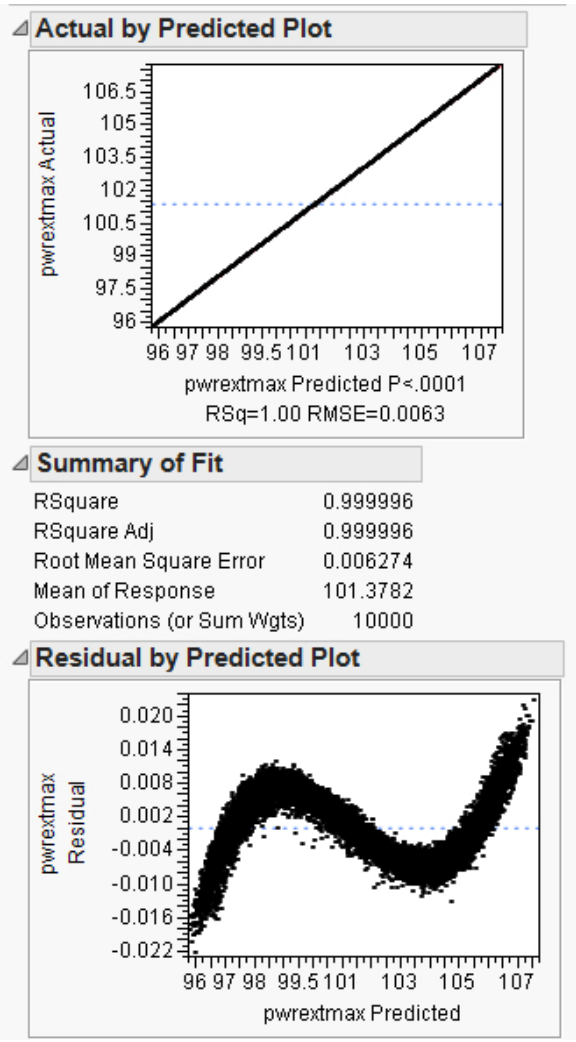

Figure 140: Hybrid Architecture Maximum Power Extraction RSE Fit Quality

The quality of these fits for responses TOGW, SW, subsystem weight, average power extraction, and maximum power extraction for the hydraulic architecture is examined in Figures 141, 142, 143, 144, and 145 respectively. Again, these figures show that the RSEs and trends shown in the interactive sensitivity analysis environments are valid.

The fit of TOGW in Figure 141 is an acceptable fit. (The only negative is patterns in the residual, which is acceptable as the magnitude of the residual is small.) This would enable the use of this RSE.

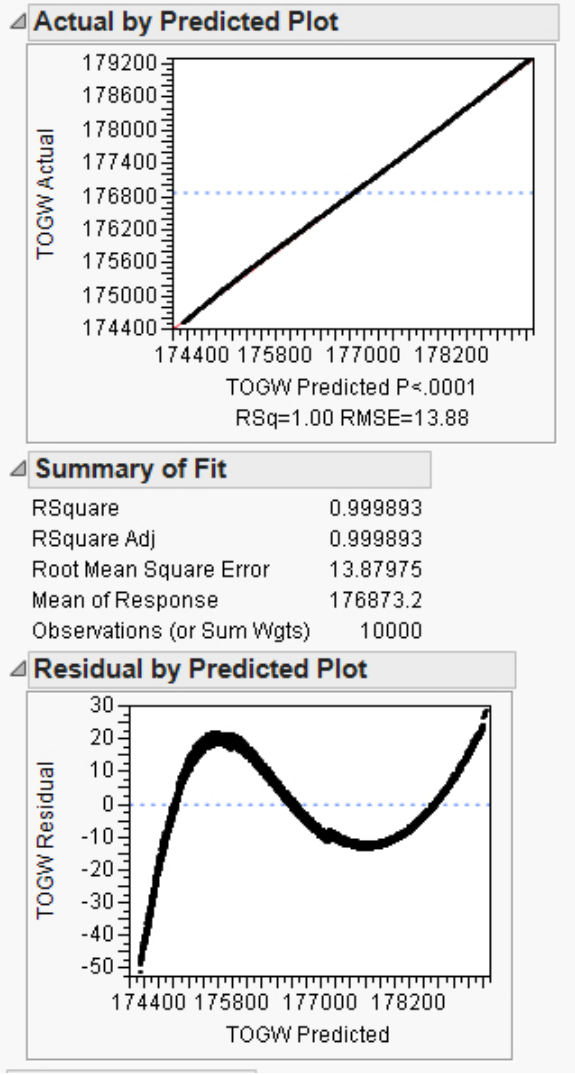

Figure 141: Hydraulic Architecture TOGW RSE Fit Quality

The RSE of SW is shown in Figure 142 and is a reasonable fit despite patterns in the residual, which is acceptable as the magnitude of the residual is small. It should again be noted that this fit is similar to the TOGW fit, as the parameters are related through W/S.

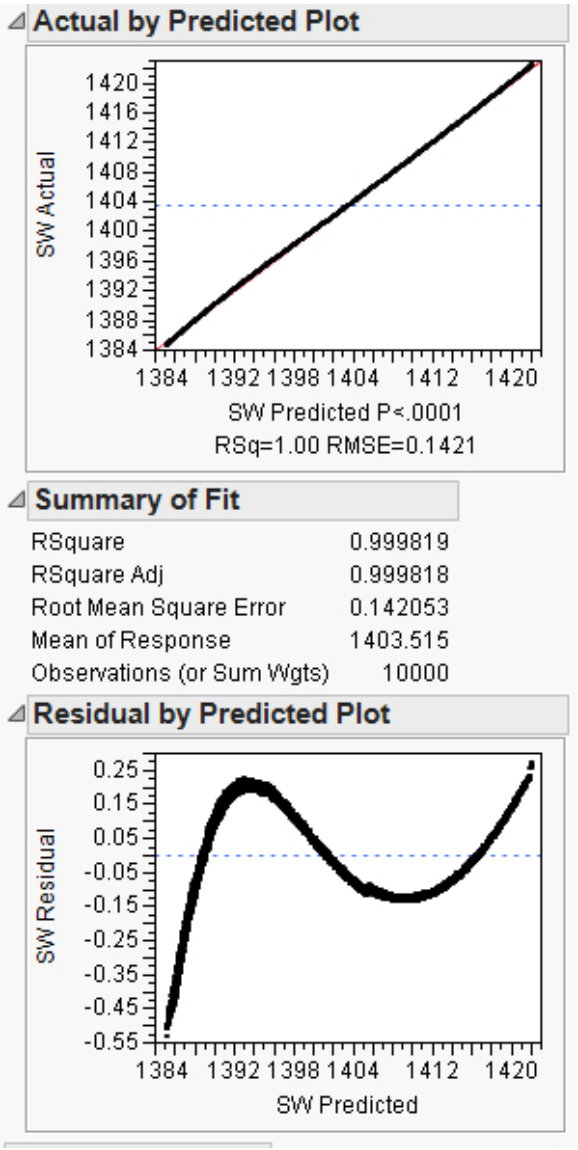

Figure 142: Hydraulic Architecture SW RSE Fit Quality

For the hydraulic architecture, Figure 143 contains the summary of fit data for subsystem weight and shows that the RSE is a good fit. (Again, the only negative is patterns in the residual, which is acceptable as the magnitude of the residual is small.)

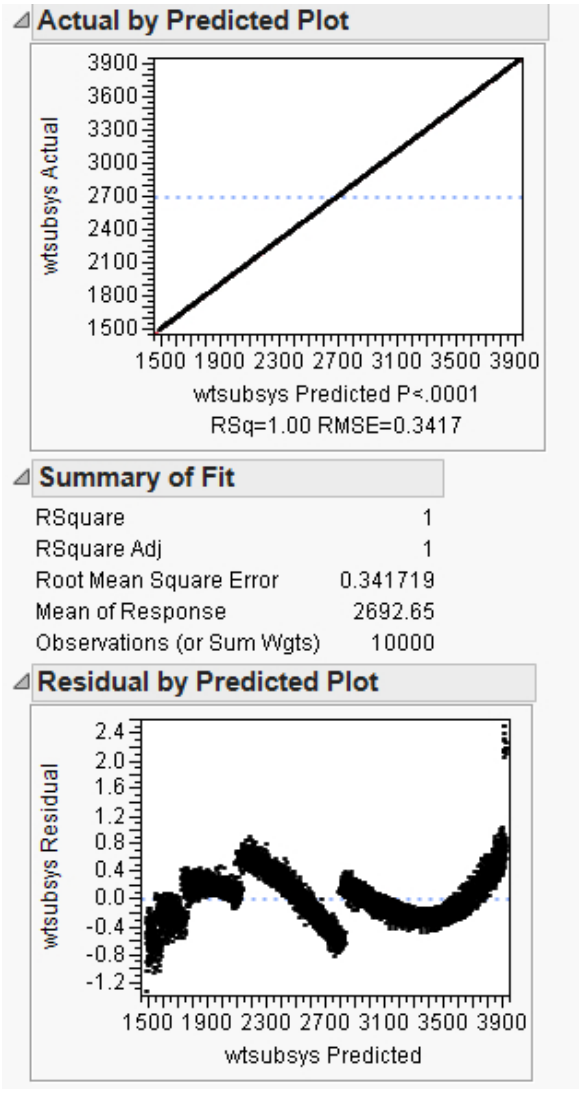

Figure 143: Hydraulic Architecture Subsystem Weight RSE Fit Quality

Summary of fit data for average power extraction for the hydraulic architecture is shown in Figure 144 which shows the RSE is an acceptable fit. (Again, the only negative is a pattern in the residual, which is acceptable as the magnitude of the residual is small.)

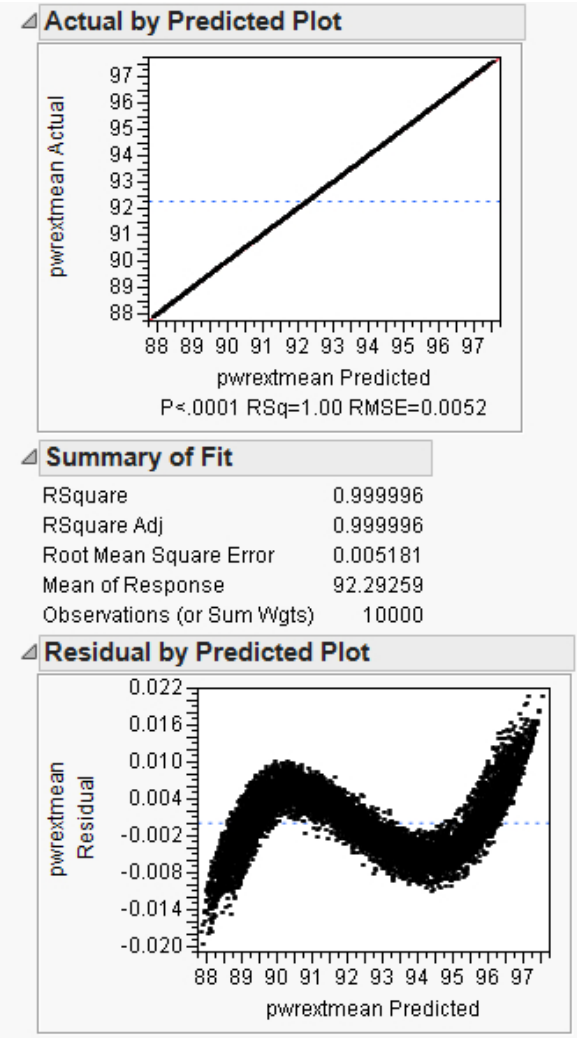

Figure 144: Hydraulic Architecture Average Power Extraction RSE Fit Quality

The summary of fit data for maximum power extraction for the hydraulic architecture is shown in Figure 145, which shows that this RSE is a decent fit despite a pattern in the residual, which is acceptable as the magnitude of the residual is small.

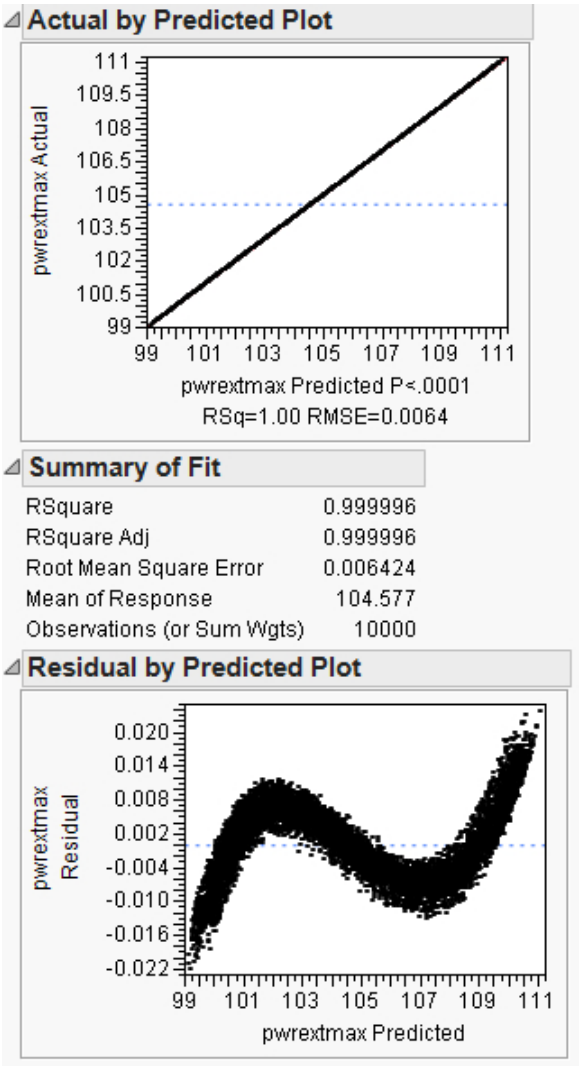

Figure 145: Hydraulic Architecture Maximum Power Extraction RSE Fit Quality

Again, for the EHA architecture, Figures 146, 130, 130, 130, and 130 examined the quality of these fits for responses TOGW, SW, subsystem weight, average power extraction, and maximum power extraction, respectively. Again, for this architecture, the RSEs and trends shown in the interactive sensitivity analysis environments are shown to be valid by the quality of fit data.

Figure 146 shows that the RSE of TOGW is a reasonable fit. (Again, the only negative is patterns in the residual, which is acceptable as the magnitude of the residual is small.)

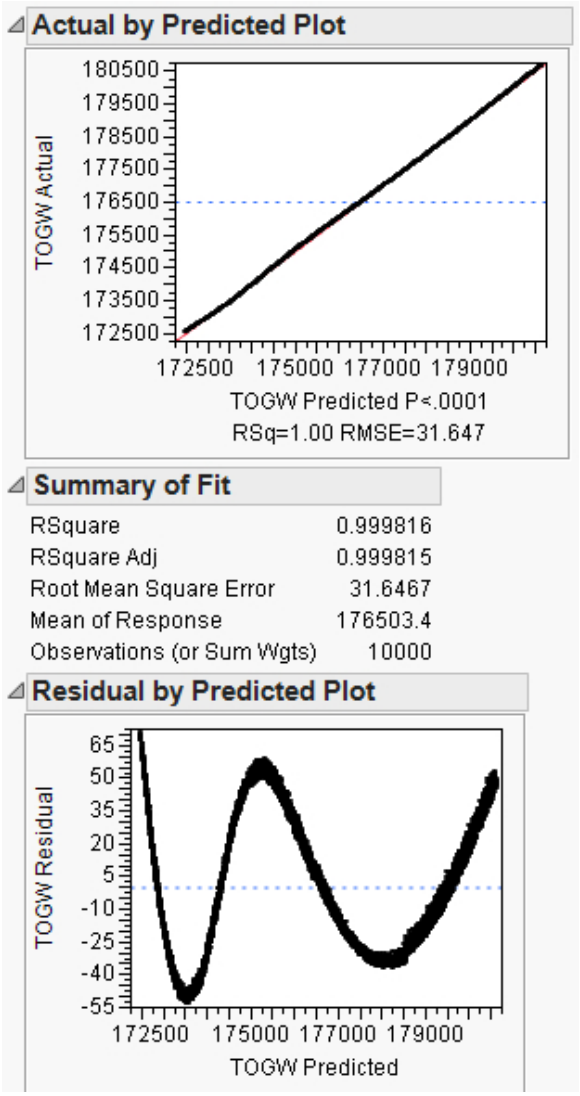

Figure 146: EHA Architecture TOGW RSE Fit Quality

Figure 147 shows that the RSE of SW is also a usable fit. (The only negative is patterns in the residual, which is acceptable as the magnitude of the residual is small.) Again, it should again be noted that this fit is similar to the TOGW fit, as the parameters are related through W/S.

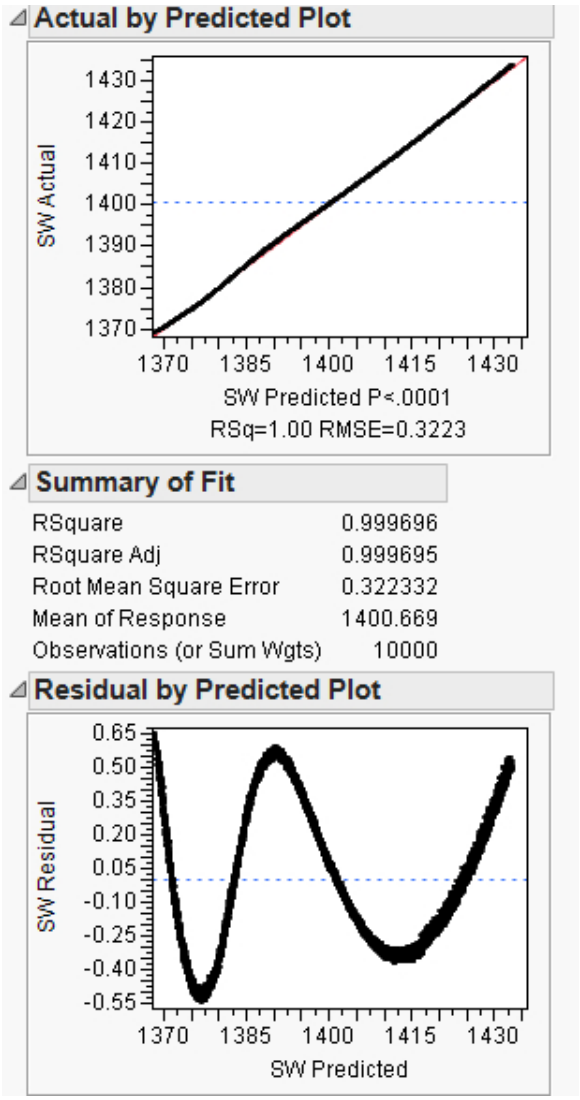

Figure 147: EHA Architecture SW RSE Fit Quality

Figure 148 contains the summary of fit data for subsystem weight and illustrates that the RSE is a good fit, for the EHA architecture despite patterns in the residual, which is acceptable as the magnitude of the residual is small.

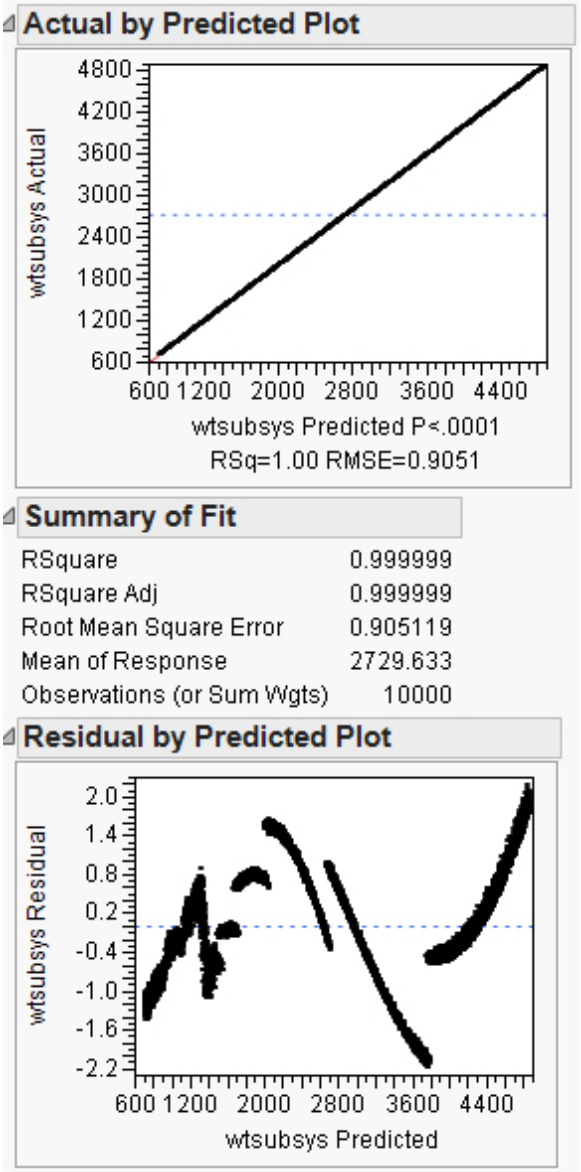

Figure 148: EHA Architecture Subsystem Weight RSE Fit Quality

Figures 149 shows that the RSEs for average power extraction for the EHA architecture is an acceptable fit. (Again, the only negative is patterns in the residual, which is acceptable as the magnitude of the residual is small.)

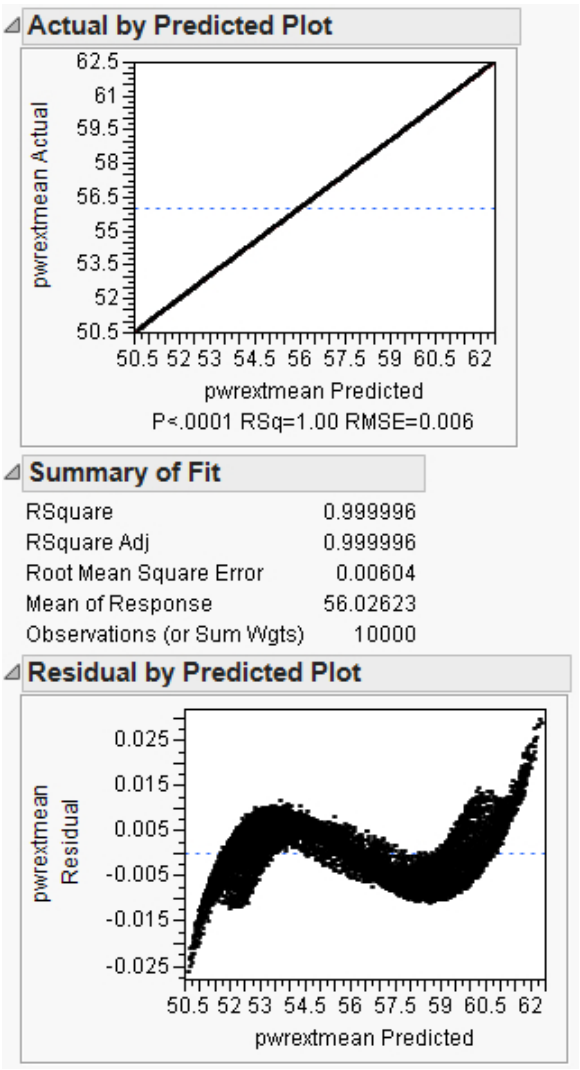

Figure 149: EHA Architecture Average Power Extraction RSE Fit Quality

Figure 150 shows that the RSE for maximum power extraction for the EHA architecture is also an acceptable fit despite patterns in the residual, which are acceptable as the magnitude of the residual is small.

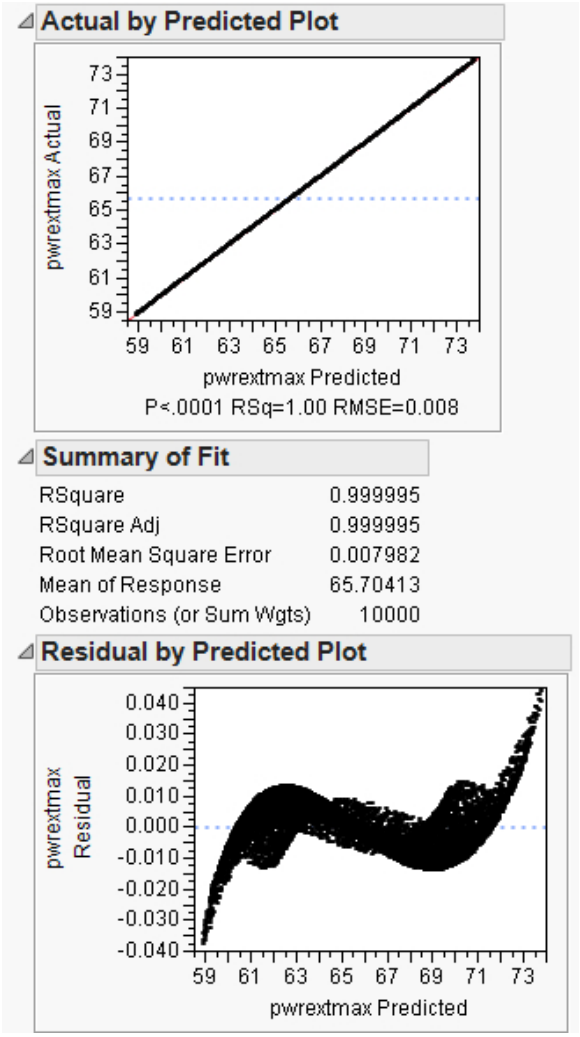

Figure 150: EHA Architecture Maximum Power Extraction RSE Fit Quality

As can be seen, the quality of fit for these RSEs is acceptable, enabling analysis utilizing the RSEs. The only negative of the fits are patterns in the residual which are deemed acceptable given that the overall magnitude of the residuals are small. As a result, conclusions drawn from these RSEs should be valid.

REFERENCES

[1] "737-NG Hydraulic System Experiences: 737-6/7/8/900."

[2] "AMJ 25.1309."

[3] "Determining electric motor load and efficiency," Tech. Rep. DOE/GO-10097-517, U.S. Department of Energy.

[4] "SAE AIR5005A: Commercial Aircraft Hydraulic Systems," 2010 05.

[5] "Advisory circular 25.1309-1a," 1988.

[6] "Massive 787 electrical system pressurizes cabin," *Aviation Week & Space Technology*, p. 47, 2005.

[7] "Exp bus technical bulletin: Aircraft wire sizes," 2011.

[8] "Maia," 2011.

[9] "Boeing 777 long-range jetliner," 2012.

[10] "FAR 25.831," 2012.

[11] "Cad 3-view drawing for airport planning purposes," 2013.

[12] "Phx modelcenter," 2013.

[13] Abraham, B., ed., *Quality Improvement Through Statistical Methods*. Statistics for Industry and Technology, Boston: Birkhauser, 1998.

[14] Air Force Research Laboratory, "Integrated vehicle energy technology demonstration (invent) solicitation number: Baa-08-03-pkpa-draft," April 2008.

[15] Air Transport Association of America Inc., "U.S. Passenger and Cargo Airline Fleet." Online, 2011.

[16] AirResearch Mfg Co of California, "Electromechanical actuation feasibility study," Tech. Rep. AD-A031 146, U.S. Department of Commerce, 1976.

[17] American Institute of Aeronautics and Astronautics, "Energy Optimized Aircraft and Equipment Systems Program - AIAA," 2011.

[18] Anderson, Jr., J., *Aircraft performance and design*. WCB/McGraw-Hill, 1999.

[19] Anderson, N. E., Loewenthal, S. H., and Black, J. D., "An analytical method to predict efficiency of aircraft gearboxes," in *Twentieth Joint Propulsion Conference*, NASA Lewis Research Center and Propulsion Laboratory and U.S. Army Research and Technology Laboratories, June 1984.

[20] Armstrong, M., "A process for function based architecture definition and modeling," Master's thesis, Georgia Institute of Technology, April 2008.

[21] Armstrong, M., *Identification Of Emergent Off-Nominal Operational Requirements During Conceptual Architecting Of The More Electric Aircraft*. PhD thesis, Georgia Institute of Technology, December 2011.

[22] ASM Aerospace Specification Metals, Inc., "Aluminum 6061-t6; 6061-t651."

[23] ASM Aerospace Specification Metals, Inc., "Titanium ti-3al-2.5v, alpha annealed."

[24] Ayyub, B. M., *Uncertainty modeling and analysis in civil engineering*. CRC Press, 1998.

[25] Bals, J., Hofer, G., Pfeiffer, A., and Schallert, C., "Virtual iron bird a multidisciplinary modelling and simulation platform for new aircraft system architectures," Deutscher Luft- und Raumfahrtkongress 2005, (Johann Bals, Gerhard Hofer, Andreas Pfeiffer, Christian Schallert), Johann Bals, Gerhard Hofer, Andreas Pfeiffer, Christian Schallert, 2005.

[26] Bals, J., Ji, Y., Kuhn, M. R., and Schallert, C., "Model based design and integration of more electric aircraft systems using modelica," in *More Electric Aircraft Forum*, (Wessling, Germany), Institute of Robotics and Mechatronics German Aerospace Centre (DLR), MOET Project Consortium, 2009.

[27] Berlowitz, I., "All/more electric aircraft engine & airframe systems implementation," in *The 9th Israeli Symposium on Jet Engines and Gas Turbines*, Israel Aerospace Industries, October 2010.

[28] Binder, K. and Heermann, D. W., *Monte Carlo Simulation in Statistical Physics: An Introduction*. Graduate Texts In Physics, New York: Springer, fifth ed., 2010.

[29] Boeing, "737-800 technical characteristics." Online, 2011.

[30] Boeing, "777-200/-200er and 777-300 general arrangements." Online, 2011.

[31] Brady, C., "The boeing 737 technical site," 1999.

[32] Chakraborty, I., Trawick, D., Hegde, C., Choi, H., Mendez-Ramos, E., and Mavris, D. N., "Development of a modeling and simulation environment for real-time performance analysis of electric actuators in maneuvering

flight," Georgia Institute of Technology, American Institute of Aeronautics and Astronautics.

[33] Cinibulk, W., "Aircraft electrical wire: Wire manufacturers perspective."

[34] Dahmann, J. S., Fujimoto, R. M., and Weatherly, R. M., "The department of defense high level architecture," in *1997 Winter Simulation Conference* (Andradttir, S., Healy, K. J., Withers, D. H., and Nelson, B. L., eds.), pp. 142–149, 1997.

[35] D'aulaire, I. and D'aulaire, E., *Book of Greek Myths*. Delacorte Press, 1962.

[36] de Tenorio, C., *Methods For Collaborative Conceptual Design Of Aircraft Power Architectures*. PhD thesis, Georgia Institute of Technology, 2010.

[37] Defense Acquistion University Press, *Systems Engineering Fundamentals*. Defense Acquistion University Press, 2001.

[38] Drakos, N., *Introduction to Monte Carlo Methods*. Computational Science Education Project, 1995. http://www.phy.ornl.gov/csep/mc/mc.html.

[39] Druflon Electronics, "Properties of ptfe and some other insulating materials," 2013.

[40] Du, X. and Chen, W., "Concurrent subsystem uncertainty analysis in multidisciplinary design," in *AIAA/NASA/USAF/ISSMO Symposium on Multidisciplinary Analysis and Optimization*, 2000.

[41] Ebert-Uphoff, I., "Tutorial on how to measure link strengths in discrete bayesian networks," Tech. Rep. Georgia Tech Research Report: GT-ME-2009-001, Georgia Institute of Technology, Atlanta, GA, September 2009.

[42] Elishakoff, I., Kulisch, U., Paola, M. D., and et al., *Whys and Hows in Uncertainty Modelling: Probability, Fuzziness, and Anti-Optimization*. No. 388 in CISM Courses and Lectures, Springer-Verlag Wien New York, 1999.

[43] Engler, W., Biltgen, P., and Mavris, D., "Concept selection using an interactive reconfigurable matrix of alternatives," in *45th AIAA Aerospace Sciences Meeting*, 2007.

[44] Fabrycky, W. J. and Blanchard, B. S., *Life-Cycle Cost and Economi Analysis*. Prentice-Hall Series in Industrial and Systems Engineering, Prentice-Hall, 1991.

[45] Faidi, A., "Effect of accessory power take-off variation on a turbofan engine performance," Master's thesis, Air Force Institute Of Technology, September 2012.

[46] Faleiro, L., "Beyond the more electric aircraft," *AEROSPACE AMERICA*, pp. 35–40, SEPTEMBER 2005.

[47] FANLIANG, M., "Actuation system design with eelectrically powered actuators," Master's thesis, Cranfiled University, January 2011.

[48] Fowlkes, W. and Creveling, C., *Engineering Methods for Robust Product Design: Using Taguchi Methods in Technology and Product Development*. Addison-Wesley Publishing Company, 1995.

[49] Gibson, S., "Pleiades mythology."

[50] Gurnani, A. P. and Lewis, K., "Decentralized design under uncertainty: Investigating the impact of designer mistakes," in *AIAA/ISSMO Multidisciplinary Analysis and Optimization Conference*, 2006.

[51] Hays, T., "Integrated digital/electric aircraft concepts studynasa cr-3841," April 2009.

[52] Heckerman, D., "A tutorial on learning with bayesian networks," Tech. Rep. MSR-TR-95-06, Microsoft Corporation, 1996.

[53] Heckerman, D., "A tutorial on learning with bayesian networks," Tech. Rep. MSR-TR-95-06, Microsoft Corporation, Redmond, WA, November 1996.

[54] Hegde, C., Chakraborty, I., Trawick, D., Choi, H., Mendez-Ramos, E., and Mavris, D. N., "A surrogate model based constrained optimization architecture for the optimal design of electrohydrostatic actuators for aircraft flight control surfaces," Georgia Institute of Technology, American Institute of Aeronautics and Astronautics.

[55] Helton, J. C. and Burmaster, D. E., "Guest editorial: treatment of aleatory and epistemic uncertainty in performance assessments for complex systems," *Reliability Engineering and System Safety*, vol. 54, pp. 91–94, 1996.

[56] Hlavacek, I., Chleboun, J., and Babuska, I., *Uncertain Input Data Problems and the Worst Scenario Method*. North-Holland Series in Applied Mathematics and Mechanics, Elsevier B.V., 2004.

[57] Hofer, E., "When to separate uncertainties and when not to separate," *Reliability Engineering and System Safety*, vol. 54, pp. 113–118, 1996.

[58] Hoffman, A. C., Hansen, I. G., Beach, R. F., Plencner, R. M., Dengler, R., Hefferies, K. S., and j. Frye, R., "Advanced secondary power system for transport aircraft," Tech. Rep. 2463, National Aeronautics and Space Administration, Cleveland, OH, May 1985.

[59] Honeywell, "Power optimized more electrical aircraft," in *Towards eEnvironment*, (Prague, Czech Republic), Honeywell, March 2009.

[60] Howe, D., *Aircraft Conceptual Design Synthesis*. Professional Engineering Publishing Limited, 2000.

[61] Huff, Jr., W. W., *Modern Engineering Methods in Aircraft Preliminary Design*, pp. 5–1 to 5–16. No. 65 in Preliminary Aircraft Design, North Atlantic Treaty Organization Adivsiory Group For Aerospace Research and Development, 1974.

[62] Huhta, S., "It architecture - for small & mid-sized organizations," 2011.

[63] Hui, C., "Multivariate robust design," in *SAE 2005 World Congress*, Society of Automotive Engineers, 2005.

[64] Hwang, C.-L. and Yoon, K., *Multiple Attribute Decision Making Methods and Applications A State-of-the-Art Survey*. Lecture Notes in Economics and Mathematical Systems, New York: Springer-Verlag, 1981.

[65] IATA, "Jet fuel price development." Online, 2011.

[66] International Council on Systems Engineering, *SYSTEMS ENGINEERING HANDBOOK: A WHAT TO GUIDE FOR ALL SE PRACTITIONERS*. International Council on Systems Engineering, 2a ed., 2004.

[67] Jenkinson, L. R., Simpkin, P., and Rhodes, D., *Civil Jet Aircraft Design*. AIAA Education Series, American Institute of Aeronautics and Astronautics, 1999.

[68] Jensen, S. C., Jenney, G. D., Raymond, B., and Dawson, D., "Flight test experience with an electromechanical actuator on the f-18 systems research aircraft," in *19th Digital Avionics Systems Conference*, NASA Dryden Flight Research Center, National Aeronautics and Space Administration, October 2000.

[69] Jimenez, H., Acuff, C., and Mavris, D., "Study of pareto-optimal aircraft technologies for next-decade environmental goals," in *51st AIAA Aerospace Sciences Meeting*, American Institute of Aeronautics and Astronautics, January 2013.

[70] Jimenez, H., Burdette, G., Schutte, J., and Mavris, D. N., "Probabilistic technology assessment for nasa environmentally responsible aviation (era) vehicle concepts," in *11th AIAA Aviation Technology, Integration, and Operations (ATIO) Conference*, American Institute of Aeronautics and Astronautics, September 2011.

[71] Jordaan, I., *Decisions under Uncertainty: Probabilistic Analysis for Engineering Decisions*. Cambridge University Press, 2005.

[72] Joy, D. C., "An introduction to monte carlo simulations," *Scanning Microscopy*, vol. 5, no. 2, pp. 329–337, 1991.

[73] Keller, G. R., *Aircraft Hydraulic Design*. Cleveland, OH: Applied hydraulics magazine, The Industrial Publishing Corporation, 1957.

[74] Keller, W. and Modarres, M., "A historical overview of probabilistic risk assessment development and its use in the nuclear power industry: a tribute to the late professor norman carl rasmussen," *Reliability Engineering and System Safety*, vol. 89, pp. 271–285, 2005.

[75] Kirby, M. R., *A Methodology For Technology Identification, Evaluation, and Selection In Conceptual and Preliminary AircraftI Design*. PhD thesis, Georgia Institute of Technology, March 2001.

[76] Kirby, M. R. and Mavris, D. N., "An approach for verification and validation of the environmental design space," in *26th International Congress of the Aeronautical Sciences*, 2008.

[77] Kirby, M. R. and Mavris, D. N., "The environmental design space," in *26th International Congress of the Aeronautical Sciences*, 2008.

[78] Lawson, C. P. and Pointon, J. M., "Thermal management of electromechanical actuation on an all-electric aircraft," in *26TH International Congress Of The Aeronautical Sciences*, Cranfield University, 2008.

[79] Liviu, D., Jenica, C., Mihai, L., and Alexandru, T., "Mathematical models and numerical simulations for electro-hydrostatic servo-actuators," *INTERNATIONAL JOURNAL OF CIRCUITS, SYSTEMS AND SIGNAL PROCESSING*, vol. 2, no. 4, pp. 229–238, 2008.

[80] Loftin, L. K., *Subsonic Aircraft: Evolution and the Maching of Size to Performance*. No. NASA Reference Publication 1060, National Aeronautics and Space Administration, August 1980.

[81] MACKAY, D., "Introduction to monte carlo methods."

[82] Mason, W. H., "Modern aircraft design techniques," May 2003.

[83] Mattingly, J. D., Heiser, W. H., and Pratt, D. T., *Aircraft Engine Design*. American Institute of Aeronautics and Astronautics, second ed., 2002.

[84] Mavris, D. N., DeLaurentis, D. A., Bandte, O., and Hale, M. A., "A stochastic approach to multi-disciplinary aircraft analysis and design," in *36th Aerospace Sciences Meeting & Exhibit*, (January), American Institute of Aeronautics and Astronautics, 1998.

[85] Mavris, D., Bandte, O., and Schrage, D., "Effect of mission requirements on the economic robustness of an hsct concept," in *Conference of the Internationa! Society of Parametric Analysis*, 1996.

[86] Mavris, D., Tenorio, C. D., and Armstrong, M., "Methodology for aircraft system architecture definition," in *46th AIAA Aerospace Sciences Meeting and Exhibit*, American Institute of Aeronautics and Astronautics, 2008.

[87] Mavris, D. N., Bandte, O., and Schrage, D. P., "Application of probabilistic methods for the determination of an economically robust hsct configuration," in *AIAA, NASA, and ISSMO, Symposium on Multidisciplinary Analysis and Optimization*, no. AIAA-96-4090, American Institute of Aeronautics and Astronautics, September 1996.

[88] Meyers, R. H. and Montgomery, D. C., *Response Surface Methodology: Process and Product Optimization Using Designed Experiments*. Wiley Series in Probability and Statistics, John Wiley & Sons Ltd., second ed., 2002.

[89] Mish, F. C. and et al., eds., *Merriam-Webster's Collegiate Dictionary*. Springfield, Massachusetts: Merriam-Webster, Incorporated, eleventh ed., 2003.

[90] MOET, "Moet project overview," November 2008.

[91] Moir, I., "Fifty years of aerospace power - full circle?," (Paris), Technologies for Energy Optimized Aircraft Equipment Systems, 2006.

[92] Moir, I. and Seabridge, A., *Military Avionics Systems*. AIAA Education Series, American Institute of Aeronautics and Astronautics and John Wiley & Sons, 2006.

[93] Moir, I. and Seabridge, A., *Aircraft Systems: Mechanical, electrical, and avionics subsystems integration*. John Wiley & Sons Ltd., 2008.

[94] Moore, R. and Lodwick, W., "Interval analysis and fuzzy set theory," *Fuzzy Sets and Systems*, vol. 135, pp. 5–9, April 2003.

[95] Moorhouse, D. J., "Proposed system-level multidisciplinary analysis technique based on exergy methods," *JOURNAL OF AIRCRAFT*, vol. 40, pp. 11–15, 2003.

[96] Murphy, K. P., "The bayes net toolbox for matlab," *Computing Science and Statistics*, October 2001.

[97] National Aeronautics and Space Administration, *NASA Systems Engineering Handbook*. National Aeronautics and Space Administration, 2007.

[98] National Research Council (U.S.), *Issues in risk assessment*. Washington, DC: National Academy Press, 1993.

[99] Navarro, R., "Performance of an electro-hydrostatic actuator on the f-18 systems research aircraft," Tech. Rep. TM-97-206224, National Aeronautics and Space Administration, Edwards, CA, October 1997.

[100] Navidi, W., *Statistics: for Engineers and Scientists*. McGraw-Hill, second ed., 2008.

[101] Neese, W. A., *Aircraft Hydraulic Systems*. Malabar, Florida: Robert E. Krieger Publishing Company, 1984.

[102] Nelson, T., "787 systems and performance," 2005.

[103] Newberry, C. F. and DeFilippo, R., *Perspectives in Aerospace Design: "Aircraft Synthesis Using Numerical Optimization Methodology"*. American Institute of Aeronautics and Astronautics: Student Programs Department, 1991.

[104] Newberry, C. F. and Eckels, W. E., *Perspectives in Aerospace Design: "Civil Transport Aircraft Design Methodology"*. American Institute of Aeronautics and Astronautics: Student Programs Department, 1991.

[105] Newberry, C. F. and Parker, J. L., *Perspectives in Aerospace Design: "Mission Requirements and Aircraft Sizing"*. American Institute of Aeronautics and Astronautics: Student Programs Department, 1991.

[106] Nicolai, L. M., *Fundamentals of Aircraft Design*. School of Engineering, University of Dayton, Ohio, 1975.

[107] Office of The Under Secretary of Defense, *DoD Guide to Integrated Product and Process Development*. United States of America Department of Defense, 1996.

[108] Ostrower, J., "A320neo does not unlock 737 customers, hurts cseries: Boeing ceo." Electronically, April 2011.

[109] Ostrower, J., "Boeing boss green-lights all-new next generation narrow-body." Electronically, February 2011.

[110] Pace, "Pacelab sysarc," 2012.

[111] Park, S. H., *Robust Design and Analysis For Quality Engineering*. New York: Chapman and Hall, 1996.

[112] Parker, "Compact eha electro-hydraulic actuators for high power density applications catalogue hy07-1310/uk," 2011.

[113] Parry, G. W., "The characterization of uncertainty in probabilistic risk assessments of complex systems," *Reliability Engineering and System Safety*, vol. 54, pp. 119–126, 1996.

[114] Pate-Cornell, M. E., "Uncertainties in risk analysis: Six levels of treatment," *Reliability Engineering and System Safety*, vol. 54, pp. 96–111, 1996.

[115] Raymer, D. P., *Aircraft Design: A Conceptual Approach Fourth Edition*. Reston, Virginia: American Institute of Aeronautics and Astronautics, 2006.

[116] Raymond, E., "Design guide for aircraft hydraulic, systems and components for use with chlorotrifluoroethylene nonflammable hydraulic fluids," Tech. Rep. AFWAL-TR-80-2111, Boeing Military Airplane Company, SEATTLE, WASHINGTON, March 1982.

[117] Regan, H. M., Ben-Haim, Y., Langford, B., Wilson, W. G., Lundberg, P., Andelman, S. J., and Burgman, M. A., "Robust decision-making under severe uncertainty for conservation management," *Ecological Applications*, vol. 15, pp. 1471–1477, August 2005.

[118] Regan, H. M., Colyvan, M., and Burgman, M. A., "A taxonomy and treatment of uncertainty for ecology and conservation biology," *Ecological Applications*, vol. 12, pp. 618–628, April 2002.

[119] Richards, M., Hastings, D., Rhodes, D., and Weigel, A., "Systems architecting for survivability: Limitations of existing methods for aerospace systems," in *6th Conference on Systems Engineering Research*, April 2008.

[120] Rosero, J., Ortega, J., Aldabas, E., and Romeral, L., "Moving towards a more electric aircraft," *IEEE A&E Systems Magazine*, March 2007.

[121] Roskam, J., *Airplane Design: Part V: Component Weight Estimation*. Roskam Aviation and Engineering Corporation, 1985.

[122] Roskam, J., *Airplane Design: Part VI: Preliminary Calculation of Aerodynamic, Thrust, and Power Characteristics*. Roskam Aviation and Engineering Corporation, 1987.

[123] Roskam, J., *Airplane Design: Part I: Preliminary Sizing of Airplanes*. Ottawa, Kansas: Roskam Aviation and Engineering Corporation, 1989.

[124] Scholz, D., "Development of a cae-tool for the design of flight control and hydraulic systems," in *Aero Tech 1995*, (London), Institution of Mechanical Engineers, October 1995.

[125] Schrage, D. P., "Technology for Rotorcraft Affordability Through Integrated Product/Process Development (IPPD)," in *American Helicopter Society 55th Annual Forum*, American Helicopter Society, Inc., 1999.

[126] Solutia Hazard Communication Group, "Skydrol 500b-4 fire resistant hydraulic fluid, solutia inc. material safety data sheet," January 2011.

[127] Stinton, D., *The Design of the Aeroplane*. Cambridge, Massachusetts: BSP Professional Books, 1983.

[128] Szekely, G. J. and Rizzo, M. L., "Brownian distance covariance," *The Annals of Applied Statistics*, vol. 3, no. 4, pp. 1236–1265, 2009.

[129] Talley, D. N., *Methodology For The Conceptual Design Of A Robust And Opportunistic System-Of-SystemS*. PhD thesis, Georgia Institute of Technology, December 2008.

[130] Targett, M., "Gulfstream-g650-cutaway.jpg," December 2011.

[131] Thompson, J. E. and Campbell, R. B., *Manual for Aircraft Hydraulics: Theory, Maintenance, Design*. Cadet Engineering Series, San Francisco, CA: Aviation Press, 1942.

[132] Thompson, K. M., "Variability and uncertainty meet risk management and risk communication," *Risk Analysis*, vol. 22, no. 3, pp. 647–654, 2002.

[133] United States Department of Transportation, "Jet fuel prices." Online, 2005.

[134] Utturwar, A., Rallabhandi, S., DeLaurentis, D., and Mavris, D., "A bi-level optimization approach for technology selection," American Institute of Aeronautics and Astronautics, 2002.

[135] Vanderplaats, G. N., *Numerical Optimization Techniques for Engineering Design*. Colorado Springs, CO: Vanderplaats Research & Development, Inc., 4th ed., 2005.

[136] Vickers, "Product News: Fluid-Cooled AC Motorpump for Boeing's727 & 737 Aircraft," 1999. PN 620-2A.

[137] Vickers Fluid Systems, "A descriptive summary of vickers inline pumps and their applications," tech. rep., Eaton Corporation, 2000.

[138] Walpole, R. E., Meyers, R. H., Meyers, S. L., and Ye, K., *Probability and Statistics for engineers & scientists*. Pearson Prentice Hall, 8th ed., 2007.

[139] Warwick, G., "New AFRL Program Focuses On Aircraft Energy," July 2010.

[140] Warwick, G., "Model design: Demand for power, cooling in advanced fighters drives a new approach to systems engineering," *Aviation Week and Space Technology*, pp. 71–72, 2011.

[141] Wood, K., *Aerospace Vehicle Design: Vol. I: Aircraft Design*. Boulder, Colorado: Johnson Publishing Company, second ed., 1966.

[142] Zwicky, F., "Morphological astronomy," *Nature*, vol. 4120, pp. 627–628, 1948.